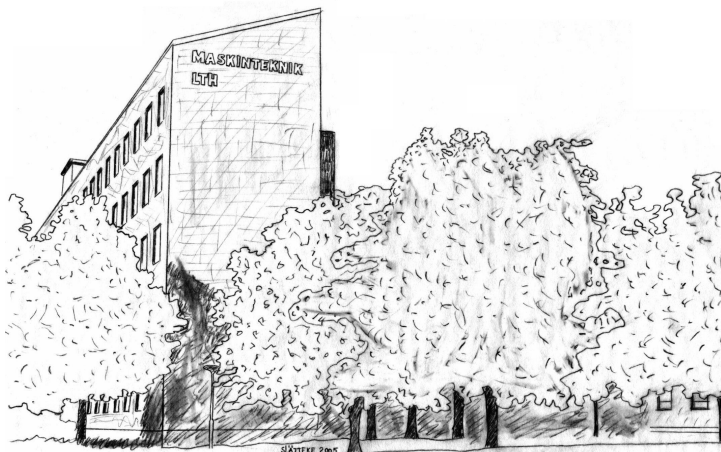# Modeling and Control of the Paper Machine Drying Section

Modeling and Control of the Paper Machine Drying Section

Ola Slätteke

Department of Automatic Control
Lund University
Lund, January 2006

To Kristin

Abstract

The topic of this thesis is modeling and control of the last part of the paper machine – the drying section. Paper is dried by letting it pass through a series of steam heated cylinders and the evaporation is thus powered by the latent heat of vaporization of the steam. The moisture in the paper is controlled by adjusting the set point of the steam pressure controllers.

There exist several commercial incentives to focus on the performance of the moisture control. The time to perform a grade change is often limited by the moisture and shorter grade change time is directly correlated to economic profit. Studies have shown that the drying section uses ⅔ of the total energy requirement in paper making. Reduced variations in moisture gives opportunity for target shifts (changed set point) which reduces the amount of raw material and steam requirement. It also creates opportunity for increased production rate.

The thesis is divided in two parts. The first part deals with the control of the steam pressure inside the cylinders. Both a black-box model and a physical model are given for the steam pressure process. A tuning rule for both PI and PID control is derived and various other controller structures are investigated. Many of the results are verified by experiments on paper machines at different paper mills.

The second part of the thesis treats the moisture controller. The physical model from the first part is expanded with a model for the paper. This gives a complete simulation model for the drying section that is implemented in the object-oriented modeling language Modelica. Two new approaches to control the moisture by feedback are evaluated. The first utilizes the air around the paper in combination with the drying cylinders to improve the controller performance. The second uses only the last part of the drying section to control the moisture, while the first part is put at an appropriate level. Finally, feedforward of a surface temperature signal is examined.

Acknowledgements

Preface

I first encountered process control in the summer of 1990. I was working as a summer intern at a pulp and paper mill at one of their winders (a machine that slits and winds the paper from the paper machine into the roll widths ordered by the customer). A winder does not have much process control but one night shift I was assigned to manage a pulper (a unit for slushing paper into pulp). I got a two minute crash course in control theory by one of the operators. For the first time in my life I heard words like set point and control signal. I remember that I did not understand much of it at that time. There were two important control loops to keep an eye on, the level control and the consistency control. Both were controlled by single-loop controllers, manufactured by Fisher & Porter, if I remember it correctly. A dangerous operating point was if the consistency was too high to physically empty the pulper at the same time as the level was too high to dilute the pulp mix. I promised the operator to not reach that point and hoped that I was right. Luckily I managed to do fine through the night and I was placed there the following nights too.

The next summer I was working at the same site but this year at the instrument department. One day we were replacing a malfunctioning flow gauge at the pulp dryer and I was watching a level controller at the instrument panel, trying to understand how it worked. I noticed that the level was too low but the controller only opened the valve by 40% and it was increasing slowly. I asked the maintenance guy who was dismounting the flow meter, why the valve was not fully opened. I thought that was the appropriate thing for the controller to do if the level was low. He then explained to me the concepts of dynamics, overshoot and stability, and from that day on I was hooked on the exciting field of process control.

During my studies I continued to work at the instrument department each summer. I learned a lot, things that are still useful for me today, every thing from repairing old pneumatic controllers with liquid solvent, programming the DCS-system and understanding different control structures. After my degree I worked there for a few years more before I went back to the university to become a PhD student.

Contents

1

Introduction

1.1 Introduction and motivation

Paper is used for printing and writing, for wrapping and packaging, and for a variety of other applications ranging from kitchen towels to the manufacture of building materials. It simply comes in an enormous variety of qualities. Some common types of paper qualities include the following:

- Copy paper for printers, copying machines and writing
- Newsprint
- Cardboard
- Light-weight coated paper for magazines
- Wrapping and packaging paper
- Hygienic tissue paper
- Currency paper

In modern times, paper has become a basic material, commonly found in almost all parts of the world. Just try to imagine a day without paper in your life. No newspaper in the morning, no tissue to clean up the coffee you spilled out on the breakfast table. No books to read in your hammock on a sunny day. No notepad to write your shopping list on before you go

to the super market. An empty mailbox each day you come home from work. No thesis to hold in your hand right now. The world simply became a better place to live in with the advent of paper some 2000 years ago.

The pulp and paper industry is a highly competitive and capital-intensive market that is under increasing price pressure. The price pressure on the finished products implies that the margins are often small and a producer can only be profitable by manufacturing high volumes [Duncan, 2003]. In Europe, the total production of paper in 2003 was 95 million tonnes with a turnover of €72 billion [CEPI, 2004]. Customers are demanding lower costs, better terms of delivery, and higher product quality. In the last decade a large number of company acquisitions and mergers has taken place in the forest industry all over the world as an answer to the high competition [FFIF, 2004], see Table 1.1. Compared to other industries such as food, chemical, and pharmaceutical, the paper industry has delivered a relatively low return on capital employed (ROCE). As a result the forest industry companies have grown by size and the industry has become more consolidated. The main objectives behind the mergers and acquisitions are lower production costs, less sensitivity to economic fluctuations, reduced transportation costs, reduced labor costs, and other positive synergy effects. Companies have realized that it might be cheaper (and certainly quicker) to buy production capacity rather than building it. At the same time there is a steady overcapacity in the world, the industry is facing increasing environmental requirements and there is an increased competition from other industries as alternatives to fiber products appear [Dumont, 1988]. The plastic packaging demand is e.g. expected to have a rapid growth in coming years. Therefore the production of paper requires constant attention on process efficiency, increasing productivity, and lower costs.

Table 1.1 Figures illustrating the consolidation trend in Europe with less number of companies and paper machines, and yet a higher capacity [CEPI, 2004].

	1991	2001	2002	2003
Number of companies	1 042	918	901	884
Number of paper machines	2 181	1 863	1 811	1 815
Employment	362 100	288 700	285 000	279 400
Turnover (million euros)	39 263	77 028	74 235	71 866
Capacity (1000 tonnes)	72 343	100 713	103 489	104 978
Consumption (1000 tonnes)	62 140	83 306	85 674	86 186

The function of a paper machine is to form the paper sheet and remove the water from the sheet. A paper machine is divided into three main parts, the wire section, the press section, and the drying section, see Figure 1.1. When the stock enters the head box in the wire section, it contains roughly 1 % of fibers or less. This low viscous mix is dispensed through a long slice onto the wire. As it travels on the wire, much of the water drains away by gravitational forces or is pulled away by suction from underneath. As the water disappears, the cellulose fibres start to adhere to one another by hydrogen bonds and form a paper web. When the paper web leaves the wire section and enters the press section, the dry solids content is around 20 %. In the press section, the newly formed sheet is pressed between rotating steel rolls and water is displaced into a press felt. After a few press nips the web enters the drying section with a solid content of approximately about 50 %. It now encounters the dryer cylinders. These are large hollow metal cylinders, heated internally with steam, which dry the paper as it passes them. Finally, the paper is wound up on a big roll and removed from the paper machine. The moisture content is now roughly 5−10 %.

Although the drying section is only responsible for removing less than 1 % of the water volume in the original stock to the head box, this is the part of the paper machine that, by far, consumes most energy. Studies have shown that the drying section uses around ⅔ of the total energy requirement in paper making [Fellers and Norman, 1998]. This implies that the drying section is the most expensive part of the paper machine in terms of energy use per kg removed water. Moreover, the drying section affects a lot of the important physical properties of the final product, such as paper sheet elasticity, twist, and curl.
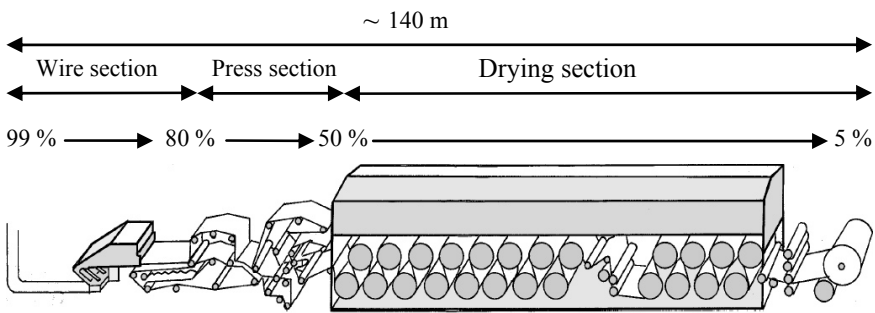
Figure 1.1 The principle of paper production is simple. The water is separated from the original stock which is smoothened out to a thin and endless paper sheet. By adding different types of fillers the paper surface obtains different properties. Typical values of moisture content are indicated. By courtesy of Skogsindustrierna.

Chapter 1. Introduction

For a paper mill, and even for a group of companies, erecting a new paper machine is a large investment. A high production rate and capacity is therefore essential to achieve a high return on the investment. One of the most important quality variables in paper manufacturing is moisture content. Below are a few reasons of why a well tuned moisture control system provides economic yield.

- Large variations in moisture can adversely affect post processing units like calendering, the converting or packaging line, or even the customer's printing press (worsen printability). During production, moisture content is therefore measured and monitored online, and the paper product is rejected if it deviates outside the specified limits. A stable and uniform moisture content during normal operation guarantees low reject and consequently high production rates.

- With reduced variance the moisture set point can be increased without changing the probability for an off-spec product, see Figure 1.2. In plain language, the paper mill is selling more water at an excessive price (paper is sold according to weight). A modern paper machine makes around 1000 tons of paper per day. A reduction of moisture by 0.1 % corresponds to 365 tons of raw material per year. With a production cost for pulp roughly around €500 per ton [Dagens Industri, 2004], this in turn means a large economical saving for the mill. An increase in moisture also gives a reduction in energy use (steam consumption). If the specific paper machine is dryer limited this also gives an opportunity to increase the machine speed, see below.

- An obvious way to increase production is to increase the machine speed. Then the drying section often becomes a bottle neck by lacking the required capacity. Maximum production is achieved by operating at maximum speed while remaining within the control constraints. Reduced variations in moisture then implies that the speed can be increased without reaching the maximum available steam pressure.

- A well tuned moisture control system will reduce the time to carry out a grade change (state transition). In practice, the moisture feedback loop is often turned off during a grade change and the process is run in open loop (feedforward). Due

to model errors in the feedforward loop the moisture will deviate from the set point when the feedback is turned on again. Hence, the moisture control is important in the last part of a grade change and a shorter grade change time is directly correlated to economic profit.

- The moisture control loop is indirectly involved during a web break by the steam pressure in the steam cylinders. A very common problem is that the cylinders become overheated since there is no longer any cooling paper around them. When the paper web is put back, picking and new web breaks easily occurs. By having an optimized steam control system during a web break, the time it takes to get the paper sheet back on the reel can be reduced.

- Many paper properties depend on moisture content, e.g. curl, stretch, tear, strength and stiffness [Gavelin, 1972].

These are some of the reasons why the drying section plays a vital role in paper manufacturing. As the title reflects, this thesis is focused on both modeling and control of the drying section of a paper machine.
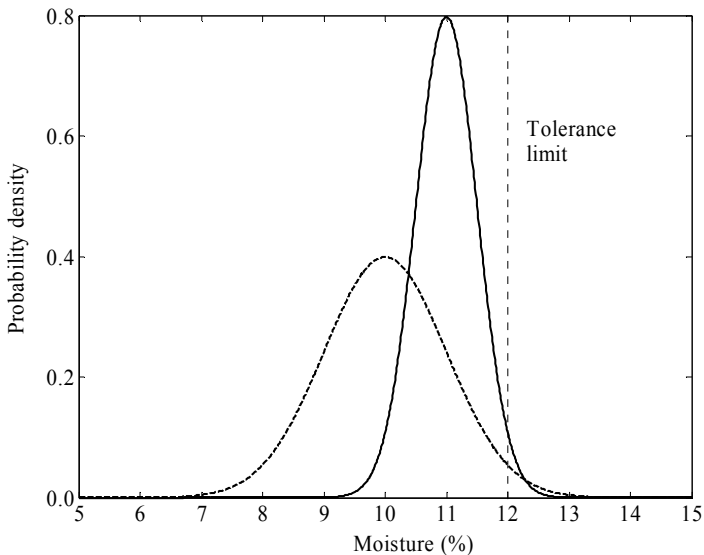
Figure 1.2 The reduction of moisture variation makes it possible to increase the set point (target shift). The solid curve represents a condition where the standard deviation has been reduced by 50 % compared to the dashed curve. Hence, it is possible to increase the set point from 10 to 11 %. The difference between the tolerance limit and mean value is sometimes called the *give-away*.

17
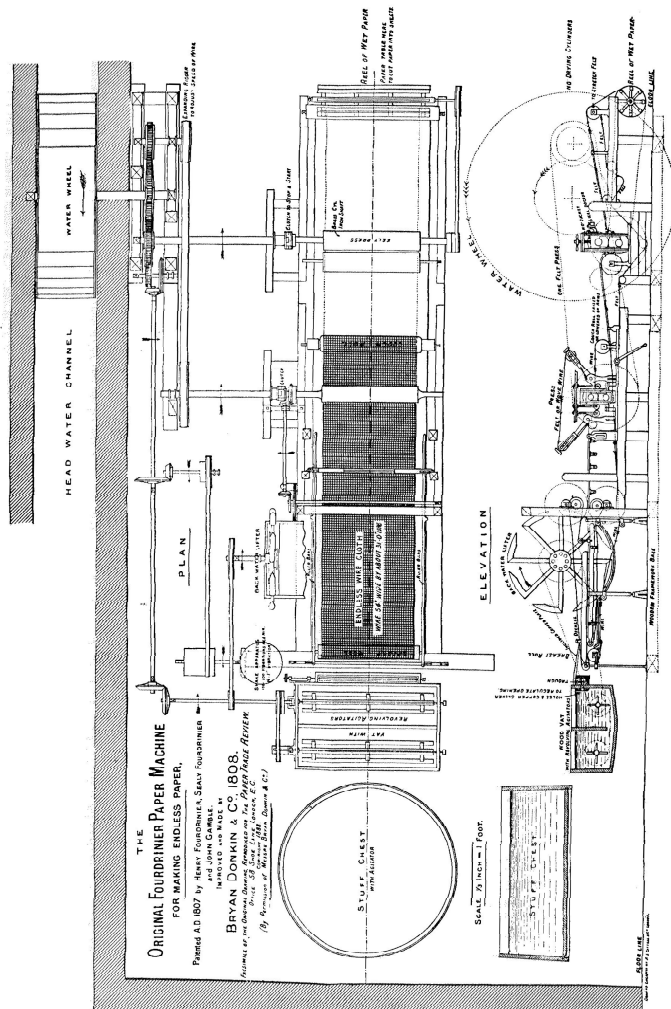
Figure 1.3 A drawing of the first paper machine from 1808, also known as the Fourdrinier paper machine [Clapperton, 1967]. It was invented in 1798 by Nicholas-Louis Robert, while working for the French paper mill owned by the Didot family. His machine used a belt of wire screen to produce a continuous web of paper. He was backed in England by the Fourdrinier brothers, who built and sold the first paper machines. By 1810, the Fourdrinier brothers found themselves in bankruptcy and Bryan Donkin, their engineer, continued to improve the basic design. Soon he was successfully manufacturing a machine that mechanized the process of making paper. A water and pulp mixture flowed across a moving, vibrating web of woven wire cloth, forming a wet mat of interlocking fibers. From the wire, the newly formed paper transferred to a moving web of woolen cloth (the felt), before being dried.

1.2 Outline and contribution of the thesis

Although the fundamental principle of producing paper has not changed since the invention of the paper machine, see Figure 1.3, very much has happened since then in terms of quality and efficiency. In those days there did not exist much automatic control in a paper mill. The pulp and paper industry first initiated computer applications to process control in the early 1960's. This was in a time when major changes occurred in the area of control theory, new concepts like state-space theory, Kalman filtering, and optimal control were introduced. Today, a large majority of all paper machines in the world are computer controlled. Some of the major breakthroughs in advanced control theory have been tested first in the pulp and paper industry, e.g. the minimum-variance controller [Åström, 1967] and the self-tuning controller [Borisson and Wittenmark, 1974], see also [Dumont, 1986] and [Bialkowski, 2000]. Since then, a significant amount of papers have been written on the subject of quality control in the paper machine but there are still opportunities for further improvements and the contributions of this thesis are

- Analysis of different controller structures for the steam pressure loop based on a previously proposed black-box model.

- Presentation of a physical steam cylinder model with the same structure as the black-box model. The purpose is to gain deeper understanding in the physics behind the process.

- A new tuning method for both PI and PID controllers based on optimization of disturbance rejection, subject to a robustness constraint. The method has one tuning parameter that adjusts the trade-off between performance and robustness. It is compared to a few other design methods and tested on a real paper machine.

- A new approach to control the moisture content in the paper sheet by using both steam pressure in the cylinders and the supply air to the hood as actuator signals. This control challenge is solved by using mid-ranging of two IMC-controllers.

- A new approach to control the moisture content in the sheet by manipulating the last steam group independently of the others. It is solved by a model predictive controller (MPC).

- Introduction of a new signal which can be used in feedforward to improve control performance. The signal is based on the temperature profile in the machine direction.

- Design of a model library in Modelica® including components for a drying section, with possibility to easily build a dynamic simulation model of a whole drying section.

Publications

The thesis is based on the following publications:

- Stenström, S., M. Karlsson, O. Slätteke, B. Wittenmark, and K. Forsman (2002): "Productivity increase from a better understanding of dynamic processes and control of the paper dryer," *Preprints 7th New Available Technologies*, pp. 70–73, Stockholm, Sweden.

- Slätteke, O., K. Forsman, T. Hägglund, and B. Wittenmark (2002): "On identification and control tuning of cylinder dryers," *Proceedings Control Systems 2002*, pp. 298−302, Stockholm, Sweden.

- Karlsson, M., O. Slätteke, B. Wittenmark, and S. Stenström (2003): "Evaluation of models for the steam supply system," *Tappi Spring Technical Conference & Trade Fare*, Chicago, IL.

- Slätteke, O. (2003): *Steam and condensate system control in paper making*, licentiate thesis, ISRN LUTFD2/TFRT--3231--SE, Department of Automatic Control.

- Karlsson, M., O. Slätteke, B. Wittenmark, and S. Stenström (2005): "Reducing moisture transients in the paper machine drying section with the mid-ranging control technique," *Nordic Pulp and Paper Research Journal*, 20(2), pp. 150−156.

- Slätteke, O., and K. J. Åström (2005): "Modeling of a steam heated rotating cylinder − A grey-box approach," *Proceedings American Control Conference 2005*, Portland, OR.

- Karlsson, M., O. Slätteke, T. Hägglund, and S. Stenström: "Feedforward control in the paper machine drying section," submitted to American Control Conference 2006.

- Slätteke, O.: "Object oriented modeling and predictive control of the moisture content in paper production," submitted to American Control Conference 2006.

Outline

This thesis is divided into two main parts. The first treats modeling and control of the steam and condensate system, and the second focuses on modeling and control of paper moisture. The different chapters are organized as follows.

Chapter 2 gives the fundamentals of the paper drying process. Much of the nomenclature used in other chapters is introduced here.

Chapter 3 presents a black-box model for the steam pressure process and a few different controller structures are investigated.

Chapter 4 derives a physical model for the steam pressure process that is compared with the black box model. It is also validated against plant data.

Chapter 5 presents a tuning rule for the steam pressure controller. It assumes PI or PID control and is compared to other tuning rules found in the literature.

Chapter 6 shows how the air system in the dryer hood can be combined with the conventional steam pressure control to enhance the moisture control performance.

Chapter 7 introduces a new feedforward signal that is based on temperature measurements of the paper surface.

Chapter 8 presents a physical model of the drying section that is implemented in the object-oriented modeling language Modelica. The model is used to evaluate a new approach to manipulate the steam pressure in the drying section to improve performance of the moisture controller.

Chapter 9 gives a conclusion and suggests possible future work.

2

Fundamentals of the Paper Drying Process

The most common way to evaporate water from the paper web is to use the latent heat of vaporization in steam. A steam-filled dryer is a cost effective method to transfer heat into the sheet. The energy in steam has proven to cost less than a quarter of any other available method [Pauksta, 1998]. Other advantages are low toxicity, easy of transportability, and high heat capacity. Since most of the heat content of steam is stored as latent heat, large quantities of heat can be transferred efficiently at a constant temperature, which is a useful attribute in paper drying and many other heating applications. Also, the energy can be extracted as mechanical work through a turbine which makes many mills more or less self-supporting in terms of electricity. For chemical pulp mills, steam is obtained simply as a by-product in the chemical recovery process line.

The moist paper can be led around a single large steam heated cylinder, called Yankee cylinder (mainly used for the drying of tissue) or a large number of steam heated cast iron cylinders in series (commonly called *cans*), called multi-cylinder drying. In this thesis, attention is only given to the multi-cylinder dryer but most of the theory can also be applied to the Yankee cylinder, see Figure 3.3. Two thorough textbooks about paper drying are [Karlsson, 2000], and [Gavelin, 1972]. A glossary can be found in Appendix A.

2.1 Cylinder configurations in the drying section

When the steam enters the cylinder it releases its thermal energy to the cast iron shell and condenses into water. This condensate is drawn off by suction with a siphon and fed back to the boiler house. The steam is typically fed to the cylinders on the backside of the machine (called the *drive side*), and the condensate is evacuated on the front side (called the *operator side*) or the backside. At some machines, especially on wide machines, the condensate is removed on both sides. Effective condensate removal is important for the heat transfer of the dryer cylinder. Therefore, it is desirable to let some steam pass through the siphon together with the condensate. This so-called blow-through steam ensures removal of condensate, air, and other noncondensable gases from the cylinder. Noncondensable gases reduce the partial pressure of the steam in the cylinders and lower the condensation temperature at a given total pressure. In addition, the air molecules tend to accumulate at the cylinder surface as they can hardly diffuse fast enough against the direction of flow of the steam and as a result the heat transfer between the steam and the cylinder shell is reduced. The effect of air in a cylinder is therefore much greater than would be expected from the average percentage of air in the cylinder [Gavelin, 1972].

On slow machines (< 300−400 m/min) the condensate forms a pool at the bottom of the cylinder. It is mainly old board machine running at these speeds. As the speed increases, the condensate starts cascading
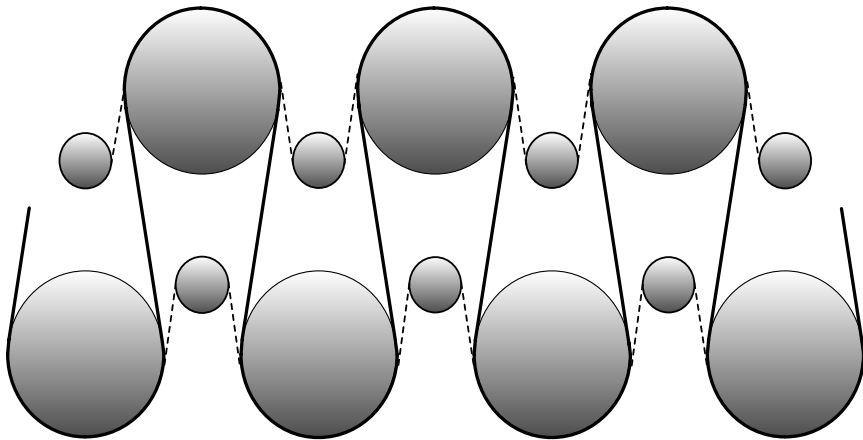
Figure 2.1 A two-tier configuration.
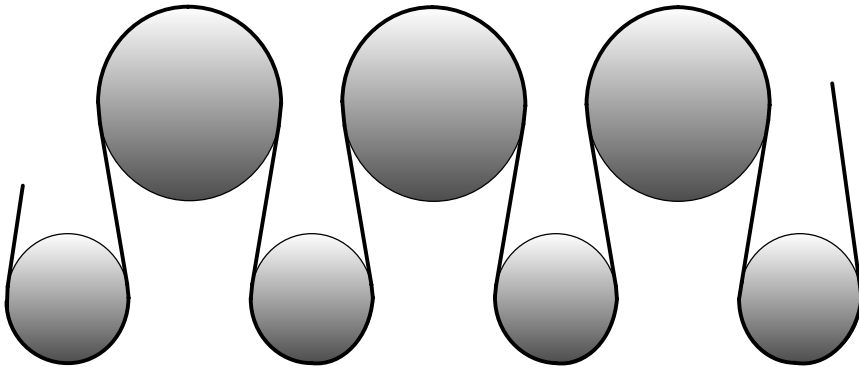
Figure 2.2 A single-tier configuration.

and suddenly a rim of condensate forms around the circumference. One immediate effect of this is that less energy is required to rotate the cylinder and the dryer load drops. If the speed is reduced, the rim will break down again but at a much lower speed than where it was first formed (hysteresis).

Almost every dryer in a modern paper machine has dryer bars on the inside of the cylinder shell. They are also called turbulent bars or spoiler bars. These provide higher and more uniform heat transfer from the steam to the cylinder by increasing the turbulent behavior of the condensate.

[Peng, *et al*, 1997] show that the condensate film thickness can be greatly reduced, and nearly eliminated, by exchanging the siphon by a rubber scraper. The condensate is then mechanically removed from the cylinder. To the author's knowledge, this technique has not yet been installed or verified on a real paper machine.

To support and transport the paper web through the drying section, dryer fabrics are utilized. The dryer fabric is also used to press the web onto the cylinders to provide good thermal contact between the two surfaces. The dryer fabrics are woven with synthetic yarns and do not absorb any water, as one might think. The water present in the web is moving directly as vapor through the fabric into the air.

There are mainly two types of dryer arrangements today, the single-tier design (single-felted) and the two-tier (double-felted). The two-tier configuration, which is the older one of the two, is shown in Figure 2.1. Here two separate fabrics are used, one is used on the top cylinders and the other on the bottom cylinders (marked as a dashed line in the figure). Wet paper is transferred unsupported from one dryer to the next, and this can cause problems like wrinkles and sheet breaks. To prevent these

runnability problems at higher machine speeds, the single-tier configuration was invented (in 1975 at Stora Enso Hylte mill [Carlberg, 1989]), see Figure 2.2. Using this technique, a single fabric is supporting the web on both the top and the bottom cylinders, as well as in the passage between them. Since the fabric is between the web and the cylinders in the bottom row, no significant drying occurs there. In modern machines, the bottom row of cylinders is therefore replaced by smaller vacuum rolls to increase the runnability even more [Asensio and Seyed-Yagoobi, 1992].

2.2 The steam and condensate system

The purpose of the steam and condensate system is to provide a sufficient amount of steam to the dryers and to handle the condensed steam. The cylinders in a drying section are divided in separate dryer groups, normally between five and ten groups, see Figure 2.3. The steam pressure in the different dryer groups can then be controlled individually to obtain the desired pressure profile through the drying section, from the first group to the last one. Since the steam inside the cylinder can be regarded as saturated because of the continuous condensation at the cylinder wall, there is a direct correlation between the steam pressure and steam temperature and you could also talk about a temperature profile. For most paper grades, dryer steam pressure is increased gradually for drying
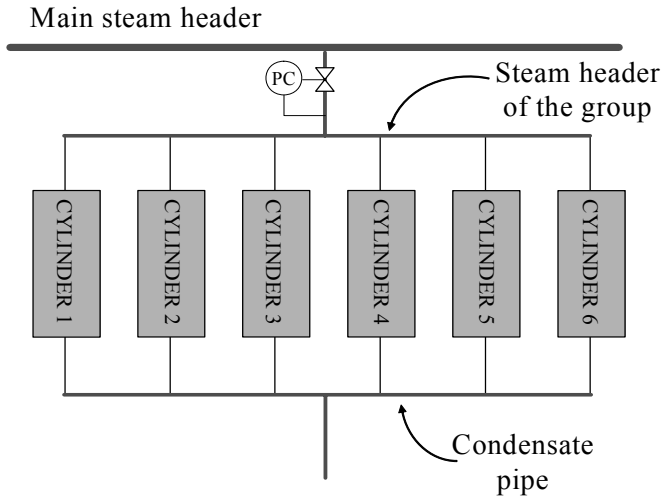
Figure 2.3 Sketch of a dryer group consisting of 6 cylinders and one common pressure gauge and controller.
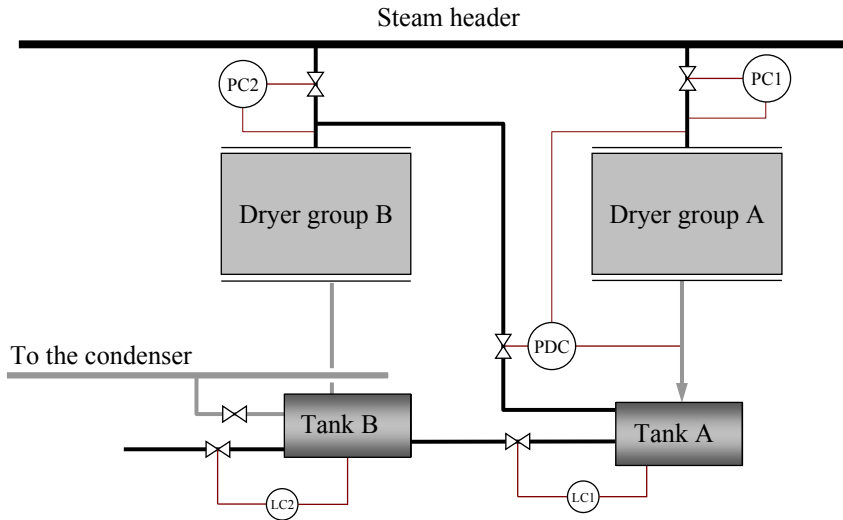
Figure 2.4 Part of a drying section with a cascade system. Sometimes the PDC-valve is installed in the pipe between group A and tank A.

capacity and runnability reasons. [Perrault, 1991], [Hill, 1993], and [Krumenacker, *et al*, 1997] give a good review of the steam and condensate system, from simple troubleshooting to advanced control schemes.

The simplest, but least energy efficient, way to supply the steam to the different steam groups would be to let them all take steam from the header and dump the blow-through to the condenser (a heat exchanger unit that heats process water by the left over steam). However, the fact that the dryer groups operate at different pressures can be utilized and this is done in the cascade system, which is an efficient arrangement from an energy usage perspective. The blow through steam from one dryer group at higher pressure is reused in a group operating at lower pressure. In Figure 2.4 we see a simple example of a system with two dryer groups. The blow through steam from Group A and flash steam (when some of the condensate meets the lower pressure in the condensate tank, it vaporizes and forms new steam) from Tank A is piped to Group B, which operates at a lower pressure. Controller PC2 then adjusts its valve, and adds some extra *make-up steam* from the header, to maintain the desired pressure in Group B. This means that there must be some minimum pressure difference between Group A and Group B in order to get a steam flow through the PDC-valve. This minimum pressure difference depends on both the operating point and machine specific properties. The differential

Steam header
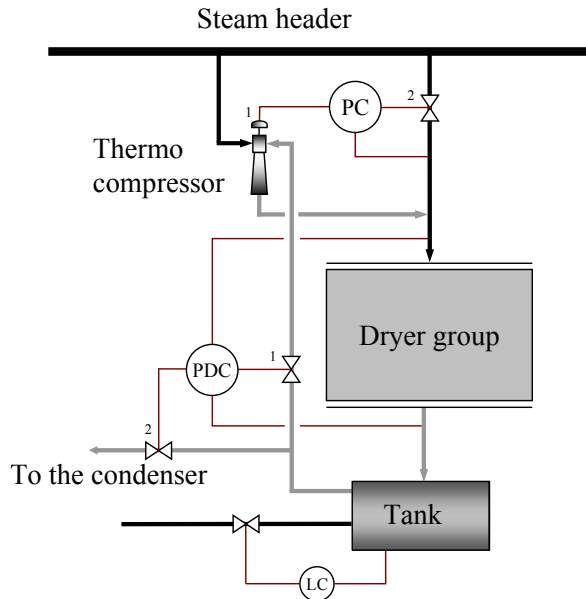
Figure 2.5 A steam group with a thermo compressor unit. Both the PC and PDC controller work in split-range and the numbers indicate in which order the actuators are manipulated. Some care must be taken since noncondensibles might be recirculated and accumulated.

pressure over Group A is preserved by controller PDC to guarantee a satisfactory condensate evacuation. In this example, Group B has the lowest pressure in the machine and therefore Tank B must dump its steam to the condenser. Often this dryer group has an operating point just above atmospheric pressure (sometimes below) and the condenser is a necessity to obtain the required low pressure in the condensate tank.

From a control perspective, the cascade system is an inconvenience, since it introduces additional interconnections between the different control loops, and provides extra pathways for disturbance distribution through the system. In general, material recycling can also severely affect the overall dynamics and in most cases leads to positive feedback [Morud and Skogestad, 1996]. Naturally, the energy perspective has higher priority and the cascade system is the dominating configuration.

The disadvantage of the interconnections from the cascade configuration can be resolved by a thermo compressor unit. A thermo compressor is a device that uses high-pressure steam from the steam header to compress blow through steam to a desired pressure. In this way, the blow through steam can be recirculated to the same steam group, making the different steam groups independent, see Figure 2.5. The PC-

27
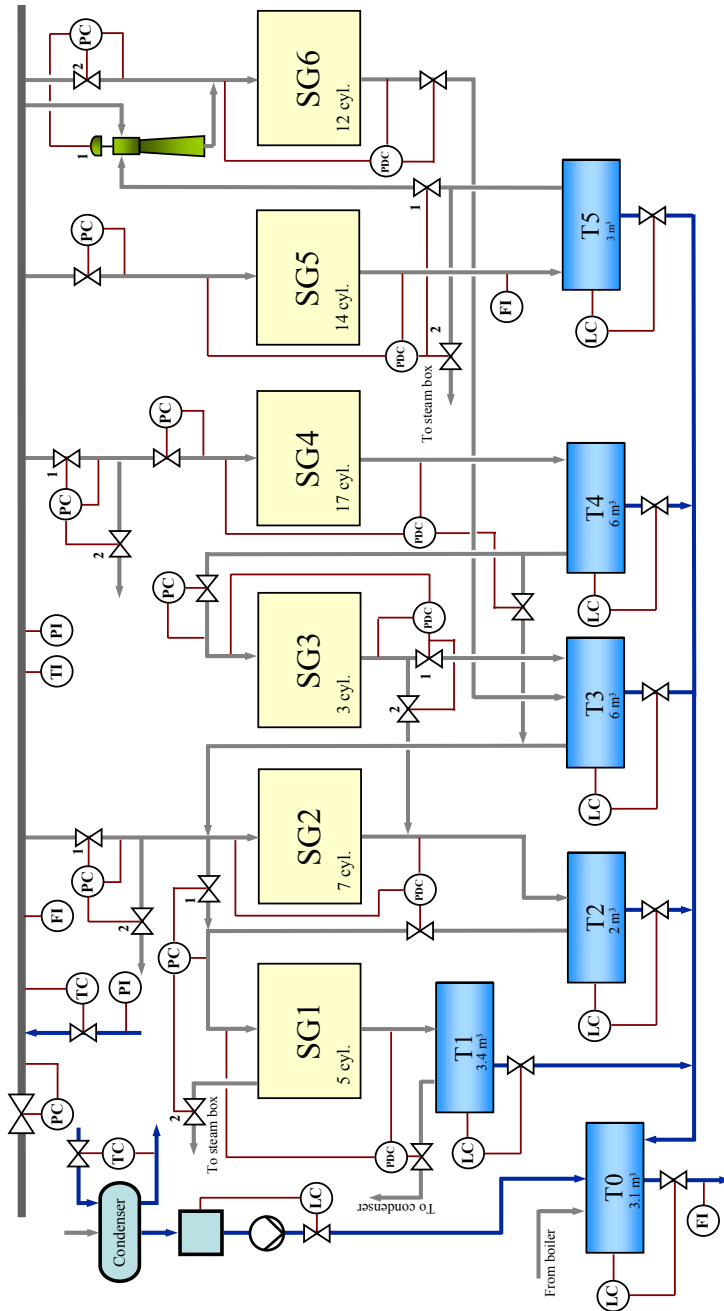
Figure 2.6 A typical piping and instrumentation diagram of the steam and condensate system.

controller primarily uses the recirculated steam from the thermo compressor but have the possibility to also use make-up steam from the header, if necessary. In the same manner, PDC leads the blow-through steam to the compressor and dumps the steam to the condenser only in exceptional cases e.g. web breaks or grades with low drying demand. Sometimes the thermo compressor is used in cascading configurations too.

Naturally, there are many other ways to structure a steam- and condensate system, and Figure 2.4 and Figure 2.5 are purely simplified cases to illustrate some basic ideas. The steam and condensate system almost always uses a case-by-case design. Figure 2.6 shows a typical, but still somewhat simplified, P&ID of a drying section, indicating both the complexity and the control engineering challenge.

2.3 The moisture control loop

The measuring principle

To control something, you must be able to measure or estimate it. Quality parameters, such as basis weight, moisture, caliper, ash content, fibre orientation, color, and brightness are measured on-line in a paper machine. The quality control system (QCS) is divided in two separate dimensions, the machine direction control (MD) and the cross direction control (CD). The conventional technique is to measure the MD and CD signals by scanning the sheet with a single sensor. The sensor is mounted in a scanner platform, where it moves back and forth in the cross direction, see Figure 2.7. Due to the MD movement of the paper, the measurements form a zigzag pattern on the paper sheet, as shown in Figure 2.8. This implies that the MD and CD variations are mixed together by the measuring principle and the two signals must be separated
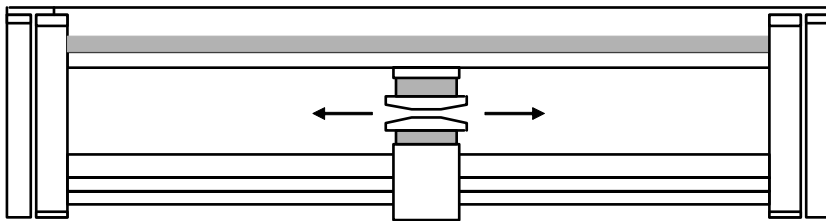
Figure 2.7 The scanner platform moves the measuring sensor back and forth across the sheet. By courtesy of ABB Ltd.
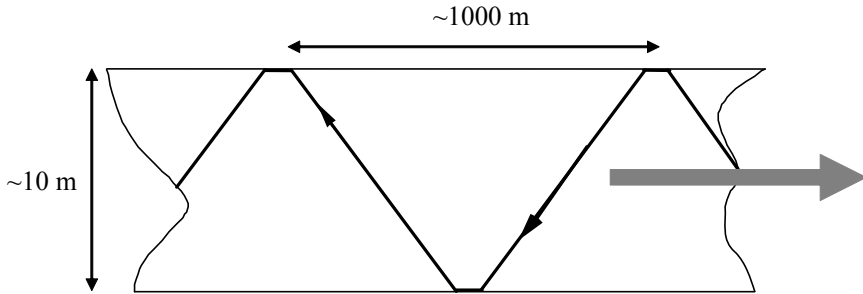
Figure 2.8 The path of the scanning sensor. The large arrow points out the direction of machine speed. Notice the different length scale in the machine direction and cross direction.

 [Kastanakis and Lizr, 1991]. In [Natarajan, *et al*, 1988] an algorithm is developed, which uses least squares to estimate the CD component and Kalman-filtering for the MD component. It is then further developed in [Dumont, *et al*, 1991], and [Chen, 1992]. A similar decomposing algorithm based on Karhunen-Loeve expansion is [Rigopoulos, *et al*, 1997], and [Chen and Subbarayan, 1999]. [Chang, *et al*, 2000] proposes an elliptic sensor trajectory by variable scanning speed or the use of two scanners traveling in opposite direction to improve the MD/CD-estimations.

   As stated above, the ultimate objective of these measurements is control. The primary mechanism today for the control of the moisture MD variations is the dryer steam pressure. Other methods have been proposed, like infrared drying [Kuang, *et al*, 1995], and [Seyed-Yagoobi, *et al*, 2001], impulse drying [Orloff and Crouse, 1999], and [Martinez, *et al*, 2001], and Condebelt drying [Lehtinen, 1995], and [Retulainen, 2001]. Most of these methods have been tested in lab-scale for many years but have not yet found acceptance in industry for various reasons [Crotogino, 2001]. The exception is Condebelt who has one installation in Finland, which has been running since 1996.

   The CD profile, on the other hand, is controlled either by remoisturizing showers, steam boxes (a device that improves the vaporization in the paper by adding superheated steam directly onto the sheet), or by infrared heating boxes located at intervals across the machine's width [Dumont, *et al*, 1993]. An even moisture content in the CD is easiest to achieve if it is low, therefore it occurs that the paper is over-dried and then remoisturized. Of course, then the gain in higher quality has to be weighted against the cost of higher energy use. This
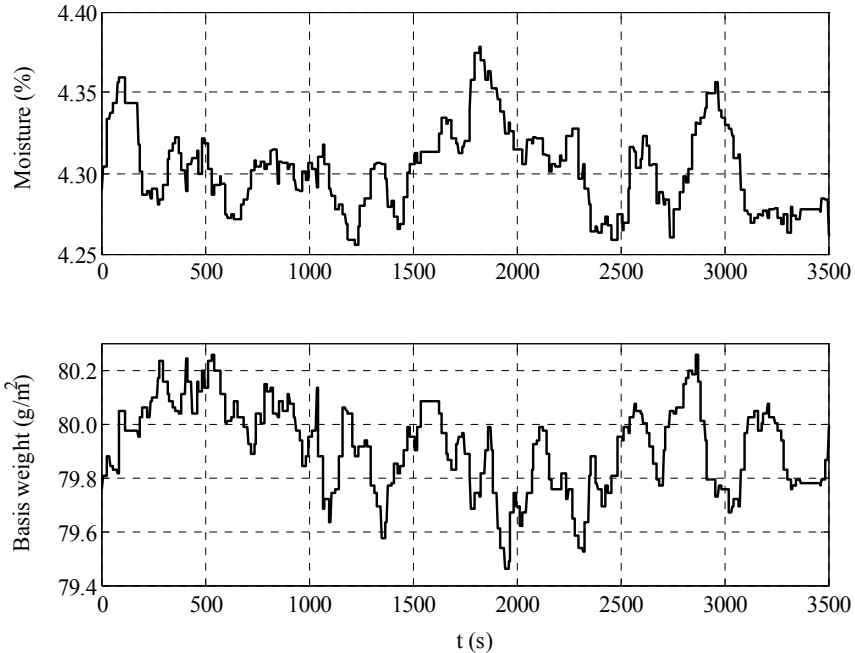
Figure 2.9 Moisture content and basis weight measurements taken from a fine paper machine. The set point for moisture in this case was 4.3% and the basis weight set point was 80 g/m². The 2-sigma values were 0.056% and 0.3 g/m² respectively.

thesis focuses solely on the MD-control. More details about CD estimation and control can be found in [Stewart, *et al*, 2003], [Heaven, *et al*, 1994], and [Kjaer, *et al*, 1995].

The performance of the control system has, in the pulp and paper industry, historically been described in "2-sigma" or two standard deviations of the controlled variables. All produced reels of paper leaves the paper machine together with a "reel-report" that include statistics like "2-sigma MD", "2-sigma CD", and "2-sigma total" for both the moisture
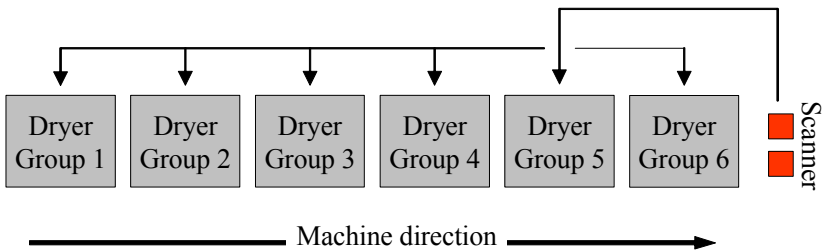
Figure 2.10 Structure for the moisture control loop with one scanner device and six steam groups.

31
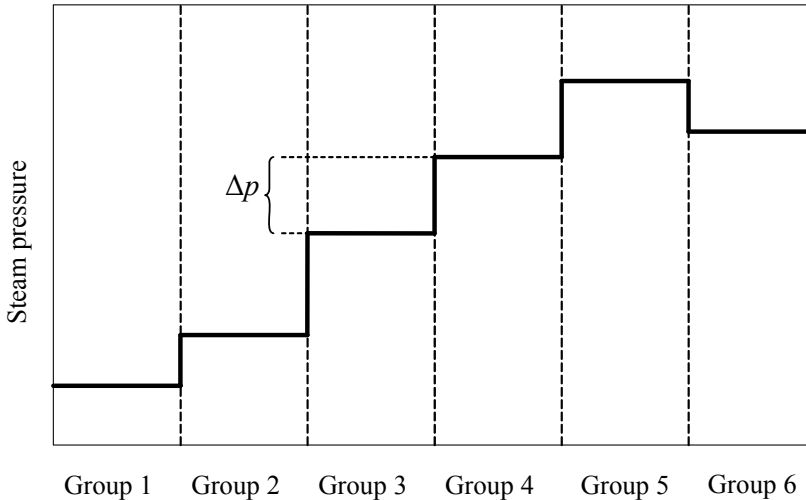
Figure 2.11 Example of feasible steam pressure distribution of the drying section in Figure 2.6 and Figure 2.10. The minimum pressure difference, Δp, between cascade groups depends on machine speed, siphon types, and steam and condensate pipe size. A typical value of Δp is 50 kPa.

and basis weight [Sell, 1995]. These are the average values for the whole reel, but it is the short term 2-sigma values that are used to make the decision if the product meets the quality requirements. To focus on the variability in this way makes sense since a consistent and uniform product is an important objective, as pointed out in Chapter 1, and the set points of the quality variables are constant during long periods and only altered at grade changes. For grade change control, see [Murphy and Chen, 1999], [Kuusisto, *et al*, 2002], and [Viitamäki, 2004]. An example of scanner measurements, in machine direction, during a normal run are shown in Figure 2.9, taken from a machine producing 80 g/m^2 of high quality copy paper. At 1500 s, there is a short period of time when the measurements are not updated, most distinct in the basis weight. This is due to the automatic calibration of the scanner, performed at constant intervals, when the measuring head is positioned at one of the ends in the CD. Also, see Section 2.5 for a comment on moisture units.

The paper moisture loop

As explained previously, the moisture in the sheet is controlled by the steam pressure in the cylinder groups. Since the drying section is divided in separately controlled groups, this is a multi-input-single-output (MISO) system. This means that the drying process has many degrees of freedom

in terms of control. Traditionally, this has been solved by letting all steam pressure controllers follow the same signal. The moisture controller then manipulates the steam pressure set point of one dryer group and the others follow that one, yielding a SISO system for the moisture controller. Figure 2.10 shows how this can be arranged with one scanner device, also called measuring frame, and the six dryer groups in Figure 2.6. Dryer group 5 (called *lead group*) operates at the highest steam pressure and receives the control signal from the moisture controller. The set points of the other groups are then calculated from that value, either as a ratio or a difference, see Figure 2.11 and Figure 2.12. The purpose of this is twofold. Firstly, the constant relation between the pressure in the groups gives good conditions for the function of the cascade system, and secondly it is also important for both runnability and the quality of the paper.

The functions *f* in Figure 2.12 are given by

$$f_n = k_n r + m_n \quad \text{where} \quad \begin{cases} 0 < k_n \leq 1, \, m_n = 0 \\ \qquad \text{or} \\ k_n = 1, \, m_n \leq 0 \end{cases}, \quad (2.1)$$

where index *n* refers to group number. These expressions can be used to achieve pressure differentials between the groups as in Figure 2.11. A combination of the two function alternatives (ratio/difference) in (2.1) is of course possible but not common. Some machines use two scanners, one in the middle of the drying section and one at the end, to improve the control. The middle scanner then controls the first part of the machine and
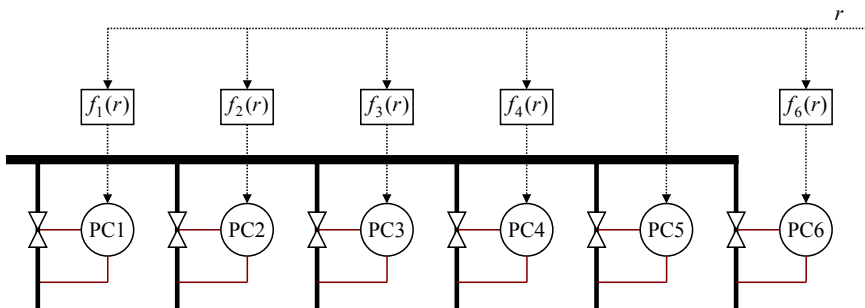
Figure 2.12 The set point *r* from the moisture controller is distributed to the steam pressure controllers by passing it through a ratio/bias-function except for the lead group, in this case group 5.
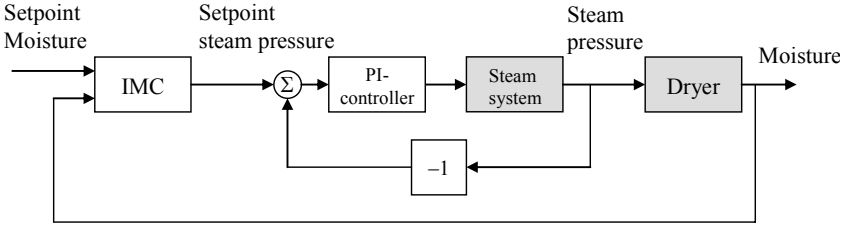
Figure 2.13 A block diagram of the moisture control loop.

the scanner at the end of the machine controls the second part. The middle scanner can of course also be used for feedforward control.

As indicated above, the moisture control loop is a cascade loop. Drawn as a block diagram, it looks like in Figure 2.13. The inner loop controls the steam pressure in the dryer groups. This is in general accomplished by a PI- or PID controller. In the outer loop there is in general a model based dead-time compensating controller, typically of the internal model control (IMC) concept [Morari and Zafiriou, 1989] or based on the Dahlin type [Dahlin, 1968] (which is a subset of IMC). The performance of these controllers are evaluated in [Bialkowski, 1996] and [Makkonen, *et al*, 1995]. The IMC controls the moisture in the paper sheet, by giving set point values to the PI-controllers in the inner loop. In Chapter 6, a mid-ranging control structure by combining two IMC-controllers is investi-
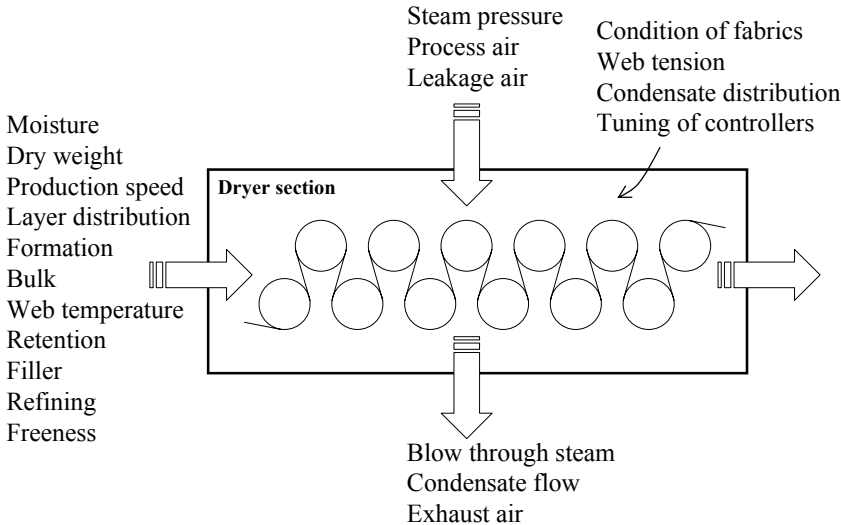
Figure 2.14 A list of variables that affect the final moisture in the paper during the drying process. A short description of some of the terms can be found in Appendix A.

gated. In this way, two single-loop controllers form a quasi-multivariable controller. The same structure is also implemented by a true multi-variable controller but with different manipulated variables, see Chapter 8. Other non-conventional moisture control schemes can also be found in [Åström, 1967], [Brown and Millard, 1993], [Xia, *et al*, 1993], [Rudd and Schweiger, 1994], [Murphy, *et al*, 1996], [Wang, 1996] and [Wells, 1999].

Apart from the steam pressure in the cylinders, there are a large number of variables that determine the moisture in the paper sheet. To indicate the complexity of the problem some of them are listed below and given in Figure 2.14.

- **Production Speed:** Affects the amount of steam needed, since high production also involves higher vaporization.

- **Dry Weight:** A thick sheet is more difficult to dry than a thin sheet at the same production speed, see Figure 2.15 and Figure 2.16.

- **Inlet Moisture**: The moisture content of the sheet after the press section is a disturbance variable that normally is unknown.

- **Degree of Refining:** This parameter naturally affects both the freeness (measure of the drainability) and the ability to dry the sheet.

- **Broke Quotient:** This is defined as the amount of broke being blended into the pulp. The broke pulp (if dried before) can be more easily dried than the new pulp.

- **Air Dew Point**: A high dew point inhibits effective evaporation.

- **Dryer Fabric Condition:** An old fabric can be clogged and give a higher evaporation resistance.

- **Bulk:** High bulk means that the water inside the web has a longer transport distance to the surface and ambient air.

- **Retention aids:** It is easier to dry the web when the retention is high since it then contains more filler.

- **Web tension:** High web tension increases the heat transfer coefficient and the drying rate.

- **Leakage air:** The air from the machine room is cooler that the preheated supply air and therefore impair the drying conditions.

- **Ply loading:** In paperboard, different layers consist of different pulps, hence different physical properties. This influences the drying.

- **Blow through steam:** In case of improper amount of blow through steam, the cylinder may be flooded. This has a large influence on the heat transfer to the paper (and the load on the drives).

Some of these disturbances are controlled variables and can therefore be regarded as known. This opens for possibilities of feedforward, which often is the case for production speed and dry weight (see below). Other variations like inlet moisture, leakage air, or amount of condensate in the cylinders can be very difficult to measure, and can only be reduced by feedback. Variations in dryer performance due to conditions of dryer fabrics can be considered as constant since this is a slowly degrading process, unless it is unevenly distributed on the fabric.
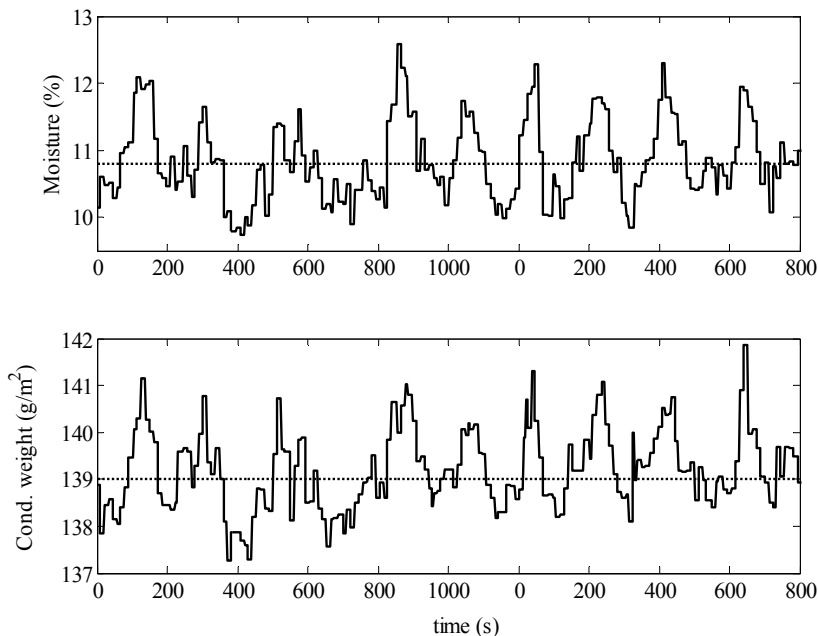
Figure 2.15 A case study from a fluting machine. At a first inspection it was found that there was a very large moisture variation with a period time of two minutes and the steam control system was thoroughly examined to find the cause. Later it turned out that the source of the disturbance was a large variation in dry weight and since the drying demand is correlated with the amount of fibers, the moisture is also affected. The set points are indicated with dotted lines.
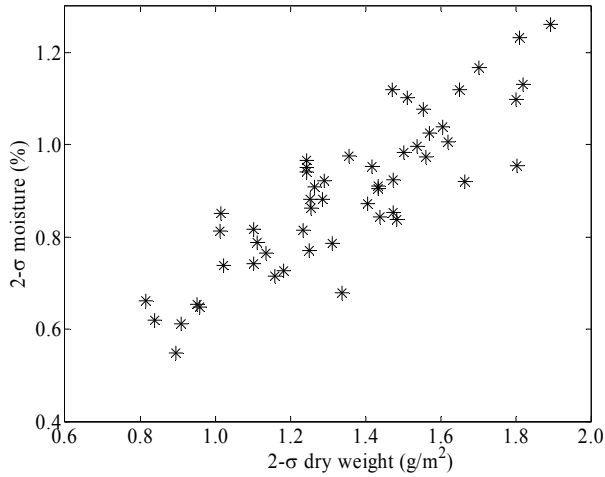
Figure 2.16 Each '*' corresponds to the mean value of a 30 minute sample from the machine in Figure 2.15. It clearly shows the strong correlation between variations in weight and moisture.
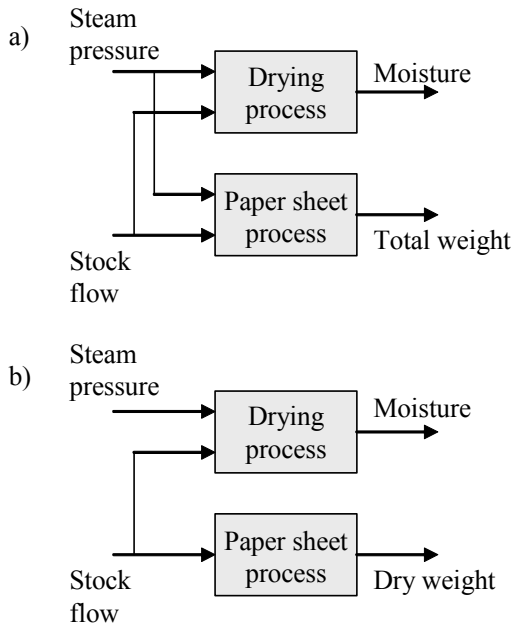
Figure 2.17 There are cross-connections between both steam pressure − total weight and stock flow − moisture (a), but one of these is easily eliminated by using dry weight as a controlled variable (b).

Apart from moisture, basis weight is also measured at the reel and controlled by using the stock flow as the manipulated variable (this is the conventional configuration, there exist others where also the machine speed is included). The total weight is naturally affected by the amount of water in the web. However, this coupling is eliminated by instead controlling the dry weight and leaving only the cross-coupling stock-moisture behind, see Figure 2.17. Since the moisture is measured, the amount of water is easy to deduct from the total weight measurement.

As a matter of curiosity, it can be mentioned that one of the first paper companies to use digital computers to control one of their machines was Billerud AB in Sweden [Åström, 1967] and [Åström, 2000a]. This was in the middle of the 1960's, and the system was an IBM 1710 with a CPU running at 100 kHz and 80 kB of memory. The system had a special real time operating system, written as a part of the installation project. All control was done in a supervisory mode, the digital computer provided set points to the analog system and it was based on stochastic control theory. The history of process control in relation to the development of computers is overviewed in [Balchen, 1999].

2.4 Disturbances in the drying section

It is important to have a good knowledge of the distribution of disturbances in the drying section when evaluating different tuning methods and control structures. By estimating an ARMAX model for closed loop data, a noise model is obtained together with a process model. Figure 2.18 illustrates an example of the power spectrum for the noise in steam pressure and moisture, taken from a fine paper machine. In Figure 2.19, a part of the corresponding time series is given, where the effect of the controller is removed. It can be seen that there is an apparent difference in frequency content between the two variables.

The steam pressure shows low frequency variations and a frequency peak at 0.1 Hz. The cut off frequency for the moisture is a decade lower (around 0.01 Hz) and there is small frequency peak at 0.003 Hz. Figure 2.18 will be used in different chapters throughout the thesis when analyzing different aspects of the control of both steam pressure and sheet moisture.
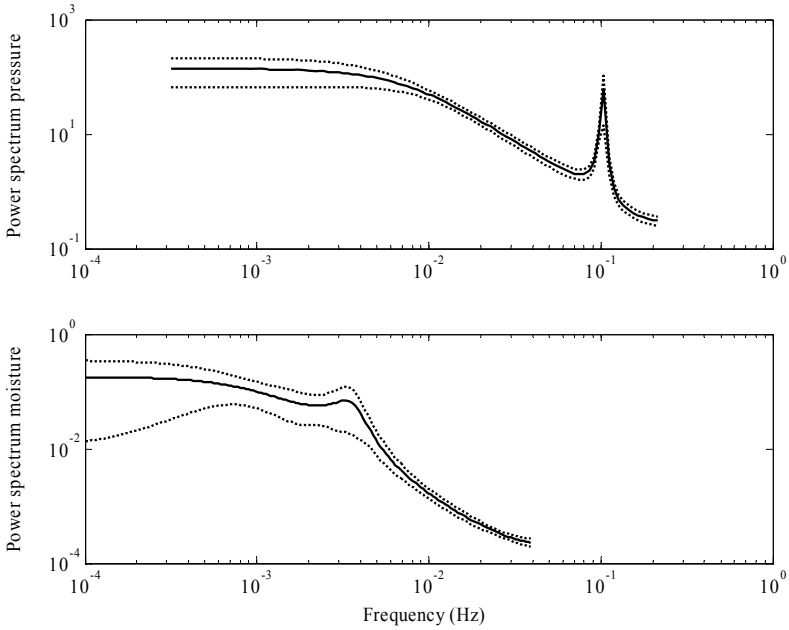
Figure 2.18 Power spectrum for steam pressure (above) and sheet moisture (below), from a fine paper machine. The dotted lines indicate the 95 % confidence interval.
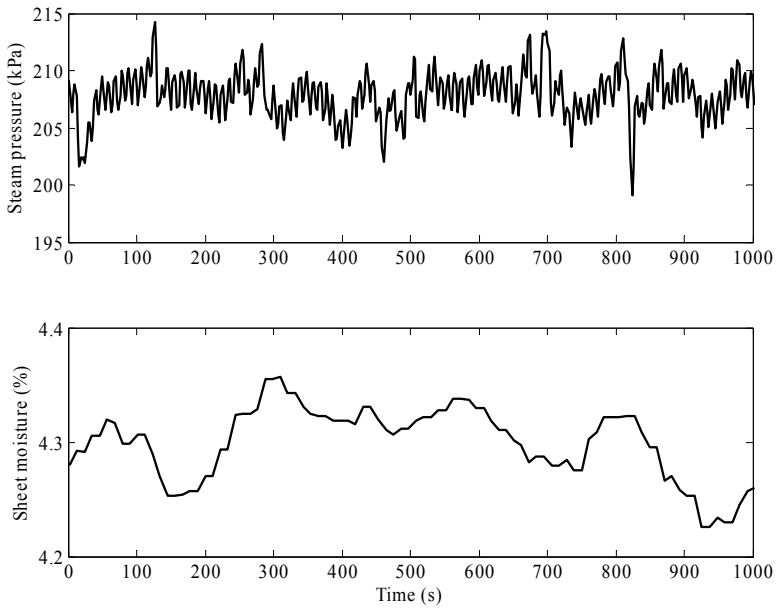
Figure 2.19 Time series for the steam pressure and moisture, used for spectrum estimations.

39

2.5 A note on the choice of units

Moisture

There exist two alternatives to express the amount of moisture in the sheet. Which one is used depends on the context. Books and articles treating control of the sheet moisture use moisture content, defined as

$$w = \frac{100 m_{wc}}{m_{wc} + m_{ds}} \quad [\%] \tag{2.2}$$

where m_{wc} is the mass of the water content in the sheet and m_{ds} is the mass of dry solids. This is the quantity used by most control system vendors and also by staff at the mills.

Alternatively, the amount of moisture can also be expressed as moisture ratio, defined as

$$u = \frac{m_{wc}}{m_{ds}} \quad [\text{kg/kg}] \tag{2.3}$$

Moisture ratio is often used in chemical engineering and literature on physical modeling of paper drying. The relation between the two quantities is

$$w = \frac{100u}{1+u}, \quad u = \frac{w}{100-w} \tag{2.4}$$

The advantage of the moisture ratio is the linearity and it better reflects variations of water content. A change in moisture content by 98 % − 99 % corresponds to a change of 50 kg water, while a change in moisture content by 8 % − 9 % corresponds to a change of 0.012 kg of water, see also Figure 2.20.

Throughout this thesis, moisture content is used in all figures and also in black-box models regarding sheet moisture. The reason for this choice is that the, by the author, expected target group for thesis, is much more familiar to that unit and different results will therefore be more prominent.

The exception for this choice is in Chapter 8 where instead moisture ratio is used in a few physical relations, since this simplifies them slightly.
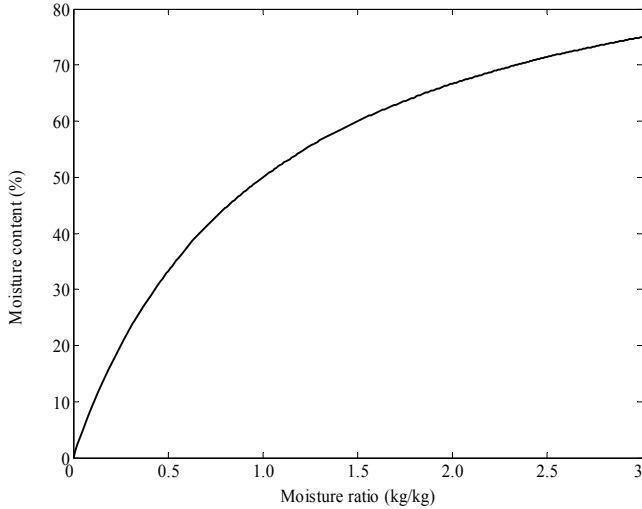
Figure 2.20 Relation between moisture content and moisture ratio.

However, it is clearly notified in those equations and the corresponding figures still show moisture content.

Pressure

All pressures are given in Pa. The value is always given in absolute pressure apart from a few exceptions where it is given in gauge pressure. It is then clearly notified. It is assumed that the absolute value is 101.325 kPa above the gauge pressure.

Temperature

Temperatures in formulas are given in K. In figures, temperatures are shown in °C for simple interpretation.

Part 1

Modeling and control of the steam and condensate system

Papermaking in the early 1900s, painted by Thomas M. Dietrich. It shows the wet end of the paper machine at the Fox River Paper mill in Appleton, Wisconsin. This painting illustrates the forerunner of the head box where stock is sprayed onto the wire. This man is adjusting valves in order to adjust the amount of stock sprayed. By courtesy of Fox Valley Corporation.

3

Black-box Models and Controller Structures

The pulp and paper industry is a highly competitive and capital-intensive market that is under increasing cost pressure. Customers are demanding lower costs, better terms of delivery, and higher product quality. To meet these requirements, much effort is spent on process modeling [Foss, *et al*, 1998]. The purpose of the models is varying. Some examples are (i) improved process understanding from experiments with "what-if" scenarios, (ii) identify the bottlenecks in a process and suggest modifications, (iii) creating process simulators for operator training, or (iv) improved control system design.

The word *model* is derived from the Latin *modus*, which means *a measure* [Bequette, 1998]. There are different classes of models and which class is best suited depends on the problem. Models can be divided into first-principles versus black-box (also known as statistical or empirical), or steady-state versus dynamical, or linear versus nonlinear, or continuous versus discrete, or lumped versus distributed.

In this thesis, preferably continuous-time dynamical models are used. They will be either black-box or first-principles, linear or nonlinear, and lumped or distributed. It all depends on the context.

This chapter introduces a linear black-box model structure for the steam pressure in a drying cylinder that is based on step response data. It

will be used to analyze the closed loop system for a few different controller structures. In the next chapter, a corresponding first-principles model is presented.

3.1 A black-box model structure − the IPZ transfer function

From experiments on a large number of different industrial paper machines, producing a whole range of different paper qualities, it has been found that a linear process model can describe the dynamics from the steam valve to the steam pressure. This model has an integrator, one pole, and one zero, therefore it is called the IPZ-model. This model structure has also been suggested in [Sell, 1995], and [Nelson and Gardner, 1996]. The IPZ-model is represented by the transfer function

$$G_{IPZ}(s) = k_v \frac{(1 + sT_1)}{s(1 + sT_2)} e^{-sL} \quad T_1 > T_2.\tag{3.1}$$
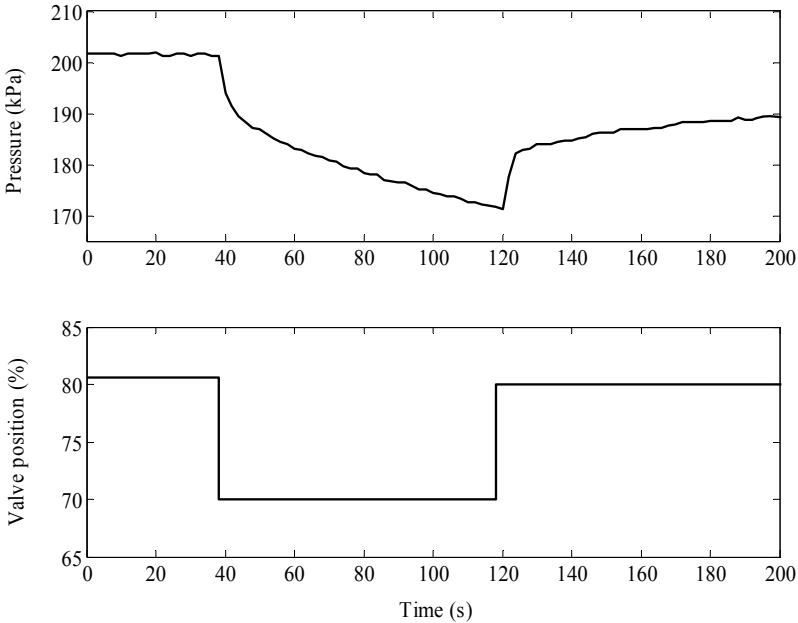
Figure 3.1 Open loop step response, taken from a liner machine. The response can be approximated by (3.1) with the process parameters k_v=0.0027, T_1=58, T_2=3.1, and L=2.0.

Note that T_1 is always larger than T_2, typically by a factor of 5 to 50. The transfer function can then be regarded as an integrator in series with a lead-network. This gives a characteristic open loop step response. It is different from most processes normally encountered in the process industry, which are often approximated by first order systems or pure integrators, possibly with a time delay. Figure 3.1 shows a step response from a liner machine. It is performed on the second of totally nine cylinder groups, which consisted of six dryer cylinders. The basis weight is 246 g/m^2 and the moisture content set point is 7.5 %.

Initially, the steam pressure makes a rapid decrease after the first step in the valve position, and then there is a distinct breakpoint in the curve with a significant change in pressure decrease rate. The same thing occurs at the second step in the control signal. This is the characteristic appearance of the IPZ-process.

[Stenström *et al*, 2002] indicates the physics behind this phenomenon. When the steam valve position is increased it will increase the pressure inside the cylinder, and consequently the saturation temperature of the steam and the condensation rate. However, the increasing condensation
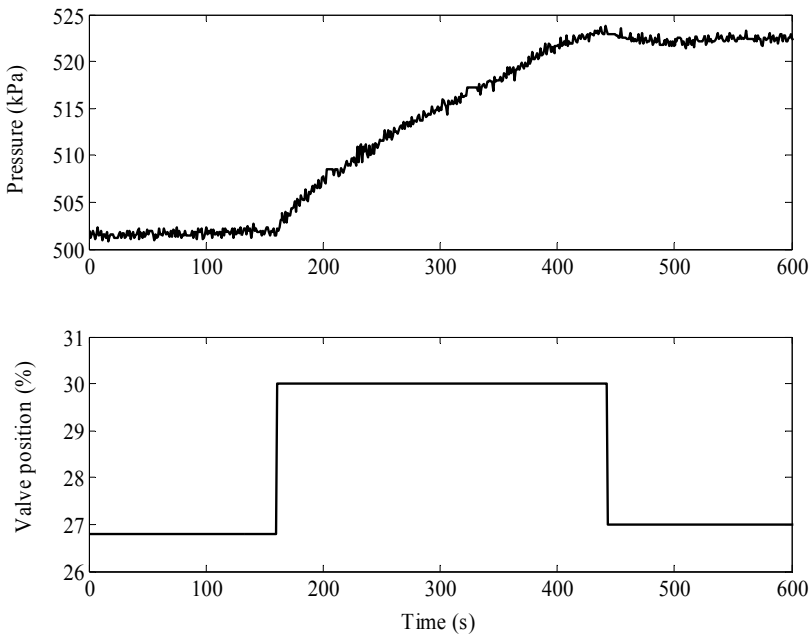
Figure 3.2 Open loop step response, taken from a board machine. The response can be approximated by (3.1) with the process parameters k_v=0.0020, T_1=73, T_2=21, and L=1.0.

rate lags behind the increasing steam inlet flow as the condensate layer heats up to the new steady state temperature. Therefore, there will be a fast initial build-up in steam pressure, before the steam consumption has reached its new value. This and many other physical properties in the drying section will be further analyzed in Chapter 8. As will be shown later, the integrator in (3.1) is an approximation of a real pole close to the origin.

In Figure 3.2, the effect of the integrator in the model structure is particularly apparent. The valve is first opened a small amount and then equally closed. When the control signal is put back to the original position, a new level of steady state pressure is reached. This is the same behavior as for the level in a tank when the influent or effluent is manipulated. In closed loop control, this implies that the controller output always returns to the original level in steady state, in absence of disturbances acting on the process.

To examine if the dimension of the cylinder has any impact on the model structure, a step response has been done on a Yankee dryer. These are mainly used for drying of tissue and have diameters up to 5.5 m
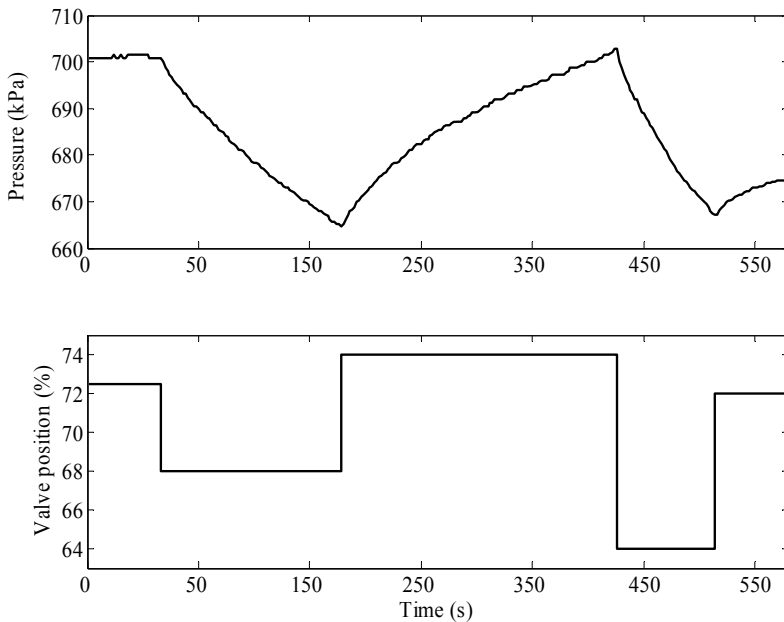
Figure 3.3 Open loop step response taken from a Yankee dryer. The model corresoinds to (3.1) with the process parameters k_v=0.0026, T_1=269, T_2=87, and L=2.0

[Karlsson, 2000]. This should be compared with multi-cylinder dryers, which normally are 1.5 or 1.8 m in diameter. The result is shown in Figure 3.3. It is not a big surprise that the response has an IPZ structure since the fundamental physical principles must be the same as in the case of a smaller cylinder. In Chapter 4, we will investigate how physical properties of the steam and dimensions of the cylinder will affect the parameters of the linear process model.

Graphical process identification from a step response

Even though there are a few commercial software tools for process identification (most DCS vendors have their own, suited for their specific control system), these are seldom systematized for identification of the IPZ-process or work preferably in discrete time. Exceptions are [Ljung, 2004] and [Wallén, 2000]. Therefore a graphical identification procedure for the IPZ model is helpful and it will now be illustrated how to obtain the four parameters, k_v, T_1, T_2, and L from a simple open loop step response.

Figure 3.4 shows a step response of an IPZ-model (3.1), where L is chosen to zero for simplicity. Start by drawing two straight lines, the
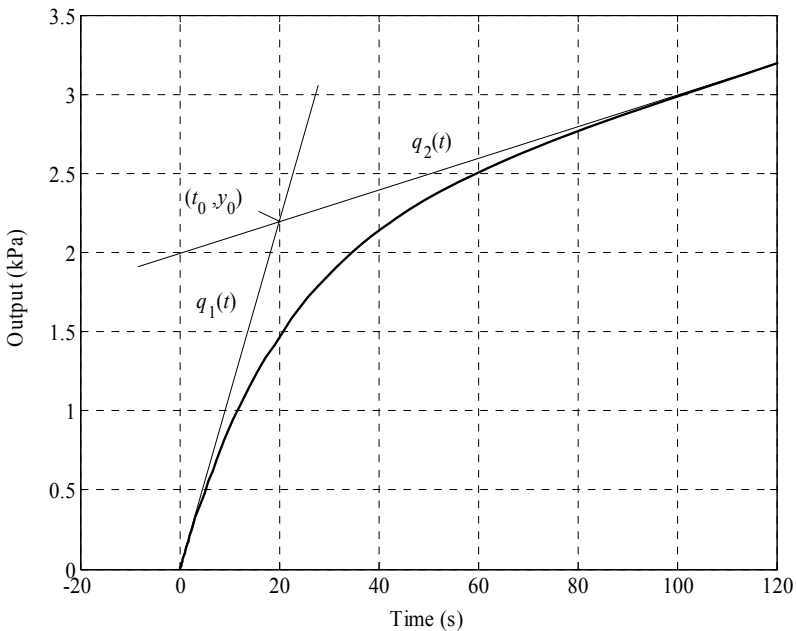
Figure 3.4 Simulated unit step response of an IPZ-process with k_v=0.01, T_1=220, T_2=20, and L=0.

tangent to the step response at time $t = 0$ (called $q_1(t)$) and the asymptote as time tends to infinity (called $q_2(t)$), both marked in the figure. Suppose that the size of the step in the control signal is u_0 and that the slope of $q_1(t)$ is k_1 and the slope of $q_2(t)$ is k_2. Also, suppose that the two lines intersect at the coordinates (t_0, y_0). Then we have

$$k_v = \frac{k_2}{u_0}, \quad T_1 = \frac{y_0}{k_2}, \quad T_2 = t_0. \tag{3.2}$$

The time delay L is obtained in a standard fashion as the time that elapses between the time when the controller output is changed and the time at which the response of the process output begins.

To derive the expressions in (3.2), start by denoting the step response by $y(t)$. To get the final slope of the step response (which also is the steady state value of the impulse response), we use the final value theorem

$$k_2 = \lim_{t \to \infty} \frac{dy(t)}{dt} = \lim_{s \to 0} s^2 G(s) \frac{u_0}{s} = \lim_{s \to 0} \frac{k_v(1 + sT_1)}{(1 + sT_2)} u_0 = k_v u_0 \tag{3.3}$$

By the initial value theorem, the initial derivative is

$$k_1 = \left. \frac{dy(t)}{dt} \right|_{t=0} = \lim_{t \to 0} \frac{dy(t)}{dt} = \lim_{s \to \infty} s^2 G(s) \frac{u_0}{s} = \lim_{s \to \infty} \frac{k_v(1 + sT_1)}{(1 + sT_2)} u_0 = \frac{k_v T_1}{T_2} u_0. \tag{3.4}$$

Thus the tangent of $y(t)$ at $t = 0$ is

$$q_1(t) = \frac{k_v T_1 u_0}{T_2} t, \tag{3.5}$$

since the response starts in the origin. By the inverse Laplace transform, the step response can also be written as

$$y(t) = k_v u_0 \left((T_1 - T_2)(1 - e^{-t/T_2}) + t \right), \tag{3.6}$$

and to get the equation for the asymptote of the step response we observe that

$$\lim_{t \to \infty}\left(y(t) - k_v u_0 t\right) = k_v u_0\left(T_1 - T_2\right),\qquad(3.7)$$

which is the value of $q_2(0)$. Consequently, we have

$$q_2(t) = k_v u_0\left(t + T_1 - T_2\right),\qquad(3.8)$$

and the two lines $q_1(t)$ and $q_2(t)$ intersect at $t = T_2$, since

$$q_1(T_2) = q_2(T_2) = k_v T_1 u_0.\qquad(3.9)$$

A note on the identification procedure

When doing graphical identification of a step response of a steam cylinder process, it has often been observed that the individual parameters may vary between different experiments on the same cylinder process while the products $k_v T_1$ and $k_v T_1/T_2$ are more or less constant. This is probably due to difficulties with finding the slope of the asymptote q_2, see Figure 3.4. If the effect from the low-pass filter part with time constant T_2 has not vanished from the response, the final slope is hard to acquire and the identified value will depend the length of the response.

By analyzing the sensitivity of the parameter estimation, given in (3.2), the observation can be verified analytically. Let the two lines in Figure 3.4 be given by

$$q_1(t) = k_1 t, \quad q_2(t) = k_2 t + y_2.\qquad(3.10)$$

The intersection of the two lines is the given by

$$y_0 = k_1 t_0, \quad y_0 = k_2 t_0 + y_2,\qquad(3.11)$$

which can be rewritten as

$$y_0 = \frac{k_1}{k_1 - k_2}\, y_2, \quad t_0 = \frac{1}{k_1 - k_2}\, y_2.\qquad(3.12)$$

We also have

$$k_v = \frac{k_2}{u_0}, \quad T_1 = \frac{k_1 y_2}{(k_1 - k_2)k_2}, \quad T_2 = \frac{y_2}{k_1 - k_2},\qquad(3.13)$$

and

$$E_1 = k_v T_1 = \frac{k_1 y_2}{(k_1 - k_2) u_0}, \quad E_2 = \frac{k_v T_1}{T_2} = \frac{k_1}{u_0}, \tag{3.14}$$

where E_1 and E_2 are the two expressions of interest. Assume an error in k_2, and differentiate T_1 with respect to k_2.

$$\frac{dT_1}{dk_2} = -\frac{k_1 y_2 (k_1 - 2k_2)}{(k_1 - k_2)^2 k_2^2}, \tag{3.15}$$

and rewrite as a relative error

$$\frac{dT_1}{T_1} = -\frac{k_1 - 2k_2}{k_1 - k_2} \frac{dk_2}{k_2} \tag{3.16}$$

Similar calculations for the other parts of (3.13) gives

$$\frac{dk_v}{k_v} = \frac{dk_2}{k_2}, \quad \frac{dE_1}{E_1} = \frac{k_2}{k_1 - k_2} \frac{dk_2}{k_2}, \quad \frac{dE_2}{dk_2} = 0. \tag{3.17}$$

The first thing to notice is that E_2 is independent of the slope k_2, so it is therefore obvious that $k_v T_1 / T_2$ tends to be independent of different experiments, if there is an uncertainty in k_2. Also, since, k_1 is larger than k_2, the relative error of E_1 is smaller than the relative errors of k_v and T_1. Consequently the observation is confirmed. It is also clear from (3.5) that $k_v T_1 / T_2$ is independent of line q_2.

The product $k_v T_1$ can be interpreted as follows. Rewrite (3.1) as

$$G_{IPZ}(s)\big|_{T_2 = 0} = \left(\frac{k_v}{s} + k_v T_1 \right) e^{-sL} \tag{3.18}$$

The step response of this function is shown in Figure 3.5. A constant product $k_v T_1$ is equal to a constant initial height in the response. If the identification procedure tends to get a good estimate of the height but a slightly altered k_v, this will give a small variation in T_1 too. It is not only short durations of the step response that can cause this difficulty. As we will see later, long durations have the same effect due to the
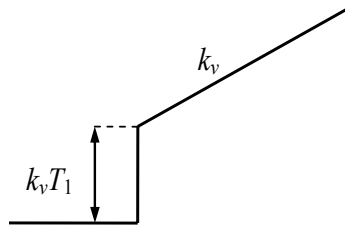
Figure 3.5 A unit step response of the IPZ process, if the low-pass filtering part is removed or equivalently $T_2 \equiv 0$.

approximation done when the slow time constant is assumed to be an integrator.

3.2 PID control of the steam pressure

It is probably fair to say that in today's paper machine control systems, the standard PI or PID controller is the most frequent controller element used to regulate the steam pressure. In general, more than 95% of the control loops in process industry are of PID type [Åström and Hägglund, 2005]. The advantage of PID control is that its function is easy to understand, even for people without knowledge in control theory. It is also possible to tune it, at least with an acceptable performance, without having any process model (you need to know the direction of the process response though). The PID controller can be found in all major DCS systems, sometimes with more advanced features like auto-tuning, gain scheduling, and loop performance analysis.

The PID controller, in ideal form, can be written as

$$u_c(t) = k_c\big(\beta r(t) - y(t)\big) + \frac{k_c}{T_i}\int_0^t \big(r(\tau) - y(\tau)\big)d\tau + k_c T_d \frac{d}{dt}\big(\gamma r(t) - y(t)\big)$$

$$(3.19)$$

where $u_c(t)$ is the control signal, $y(t)$ is the process output, $r(t)$ is the set point, and k_c, T_i, T_d, β, and γ are controller parameters. Often the set point is not included in the derivative part ($\gamma = 0$) and there is also a first order filter on the derivative part. Written in the frequency domain using the Laplace operator, (3.19) becomes

$$C_{ff} = k_c\left(\beta + \frac{1}{T_i s} + \gamma T_d s\right), \quad C_c = k_c\left(1 + \frac{1}{T_i s} + T_d s\right), \qquad (3.20a)$$
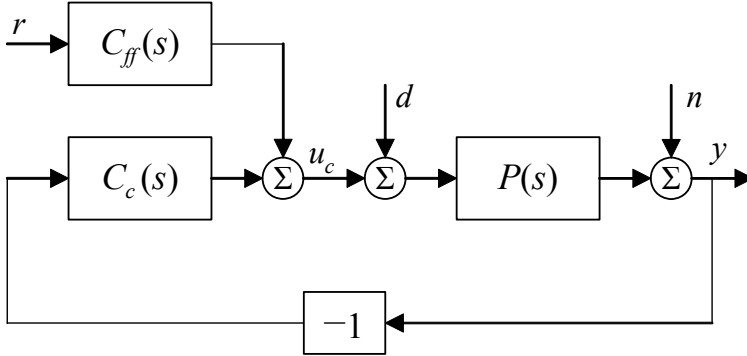
Figure 3.6 Block diagram of the PID-controller used in this thesis, together with the process. r is the set point, u_c the control signal, y the measurement, d a load disturbance, and n measurement noise.

where C_{ff} and C_c are transfer functions, defined by the block diagram in Figure 3.6. A low-pass filter added to the derivative part gives

$$C_{ff}(s) = k_c\left(\beta + \frac{1}{T_i s} + \frac{\gamma T_d s}{1 + \frac{T_d}{N}s}\right), \quad C_c(s) = k_c\left(1 + \frac{1}{T_i s} + \frac{T_d s}{1 + \frac{T_d}{N}s}\right),$$

(3.20b)

where $N = 2-20$ [Åström and Hägglund, 2005]. The purpose of the filter is to attenuate the high frequency gain of the derivative part but it can also be regarded as an inherent part of the control design, like the other parameters in the controller [Isaksson and Graebe, 2002].

The closed loop behavior

The pressure loop is in cascade control with the moisture control, as noted before, and therefore its set point varies more or less continuously during normal operation. But it is not unusual that the steam pressure in the first dryer group is run with a constant set point, given by the operator, to avoid sheet picking, fibre rising, dusting, and other runnability problems caused by too rapid heating of the sheet. Figure 3.7 shows a typical behavior of the pressure when there is a step in the reference value. The step response has an overshoot, which turns out to be caused by the integral action in the controller. To see this, let the
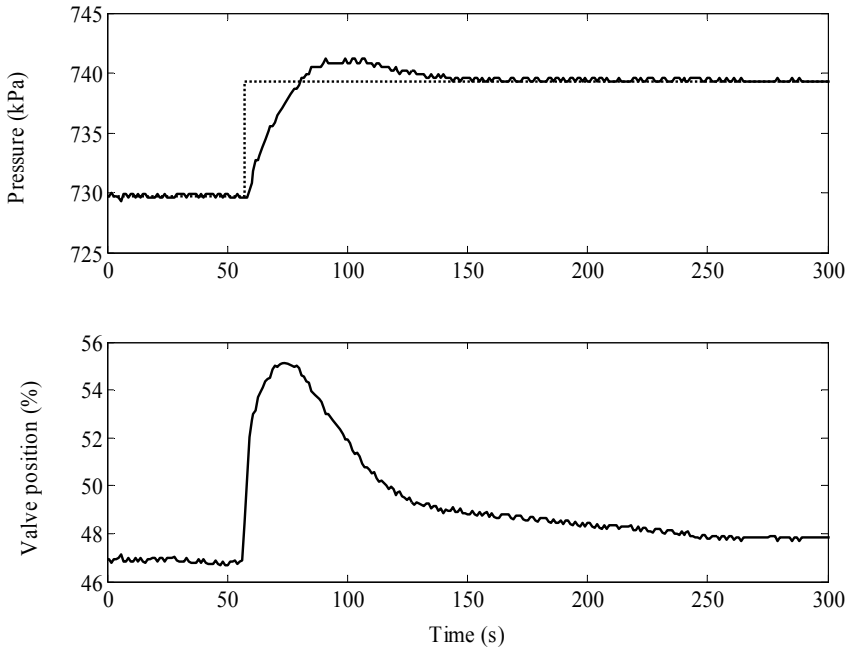
Figure 3.7 Typical closed loop step response of the pressure loop when using a PID controller, taken from a fluting machine.

controller be given by (3.20a). Now, assume that the process has an integrator. Write the process transfer function as

$$P(s) = \frac{1}{s}\hat{P}(s), \tag{3.21}$$

where

$$\hat{P}(0) \neq 0 \text{ and } \lim_{s \to 0} s\hat{P}(s) = 0, \tag{3.22}$$

and since

$$E(s) = R(s) - Y(s) = \left(1 - G_{ry}(s)\right)R(s) = G_{re}(s)R(s), \tag{3.23}$$

where $G_{ry}(s)$ is the transfer function from set point to process output and $G_{re}(s)$ is the transfer function from set point to control error, we can write the transfer function from set point to control error as

55

$$G_{re}(s) = 1 - G_{ry}(s) = 1 - \frac{k_c\left(\beta + \dfrac{1}{T_i s} + \gamma T_d s\right)\dfrac{1}{s}\hat{P}(s)}{1 + k_c\left(1 + \dfrac{1}{T_i s} + T_d s\right)\dfrac{1}{s}\hat{P}(s)}$$

$$= \frac{1 + k_c\left(1 + \dfrac{1}{T_i s} + T_d s\right)\dfrac{1}{s}\hat{P}(s) - k_c\left(\beta + \dfrac{1}{T_i s} + \gamma T_d s\right)\dfrac{1}{s}\hat{P}(s)}{1 + k_c\left(1 + \dfrac{1}{T_i s} + T_d s\right)\dfrac{1}{s}\hat{P}(s)}$$

$$= \frac{T_i s^2 + k_c\left(T_i s + 1 + T_i T_d s^2\right)\hat{P}(s) - k_c\left(\beta T_i s + 1 + \gamma T_i T_d s^2\right)\hat{P}(s)}{T_i s^2 + k_c(T_i s + 1 + T_i T_d s^2)\hat{P}(s)}$$

$$= \frac{T_i s^2 + \left(1 - \beta + (1-\gamma)T_d s\right)\hat{P}(s)k_c T_i s}{T_i s^2 + k_c(T_i s + 1 + T_i T_d s^2)\hat{P}(s)}.$$

$$(3.24)$$

Now let us study the integral of the controller error as time goes to infinity and the set point is a step.

$$\int_0^\infty e(t)dt = \lim_{s\to 0} s \cdot \frac{1}{s^2} G_{re}(s)$$

$$(3.25)$$

$$= \lim_{s\to 0} \frac{T_i s + \left(1 - \beta + (1-\gamma)T_d s\right)\hat{P}(s)k_c T_i}{T_i s^2 + k_c(T_i s + 1 + T_i T_d s^2)\hat{P}(s)} = (1 - \beta)T_i.$$

In the classical case, when $\beta = 1$, the integral of the control error is zero. This implies that there must be an overshoot in the set point step response to compensate the initial positive area in the time plot. We can also conclude that $\beta > 1$ will give an overshoot in the step response since the integral has a negative value. The range of β is normally defined as

$$0 \le \beta \le 1,$$

$$(3.26)$$
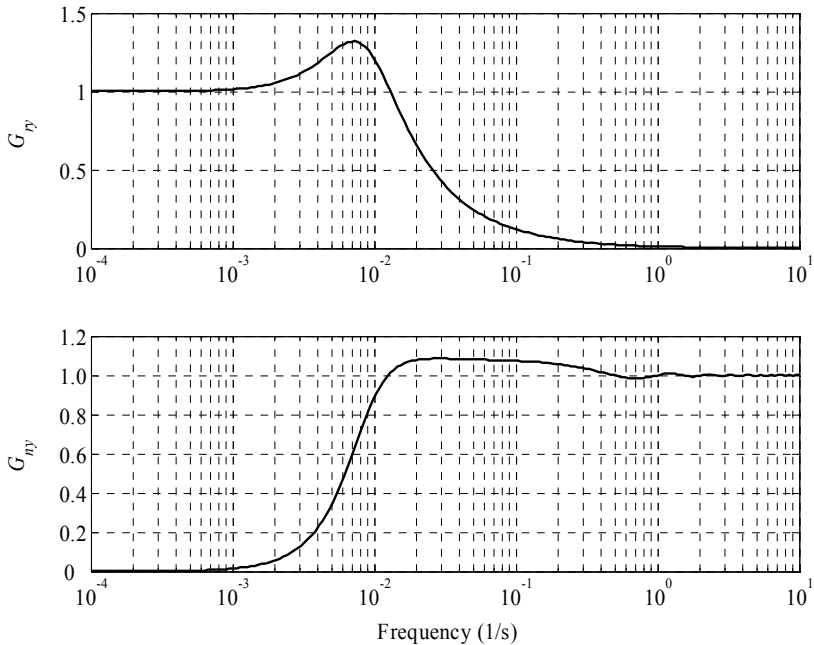
Figure 3.8 Frequency response from set point to output (above) and frequency response from noise to output (below) for the closed loop system in Figure 3.7, when governed by a PID-controller.

and extensive simulation results have indicated that there will be an overshoot in this case too. Note that the integral error is independent of the controller gain, k_c, in (3.25).

Figure 3.8 shows two closed loop frequency plots for the process in Figure 3.7. G_{ry} is the response from set point r to output y. G_{ny} is the response from noise n to output y (the sensitivity function) and has implications for the robustness as will be discussed later. An interesting observation is the resonance peak in G_{ry}, showing how some frequencies are amplified by the controller. This is obviously an undesired feature and problems might occur if all steam pressure loops amplify r in the same frequency region. In practice it has been observed that often the pressure variations in the steam and condensate system are in that specific frequency region, possibly because of this response amplification. We will now show how this peak can be avoided by having controllers with more degrees of freedom than the standard PID.

3.3 Improved set point response by feedforward

Normally feedforward is introduced as a method to reduce the impact of measurable disturbances. However, it can also be used to improve set point responses, see [Åström and Wittenmark, 1997] and [Åström and Hägglund, 2005]. In fact, this has already been introduced for the PID controller in Section 3.2 with the set point weights β and γ. Here, we will have a more systematic treatment for a general controller but assume that the process is given by (3.1).

Assume that we have a controller structure as in Figure 3.9, also known as a two-degree-of-freedom controller. The transfer function from set point to process output is then

$$G_{ry} = \frac{P(CM_y + M_u)}{1 + PC} = M_y + \frac{PM_u - M_y}{1 + PC}, \qquad (3.27)$$

where M_y is the desired response from r to y. The condition for ideal feedforward is

$$M_u = P^{-1}M_y. \qquad (3.28)$$

If we require that M_u is realizable, M_y should have a time delay that is equal to or larger than the time delay of the process and the pole excess of M_y should be at least as large as the pole excess of P. In addition, M_y should have the same zeros in the right half plane as P.
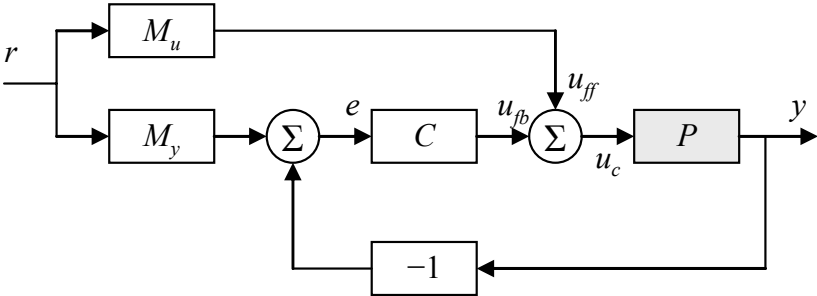
Figure 3.9 A two-degree-of-freedom controller (2DOF), where P is the process, C the controller, and M_u and M_y are feedforward filters. The advantage of this configuration is that the servo and regulation problems are separated.

Let P be given by the IPZ transfer function

$$P = k_v \frac{1 + sT_1}{s(1 + sT_2)} e^{-sL}, \tag{3.29}$$

and choose the desired set point response to

$$M_y = \frac{1}{1 + sT_{cl}} e^{-sL}, \tag{3.30}$$

then

$$
\begin{aligned}
M_u &= \frac{s(1 + sT_2)}{k_v(1 + sT_1)(1 + sT_{cl})} \\
&= \frac{T_2}{k_v T_{cl} T_1} + \frac{T_{cl} - T_2}{k_v T_{cl}(T_1 - T_{cl})} \frac{1}{(1 + sT_{cl})} - \frac{T_1 - T_2}{k_v T_1(T_1 - T_{cl})} \frac{1}{(1 + sT_1)},
\end{aligned} \tag{3.31}
$$

and u_{ff} can be generated as the output of the sum of a constant gain and two low pass filters. This is necessary if the DCS-systems have no component for high order filters or no possibility to implement the pure derivative. Observe that the calculations made above are independent of the feedback controller C. Under ideal conditions, the control signal u_{fb} remains constant during a set point change and the purpose of C is simply
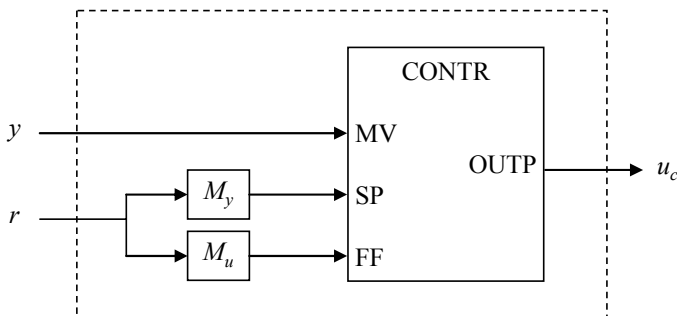
Figure 3.10 Implementation of the feedforward structure in Figure 3.9 in a DCS system. To let the operator manipulate the correct set point, the objects should be grouped together and presented as one controller element in the operator station, as indicated by the dashed line.

to give good disturbance rejection and robustness. In reality, there will be a control error during a set point change due to modeling errors which the feedback loop takes care of by driving e to zero. Figure 3.10 shows how the feedforward part could be implemented in an industrial control system to make use of its anti-windup, bumpless transfer, and other functions. Observe that normally there is a pure time delay in M_y, which also should be implementable in the control system.

How should T_{cl} be chosen? Looking at the shape of the control signal gives a hint. The transfer function from set point to control signal is

$$G_{ru} = M_u = \frac{s}{k_v(1+sT_1)} \frac{(1+sT_2)}{(1+sT_{cl})}, \qquad (3.32)$$

and we have lead-network (low-pass filtered derivative) followed by a zero-pole-network. If $T_{cl} < T_2$, more lead action is added to the first lead-network, and $T_{cl} > T_2$ gives a low-pass filter. Observe that T_1 is always greater than T_2.
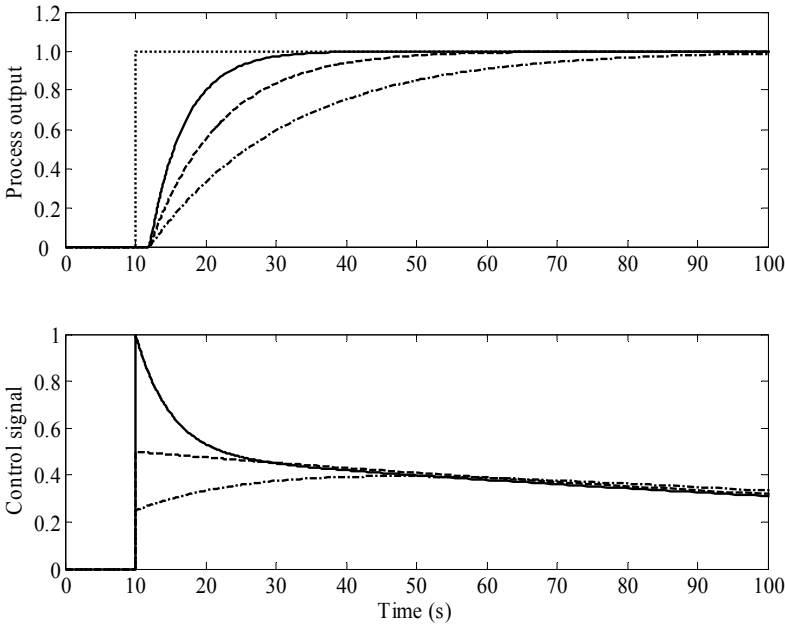
Figure 3.11 Set point step response of the 2DOF-controller. $T_{cl} = 5$ (solid), $T_{cl} = 10$ (dashed), and $T_{cl} = 20$ (dash-dotted). The dotted line is the set point.

If r is a unit step, the initial value theorem gives

$$u_c(0) = \frac{T_2}{k_v T_{cl} T_1}.$$

(3.33)

This can also be seen in the partial fraction expansion of M_u in (3.31). Figure 3.11 shows a simulation where the process is given by k_v=0.01, T_1=200, T_2=10, L=2. It clearly shows how the relation between T_{cl} and T_2 affects the shape of u_c. The selection of T_{cl} will be a trade-off between performance and control action, and letting $T_{cl} \geq T_2$ is a good choice.

Since there is an integrator in the process, the control signal will always go to zero in absence of disturbances. However, due to the cancellation of the slow process zero in $-1/T_1$ by (3.32), the control signal is slowly brought back to zero long after we have reached the set point. But the control signal must behave like this to maintain the output at the
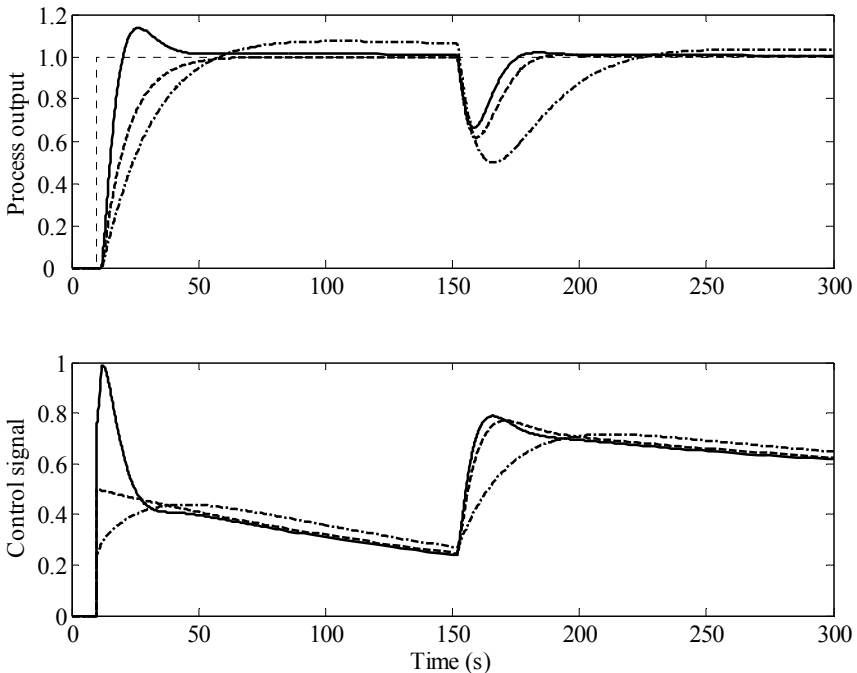
Figure 3.12 Dashed − 2DOF-controller T_{cl} = 10, solid − PI with aggressive tuning, and dash-dotted − PI with robust tuning. The thin dashed curve is the set point. Note that the 2DOF-controller cancels process dynamics from $r \rightarrow y$ but not from load disturbance d, therefore there is a slight overshoot when the disturbance acts on the system.
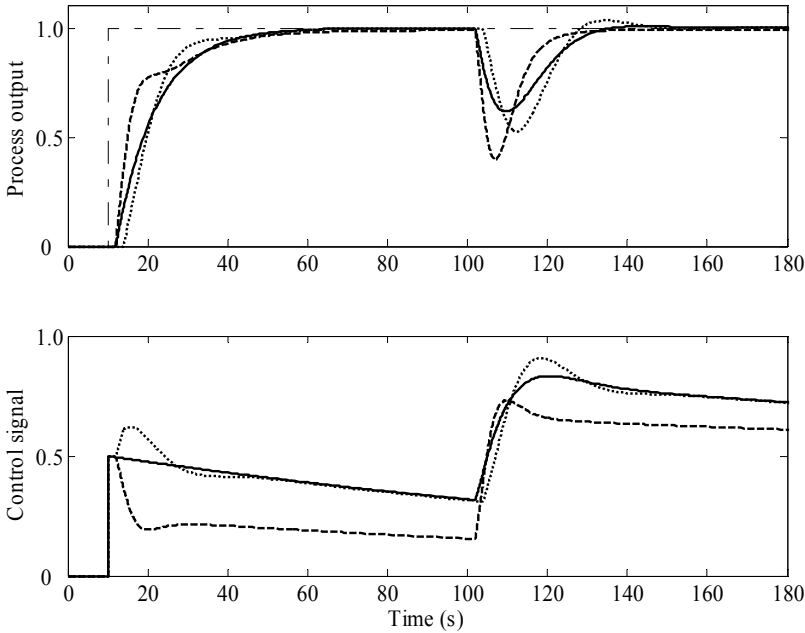
Figure 3.13 Robustness analysis to modeling errors of the 2DOF-controller. Perfect process model (solid), doubled time delay in process (dotted), and doubled process gain (dashed). The dash-dotted line is the set point.

desired value. The physical explanation is that the energy flow from the steam to the cylinder and paper is slowly increasing which implies that the steam consumption is slowly increasing. To compensate for this the controller must add extra steam to the cylinder long after the set point has been reached. Therefore, even though the set point has been reached the system has not reached steady-state, and the cylinder and paper temperatures are still increasing.

Figure 3.12 shows how a well-tuned PI controller behaves without the feedforward compared to the 2DOF-controller. What is meant by well tuned is obviously relative. The tuning method used for the PI controller is introduced in Chapter 5. The method has one user parameter that determines the robustness of the loop and two different settings are used in the figure, here denoted as aggressive and robust. The two settings are chosen to give both a faster and slower response compared to the 2DOF-controller. The 2DOF-controller gives a smoother performance in set point response. Since the transfer function from r to y is a first order system, the frequency response does not have a peak as in Figure 3.8, which is a nice feature of the 2DOF-controller structure. It is also an advantage that this structure is easy to implement into most commercial

DCS-systems, which is not the case for the controller structure presented in the following section.

Finally, the sensitivity to modeling errors is investigated. Figure 3.13 shows closed loop simulations where the time delay and gain in the process is increased by a factor two. The response in process output is no longer equal to the desired response in presence of modeling errors since the feedback loop is active, and the second term in (3.27) is not canceled by M_u. However, the control system proves to handle model errors well.

3.4 A state feedback controller

As we have shown, when the steam pressure is governed by a standard PID controller there will be an overshoot in the step response and a peak in the frequency response of the closed loop system from r to y. In the previous section, a feedforward filter was introduced which gives a closed loop response without this overshoot and peak. This is also possible to obtain by a state feedback controller as will be shown here. The zeros of the closed loop systems can not be positioned with state feedback but the poles can be located arbitrarily, which is sufficient to avoid the overshoot. Since a time delay in continuous time can not be represented by a finite number of poles and zeros, and the purpose here is merely to show the idea, the delay is assumed to be zero. In practice, the design should be done in the discrete time domain and the delay will then augment the transfer function with extra poles in the origin and possibly an extra zero.

Let the process be given by

$$G(s) = k_v \frac{sT_1 + 1}{s(sT_2 + 1)} = \frac{\dfrac{k_v T_1}{T_2} s + \dfrac{k_v}{T_2}}{s\left(s + \dfrac{1}{T_2}\right)} = \frac{b_1 s + b_2}{s(s + a_1)}. \tag{3.34}$$

Assume that the model is written in observable canonical form

$$\begin{cases} \dot{x}(t) = Ax(t) + Bu_c(t) = \begin{bmatrix} -a_1 & 1 \\ 0 & 0 \end{bmatrix} x(t) + \begin{bmatrix} b_1 \\ b_2 \end{bmatrix} u_c(t) \\ y(t) = Cx(t) = \begin{bmatrix} 1 & 0 \end{bmatrix} x(t) \end{cases} \tag{3.35}$$

By definition this system is observable. It is also controllable unless $T_1 = T_2$ which implies that we have a pure integrator instead of an IPZ process.

Let the state feedback be given by

$$u_c(t) = -Lx(t) + l_r r(t) = -\begin{bmatrix} l_1 & l_2 \end{bmatrix} x(t) + l_r r(t). \tag{3.36}$$

The closed loop system then becomes

$$\begin{cases} \dot{x}(t) = \begin{bmatrix} -a_1 - b_1 l_1 & 1 - b_1 l_2 \\ -b_2 l_1 & -b_2 l_2 \end{bmatrix} x(t) + l_r \begin{bmatrix} b_1 \\ b_2 \end{bmatrix} r(t) \\ y(t) = \begin{bmatrix} 1 & 0 \end{bmatrix} x(t) \end{cases}, \tag{3.37}$$

which in input-output form becomes

$$G_{ry}(s) = \frac{(b_1 s + b_2) l_r}{s^2 + (a_1 + b_1 l_1 + b_2 l_2)s + a_1 b_2 l_2 + b_2 l_1}. \tag{3.38}$$

By choosing

$$l_r = l_1 + a_1 l_2, \tag{3.39}$$

we get unit steady-state gain. If we choose to place the poles in λ_1 and λ_2, we get the equation system

$$\begin{bmatrix} b_1 & b_2 \\ b_2 & a_1 b_2 \end{bmatrix} \begin{bmatrix} l_1 \\ l_2 \end{bmatrix} = \begin{bmatrix} -\lambda_1 - \lambda_2 - a_1 \\ \lambda_1 \lambda_2 \end{bmatrix}. \tag{3.40}$$

Note that we have assumed that the two states of the system are measurable, which practically is unlikely. What is also needed then is a Kalman filter to estimate the states, which is feasible since the system is observable. However, since an observer will not affect the dynamics of the closed loop system from set point r to output y, except for initial transients in the estimation, it is adequate to consider simply the state feedback in this analysis.

A Simulation Example

Assume that we have the system

$$G(s) = 0.02 \frac{50s + 1}{s(10s + 1)} = \frac{0.1s + 0.002}{s^2 + 0.1s} = \frac{b_1 s + b_2}{s^2 + a_1 s}. \tag{3.41}$$

The open loop poles are in $p_1 = 0$ and $p_2 = -0.1$, and the zero is in $z = -0.02$. To examine a cancellation of the process zero, place one pole at $\lambda_1 = -0.2$, and let the other one be at $\lambda_2 = -0.04$, -0.02, and -0.01 (in three different simulations). In other words, we have one case where both closed loop poles are faster than the process zero, one case where one pole cancels the zero, and finally one case where one pole is slower than the zero.

The controller parameters can then be calculated as

$$l_1 = 1.25 + 12.5\lambda_2,$$
$$l_2 = -12.5 - 1125\lambda_2, \tag{3.42}$$
$$l_r = -100\lambda_2.$$

Figure 3.14 shows the simulation results. We can see that when both poles are faster than the process zero we get an over-shoot due to the lead action of the zero (which is closer to the origin). When $\lambda_2 = -0.02$, we cancel the zero and get a first order response. In this case, the performance of the system is given only by the position of the other pole. Finally, we let $\lambda_2 = -0.01$, and the closed loop system has one fast and one slow pole. The slow pole is clearly visible in the step response.

Adding Integral Action

The feedback loop in Figure 3.14 has one drawback. In presence of disturbances, there will be a steady state error in the output. By introducing integral action, the asymptotic error becomes zero. This can be accomplished by augmenting the system with an extra state, called x_3

$$\dot{x}_3 = r - y = r - Cx. \tag{3.43}$$

The new system can then be written as
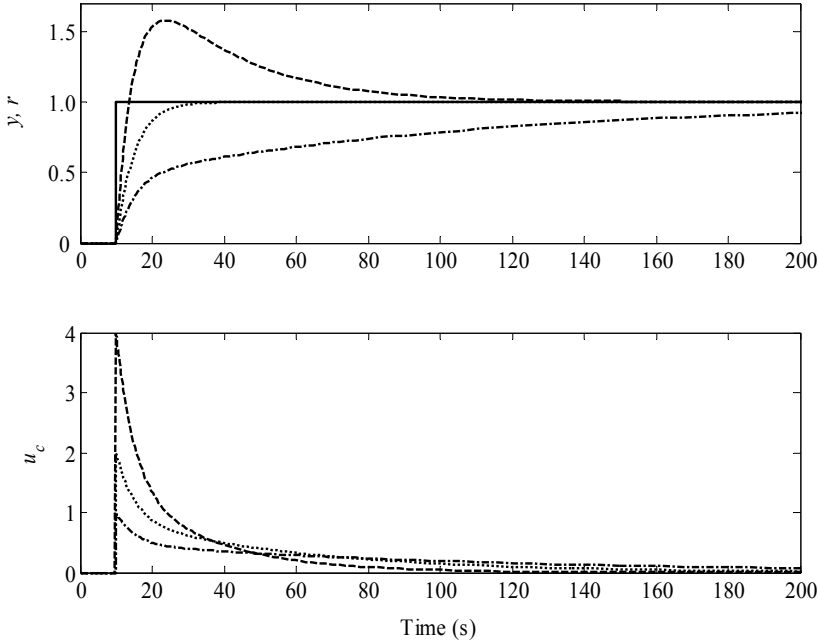
Figure 3.14 Simulation of the three different cases of state feedback. Set point (solid), λ_2 = −0.04 (dashed), λ_2 = −0.02 (dotted), and λ_2 = −0.01 (dash-dotted).

$$
\begin{bmatrix} \dot{x}_1 \\ \dot{x}_2 \\ \dot{x}_3 \end{bmatrix} = \begin{bmatrix} -a_1 & 1 & 0 \\ 0 & 0 & 0 \\ -1 & 0 & 0 \end{bmatrix} \begin{bmatrix} x_1 \\ x_2 \\ x_3 \end{bmatrix} + \begin{bmatrix} b_1 \\ b_2 \\ 0 \end{bmatrix} u_c + \begin{bmatrix} 0 \\ 0 \\ 1 \end{bmatrix} r.
\tag{3.44}
$$

This augmented system is also controllable from u_c unless $T_1 = T_2$. By using the standard state feedback law

$$
u_c = -Lx - l_3 x_3,
\tag{3.45}
$$

we get the following closed loop system

$$
\begin{bmatrix} \dot{x}_1 \\ \dot{x}_2 \\ \dot{x}_3 \end{bmatrix} = \begin{bmatrix} -a_1 - b_1 l_1 & 1 - b_1 l_2 & -b_1 l_3 \\ -b_2 l_1 & -b_2 l_2 & -b_2 l_3 \\ -1 & 0 & 0 \end{bmatrix} \begin{bmatrix} x_1 \\ x_2 \\ x_3 \end{bmatrix} + \begin{bmatrix} 0 \\ 0 \\ 1 \end{bmatrix} r,
\tag{3.46}
$$
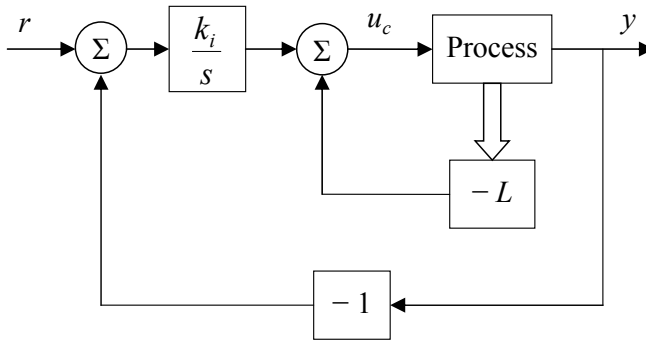
Figure 3.15 Adding integral action to a state feedback system

which has the transfer function

$$G_{ry}(s) = \frac{-l_3(b_2 + b_1 s)}{s^3 + (a_1 + b_1 l_1 + b_2 l_2)s^2 + (a_1 b_2 l_2 + b_2 l_1 - b_1 l_3)s - b_2 l_3}. \quad (3.47)$$

The new state, x_3, can be added by having an additional feedback loop as shown in Figure 3.15. The integrator gain, k_i, is then given by

$$k_i = -l_3. \quad (3.48)$$

A Simulation Example, Cont'd

We add an integrator to the state feedback controller and let one closed loop pole be placed in $\lambda = -0.02$ (cancellation) and a double pole in $\lambda = -0.2$. In other words, we want the characteristic equation to be given by

$$s^3 + 0.42s^2 + 0.048s + 0.0008 = 0, \quad (3.49)$$

and get the following system of equations

$$\begin{cases} a_1 + b_2 l_2 + b_1 l_1 = 0.42 \\ a_1 b_2 l_2 + b_2 l_1 - b_1 l_3 = 0.048 \\ -b_2 l_3 = 0.0008 \end{cases}, \quad (3.50)$$

which has the solution $l_1 = 3$, $l_2 = 10$ and $l_3 = -0.4$. Figure 3.16 shows the simulation result. Since there is an extra pole in the closed loop system
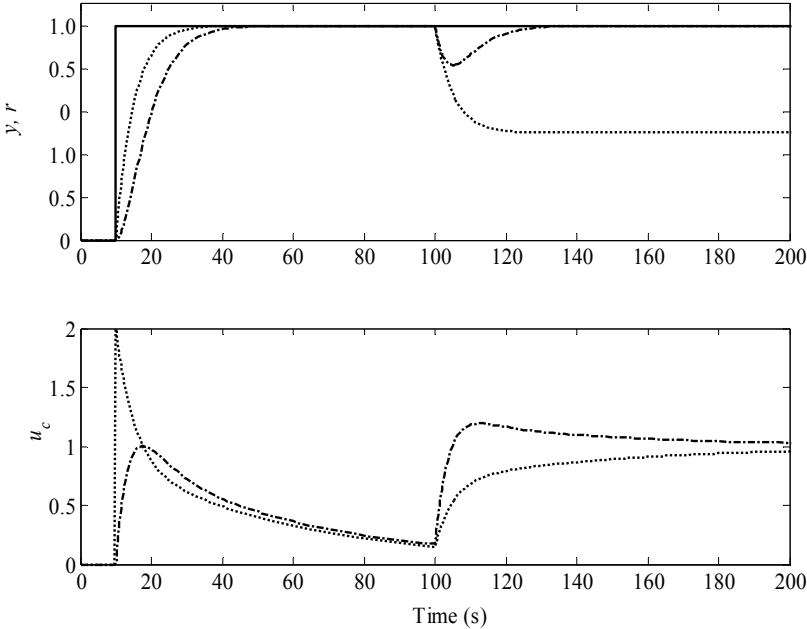
Figure 3.16 A simulation where a disturbance acts on the controller output for the case when there is a cancellation of the process zero. Without integral action in the controller (dotted − same as the dotted curve in Figure 3.14), and with integral action (dash-dotted). Observe that the dynamics are different in the two cases since the number of closed loop poles is different.

due to the integrator state, x_3, the dynamics of the set point step response is different from the system in (3.42).

A Remark

In Section 3.3 the overshoot in set point step response, as the standard PID-controller introduces, is eliminated by canceling process dynamics by feedforward. Here we have shown how the process zero can be cancelled by one of the closed loop poles introduced by feedback. By letting the remaining two poles (in the case of integral action in the controller) be real, we avoid both overshoot in the step response and resonance in the frequency response.

   The practical disadvantage with state feedback is that most commercial DCS do not have any support for this controller type. Instead, it must be implemented by the user together with features like windup protection, bumpless transfer, and bumpless parameter change.

3.5 A two-pole model of the steam pressure

Since the steam pressure in a cylinder group finally must reach some steady state value, the integrator in (3.1) is more likely to be a long time constant. This implies that the model does not capture the low frequency behavior well and this has been one of the criticisms against it. However, the purpose of the model is not simulation and the question is if its complexity is sufficient for a control design usage. With an extra pole, we get

$$G_{PPZ}(s) = k_p \frac{(1 + sT_1)}{(1 + sT_2)(1 + sT_3)} e^{-sL}, \quad T_3 > T_1 > T_2, \quad (3.51)$$

instead of (3.1). Here the integrator is replaced by a new pole close to the origin, and instead we call the model structure PPZ (pole-pole-zero). Since it in most practical cases is not desirable to let the steam pressure in an open loop step response reach steady state, because of the influence on the paper qualities, this slow pole can be difficult to identify graphically
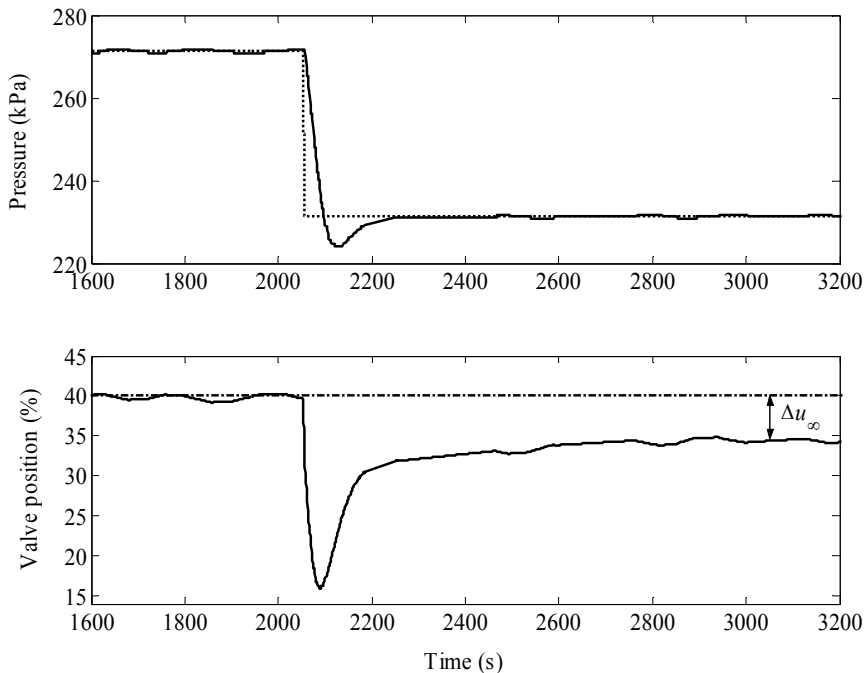
Figure 3.17 Closed loop step response. Taken from a liner machine.

from a single step. It can be identified from well excited closed or open loop data with system identification techniques for linear parametric models, such as the prediction-error methods, though.

In Figure 3.17 a closed loop step response from a steam group in a liner machine, consisting of 13 cylinders, is shown. We will now see that the fact that the control signal does not return to the same steady state value as before the step in the set point, exposes the PPZ-structure of the process.

Start by defining the change in control signal as time goes to infinity, and assume a step in the set point with size Δr

$$\Delta u_\infty \equiv u_0 - \lim_{t \to \infty} u_c(t) = u_0 - \lim_{s \to 0} s \cdot G_{ru}(s) \frac{\Delta r}{s} = u_0 - G_{ru}(0)\Delta r, \quad (3.52)$$

where $G_{ru}(s)$ is the transfer function from the set point r to the control signal u_c. Assume that the process dynamics are described by the IPZ-model given in (3.1). Also, assume that the controller is given by (3.20a). Then we have

$$G_{ru}(s) = \frac{G_{ff}(s)}{1 + G_c(s)G(s)} = \frac{k_c\left(\beta + \dfrac{1}{sT_i} + s\gamma T_d\right)}{1 + k_v k_c\left(1 + \dfrac{1}{T_i s} + T_d s\right)\dfrac{(sT_1 + 1)}{s(sT_2 + 1)}e^{-sL}} \quad (3.53)$$

$$= \frac{k_c s\left(s^2 \gamma T_i T_d + s\beta T_i + 1\right)(sT_2 + 1)}{s^2 T_i (sT_2 + 1) + k_v k_c\left(s^2 T_i T_d + sT_i + 1\right)(sT_1 + 1)e^{-sL}}.$$

The steady state value of the control signal is then

$$\Delta u_\infty = G_{ru}(0)\Delta r = 0, \quad (3.54)$$

and we can see that the final value of the control signal must be equal to zero. This is obviously because of the integrator in the process and it means that the control signal in Figure 3.17 should have returned to its original steady state value (to the level it had before the step in the set point). If we instead let the process be of PPZ-type, see (3.51), then the steady state value of the control signal will become

$$\frac{G_{ff}(0)}{1+G_c(0)G_{PPZ}(0)}\Delta r$$

$$= \left. \frac{k_c\left(1+s\beta T_i + s^2\gamma T_i T_d\right)\left(1+sT_2\right)\left(1+sT_3\right)\Delta r}{sT_i\left(1+sT_2\right)\left(1+sT_3\right)+k_c k_p\left(1+sT_i + s^2 T_i T_d\right)\left(1+sT_1\right)e^{-sL}}\right|_{s=0} = \frac{\Delta r}{k_p} \qquad (3.55)$$

and it depends of the process gain and the size of the step.

Normally, the difference between the PPZ- and the IPZ-model is only exposed in long time series. Figure 3.18 shows an example from a paper board machine (a group consisting of 12 cylinders) where almost two
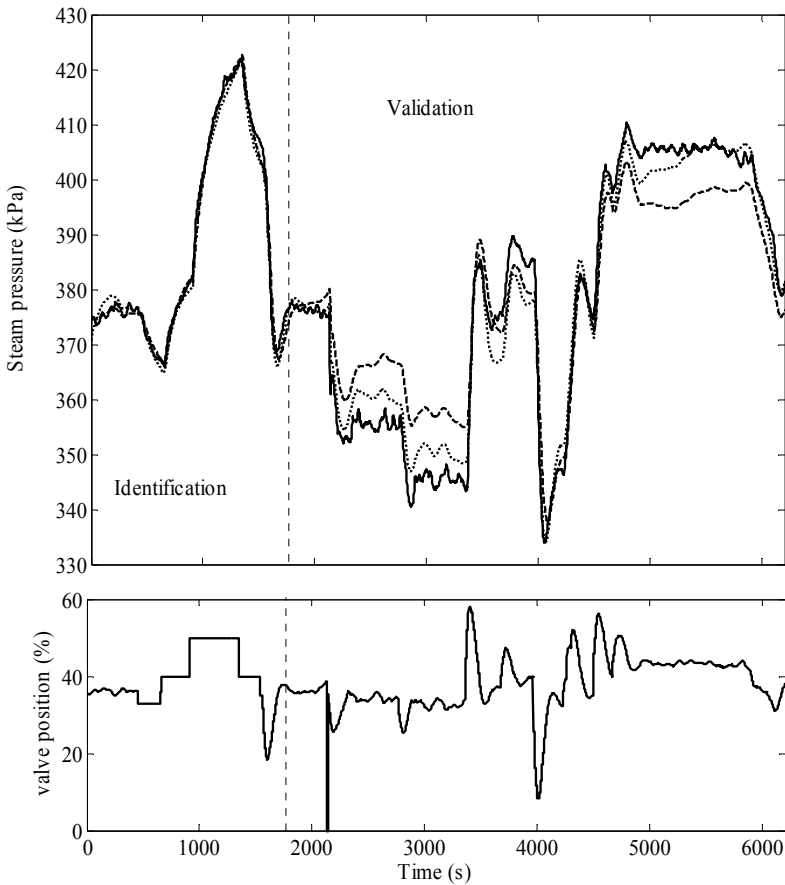
Figure 3.18 Model validation showing the difference between the IPZ (dashed) and the PPZ (dotted) process. Measurements taken from a board machine.

hours of logged data is used. Both an IPZ (dotted line) and a PPZ (dashed line) model have been identified and their simulations are plotted together with the measured value (solid line). The first part of the time series is used for identification (marked in the figure) and the second part is a pure simulation. The estimated PPZ model is

$$G_1(s) = 15.5 \frac{(1+291s)}{(1+797s)(1+74.2s)} e^{-2.83s} \qquad (3.56)$$

and the estimated IPZ model is

$$G_2(s) = 0.00421 \frac{(1+1896s)}{s(1+138s)} e^{-2.83s} \qquad (3.57)$$

The difference between the two models is apparent. The IPZ-model does not capture the low frequency component of the process as well as the PPZ-model does. By manipulating the parameters in the IPZ-model, the graphical fit can be improved in the validation part of the figure, to the other part's disadvantage.

The question that we posed in the beginning of this section was if the IPZ model is sufficient for control design purposes or do we need to use a PPZ model instead? To answer that question we start by quoting [Ljung, 1999]: "Feedback control is both forgiving and demanding in the sense that we can have good control even with a mediocre model, as long as it is reliable in certain frequency ranges. Loosely speaking, the model has to be reliable around the cross-over frequency ($\approx$ the bandwidth of the closed loop system), and it may be bad where the closed loop sensitivity function is small."

Figure 3.19 shows the open-loop Bode plot for the models in equation (3.56) and (3.57). Both in the magnitude and the phase plot, there is a large discrepancy for low frequencies but the disparity between the models is negligible in the high frequency region. Also around the cross-over frequency, the two different process models have similar appearance. This means that the IPZ-model is adequate and well suited for control design usage. We also note that compared to the PPZ-model, the IPZ-model in general has larger phase lag. Thus, we can, by using the IPZ-model for design, be sure to have a stable controller even if the process is of PPZ-type.
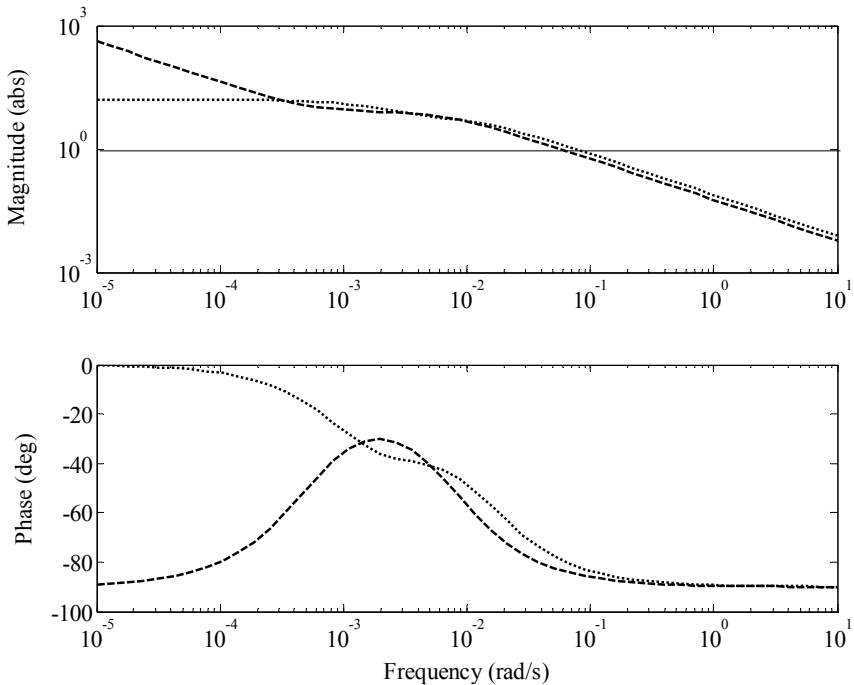
Figure 3.19 Bode plot for the IPZ (dashed) and PPZ (dotted) models.

We have previously referred to the identification issue and pointed out the advantage with the IPZ model. From an open loop step response it is simple to graphically obtain the parameters of the transfer function. Practically it is more difficult to get a good PPZ model since it has more parameters to identify.

   Let us finally regard another quotation that agrees with the conclusions we have already made. In [Ljung, 2004] it is indicated that a model validation as in Figure 3.18 in terms of a pure simulation, can portray a good model in an unpromising manner. "If the model is unstable, or has integration or very slow time constants, the levels of the simulated and the measured output may drift apart, even for a model that is quite good (at least for control purposes). It is then a good idea to evaluate the model's predicted output rather than the simulated one".

3.6 The differential pressure loop

The main objective in this thesis is to give a systematic treatment of the moisture control loop, shown in Figure 2.13. That involves a steam pressure process with a steam pressure controller, and a paper process with a moisture controller. But there is a third controller loop described in Section 2.2, the differential pressure, which here will be shortly analyzed.

It is easy to realize that there ought to be cross-connections between the pressure and differential pressure, since they are both acting on the same physical unit. We then have a two-input-two-output (TITO) system. To examine this, an experiment has been performed on a fine paper machine, see Figure 3.20. The processes are excited by step responses in the control valves, one loop at a time, see Figure 3.21. The model is found to be

$$
\begin{bmatrix} y_P \\ y_{dP} \end{bmatrix} = \begin{bmatrix} 0.186 \dfrac{29s+1}{s(1.9s+1)} e^{-1.7s} & 0 \\ 0.0395 \dfrac{122s+1}{s(2.3s+1)} e^{-2s} & 0.0029 \dfrac{343s+1}{s(3.1s+1)} e^{-2.6s} \end{bmatrix} \begin{bmatrix} u_P \\ u_{dP} \end{bmatrix} \quad (3.58)
$$
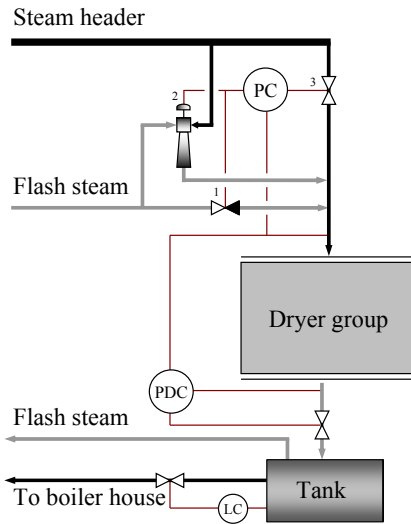
Figure 3.20 A P&ID of the dryer group where the TITO experiment was performed. The pressure controller PC primarily uses flash steam (from another group operating at higher pressure), secondly steam from the compressor, and thirdly live steam from the header.
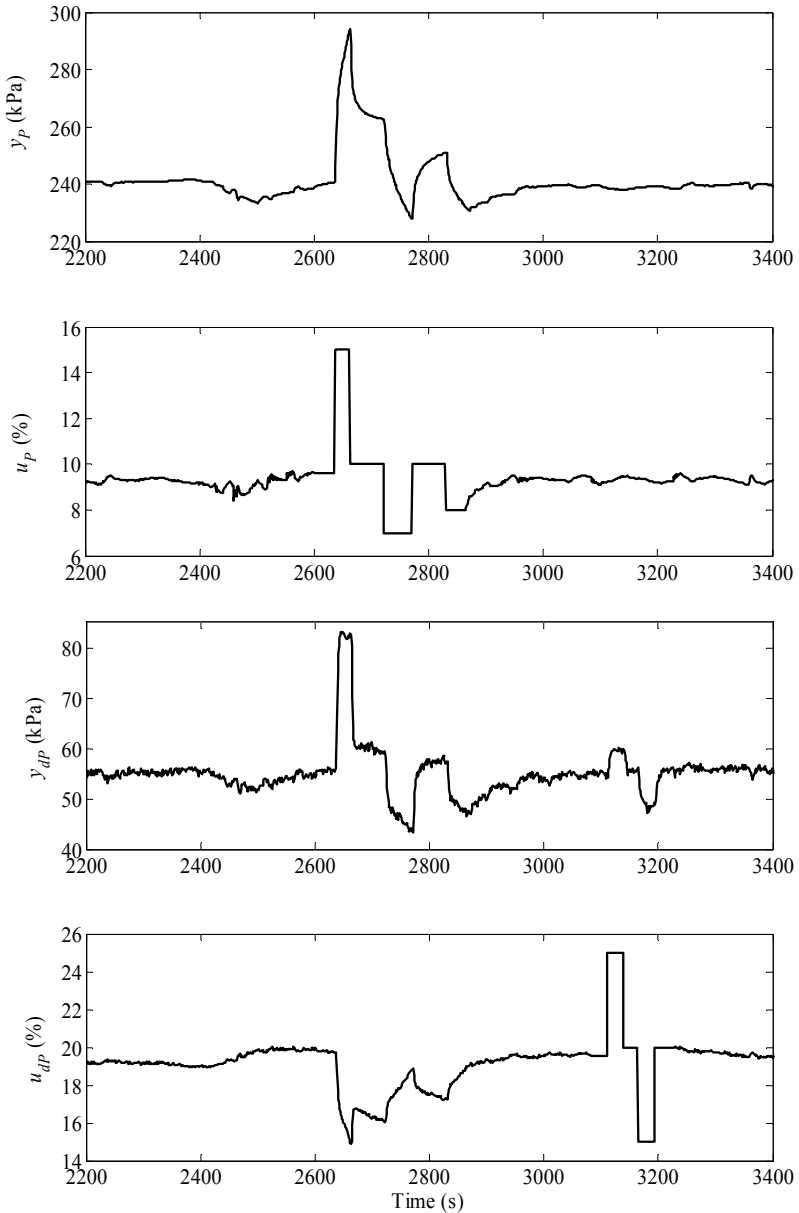
Figure 3.21 The step response experiment of the pressure and differential pressure loops. The identified model is given in (3.58). Taken from a fine paper machine.
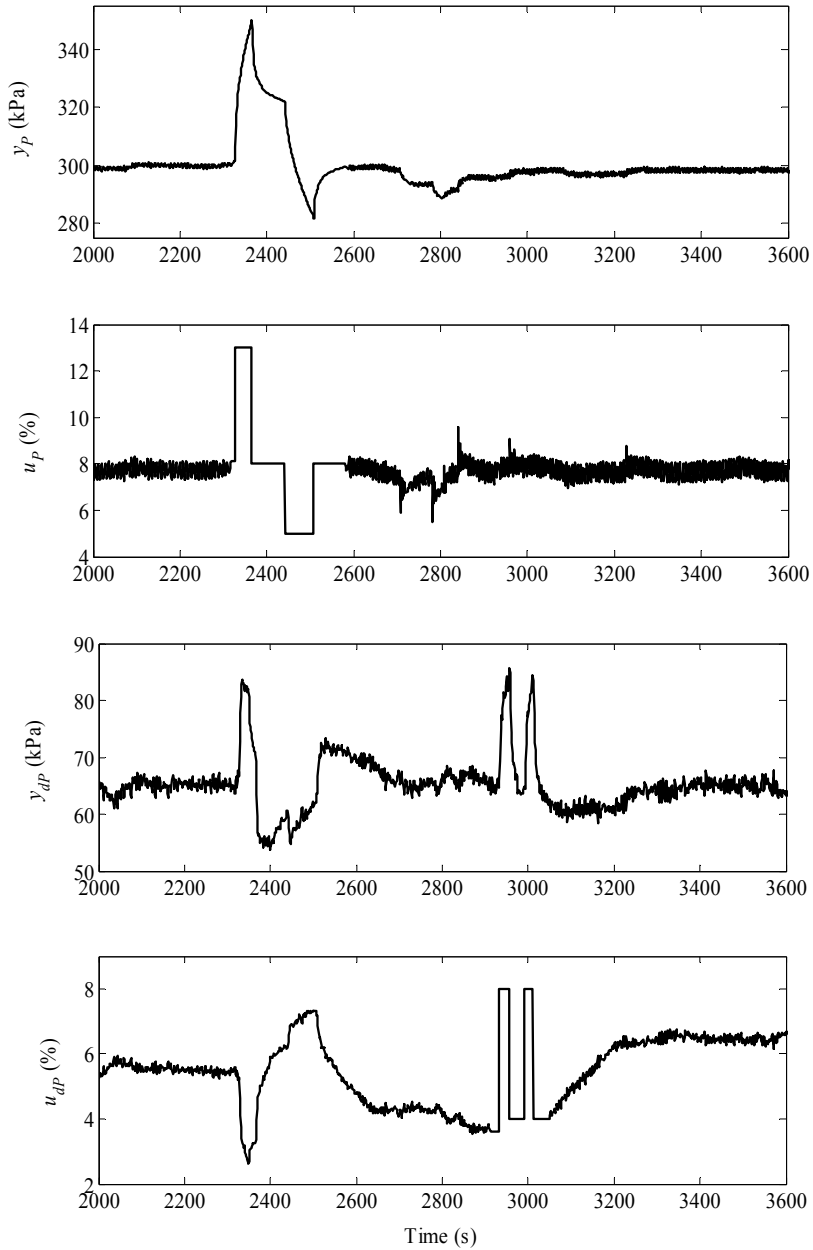
Figure 3.22 A second step response model of a similar process as in Figure 3.20. Taken from a fine paper machine.

where y_P and u_P are output and input of the steam pressure process, respectively, and y_{dP} and u_{dP} are output and input of the differential pressure process, respectively. Most conspicuous of this model is that the differential pressure valve, u_{dP}, has no influence on the pressure, y_P. This is also very clear from the figure. This is a nice property since the pressure controller can then be tuned without regarding the differential pressure, y_{dP}. The differential pressure, however, is significantly affected by the pressure valve, most easily seen in Figure 3.21. This interconnection has to be regarded when tuning the PDC controller. The purpose of this loop is to maintain good condensate evacuation and even short term deviations from the set point will influence the drying effect. However, since the PC loop has a larger effect on the drying, good regulation of this is more important and the performance of the PDC loop is of minor importance. Figure 3.22 shows a similar experiment as in Figure 3.21, but on a different dryer group. This experiment gives equivalent results.

It is not a big surprise that also the differential pressure can be modeled as an IPZ process, just like the pressure. Both are acting on the same system and must, to some extent, be governed by the same physical equations. However, it should be noted that in some cases it has shown sufficient to model it as a first order system. Deep analysis of the differential pressure loop is not covered in this thesis, and from here on only the moisture cascade loop will be treated

3.7 Summary

In this chapter a black-box model structure has been presented and some controller structures have been analyzed. First, the closed loop properties when using a PID controller are examined. It is then followed by two different controller structures. The main purpose of this is to avoid resonances in the frequency response, $r \rightarrow y$, as feedback with a simple PID gives, see Figure 3.8. In Section 3.3 this is accomplished by canceling process dynamics by feedforward in terms of a two-degree-of-freedom controller. In Section 3.4 dynamics are instead cancelled by state feedback. The 2DOF controller is best suited for implementation since the existing DCS today seldom support state feedback controllers.

A different type of model for the steam pressure has also been investigated where the integrator is replaced by a pole. The conclusion is, however, that the integrator model is sufficient for controller tuning purposes and therefore the natural choice.

Finally, a multi-variable model for the pressure and differential pressure loop has been given. The main conclusion of this is that the pressure loop can be tuned without regarding the differential pressure.

4

A Physical Model of a Steam Heated Cylinder

In Chapter 3, an empirical black-box model structure for the steam pressure in a dryer cylinder is presented. This class of models is adequate for controller tuning purposes but does not tell anything about the physics that generate the dynamic behavior. Here we will present a first principles model, initially proposed by [Åström, 2003]. The foundation of the model is simple mass and energy balances. The primary model is a nonlinear differential-algebraic equation set, but by algebraic manipulations and a linearization, it will have the same structure as the IPZ model. The steam pressure and the cylinder shell temperature are chosen as state variables, since both these variables are possible to measure. One of the main purposes of this grey-box model is to gain insight into which physical characteristics and mechanisms have key effect on the parameters in the IPZ model. A similar approach for a drum boiler has been presented in [Åström and Bell, 2000b]. For more on grey-box modeling, see [Allison *et al*, 1997], [Bohlin and Graebe, 1995] and [Bohlin, 1994]. Two comprehensive books on physical modeling and model analysis is [Hangos and Cameron, 2001] and [Thomas, 1999]. A nomenclature can be found at the end of the thesis.

   The nonlinear model will be further examined in Chapter 8, where it is expanded with dynamics for the paper web to give a complete simulation model for a whole drying section.

4.1 The model

Let q_s (kg/s) be the mass flow rate of steam into the cylinder, q_c (kg/s) be the condensation rate, and q_w (kg/s) be the siphon flow rate. Also, let V_s (m³) and V_w (m³) be the volume of steam and water in the cylinder, and let ρ_s (kg/m³) and ρ_w (kg/m³) be the densities of steam and water. The mass balances for water and steam are then

$$\frac{d}{dt}(\rho_s V_s) = q_s - q_c, \qquad (4.1a)$$

$$\frac{d}{dt}(\rho_w V_w) = q_c - q_w, \qquad (4.1b)$$

where no blow-through steam is assumed. Sometimes the blow-through steam is modeled as a fraction of q_s [Karlsson *et al*, 2002]. This does not affect the dynamics of the system, only the steady state gain. The energy balances for steam, water and metal are

$$\frac{d}{dt}(\rho_s u_s V_s) = q_s h_s - q_c h_s, \qquad (4.2a)$$

$$\frac{d}{dt}(\rho_w u_w V_w) = q_c h_s - q_w h_w - Q_m, \qquad (4.2b)$$

$$\frac{d}{dt}(mC_{p,m}T_m) = Q_m - Q_p, \qquad (4.2c)$$

where Q_m (W) is the power supplied from the water to the metal, Q_p (W) is the power supplied from the metal to the paper, h_s (J/kg) is the steam enthalpy, h_w (J/kg) is the water enthalpy, m (kg) the mass of the cylinder shell, $C_{p,m}$ (J/(kg·K)) the specific heat capacity of the shell, T_m (K) the mean temperature of the metal, u_s (J/kg) and u_w (J/kg) are the specific internal energies of steam and water. For the period of one revolution, the cylinder is in contact with the paper or dryer fabric one part of the time, and in contact with the surrounding air the other part. Due to higher resistance for heat transfer, the energy loss to the air is only a fraction of the energy flow to the paper or fabric. However, [Janson and Nordgren, 1958] found that the temperature variation during one revolution is negligible (less that 0.3°C) and the metal temperature is therefore assumed to be independent of the cylinder rotation. The energy flow to the metal is given by
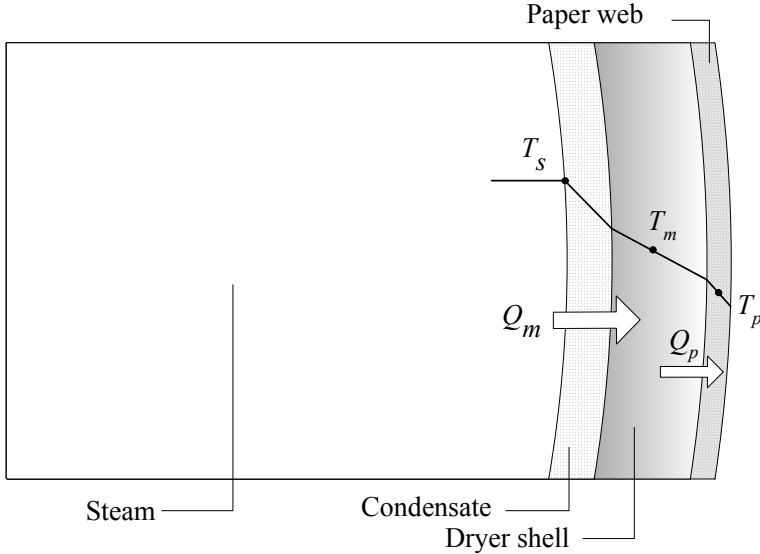
Figure 4.1 A piece of the cross-section of a drying cylinder, visualizing the assumption on the temperature profile and the energy flows.

$$Q_m = \alpha_{sc} A_{cyl} (T_s - T_m),\qquad(4.3)$$

where α_{sc} (W/(m²·K)) is the heat transfer coefficient from the steam-condensate interface to the centre of the cylinder shell, A_{cyl} (m²) is the inner cylinder area, and T_s (K) the steam temperature. The outer surface area of the cylinder is assumed to be equal to its inside area. The error is negligible (less than 5%), because the thickness of the cylinder shell is much smaller than the outer cylinder diameter. The energy flow to the paper is given by

$$Q_p = \alpha_{cp} A_{cyl} \eta (T_m - T_p),\qquad(4.4)$$

where α_{cp} (W/(m²·K)) is the heat transfer coefficient from the center of the cylinder shell to the centre of the paper sheet, η (unitless) is the fraction of dryer surface covered by the paper web, and T_p (K) is the paper temperature. Fraction η is between 0.5 and 0.7.

For simplicity, all steam within the cylinder cavity is assumed to be homogeneous with the same pressure and temperature. From (4.3) and (4.4), we make the assumption of a temperature gradient in the condensate layer, cylinder shell, and paper web, as illustrated in Figure 4.1.

Equations (4.1), (4.2), and (4.3) are a crude nonlinear model for the steam and condensate system in the cylinder cavity. To obtain a linear second-order model, we make a few simplifications.

i. First assume that the steam in the cylinder is saturated. This because there is a continuous condensation occurring at the cylinder wall. This means that the state of the steam can be characterized by one variable only and that it is sufficient to use either the mass balance or energy balance. Therefore, we leave out the energy balance (4.2a).

ii. When the inflow of steam is varied, the temperature of the paper, T_p, is likely to vary slowly compared to the steam- and cylinder dynamics, due to the low pass effect of the cylinder shell. Therefore, we assume that T_p is constant (otherwise we would also need an energy balance for the paper web).

iii. In addition, the thermal dynamics of the water is very fast compared to the cylinder, so we replace it by a static model.

iv. Observing that the volumes are constrained by $V_s + V_w = V$, where V is the total cylinder volume, the second mass balance in (4.1) can be eliminated. Since the water volume is small we also have $V \approx V_s$.

Summarizing, we find that the system can be described by the equations

$$
\begin{aligned}
\frac{d}{dt}\left(\rho_s V\right) &= q_s - q_c, \\
\frac{d}{dt}\left(m C_{p,m} T_m\right) &= Q_m - Q_p, \\
0 &= q_c h_s - q_w h_w - Q_m, \\
Q_m &= \alpha_{sc} A_{cyl}\left(T_s - T_m\right), \\
Q_p &= \alpha_{cp} A_{cyl}\eta\left(T_m - T_p\right),
\end{aligned}
\tag{4.5}
$$

which are a mass balance for the steam, an energy balance for the metal, a static energy balance for the water, and an algebraic equation for the energy flow. Eliminating the variables q_c and Q_m, the model becomes

$$h_s \frac{d}{dt}(\rho_s V) = q_s h_s - q_w h_w - \alpha_{sc} A_{cyl}(T_s - T_m),$$

$$\frac{d}{dt}(mC_{p,m}T_m) = \alpha_{sc} A_{cyl}(T_s - T_m) - \alpha_{cp} A_{cyl}\eta(T_m - T_p). \tag{4.6}$$

Assuming that the steam in the cylinder is saturated, enthalpies h_s, h_w, density ρ_s and the temperature T_s, are all functions of the pressure p. The model can thus be written as

$$h_s(p)V \frac{d\rho_s}{dp}\frac{dp}{dt} = q_s h_s(p) - q_w(p)h_w(p) - \alpha_{sc} A_{cyl}(T_s(p) - T_m),$$

$$mC_{p,m}\frac{dT_m}{dt} = \alpha_{sc} A_{cyl}(T_s(p) - T_m) - \alpha_{cp} A_{cyl}\eta(T_m - T_p), \tag{4.7}$$

where the states are pressure p and mean metal temperature T_m. The steam inlet flow, q_s, is the input. The equilibrium gives the relations

$$0 = q_s^0 h_s(p^0) - q_w(p^0)h_w(p^0) - \alpha_{sc} A_{cyl}(T_s(p^0) - T_m^0),$$

$$0 = \alpha_{sc} A_{cyl}(T_s(p^0) - T_m^0) - \alpha_{cp} A_{cyl}\eta(T_m^0 - T_p^0). \tag{4.8}$$

Hence

$$T_p^0 = T_m^0 - \frac{q_s^0 h_s(p^0) - q_w^0 h_w(p^0)}{\alpha_{cp} A_{cyl}\eta}. \tag{4.9}$$

The numerator in (4.9) is the amount of energy delivered to the cylinder shell (difference between inflow and outflow of energy). Dividing this by the conductivity for the surface covered by paper gives the reduction in temperature from cylinder to paper. Linearizing around the equilibrium gives

$$h_s(p^0)V\left.\frac{d\rho_s}{dp}\right|_{p=p^0}\frac{d\Delta p}{dt}$$

$$=\left(q_s^0\frac{dh_s}{dp}-q_w(p^0)\frac{dh_w}{dp}-h_w(p^0)\frac{dq_w}{dp}-\alpha_{sc}A_{cyl}\frac{dT_s}{dp}\right)_{p=p^0}\Delta p \qquad (4.10)$$

$$+\alpha_{sc}A_{cyl}\Delta T_m+h_s(p^0)\Delta q_s,$$

$$mC_{p,m}\frac{d\Delta T_m}{dt}=\alpha_{sc}A_{cyl}\left.\frac{dT_s}{dp}\right|_{p=p^0}\Delta p-\alpha_{sc}A_{cyl}\Delta T_m-\alpha_{cp}A_{cyl}\eta\Delta T_m,$$

where the states are expressed in terms of deviations and the equilibrium point in (4.8) have been used to simplify the expression. Assuming that

$$\left|q_s^0\frac{dh_s}{dp}-q_w(p^0)\frac{dh_w}{dp}-h_w(p^0)\frac{dq_w}{dp}\right|<<\alpha_{sc}A_{cyl}\left|\frac{dT_s}{dp}\right|, \qquad (4.11a)$$

and

$$\alpha_{cp}\eta<<\alpha_{sc}, \qquad (4.11b)$$

the model becomes

$$h_s(p^0)V\left.\frac{d\rho_s}{dp}\right|_{p=p^0}\frac{d\Delta p}{dt}=-\alpha_{sc}A_{cyl}\left.\frac{dT_s}{dp}\right|_{p=p^0}\Delta p+\alpha_{sc}A_{cyl}\Delta T_m+h_s(p^0)\Delta q_s,$$

$$mC_{p,m}\frac{d\Delta T_m}{dt}=\alpha_{sc}A_{cyl}\left.\frac{dT_s}{dp}\right|_{p=p^0}\Delta p-\alpha_{sc}A_{cyl}\Delta T_m.$$

$$(4.12)$$

Assumption (4.11b) is another way of saying that Q_p is varying much more slowly than Q_m when the inlet steam flow is changed. The interface between the cylinder and paper then acts as a large heat transfer barrier. From experimental values in [Karlsson, 2000], it is found that the right hand side is $2-20$ times larger than the left hand side in (4.11b). For the lower region of that range, it is probably unsatisfying to use model (4.12). However, experiments show that large values of α_{cp} only occur for high moisture contents (>40 %) and high fabric tensions. It is therefore the belief of the author that this is an uncommon situation and the right hand

side of (4.11b) is generally much larger that the left hand side. This is further discussed in Section 4.4 and Chapter 8. The inequality in (4.11a) will be commented and examined later in the simulations, and also in Chapter 8.

Writing the system in standard state-space form, we find that

$$
\begin{aligned}
\dot{x} &= Ax + B\Delta q_s, \\
y &= Cx + D\Delta q_s,
\end{aligned}
\tag{4.13}
$$

where $x = \begin{bmatrix} \Delta p & \Delta T_m \end{bmatrix}^T$ and

$$
A = \alpha_{sc}
\begin{bmatrix}
-\dfrac{A_{cyl}\dfrac{dT_s}{dp}}{h_s V \dfrac{d\rho_s}{dp}} & \dfrac{A_{cyl}}{h_s V \dfrac{d\rho_s}{dp}} \\[4mm]
\dfrac{A_{cyl}\dfrac{dT_s}{dp}}{mC_{p,m}} & -\dfrac{A_{cyl}}{mC_{p,m}}
\end{bmatrix}, \quad
B =
\begin{bmatrix}
\dfrac{1}{V\dfrac{d\rho_s}{dp}} \\[4mm]
0
\end{bmatrix},
\tag{4.14}
$$

$$
C = \begin{bmatrix} 1 & 0 \end{bmatrix}, \qquad\qquad D = 0.
$$

The steam properties are here assumed to in given in their equilibrium values. The matrix A has an eigenvalue at the origin and one eigenvalue on the negative real axis. The transfer function from steam flow to pressure is

$$
G(s) = b_1 \frac{s - a_{22}}{s(s - a_{11} - a_{22})} = b_1 \frac{s + z}{s(s + \lambda)} = \frac{b_1}{\lambda}\left(\frac{z}{s} + \frac{\lambda - z}{s + \lambda}\right),
\tag{4.15}
$$

where

$$b_1 = \frac{1}{V\dfrac{d\rho_s}{dp}}, \quad z = -a_{22} = \frac{\alpha_{sc}A_{cyl}}{mC_p},$$

$$\lambda = -a_{11} - a_{22} = \alpha_{sc}\left(\frac{A_{cyl}\dfrac{dT_s}{dp}}{h_sV\dfrac{d\rho_s}{dp}} + \frac{A_{cyl}}{mC_{p,m}}\right). \qquad (4.16)$$

Note that the model (4.15) has an IPZ structure. The essential parameters of the model are

- Cylinder volume V
- Cylinder mass m
- Specific heat capacity of metal $C_{p,m}$
- Area of the cylinder surface A_{cyl}
- Steam properties h_s, $d\rho_s/dp$, dT_s/dp
- Heat transfer coefficient α_{sc}

All parameters, except the heat transfer coefficient, α_{sc}, are known beforehand, either by machine specifications or from a physics handbook which includes a steam table and heat capacities. The heat transfer coefficient depends on both amount of condensate and its degree of turbulence, and is very difficult to predict. Therefore it is used to fit the model to the measured data. Note that it is only the last two items in the parameter list that depend on the operating point.

The following assumptions have been made in the development of the model

- No blow-through steam
- The steam in the cylinder is saturated
- Paper temperature is constant
- The thermal dynamics of the condensate is fast compared to the cylinder shell
- The condition (4.11)

The pole λ and the zero z are both proportional to the heat transfer coefficient α_{sc}. For large s the transfer function (4.15) is approximated by

$$G(s) \approx \frac{b_1}{s},\qquad (4.17)$$

where b_1 does not depend on α_{sc}. For small s the transfer function can be approximated by

$$G(s) \approx \frac{b_1 z}{\lambda s},\qquad (4.18)$$

where

$$\frac{b_1 z}{\lambda} = \frac{h_s}{mC_{p,m}\frac{dT_s}{dp} + Vh_s\frac{d\rho_s}{dp}},\qquad (4.19)$$

does not depend on α_{sc}. Therefore neither the initial part of a step response nor the slope of the asymptote depend on the heat transfer coefficient. Finally, the relations between the black-box and grey-box parameters are

$$k_v = \frac{h_s}{mC_{p,m}\frac{dT_s}{dp} + Vh_s\frac{d\rho_s}{dp}}, \qquad T_1 = \frac{mC_{p,m}}{\alpha_{sc}A_{cyl}},$$

$$T_2 = \frac{mC_{p,m}h_sV\frac{d\rho_s}{dp}}{\alpha_{sc}A_{cyl}\left(mC_{p,m}\frac{dT_s}{dp} + Vh_s\frac{d\rho_s}{dp}\right)}.\qquad (4.20)$$

Note that the velocity gain, k_v, above is not normalized by the measuring or any actuator range.

As can be noticed, the grey-box model does not explain the time delay often seen in the black-box model. It is important to remember that we often are dealing with sampled measurements and it has been observed, in practice, that the time delay of the system often is close to the sampling time. Moreover, we have seen from the derivation of the grey-box model that there are neglected dynamics in the model, which may possibly give rise to an estimation of the dead-time that is larger than the true value.

Chapter 4. A Physical Model of a Steam Heated Cylinder

Remark 1
A unit analysis of the expressions in (4.20) shows that T_1 and T_2 are given in seconds, while k_v is given in Pa/kg. Since k_v is a velocity gain, one would expect its unit to include seconds. However, the inflow of steam is given in kg/s and the time unit is therefore canceled.

Remark 2
The energy flow to the metal (4.3) can be derived as the solution of Fourier's law of heat conduction

$$Q = -kA\nabla T, \tag{4.21}$$

where k is the thermal conductivity, A is the area, T the temperature, and Q the energy flow. The negative sign indicates that the temperature gradient is in the opposite direction of the energy flow. Assuming there is no build-up of heat at any point along the path of the heat flow, Q is constant along the path. Consider a one-dimensional and homogeneous system, and integrate (4.21) from point "0" to point "1"

$$\int_{x_0}^{x_1} Q\,dx = -kA \int_{T_0}^{T_1} dT \tag{4.22}$$

or equivalently

$$Q = kA\frac{T_0 - T_1}{x_1 - x_0} = \frac{k}{\Delta x} A(T_0 - T_1). \tag{4.23}$$

Writing the quotient $k/\Delta x$ as a heat transfer coefficient α, we have the relation in (4.3). It might appear as a large restriction to assume constant energy flow along the path but it can still vary with time, there is simply no build-up. By combining the energy balance for the metal in (4.2c) with

$$Q_m = \alpha_{sc} A_{cyl}(T_s - T_m), \tag{4.3}$$

we get a first-order system from steam temperature to mean metal temperature, which also corresponds to the solution given by the distributed heat equation (with constant energy flow to the paper as boundary condition), see Appendix C (Figure C.5).

Remark 3
The steady-state solution to (4.1) and (4.2) is

$$q_s = q_c = q_w$$
$$Q_m = q_c(h_s - h_w) \qquad (4.24)$$
$$Q_m = Q_p$$

As expected, both the mass flows and energy flows are equal. The energy flow to the metal, Q_m, is given by the condensation rate times the difference in enthalpy due to condensation. The drying is, in other words, powered by the latent heat of vaporization of the steam.

4.2 Time and frequency domain analysis

To investigate the dynamic behavior of the linearized model, given by (4.13), we will look at the Bode plot and a step response. The machine dependent parameters are taken from a steam group of a fluting machine, running at an operating point with a steam pressure of 90 kPa (gauge pressure), a nominal speed of $450 - 600$ m/min and a basis weight between $110 - 200$ g/m^2. The machine dependent values used for the simulation are

- Cylinder volume: $V = 12.6$ m^3
- Cylinder mass: $m = 7610$ kg
- Cylinder area: $A_{cyl} = 37.2$ m^2
- Heat capacity for cast iron: $C_{p,m} = 500$ J/(kg·K)
- Steam properties for the given operating point

The nominal steam mass flow rate to each cylinder is approximately 0.25 kg/s. This value is obtained by simply dividing a measurement of the total machine steam consumption by the number of cylinders. Figure 4.2 shows the Bode plot of the process, where the gain is normalized by the measuring range of the pressure.

The amplitude gain is independent of α_{sc}, both at high and low frequencies, as shown in (4.17) and (4.18). The heat transfer coefficient has a considerable influence on both the gain and phase in the mid-frequency range. For the purpose of designing a PID-controller, this difference in gain and phase influences the controller parameters. Otherwise it would be possible to tune the controller solely from cylinder
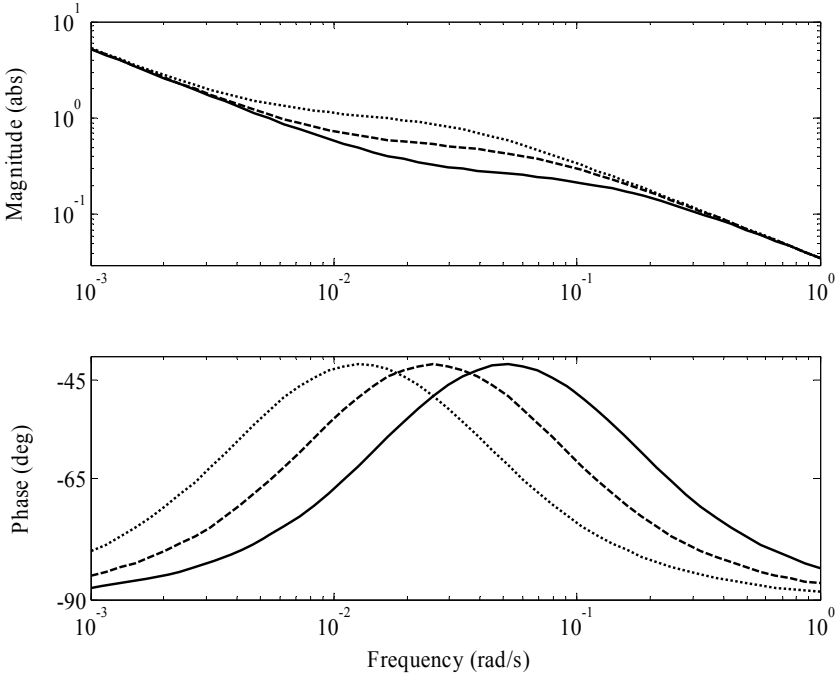
Figure 4.2 Frequency properties for different values of the heat transfer coefficient α_{sc} = 500 (dotted), 1000 (dashed), and 2000 (solid).

dimensions and a steam table. It can also be seen that, a higher heat transfer coefficient yields a lower steam pressure gain, since there is a larger heat transfer to the cylinder and a higher condensation rate.

The linearized model has also been simulated with a step in the input signal, shown in Figure 4.3. As the figures illustrate, a higher heat transfer coefficient gives a lower steam pressure, at a given time instance, due to a larger heat transfer to the cylinder shell. This has also been pointed out in [Nelson and Gardner, 1996]. A greater energy flow through the cylinder shell gives a higher cylinder temperature even though the steam has a lower temperature, at any time index. The effect of a larger α_{sc}, in basic terms, dominates over the effect of a lower steam temperature. It is essential to remember that there are two effects taking place in this pressure−temperature process. The heat transfer coefficient varies between the simulations and the steam temperature is changing with time, and the cylinder temperature depends on both.

In (4.11a) an inequality that depends on the operating point and cylinder dimensions was utilized to make a significant simplification. Using values from this example, we can examine its justification. Apart
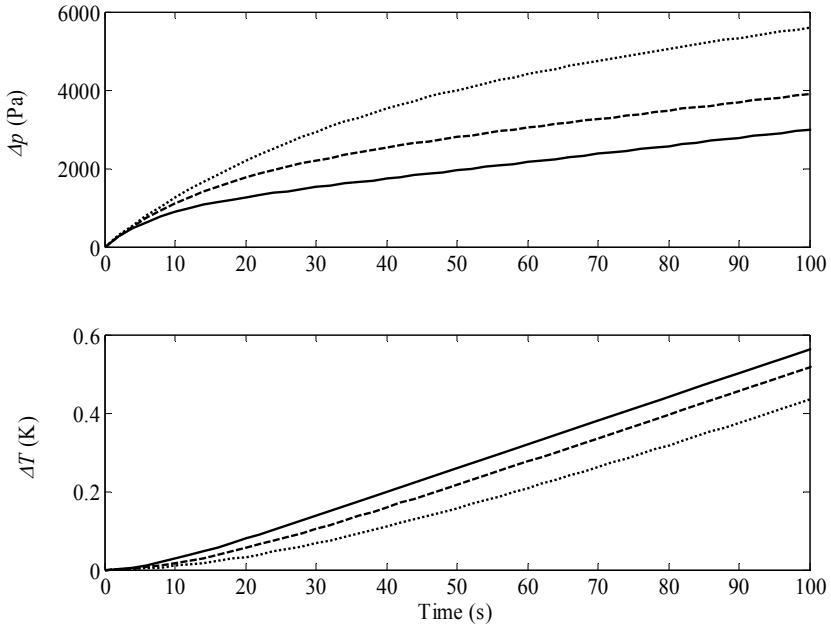
Figure 4.3 Step responses for different values of the heat transfer coefficient α_{sc} = 500 (dotted), 1000 (dashed), and 2000 (solid). The upper graph shows the steam pressure and the lower shows the cylinder temperature.

from the steam properties, we also need an expression for the derivative of siphon flow rate, q_w, with respect to the cylinder pressure. Some experimental values are given in [Stenström and Svanquist, 1991] and using those, we find that the right hand side of (4.11a) is 10 to 20 times larger than the left hand side. The next section shows that the model has a good fit to experimental data.

4.3 Comparisons with plant data

To evaluate the accuracy of the grey-box model it has been calibrated and validated against measurements from a steam- and condensate system. The experiments have been carried out on a paperboard machine and signals have been measured with a sampling time of 1 s. The cylinder data is

- Cylinder volume: V = 18.4 m^3
- Cylinder mass: m = 8300 kg
- Cylinder area: A_{cyl} = 45.5 m^2

Since the input signal (steam input flow) is not manipulated directly, neither measured, a model for a steam valve has to be added to (4.13). A simple approach is to assume a static linear relationship between the controller signal, u_c, and the steam input flow, q_s, namely

$$q_s = d_v u_c, \tag{4.25}$$

where d_v is a valve constant which will be the second calibration parameter together with the heat transfer coefficient, α_{sc}. Using this valve description, we keep the linearity and IPZ-structure in the model, given in (4.13).

To calibrate the model, the functions `idgrey.m` and `pem.m` in System Identification Toolbox for Matlab, were used to find the optimal calibration parameters. The optimization method is based on minimizing the prediction error, see [Ljung, 1999].

Figure 4.4 shows an open loop response together with the calibrated model, where the control signal and model output are bias corrected (by the linear model, a steady-state pressure level can only be reached for a closed valve). The calibration parameters obtained are

$$\alpha_{sc} = 1820 \text{ W/(m}^2\cdot\text{K)}, \quad d_v = 0.00308 \text{ kg/(s}\cdot\%). \tag{4.26}$$

To compare the result with nominal values cited in literature, we need a heat transfer coefficient through only the condensate film, α'_{sc}. From [Karlsson, 2000] the relationship

$$\alpha_{sc} = \frac{1}{\dfrac{1}{\alpha'_{sc}} + \dfrac{\delta_{cyl}}{\lambda_{cyl}}}, \tag{4.27}$$

is given, where δ_{cyl} is the distance into the cylinder where the temperature is equal to the mean cylinder temperature, and λ_{cyl} is the thermal conductivity of the cylinder shell. In this example, the cylinder thickness is 25 mm (the mean temperature, T_m, occurs in the middle of the cylinder shell), and the thermal conductivity is 50 W/(m·K). The heat transfer coefficient through the condensate is then

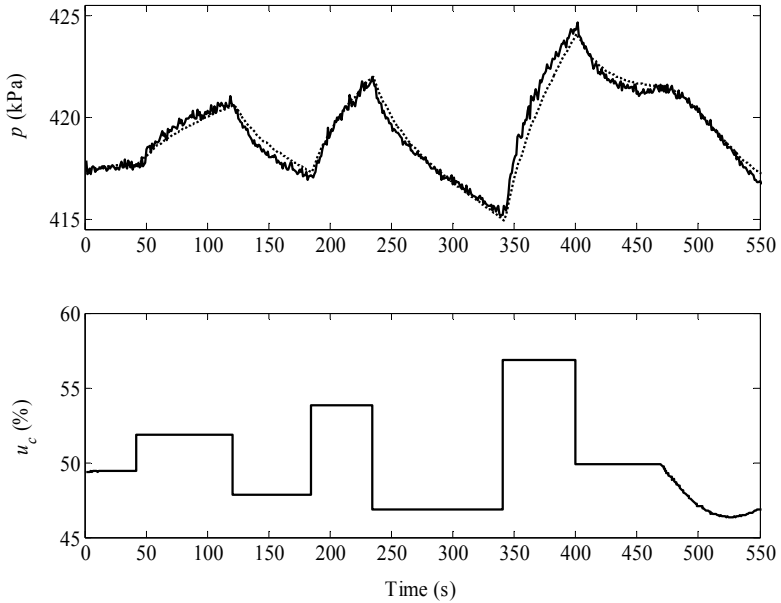$$\alpha'_{sc} = 3340 \text{ W/(m}^2\cdot\text{K)}. \tag{4.28}$$

Figure 4.4 Calibrated model (dotted) and measured data (solid).
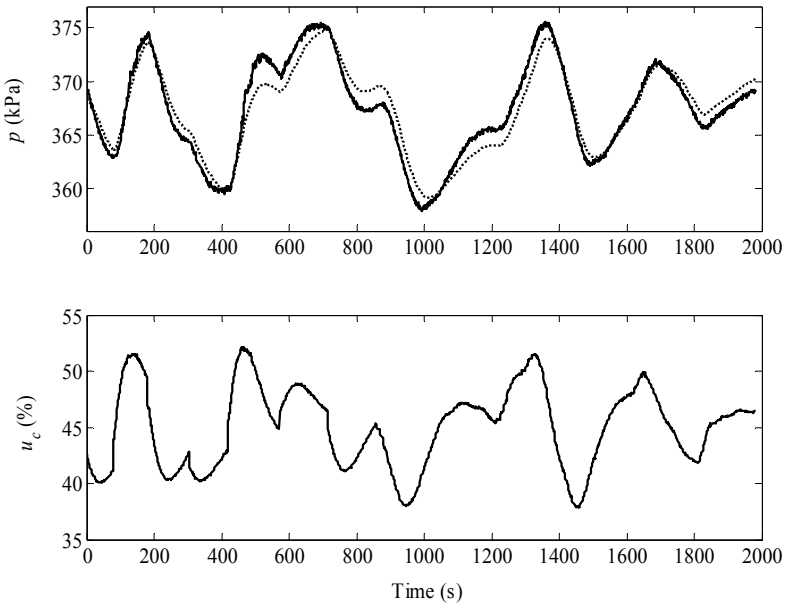
Figure 4.5 Validation of model (dotted) against measured data (solid).

In [Karlsson, 2000], typical values of the heat transfer coefficient are given. They depend strongly on the condensate thickness and turbulence, and can vary between 1000 and 4000 W/(m²·K), where 2000 is a nominal value. Nevertheless, the fact that our estimated value from the model is within that range, gives support for the legitimacy of the model.

The total mass flow rate of steam, during the experiment, to the drying section is 85 ton/h. The machine has 93 cylinders, so the average steam flow per cylinder is 0.254 kg/s. The parameter d_v, in (4.26), and the average valve opening gives the steam flow to the particular cylinder in the model, namely 0.154 kg/s. The steam flow is likely to vary a great deal between different drying groups but by comparing the two values, we know that also the second calibration parameter is realistic.

In (4.29) the grey-box model is compared with the corresponding black-box model, adjusted on the same data set. The velocity gain in the models is normalized with the measuring range of the pressure gauge. The black-box model is not shown in the figures but it gives a slightly better fit to the data, since it has more degrees of freedom (three parameters to adjust instead of two). There is also a difference in the parameters of the transfer functions. The time delay is equal to the sampling time and comes from the identification procedure (`pem.m` in System Identification Toolbox for Matlab).

$$G_{grey}(s) = 0.00243 \frac{(50.1s + 1)}{s(20.4s + 1)} e^{-s}$$

$$G_{black}(s) = 0.00176 \frac{(77.8s + 1)}{s(21.3s + 1)} e^{-s}$$

(4.29)

The grey-box model has also been validated graphically by using the control signal values to simulate an output. The model output is then compared with the measured steam pressure. Figure 4.5 shows such an evaluation. The excitation in the control signal is generated by a series of steps in the set point (closed loop), which is not shown in the figure to keep it clear.

4.4 A modified model

In Chapter 3, it was discussed that in some cases the IPZ-structure is not sufficient to describe the pressure dynamics in a steam cylinder. This can be resolved by changing the integrator to a real pole. In the grey-box

model this can be accomplished by disregarding the assumption from (4.11b), saying that

$$\alpha_{cp}\eta << \alpha_{sc}. \tag{4.11b}$$

It was previously discussed that for high moisture contents and high fabric tensions, this assumption might not be valid. By letting T_p be constant, (4.14) instead becomes

$$A' = \begin{bmatrix} -\dfrac{\alpha_{sc}A_{cyl}\dfrac{dT_s}{dp}}{h_sV\dfrac{d\rho_s}{dp}} & \dfrac{\alpha_{sc}A_{cyl}}{h_sV\dfrac{d\rho_s}{dp}} \\[4mm] \dfrac{\alpha_{sc}A_{cyl}\dfrac{dT_s}{dp}}{mC_{p,m}} & -\dfrac{A_{cyl}(\alpha_{sc}+\alpha_{cp}\eta)}{mC_{p,m}} \end{bmatrix}, \tag{4.30}$$

and the other matrices are unchanged. By examining time series where the IPZ-structure is sufficient with cases where it is not, an explanation to the modeling problem is found. If $\alpha_{sc} >> \alpha_{cp}$ then model (4.13) is adequate and $\alpha_{sc} \approx \alpha_{cp}$ means that (4.30) is a better structure. This has also been verified by simulation of the primary DAE system (4.1)–(4.3) in Modelica, see Chapter 8. Closer examination of (4.30) shows that $\alpha_{sc} >> \alpha_{cp}$ gives a system with one fast pole and one close to the origin. When α_{cp} is increased, the slow pole moves along the real negative axis towards the other pole, and it can then no longer be regarded as an integrator.

It can be shown, knowing that all factors in the elements of (4.30) are positive, that the eigenvalues of A' are real and negative. This is nice since it would be unsatisfying to have a model that is unstable for some combinations of physical parameters, when it is clear that the process is stable in reality. The characteristic equation of (4.30) is

$$s^2 - (a_{11} + a_{22})s + a_{11}a_{22} - a_{12}a_{21}, \tag{4.31}$$

where a_{11}, a_{12}, a_{21}, and a_{22} are the elements of matrix A'. Identification of the parameters gives

$$a_{11} + a_{22} = -\frac{\alpha_{sc} A_{cyl} \dfrac{dT_s}{dp}}{h_s V \dfrac{d\rho_s}{dp}} - \frac{A_{cyl}(\alpha_{sc} + \alpha_{cp}\eta)}{mC_{p,m}} < 0,$$

$$(4.32)$$

$$a_{11}a_{22} - a_{12}a_{21} = \frac{\eta \alpha_{sc} \alpha_{cp} A_{cyl}^2 \dfrac{dT_s}{dp}}{h_s V m C_{p,m} \dfrac{d\rho_s}{dp}} > 0,$$

and since the coefficients of the polynomial (4.31) are all positive, the system is stable. The roots of (4.31) are

$$s_{1,2} = \frac{a_{11} + a_{22}}{2} \pm \sqrt{\frac{(a_{11} - a_{22})^2}{4} + a_{12}a_{21}},$$

$$(4.33)$$

and since both a_{12} and a_{21} are positive, the solution has no complex parts. The relation between the position of the poles and the physical parameters is a bit more complicated than in (4.16).

   It can also be shown that the initial dynamics of the modified model in (4.30) are equal to (4.17). For large s we have

$$G(s) \approx \frac{1}{V \dfrac{d\rho_s}{dp} s}.$$

$$(4.34)$$

The low frequency properties will be different for the two models however, since (4.13) contains an integrator and has no steady state gain. For small s the modified model becomes

$$\lim_{s \to 0} G(s) = \frac{h_s(\alpha_{sc} + \alpha_{cp}\eta)}{\alpha_{sc} A_{cyl} \eta \alpha_{cp} \dfrac{dT_s}{dp}}.$$

$$(4.35)$$

4.5 Summary

Chapter 3 introduced a black-box model structure for the steam pressure dynamics. In this chapter an additional model has been presented, a grey-box model. Both have the same structure but different purposes. The intention of the black-box model is purely controller tuning and the main purpose of the grey-box model is to gain insight into the physical laws behind the black-box model. Issues like how the heat transfer coefficient, cylinder diameter, condensate removal, selection of materials or steam pressure affect the dynamical performance of the system can then be answered. This might have effect on the mechanical design of the drying section, such as the siphon shape and form, dryer bars, cylinder dimensions etc.

There is also a potential to make a recursive identification of the heat transfer coefficient for fault detection with respect to condensate evacuation. It would then be beneficial to have a separate pressure meter and mass flow meter installed at the drying cylinder of interest, to acquire an accurate estimate. An important thing to remember here is that the model is an approximation of the real process. Model errors will therefore be included in the calibration parameter and its absolute value might be uncertain. The relative value is a useful parameter though.

The grey-box model has been validated by measurement from a paper machine with good results. Further examination of the model can be found in Chapter 8, where it is combined with a paper web model.

5

A Tuning Method for IPZ Models

From practical experience, it has been seen that there can be significant disturbances in the drying section, which makes disturbance attenuation an important issue. Since the prevalent machine design standard is to connect all the dryer groups to the same steam header, a disturbance in one group easily affects the other groups. In this section, a simple tuning rule for both PI and PID control is presented. Many tuning methods for PI and PID control have been proposed previously but most of them exclusively suppose a first-order system with dead time or an integrating process with dead time. Since this does not fit very well to the IPZ-process, a new method is necessary. The design goal is to obtain good load disturbance response. The tuning rule is based on the four process parameters of the IPZ transfer function and is therefore denoted as IPZ-tuning. The idea is to provide operators and control engineers at the paper mill with a simple tuning tool, which can be used without any complex optimization calculations. To give the user the option to balance between robustness and performance, the tuning rule has a design parameter. This parameter is derived from the Nyquist stability theory and is dimensionless, which is a nice property since it is then independent of unit selections. The IPZ-tuning rule is tested and evaluated on an industrial paper machine. It is also compared with a few other design methods.

5.1 A design method based on optimization

The word optimize comes from the Latin word *optimus* which means *the best* (maximize comes from *maximus* which means *the highest*). Optimization methods are an important tool in nearly all engineering domains, and the control field is indeed no exception. Many control methods are based on optimization of some vital criteria, subject to one or a few constraints. However, it is important to consider how the optimization problem is set up, since this obviously very much affects the result and it is not necessarily a good controller that comes out of an optimal solution. If the optimization problem is not correctly formulated, the optimal controller might not even be stable. The formulation of the problem also affects how easily it is solved. There exist very powerful numerical tools that solve linear or quadratic programming problems, while non-convex optimization is much more demanding due to less effective numerics and the existence of several local optimal solutions.

The derivation of the IPZ-tuning rule is based on a design proposal in [Åström, *et al*, 1998] and [Åström and Hägglund, 2004]. The idea is to maximize the integral gain, defined as $k_i = k_c / T_i$, subject to a robustness constraint. Due to the form of the constraint, the optimization problem is non-convex. Therefore, much effort is put on finding a simple relation between the process parameters and the optimal solution of controller parameters, so that the user is relieved from the optimization issue. Instead, he or she will get an approximate solution from just a few button pushes on a pocket calculator.

By maximizing the integral gain, the absolute value of the integrated error (IE) of a step load disturbance is minimized. This can easily be seen by using the nomenclature in Figure 3.6 and writing the error as

$$E(s) = R(s) - Y(s)$$

$$= R(s) - \left(\frac{P(s)}{1 + P(s)C_c(s)} D(s) + \frac{P(s)C_{ff}(s)}{1 + P(s)C_c(s)} R(s) \right) \quad (5.1)$$

$$= \left(1 - \frac{P(s)C_{ff}(s)}{1 + P(s)C_c(s)} \right) R(s) - \frac{P(s)}{1 + P(s)C_c(s)} D(s).$$

Assume a step unit load disturbance and that the set point is zero. Evaluate the integral of the error by the final value theorem

$$\mathrm{IE} = \int_0^\infty e(t)dt = \lim_{s \to 0} - \frac{P(s)}{1 + P(s)C_c(s)} \frac{1}{s}$$

$$= \lim_{s \to 0} - \frac{P(s)}{1 + P(s)k_c \dfrac{1 + T_i s + T_i T_d s^2}{T_i s}} \frac{1}{s} \qquad (5.2)$$

$$= \lim_{s \to 0} - \frac{T_i P(s)}{T_i s + k_c (1 + T_i s + T_i T_d s^2)P(s)} = -\frac{T_i}{k_c}.$$

By maximizing the integral gain, this integrated error is minimized if the sign is disregarded. However, to only maximize the integral gain is not sufficient since there is no guarantee that the control loop is stable, see Figure 5.1. Therefore, an additional constraint is needed. The robustness constraint used here is characterized by a circle with its centre at the point −1 in the Nyquist diagram, see Figure 5.2. By avoiding the point of instability with a certain distance, R_0, stability is guaranteed. The radius of the circle will then be the design parameter, and the smaller R_0 is the more aggressive the controller will be. This can also be expressed in terms of the sensitivity function, defined as
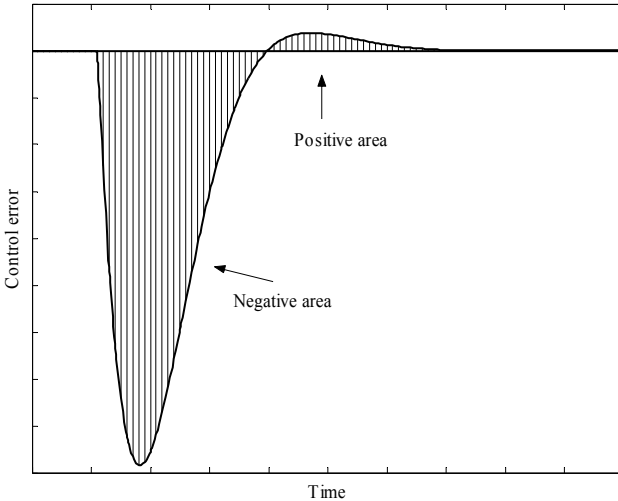
Figure 5.1 A characteristic response to a load disturbance on the IPZ process, controlled by a PID controller. It is crucial add a constraint to the optimization problem to avoid an oscillatory solution, since equally large positive and negative areas cancel each other by the IE criteria.
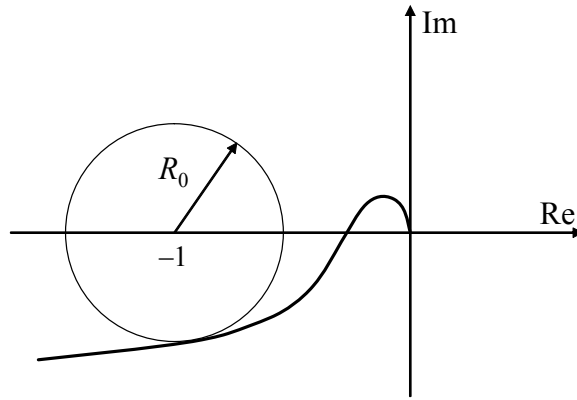
Figure 5.2 The robustness constraint of the design method. By varying the radius of the circle, the degree of robustness is changed.

$$S(s) = \frac{1}{1 + L(s)},\qquad(5.3)$$

where $L(s)$ is the loop transfer function. The maximum sensitivity, M_s, is then given by

$$M_s = \max_{\omega} |S(i\omega)| = \max_{\omega} \left| \frac{1}{1 + L(i\omega)} \right|.\qquad(5.4)$$

Since $|1+L(i\omega)|$ is the distance from a point on the Nyquist curve to the critical point -1, the shortest distance from the Nyquist curve to the point -1 is thus $1/M_s$. Therefore, we get

$$M_s = \frac{1}{R_0},\qquad(5.5)$$

and we can then use M_s as our design parameter, when deriving the tuning rule. The nice thing about the maximum sensitivity function is that it connects the open loop Nyquist curve with a closed loop property. It is also dimensionless which is a nice property. The disadvantage is that it can be difficult to relate to for the unfamiliar user. A common question, e.g., can be what $M_s = 1.2$ means in practice. Simulations and familiarization is one answer to that issue.
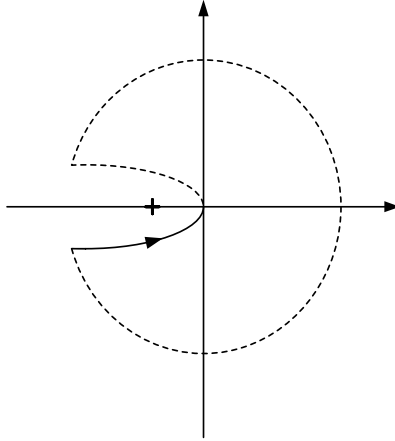
Figure 5.3 The complete Nyquist curve for the IPZ-process and a PID controller if the dead time is assumed to be zero. Otherwise, there will be the typical circular appearance in the origin.

The shape of the Nyquist curve is changed by varying the controller parameters, in order to avoid the M_s-circle while achieving a high integral gain. The derivative time T_d, affects the curve close to the origin (high frequencies), the integral time T_i affects low frequencies, while the gain k_c affects all frequencies equally. However, a few properties of the Nyquist curve are independent of the controller parameters. Since both the IPZ-process and a PID controller contain one integrator each, the Nyquist curve starts at the phase lag $-\pi$. At high frequencies the phase is $-\pi/2$, if we assume no dead time. The complete Nyquist plot then appears as in Figure 5.3.

Note that this design method does not give any suggestion about the feedforward parameters β or γ of the controller, see (3.19), since these parameters have no influence on the sensitivity function or the disturbance rejection.

The design method puts emphasis on disturbance rejection. In [Slätteke, *et al*, 2002] it was shown that for a certain value of the maximum sensitivity ($M_s = 1.2$), maximizing the integral gain or maximizing the bandwidth of the closed loop system (from set point to measurement) gave essentially the same controller parameters. That means that emphasis is put on both the regulator and servo problem. This does not always hold though, even if the two criteria prove to be close.

Remark

Apart from IE, a few other minimization criteria have been proposed in different contexts, e.g. the integrated absolute error (IAE), integrated square error (ISE), and integrated absolute time weighted error (IATE). A disadvantage with ISE is that it penalizes large errors and gives a small but long-term error. IAE have the advantage to avoid oscillatory responses. However, if the system is well damped, IE and IAE give similar results. Keep in mind that IE = IAE, if the error is positive. This is also noted in [Åström, *et al*, 1998]. IE is therefore chosen as the optimization criterion, since it also is computationally effortless.

5.2 The IPZ tuning rule for PI control

A large number of different IPZ models, see (3.1), have been tuned according to the method described in the previous section, with respect to different M_s-values. The M_s-values have been chosen to give practically reasonable and sound controller settings. The models have been chosen to represent a large variety of cylinder pressure processes encountered at different paper machines, producing different grades and qualities. The models cover many different cases, from $L << T_2$ to $L > T_2$, T_1 from 50 to 800, and T_2 from 2 to 400. However, process parameters T_1, T_2, and L are presumed to be positive. This implies that, e.g. non-minimum phase systems are not included. Furthermore, T_1 is always larger than T_2 but cases where T_2 is almost as large as T_1 are also included in the batch of models. The purpose of this is to cover the whole range of models found in the industry. This is also of interest in other process areas since a PPZ structure appears when two first order models are added (parallel paths in integrated plants) and if the two time constants differ in magnitude, it can be modeled as an IPZ process.

The result for $M_s = 1.1$ is plotted in Figure 5.4, where each circle represents one set of process parameters and the corresponding optimal controller parameters. In the plot, the controller gain and integral time have been drawn in combination with the process parameters to give a linear dimensionless relationship. The advantage with dimensionless parameters is that they are independent of the selection of units. Whether the unit of the velocity gain k_v, for example, is given in kPa/(%·s) or simply s^{-1}, does not affect the plot in Figure 5.4.

Even though there is some experimental work in finding combinations that give a clear relationship between the parameters, there is also a structure in the selection. Due to their units, k_v and k_c belongs together, in
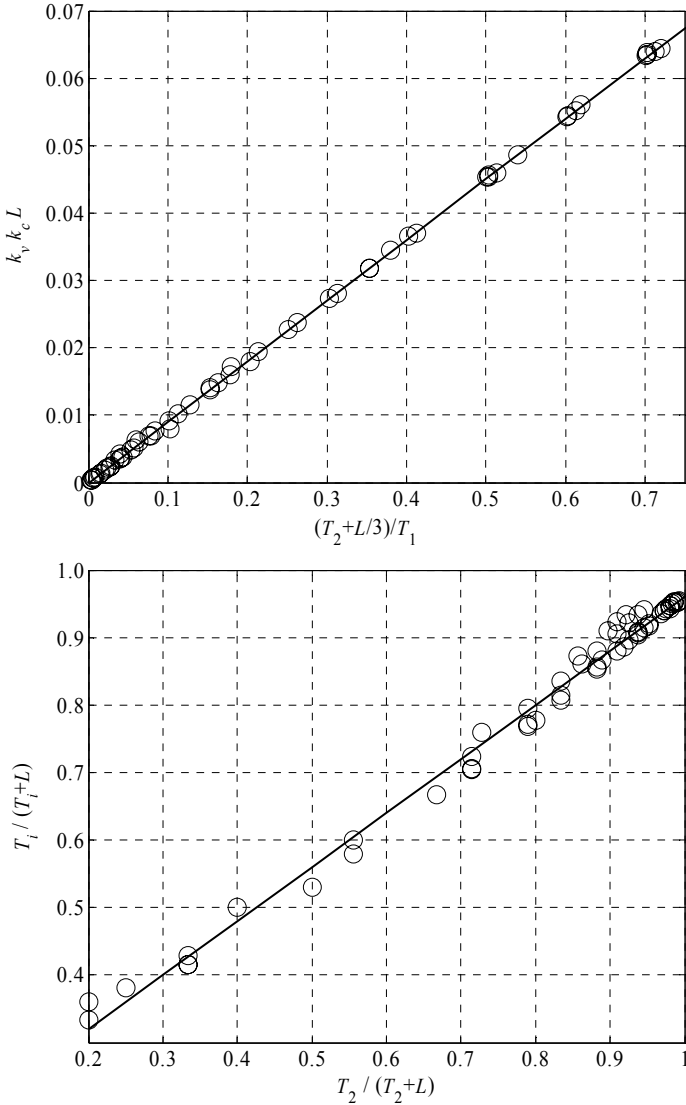
Figure 5.4 The linear relationship between the PI controller parameters and process parameters for $M_s = 1.1$. Each circle represents one set of process parameters from the investigated batch and corresponding control parameters from the optimization routine.

combination with a parameter that is given in seconds (T_1, T_2, T_i, or L). As will be obvious shortly, it must be L because of the influence it has on the controller gain. Moreover, larger T_1 compared to T_2 give more lead action in the process, which must results in a smaller controller gain, given a

certain robustness. Therefore the ratio between T_1 and T_2 (together with a correction term $L/3$, that is found ad hoc) is related to k_c. Also, it seems natural to expect T_i depend on the 'time constant' T_2, compare e.g. lambda tuning [Morari and Zafiriou, 1989], and here it is also affected by L in a way that the expressions on both axes, in Figure 5.4, ranges between zero and one.

The figure shows an apparent linearity. The least squares method has been used to get an equation for this relationship, given in the controller parameters. Obviously, linearity is not a necessity. Curves of higher degrees are possible to use, as long as the desired parameters can be analytically solved for.

The chosen M_s-values are 1.1, 1.2, 1.3, and 1.4. The resulting controller parameters are given by

$$M_s = 1.1 \quad : \quad k_c = 0.09 \frac{T_2 + \dfrac{L}{3}}{T_1 k_v L}, \quad T_i = 4L \frac{6T_2 + L}{T_2 + 21L},$$

$$M_s = 1.2 \quad : \quad k_c = 0.16 \frac{T_2 + \dfrac{L}{3}}{T_1 k_v L}, \quad T_i = 5L \frac{23T_2 + 4L}{9T_2 + 105L},$$

$$M_s = 1.3 \quad : \quad k_c = 0.23 \frac{T_2 + \dfrac{L}{3}}{T_1 k_v L}, \quad T_i = L \frac{100T_2 + 17L}{11T_2 + 94L},$$

$$M_s = 1.4 \quad : \quad k_c = 0.28 \frac{T_2 + \dfrac{L}{3}}{T_1 k_v L}, \quad T_i = L \frac{88T_2 + 15L}{12T_2 + 85L}.$$

$$(5.6)$$

By looking at the controller gain for the different M_s-values, it is easy to interpret the implication of the tuning parameter. The larger the maximum sensitivity is chosen to be (remember that a large value means a less robust controller); the larger is the controller gain, as expected. The interpretation of the integral time is not so obvious by simply looking at the equations. In Figure 5.5 the integral time is plotted against the time constant T_2 of the IPZ model, for a specific time delay L. Here we can see that the larger the value of the design parameter, M_s, is the smaller will the integral time be, for a given value of T_2. As in the analysis of k_c above, this is also expected.
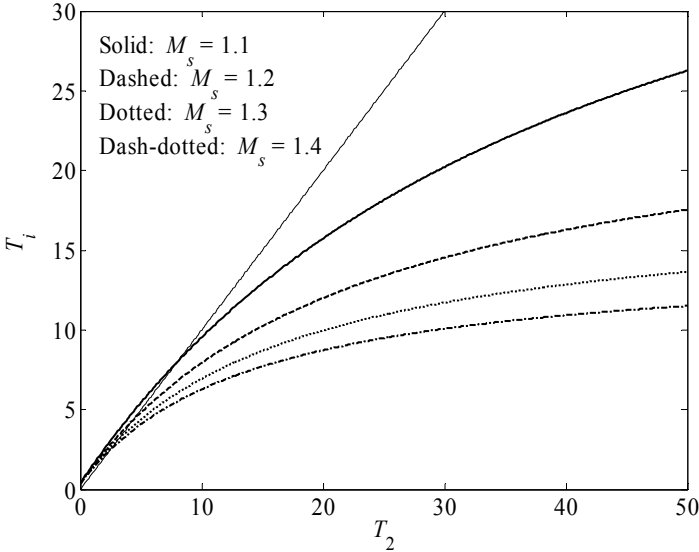
Figure 5.5 The integral time, T_i, as function of the time constant T_2, for the PI tuning rule. For small T_2, the two variables are almost equal, otherwise T_i is smaller that T_2. The thin solid line shows $T_i = T_2$, as a comparison. This is also suggested in a tuning method by [Nelson and Gardner, 1996].

If the time delay in the IPZ-model is very short, the gain will become increasingly large and the integral time short, in the formulas above. This is theoretically correct, since the constraint is still fulfilled for the control loop. By considering the root locus of the feedback loop and assuming $L = 0$, shown in Figure 5.6, we can see that an increasing gain does not move any of the closed loop poles into the right half plane. Neither by varying the integral time, the loop will become unstable at any time as long as it is positive. There is no limitation because of system dynamics. It has infinite gain margin and any combination of positive k_c and T_i can be achieved. But, high controller gain amplifies measurement noise and gives large control signals, which will saturate actuators. Limitations are instead given by [Åström, 2000b]

- Sensor noise

- Unmodeled process dynamics

- Actuator saturation

- Admissible control signal variations

- Sensor and actuator resolution

We can conclude that the dead time of the process is directly related to the stability of the feedback system. However, it is unusual to obtain a dead time equal to zero, when identifying the steam pressure process, partly because of the sample time in today's discrete DCS-systems. Thus, this should not impose large restrictions to the usefulness of the method.

In Figure 5.7 and Figure 5.8 simulations of an IPZ-tuned PI controller for different values of M_s and with $\beta = 1$ or $\beta = 0$. The process is given by

$$P(s) = 0.01 \frac{(200s + 1)}{s(20s + 1)} e^{-s}. \tag{5.7}$$

With $\beta = 0$ the control signal smoother and the overshoot smaller for the step in set point compared to the case with $\beta = 1$. This can also be accomplished with a more sophisticated set point filter. Remember that the IPZ tuning is based on optimization of disturbance rejection and can with advantage be combined with e.g. the 2DOF-controller described in Section 3.3.

Remark 1
By looking at the root locus in Figure 5.6, an interesting observation can be made. If the dead time is not dominating the process dynamics, higher controller gain makes the closed loop system less oscillatory. This counter-intuitive phenomenon can also be seen when controlling a pure integrating process with a PI or PID controller.
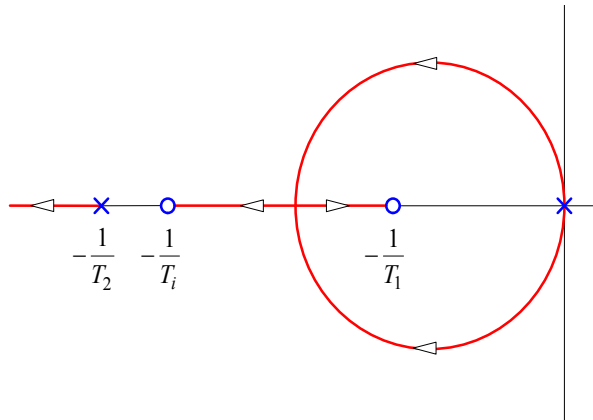
Figure 5.6 The root locus for the IPZ-process in connection with a PI controller for the case $T_1 > T_i > T_2$. Good tuning normally requires $T_1 \gg T_i \approx T_2$.

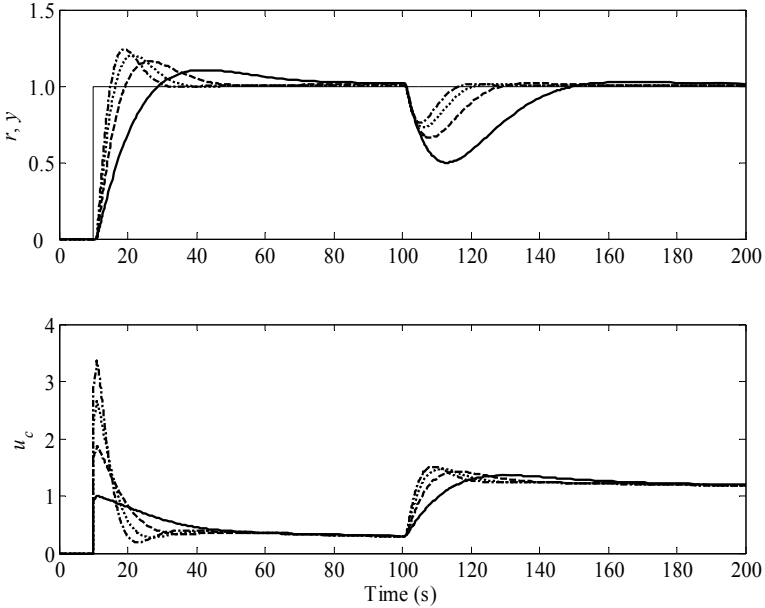**Figure 5.7** Closed loop response of (5.7) and an IPZ-tuned PI controller for $M_s = 1.1$ (solid), $M_s = 1.2$ (dashed), $M_s = 1.3$ (dotted), and $M_s = 1.4$ (dash-dotted). $\beta = 1$.
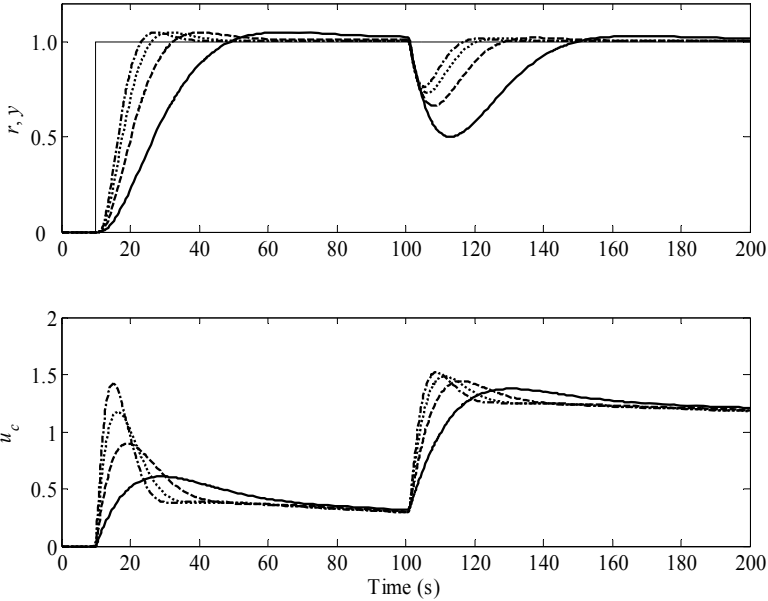

Figure 5.8 Simulation with the same process and controller as in Figure 5.7 but with $\beta = 0$.

Remark 2

The root locus also shows why the open loop zero in the process can not be canceled by a PI controller, as discussed in Chapter 3. It is only by having infinite controller gain that one of the feedback poles will reach the process zero in $-1 / T_1$.

Remark 3

The feature of the IPZ-tuning, to give a non-realizable controller when the process dead time is zero, is not unique for this method. Many other tuning methods for minimum phase systems have the same property, see e.g. [Ziegler and Nichols, 1942], [Chien, *et al*, 1952], [Cohen and Coon, 1953], [Ho, *et al*, 1995], [Poulin and Pomerleau, 1999], and [Visioli, 2001].

Remark 4

Small values of T_2 will generally give a short integral time, T_i by the IPZ-tuning. Then it is also important to consider the sample time so that the process is sampled sufficiently fast [Åström and Hägglund, 2005].

5.3 The IPZ tuning rule for PID control

The same technique used in the previous section was also used to obtain tuning parameters for the PID controller. Using (3.20a) the high frequency gain for the open loop system is

$$\lim_{\omega \to \infty} \left| k_c k_v \left(1 + \frac{1}{T_i i \omega} + T_d i \omega \right) \frac{1 + i \omega T_1}{i \omega (1 + i \omega T_2)} e^{-i \omega L} \right| = \frac{k_c k_v T_1 T_d}{T_2}. \qquad (5.8)$$

Physically this means that the open loop system has infinite bandwidth which is unrealistic. To obtain a finite bandwidth, (3.20b) is used instead, where N is chosen to 10. The result for $M_s = 1.1$ is shown in Figure 5.9. The integral time proves to have a more complex appearance that in the case of PI control, compare to Figure 5.4. This is also the case for the derivative time and therefore second-degree curves have been fitted to the optimal parameters, except for the controller gain. The resulting controller parameters are given in (5.9). We see that the equations are a bit more complex than compared to PI control (5.6), but have the same property of giving infinite controller gain and zero integral time for zero dead time.

   In Figure 5.10 and Figure 5.11 simulations of an IPZ-tuned PID controller for different values of M_s and with $\beta = 1$ or $\beta = 0$.
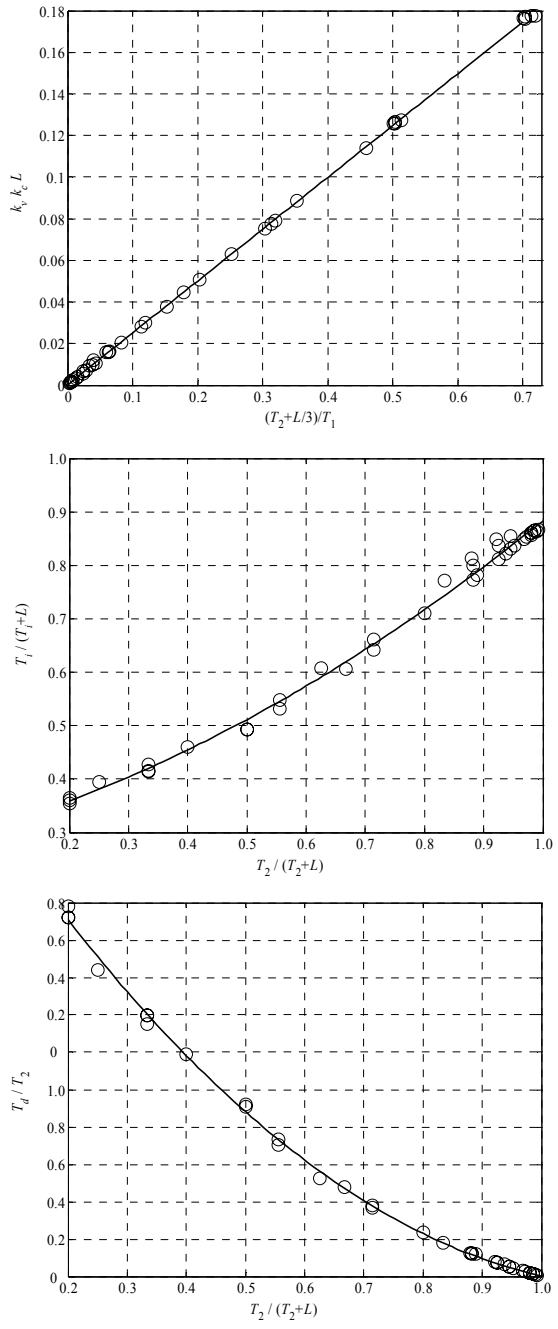
Figure 5.9 The relationship between the PID controller parameters and process parameters for $M_s = 1.2$.

$$M_s = 1.1: \quad \begin{aligned} k_c &= \frac{3T_2 + L}{22k_v T_1 L} \\[2mm] T_i &= \frac{L(472T_2^2 + 471T_2 L + 146L^2)}{(28T_2^2 + 529T_2 L + 354L^2)} \\[2mm] T_d &= \frac{T_2(7T_2^2 + 264T_2 L + 1359L^2)}{1000(T_2^2 + 2T_2 L + L^2)}, \quad N = 10 \end{aligned}$$

$$M_s = 1.2: \quad \begin{aligned} k_c &= \frac{3T_2 + L}{12k_v T_1 L} \\[2mm] T_i &= \frac{L(883T_2^2 + 875T_2 L + 286L^2)}{3(39T_2^2 + 375T_2 L + 238L^2)} \\[2mm] T_d &= \frac{T_2(T_2^2 + 361T_2 L + 1400L^2)}{1000(T_2^2 + 2T_2 L + L^2)}, \quad N = 10 \end{aligned}$$

$$(5.9)$$

$$M_s = 1.3: \quad \begin{aligned} k_c &= \frac{3(3T_2 + L)}{26k_v T_1 L} \\[2mm] T_i &= \frac{L(835T_2^2 + 842T_2 L + 277L^2)}{3(55T_2^2 + 386T_2 L + 241L^2)} \\[2mm] T_d &= \frac{2T_2(3T_2^2 + 176T_2 L + 736L^2)}{1000(T_2^2 + 2T_2 L + L^2)}, \quad N = 10 \end{aligned}$$

$$M_s = 1.4: \quad \begin{aligned} k_c &= \frac{3(3T_2 + L)}{20k_v T_1 L} \\[2mm] T_i &= \frac{L(786T_2^2 + 851T_2 L + 278L^2)}{214T_2^2 + 1149T_2 L + 722L^2)} \\[2mm] T_d &= \frac{T_2(8T_2^2 + 367T_2 L + 1443L^2)}{1000(T_2^2 + 2T_2 L + L^2)}, \quad N = 10 \end{aligned}$$
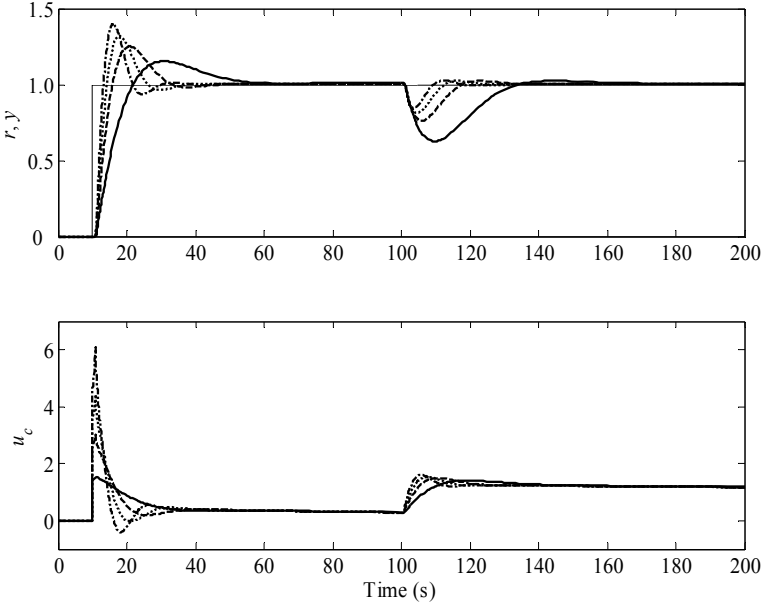
Figure 5.10 Closed loop response of (5.7) and an IPZ-tuned PID controller for $M_s = 1.1$ (solid), $M_s = 1.2$ (dashed), $M_s = 1.3$ (dotted), and $M_s = 1.4$ (dash-dotted). $\beta = 1$ and $\gamma = 0$.
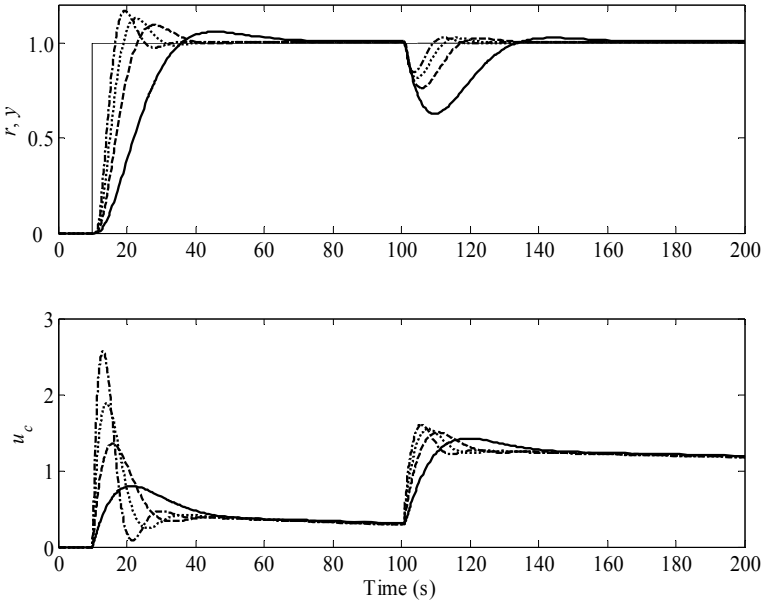

Figure 5.11 Simulation with the same process and controller as Figure 5.10 but with $\beta = 0$.

5.4 Stability regions

A nice tool to graphically examine stability is stability regions [Åström and Hägglund, 2001]. It will be used here to relate the parameters suggested by the IPZ-tuning and the stability boundary. It will later be applied in Section 5.7 also, when comparing other tuning methods. Obviously, staying inside this boundary does not automatically imply good tuning, only that the closed loop is stable. Start by writing the process as

$$G(i\omega) = r(\omega)e^{i\varphi(\omega)} = r(\omega)\big(\cos\varphi(\omega) + i\sin\varphi(\omega)\big), \qquad (5.10)$$

and let the controller be given by

$$C(s) = k_c + \frac{k_i}{s} + k_d s, \qquad (5.11)$$

where $k_d = k_c T_d$. The condition for oscillation is then given by Nyquist's theorem

$$G(i\omega)C(i\omega) = r(\omega)\big(\cos\varphi(\omega) + i\sin\varphi(\omega)\big)\left(k - i\frac{k_i}{\omega} + ik_d\omega\right) = -1. \quad (5.12)$$

Identifying the real and imaginary parts, we find that the boundary of the stability region can be represented by

$$k_c = -\frac{\cos\varphi(\omega)}{r(\omega)}, \quad k_i = \omega^2 k_d - \frac{\omega\sin\varphi(\omega)}{r(\omega)}. \qquad (5.13)$$

For the IPZ process, we have

$$r(\omega) = k_v \frac{(1 + \omega^2 T_1^2)^{0.5}}{\omega(1 + \omega^2 T_2^2)^{0.5}}, \qquad (5.14)$$

$$\varphi(\omega) = \arctan(\omega T_1) - \arctan(\omega T_2) - \frac{\pi}{2} - \omega L.$$

Figure 5.12 and Figure 5.13 show examples of stability regions and IPZ-tuning. The IPZ-tuning gives parameters rather distant from the boundary
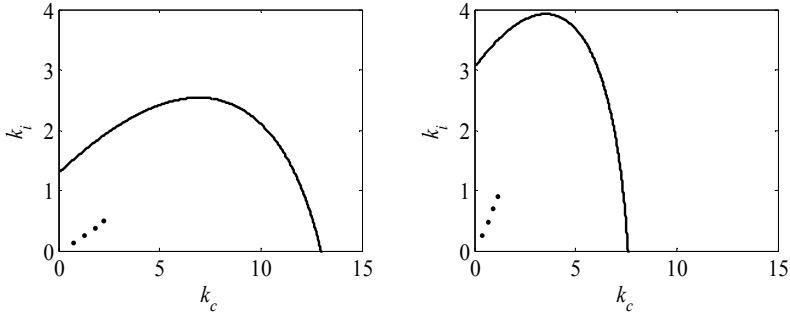
Figure 5.12 Stability regions for the IPZ-process controlled by a PI controller. Left: $k_v = 0.005$, $T_1 = 50$, $T_2 = 5$, $L = 3$; Right: $k_v = 0.001$, $T_1 = 200$, $T_2 = 1$, $L = 2$. The points indicate the position of the IPZ-tuning for the different M_s-values in (5.6). The indications are moving from the origin to larger k_c and k_i with larger M_s.
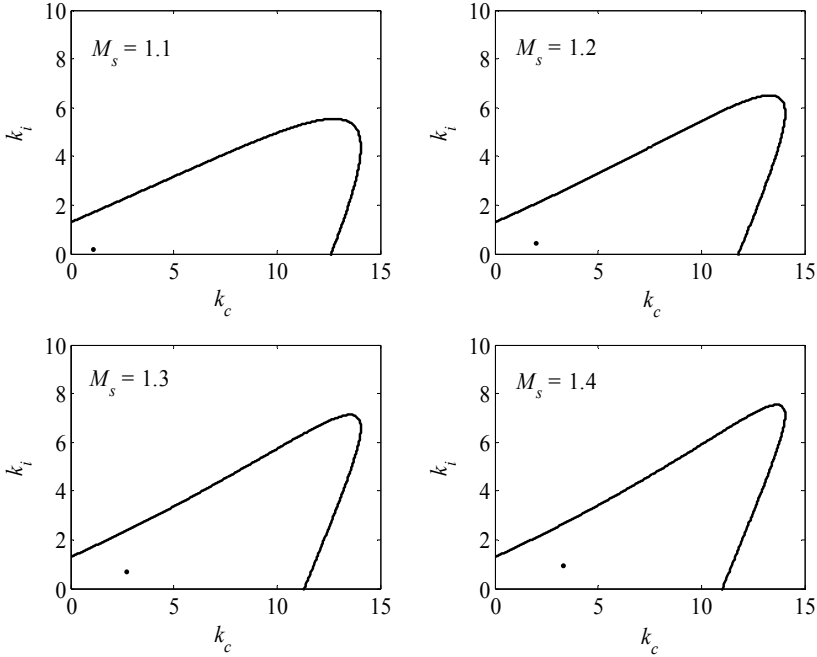
Figure 5.13 Stability region for the IPZ-process controlled by a PID controller. The process is given by $k_v = 0.005$, $T_1 = 50$, $T_2 = 5$, $L = 3$. The stability region forms a three dimensional surface in the k_c–k_i–k_d plane. Here, it is visualized in two dimensional plots by looking at the k_c–k_i plane for the optimal k_d (constant in each plot) given by the IPZ-tuning rule.

114

of stability. With higher robustness (lower M_s-values), the tuning moves closer to the origin. With lower robustness, the proposed tuning moves in direction to the maximum k_i-value in the stability region. This implies that if we assume a stable controller, there is lower boundary for the achievable IE, for a given process. Also, note that, if the dead time of the IPZ-process is zero, the stability region fills the whole first quadrant, and any and k_i is feasible.

5.5 Industrial verification of the tuning rule

To verify the tuning rule it has been tested on a real paper machine, for a PI controller and different M_s-values. It is the first group in a fluting machine consisting of five cylinders. The process transfer function has been obtained from a step response and is given by

$$P(s) = 0.0196 \frac{(51.6s + 1)}{s(7.79s + 1)} e^{-1.30s}. \tag{5.15}$$

The controller settings are calculated for all the values of the maximum sensitivity function in (5.6) and the obtained values are given in Table 5.1. The results are presented in Figure 5.14 and Figure 5.15 by a series of closed loop step responses.

Table 5.1 The controller settings for (5.15)

	K_c	T_i
M_s=1.1	0.56	7.1
M_s=1.2	1.0	5.8
M_s=1.3	1.4	5.0
M_s=1.4	1.8	4.5

The step responses in the figures and the table show very well the difference between various values of the tuning parameter M_s. A higher value provides a more quick response and tighter control, but the valve must also work harder. This is essential to remember since an aggressive control signal can introduce disturbances in adjacent dryer groups through the steam header and must be considered when tuning a whole drying section of a paper machine.
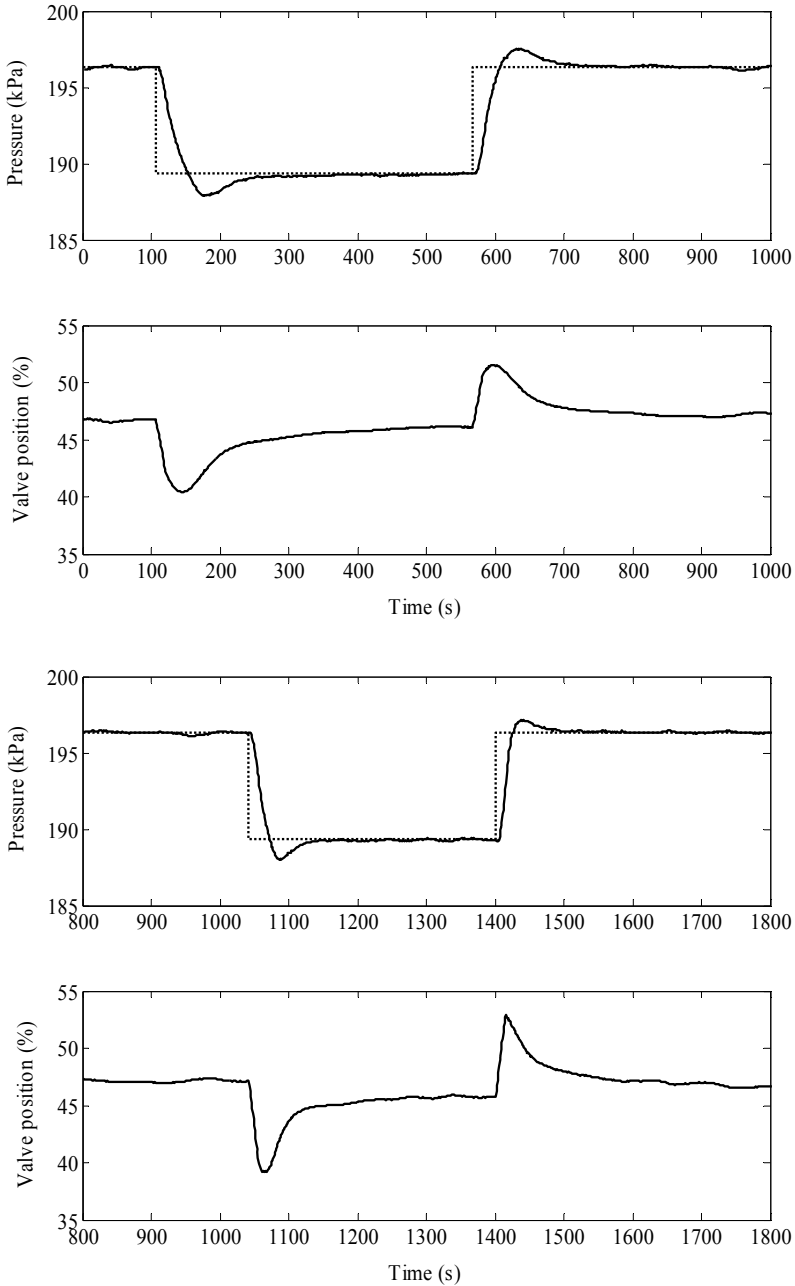
Figure 5.14 Experiment on a real paper machine showing a closed loop step response, using IPZ-tuning for a PI controller. $M_s = 1.1$ (above) and $M_s = 1.2$ (below). Controller parameters $\beta = 1$.
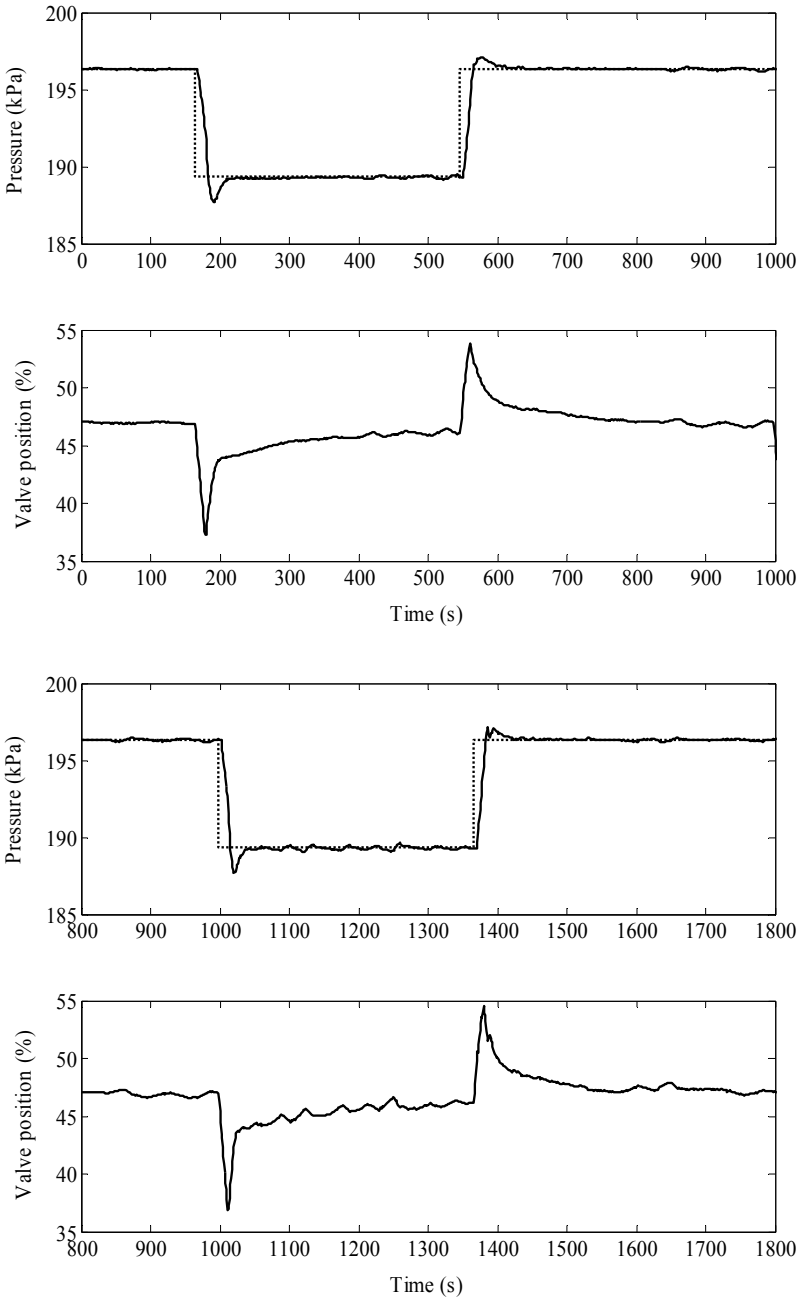
Figure 5.15 Experiment on a real paper machine showing a closed loop step response, using IPZ-tuning for a PI controller. $M_s = 1.3$ (above) and $M_s = 1.4$ (below). Controller parameter $\beta = 1$.

117

Another important issue is the steam load to the boiler house. Large variations in the paper machines steam demand can put out the recovery boiler and this has to be considered when tuning the drying section too.

For $M_s = 1.4$, a high frequency component becomes evident, most easily seen at $t = 1000 - 1400$. This is probably due to actuator nonlinearities or disturbances (as a result of the tuning, some disturbance frequencies are amplified by 40 %).

5.6 Comparison between PI and PID control

An interesting question is if PID control gives any enhanced performance compared to PI control, in the case of an IPZ-process. It is a well-known fact that for a first-order process, PI control is adequate (two closed loop poles and two controller parameters) and for high order process dynamics, derivative action can speed up the response [Åström and Hägglund, 2005]. Also, if the dynamics are delay dominated, derivative action gives modest performance improvements compared to PI control but derivative action gives significant improvements for processes that are lag dominated.

To evaluate this for the IPZ-process the integral error (IE) is calculated for a few different processes and M_s-values, when a unit step disturbance acts on the system, see Table 5.2. The table clearly shows a large difference in IE when comparing PI and PID control for the same IPZ-process. The integrated area is more or less reduced by a factor two by derivative action. What happens is that the derivative-term increases the phase margin by adding phase lead to the open loop system, making it possible to increase the integral gain without changing the stability margin. So it seems that a PID control is superior to PI control in this sense. But there are a few more other central aspects to regard.

Table 5.2 Controller settings for both PI and PID control, giving minimal IE w.r.t the maximum sensitivity constraint. Row three is marked in italics to highlight the settings used for the example in Figure 5.12.

M_s	k_v	T_1	T_2	L	k_c	T_i	k_c	T_i	T_d	IE PI	IE PID
1.2	0.01	400	40	4	0.42	22.9	0.64	15.89	1.88	54.52	24.83
1.2	0.01	100	8	1	1.35	5.0	2.05	3.57	0.48	3.70	1.74
1.2	*0.01*	*50*	*15*	*3*	*1.74*	*13.7*	*2.63*	*10.15*	*1.37*	*7.87*	*3.86*
1.2	0.01	25	2	1	1.47	1.9	2.33	1.68	0.45	1.29	0.72
1.4	0.01	400	40	4	0.72	17.0	1.10	10.45	1.97	23.61	9.50
1.4	0.01	100	8	1	2.29	3.8	3.52	2.42	0.50	1.66	0.69
1.4	0.01	50	15	3	2.91	10.5	4.51	6.98	1.45	3.61	1.55
1.4	0.01	25	2	1	2.51	1.7	3.92	1.33	0.49	0.68	0.34
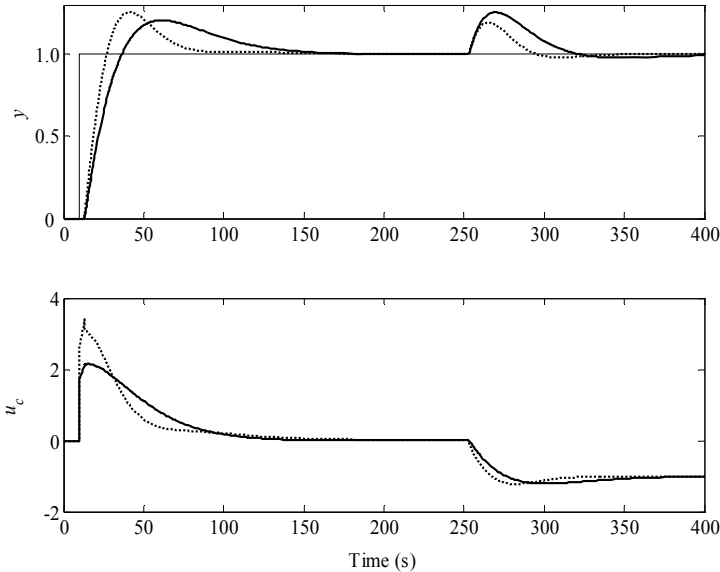
Figure 5.16 Comparison between a PI controller (solid) and a PID controller (dotted) regulating (5.16). Both controllers are tuned for $M_s = 1.2$, see Table 5.2. The other controller parameters are chosen as $\beta = 1$, $\gamma = 0$, $N = 10$, see (3.20b). There is a set point change at $t = 10$, and a load disturbance starting at $t = 250$ s.

Apart from the disturbance rejection, set point following is also an important property for the closed loop system. Figure 5.16 shows both a set point change and a load disturbance, acting on the process

$$P(s) = 0.01\frac{1+50s}{s(1+15s)}e^{-3s}. \tag{5.16}$$

The figure clearly shows that the PID controller puts back the process value to the set point more quickly than the PI controller during the load disturbance. The process also reacts faster to a set point change with the PID controller. However, in both those cases the control signal is slightly more aggressively used by the PID, which might be a disadvantage due to cross couplings to adjacent steam groups and increased variations in the steam demand to the boiler house.

Figure 5.17 shows the gain of the transfer function from r to y and also the sensitivity function. Figure 5.18 shows the corresponding Nyquist curves. The PID controller gives a somewhat larger peak in the amplitude curve for G_{ry}. However, this can be adjusted by the feedforward parameters β and γ of the PID controller, or by a more general set point

119
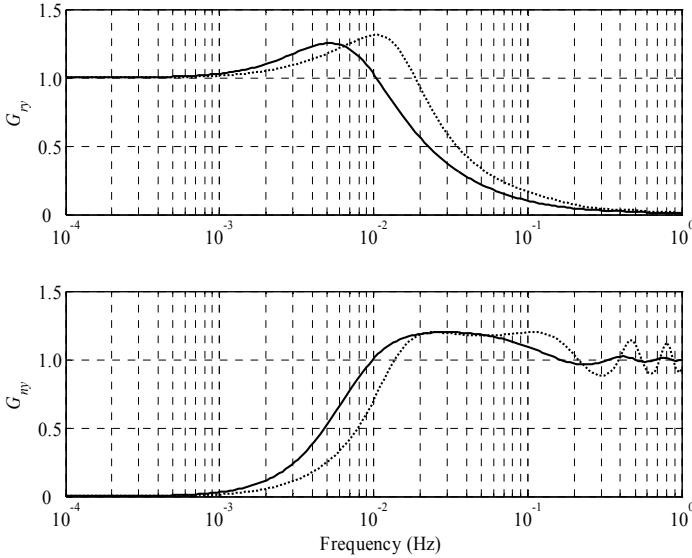
Figure 5.17 Amplitude diagram for the transfer functions from set point *r* to process output *y*, G_{ry}, and from noise *n* to process output *y*, G_{ny}. G_{ny} is equal to the sensitivity function and G_{ry} is equal to the complementary sensitivity function, if $\beta = 1$ and $\gamma = 1$. PI − solid, and PID − dotted. Note that the maximum sensitivity is equal for the to controllers as the tuning prescribes.
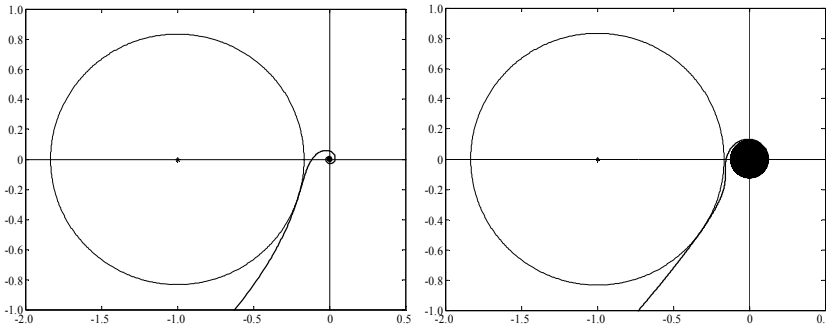
Figure 5.18 Nyquist curves for the marked controllers in Table 5.2 and the process in (5.16), PI − left, PID − right. An often occurring difference between the two optimized Nyquist curves is that for the PID controller the curve touches the M_s-circle in two points but only once for the PI controller. This can also be seen in the sensitivity function in Figure 5.17.

filter, so this is actually not an issue of the feedback loop. The sensitivity function shows that some disturbances are amplified more by the PID controller. By looking at the spectrum of pressure disturbances in Figure 2.18, it can be seen that this extra peak in the sensitivity function

coincides with the variations found in that specific case study. Therefore, the gain of higher performance by PID control is put in the shade by the amplification of specific disturbances (the problem should evidently be resolved by finding the root cause of the disturbances and resolve it, if possible).

The IPZ-tuning, presented in this chapter, is based on stability of the closed loop system and disturbance rejection, and does not give any recommendations on the feedforward settings. However, in Chapter 3 a two-degree-of-freedom controller structure with set point feedforward is given that can be combined with the PI or PID controller. Then the regulation problem and servo problem are separated in a nice way and a design procedure is given for both.

The conclusion is that PID control of the IPZ-process is more effective than PI control but it will give a controller with slightly more aggressive use of the control signal, and also a bit more over-shoot in the set point response for the standard PID structure. It is therefore difficult to dogmatically say that the one or the other is better. It simply depends on how sensitive the steam system is to disturbances and how severe the cross-couplings between the different steam groups are.

5.7 Comparison to other design methods

This chapter has presented a tuning method for a PI and PID controller regulating an IPZ-process. Many different tuning methods have been presented previously, but they mostly suppose a first or second-order process, see e.g. [Chien, *et al*, 1952], [Cohen and Coon, 1953], [Zhuang and Atherton, 1993], [Ho, *et al*, 1996], and [Skogestad, 2003], or an integrating process, see e.g. [Poulin and Pomerleau, 1999], [Wang and Cai, 2001], [Visioli, 2001], and [Chidambaram and Sree, 2003]. Since the IPZ-process is not a self-regulating process, it is most natural to use the latter. However, it is not obvious how to match the IPZ-process to a pure integrator and these methods do not always give a satisfactory result. Nevertheless, there a few examples, which are modifications of the Ziegler-Nichols method that give reasonable tuning, e.g. [Tyreus and Luyben, 1992], and [Poulin and Pomerleau, 1999], but these methods have no design parameter which is a deficiency.

In this section, a few design methods found in the literature are examined to see how well they are compared to IPZ-tuning. The purpose is not to discredit these methods but to demonstrate the need for a new

tuning method for the steam pressure process. All examples are based on the process model

$$P(s) = 0.05 \frac{1 + 100s}{s(1 + 20s)} e^{-s}. \tag{5.17}$$

The simulations of IPZ-tuning use $M_s = 1.2$ and $M_s = 1.3$, while the obtained M_s-value for the other design methods are also given for a comparison. Remember that these other methods are sometimes based on a different criterion than the IPZ-tuning. The resulting parameters for the IPZ-tuning are

$$M_s = 1.2 \quad \text{PI:} \quad k_c = 0.67, \ T_i = 8.1,$$

$$M_s = 1.3 \quad \text{PI:} \quad k_c = 0.92, \ T_i = 6.4,$$

$$M_s = 1.2 \quad \text{PID:} \quad k_c = 1.0, \ T_i = 5.3, \ T_d = 0.41,$$

$$M_s = 1.3 \quad \text{PID:} \quad k_c = 1.4, \ T_i = 3.9, \ T_d = 0.49.$$

(5.18)

5.7.1   Ziegler-Nichols two tuning methods

The Ziegler-Nichols rules are the most famous tuning rule for the PID controller [Ziegler and Nichols, 1942]. It was presented in 1942 and consists of two different methods. One is based on frequency response data (a closed loop test) and the other one is a step test method (an open loop test). Both these methods are known to give only reasonable performance. Nevertheless, they are used here for comparison due to their widespread use.

The frequency method

The frequency method uses information of one point in the Nyquist curve, namely the frequency where $k_c P(i\omega)$ pass through the point -1. This point can be found without knowing the transfer function $P(s)$ by a straightforward closed loop experiment. Simply disable any integral or derivative action and increase the controller gain until a stable oscillation is achieved. This gain is called the ultimate gain, k_0, and the oscillation period is T_0. The controller settings are then
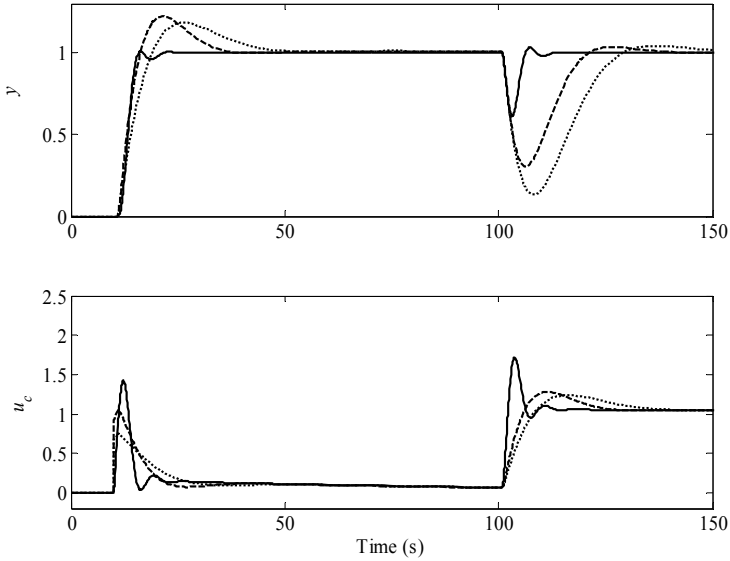
Figure 5.19 Evaluation of Ziegler-Nichols frequency response method for PI control (solid line) given the process in (5.17). Also shown is the IPZ-tuning for $M_s = 1.2$ (dotted) and $M_s = 1.3$ (dashed).
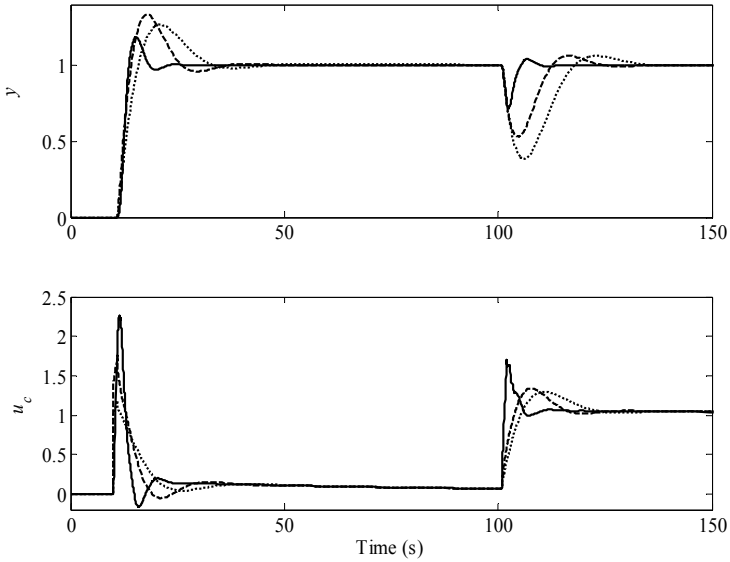
Figure 5.20 Evaluation of Ziegler-Nichols frequency response method for PID control (solid line) given the process in (5.17). Also shown is the IPZ-tuning for $M_s = 1.2$ (dotted) and $M_s = 1.3$ (dashed).

123
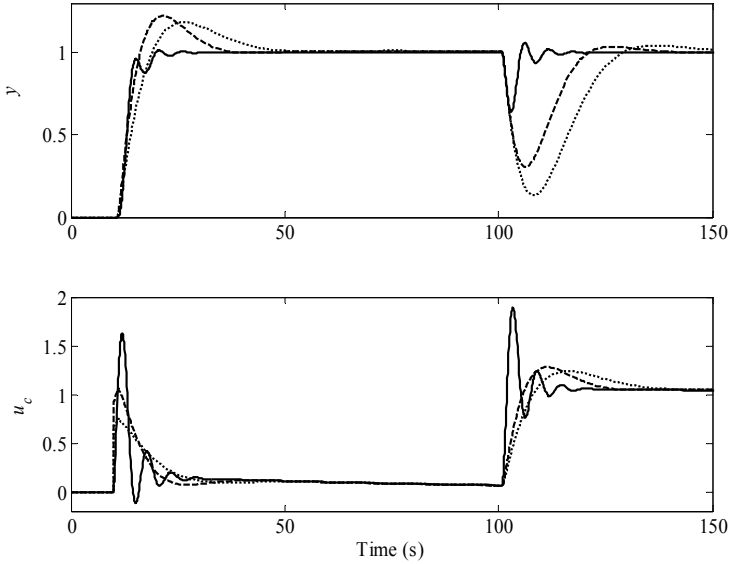
Figure 5.21 Evaluation of Ziegler-Nichols step response method for PI control (solid line) given the process in (5.17). Also shown is the IPZ-tuning for $M_s = 1.2$ (dotted) and $M_s = 1.3$ (dashed).
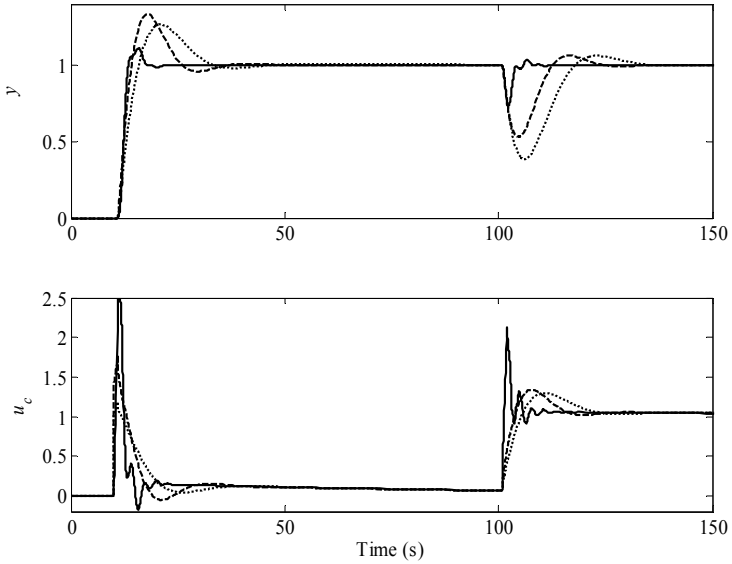
Figure 5.22 Evaluation of Ziegler-Nichols step response method for PID control (solid line) given the process in (5.17). Also shown is the IPZ-tuning for $M_s = 1.2$ (dotted) and $M_s = 1.3$ (dashed).

$$\text{PI:} \quad k_c = 0.45k_0, \quad T_i = \frac{T_0}{1.2}, \tag{5.19}$$

and

$$\text{PID:} \quad k_c = 0.6k_0, \quad T_i = \frac{T_0}{2}, \quad T_d = \frac{T_0}{8}. \tag{5.20}$$

The ultimate gain and oscillation period can also be calculated directly from the transfer function. Assume the IPZ process and a P controller. The condition for the point of instability is

$$k_c \frac{1 + sT_1}{s(1 + sT_2)} e^{-sL} = -1. \tag{5.21}$$

By letting $s = i\omega$, and equating the complex and real parts, the following controller settings and M_s-values are obtained

$$\text{PI:} \ k_c = 2.87, \ T_i = 3.28, \quad M_s = 2.7, \tag{5.22}$$

and

$$\text{PID:} \ k_c = 3.83, \ T_i = 1.97, \ T_d = 0.49, \quad M_s = 2.55. \tag{5.23}$$

As mentioned before, the Ziegler-Nichols method is known to give oscillatory results and it is no surprise that the maximum sensitivity functions are very high. Figure 5.19 shows simulation results for PI control and Figure 5.20 shows results for PID control. In both cases, it is related to IPZ-tuning, even though they are not completely comparable. This is since the simulated IPZ-tuning has different M_s-values. Figure 5.21 and Figure 5.22 show the corresponding simulations for the step response method, which is presented next.

The step test method

The step test method is based on two parameters of an open loop step test, *a* and *L*, see Figure 5.23. They are achieved by finding the point of inflection, which is the point where the response has the maximum derivative. The tangent through this point gives the two parameters of interest. The method now suggests the controller settings as
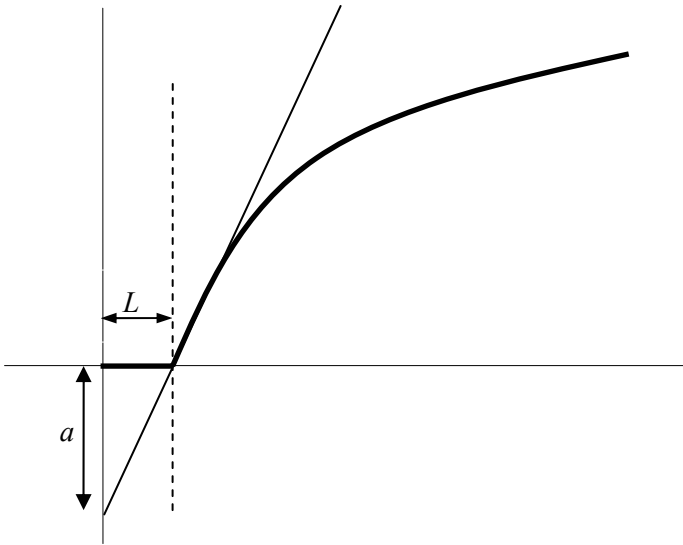
Figure 5.23 The two parameters used in the Ziegler-Nichols step response method.

$$\text{PI:} \qquad k_c = \frac{0.9\Delta u_c}{aL}, \quad T_i = 3.33L, \qquad (5.24)$$

and

$$\text{PID:} \qquad k_c = \frac{1.2\Delta u_c}{aL}, \quad T_i = 2L, \quad T_d = 0.5L, \qquad (5.25)$$

where Δu_c is the size of the step. Like in the case of the frequency method, (5.17) is examined by a simulation. The obtained settings are

$$\text{PI: } k_c = 3.6, \, T_i = 3.33, \quad M_s = 3.8 \qquad (5.26)$$

and

$$\text{PID: } k_c = 4.8, \, T_i = 2, \, T_d = 0.5, \quad M_s = 4.3. \qquad (5.27)$$

The controller settings are somewhat more aggressive than in the frequency response method. This is also confirmed in the simulations.

5.7.2   Tyreus-Luyben's modified ZN tuning rule

The Ziegler-Nichols tuning rules are derived to give decay ratio of ¼. For many process control system this is too aggressive, which led [Tyreus and Luyben, 1992] to derive a more conservative PI tuning rule. The method is obtained by maximizing the closed loop resonant frequency given a maximum complementary sensitivity function of 2 dB (≈ 1.26). The result is given by

$$\text{PI:} \quad k_c = \frac{k_0}{3.22}, \quad T_i = 2.2T_0, \tag{5.28}$$

where k_0 and T_0 is defined as in Section 5.7.1. This gives the following values for the process in (5.17)

$$\text{PI:} \; k_c = 1.97, \, T_i = 8.66, \quad M_s = 1.65 \tag{5.29}$$

Figure 5.24 shows the simulation results and the method gives a reasonable good tuning. However, the maximum complementary sensitivity function is different (in this case 1.16) from the value prescribed by the method, since it is derived for a different process. Both the set point response and disturbance rejection is faster than the IPZ-tuning, but it is also less robust (larger M_s) and the control signal is much more aggressive. As a comparison, Figure 5.25 shows IPZ-tuning for $M_s = 1.65$. The disturbance rejection is then better for IPZ-tuning than Tyreus-Luyben's tuning rule. The time to reach a new set point is similar for the two methods even though the size of the over-shoot is different. Remember that the over-shoot should be dealt with the feedforward part of the controller, if necessary.

As for the case of Ziegler-Nichols, the Tyreus-Luyben method lacks a tuning parameter.

5.7.3   The AMIGO tuning rule

The AMIGO-rule [Åström and Hägglund, 2005] is developed in a similar way as the IPZ-rule, with $M_s = 1.4$. However, a test batch of nine different process structures have been used (IPZ not included), and the method presumes that the process can be approximated by either a first-order system or an integrator. Given the system

$$P(s) = \frac{k_v}{s} e^{-sL}, \tag{5.30}$$

127
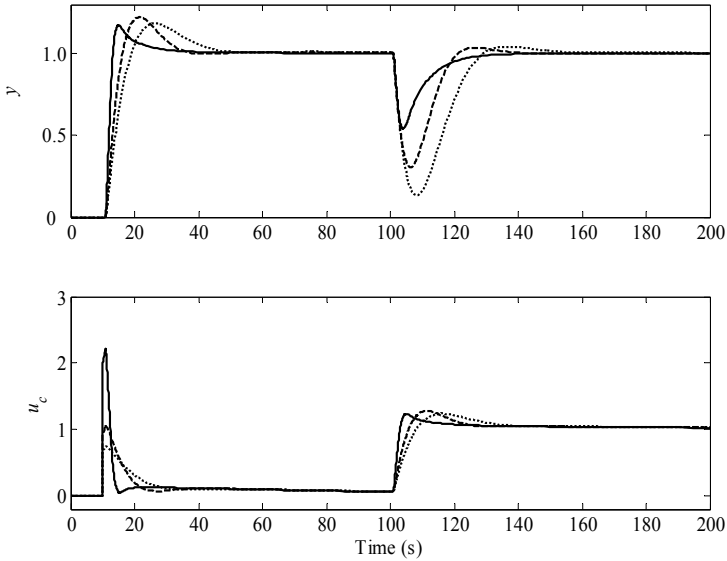
Figure 5.24 Evaluation of Tyreus-Luyben's method for PI control (solid line) given the process in (5.17). Also shown is the IPZ-tuning for $M_s = 1.2$ (dotted) and $M_s = 1.3$ (dashed).
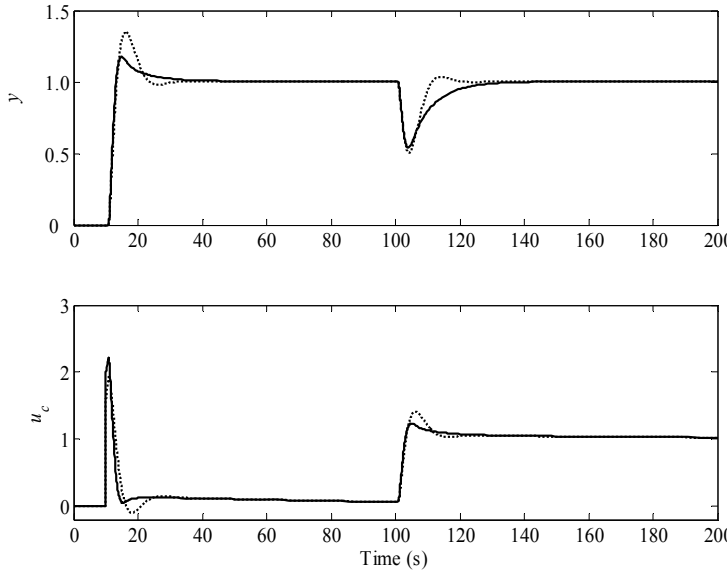
Figure 5.25 Evaluation of Tyreus-Luyben's method for PI control (solid line) given the process in (5.17). Also shown is the IPZ-tuning for $M_s = 1.65$ (dotted) ($k_c = 1.57$, $T_i = 4.09$).

Figure 5.26 Evaluation of the AMIGO tuning rule for PI control (solid line) given the process in (5.17). Also shown is the IPZ-tuning for $M_s = 1.2$ (dotted) and $M_s = 1.3$ (dashed).

Figure 5.27 Evaluation of the AMIGO tuning rule for PID control (solid line) given the process in (5.17). Also shown is the IPZ-tuning for $M_s = 1.2$ (dotted) and $M_s = 1.3$ (dashed).

129

the proposed tuning rule is

$$\text{PI: } k_c = \frac{0.35}{k_v L}, \quad T_i = 13.4L, \tag{5.31}$$

$$\text{PID: } k_c = \frac{0.45}{k_v L}, \quad T_i = 8L, \quad T_d = 0.5L. \tag{5.32}$$

The next step is to match the IPZ-process to a pure integrator with time delay. By letting k_i be equal to the maximum slope of a unit step response of the IPZ-process, (3.5) gives

$$k_v = \frac{k_v T_1}{T_2}. \tag{5.33}$$

The time delay, L, is equal to the time delay of the true process. Assuming (5.17), the controller settings and obtained maximum sensitivity are

$$\text{PI: } k_c = 1.4, \ T_i = 13.4, \quad M_s = 1.4, \tag{5.34}$$

and

$$\text{PID: } k_c = 1.8, \ T_i = 8, \ T_d = 0.5, \quad M_s = 1.4. \tag{5.35}$$

Figure 5.26 and Figure 5.27 show the simulations. We observe the AMIGO rule gives a pleasant performance for this process. There is less over-shoot in the set point response, compared to the IPZ-tuning and the controllers also bring back the process output to the set point nicely at a load disturbance.

However, if we instead let the process be given by

$$P(s) = 0.01 \frac{1 + 100s}{s(1 + 10s)} e^{-3s} \tag{5.36}$$

we get the tuning

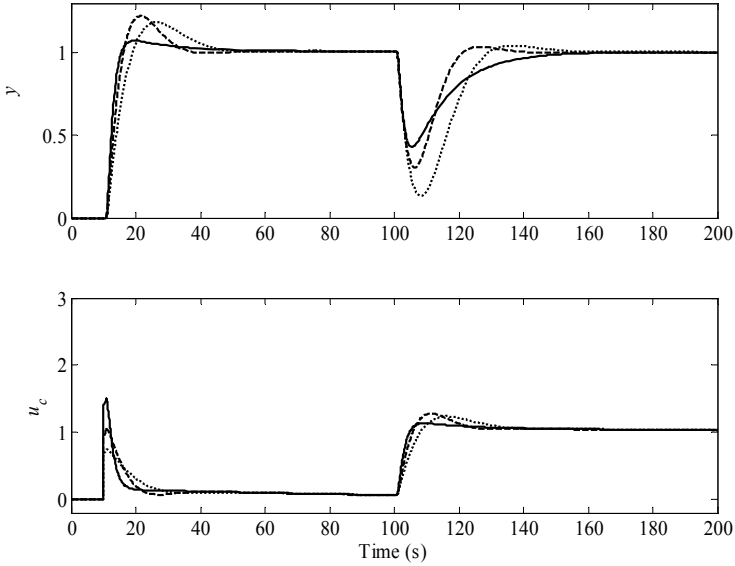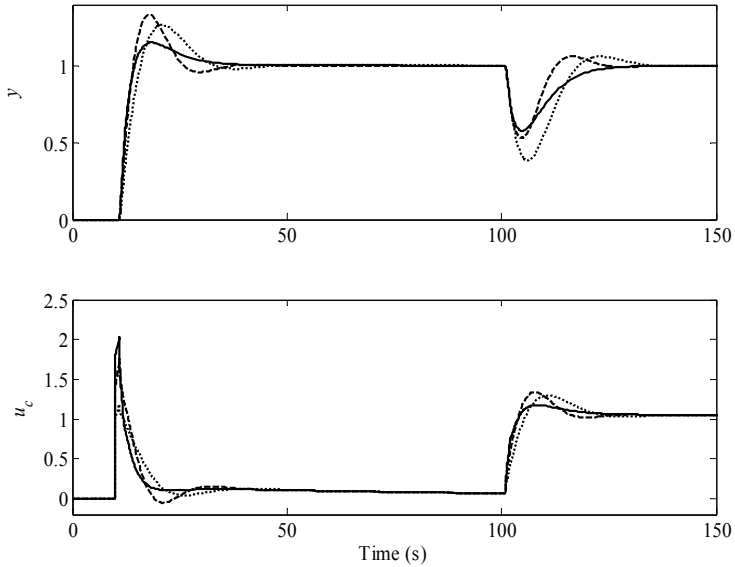$$\text{PI: } k_c = 1.17, \ T_i = 40.2, \quad M_s = 1.3, \tag{5.37}$$
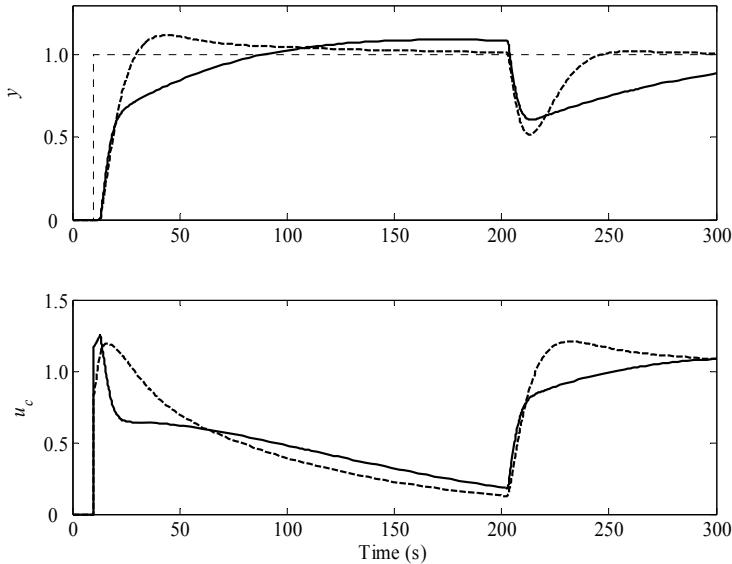
Figure 5.28 Evaluation of the AMIGO tuning rule for PI control (solid line) given the process in (5.36). Also shown is the IPZ-tuning for $M_s = 1.3$ (dashed).

and

$$\text{PID: } k_c = 1.5,\ T_i = 24,\ T_d = 1.5, \quad M_s = 1.4. \tag{5.38}$$

Figure 5.28 shows the simulation for (5.37) compared with one case of IPZ-tuning. The AMIGO tuning does not give a satisfactory result at all for this process. Note that the two controllers in the figure have the same robustness measure but still very different performance.

5.7.4 Pole placement

The idea of pole placement is to find a controller that gives a closed-loop system with a specified characteristic polynomial. In Chapter 3, this was introduced by state-feedback and all closed loop poles could be placed arbitrarily. This is not always possible when the process is controlled by a PI or PID controller. In the general case, a PI controller can give the characteristic polynomial arbitrary values for a first-order process, and a PID controller handles the same thing for a second-order process. It is clear that it is possible to find a good controller with such a general tuning method as pole placement. The difficulty can be to know where to place the poles to obtain a satisfactory feedback loop. The design method is shown by a few examples.

Nelson-Gardner's pole placement rule for PI control

In [Nelson and Gardner, 1996] a tuning rule for the IPZ process is given, that is derived from simple pole placement. It can also be found in one of the exercises in [Sell, 1995], written by Bill Bialkowski, but not as detailed. In both references the idea is given in words without carrying out the calculations and the time-delay is disregarded. Let the process be given by

$$P(s) = k_v \frac{(1+sT_1)}{s(1+sT_2)} e^{-sL} \approx k_v \frac{(1+sT_1)(1-sL)}{s(1+sT_2)}, \qquad (5.39)$$

where the time delay have been approximated by the first-order Taylor series. The controller is given by

$$C(s) = k_c \frac{1+sT_i}{sT_i}. \qquad (5.40)$$

Now, let $T_i = T_2$. This implies that the process pole is canceled by the zero of the controller. This can be compared with the IPZ-tuning rule, where the integral time follows the parameter T_2 in the sense that larger values of T_2 gives larger values of T_i, and for small T_2 the two are almost equal, see Figure 5.5. The closed loop system is now given by

$$G_{ry}(s) = \frac{k_v k_c (1+sT_1)(1-sL)}{(T_2 - k_v k_c T_1 L)s^2 + (k_v k_c T_1 - k_v k_c L)s + k_v k_c}. \qquad (5.41)$$

The two zeros of the denominators are

$$s = -\frac{k_v k_c (T_1 - L) \pm \sqrt{(k_v k_c (L+T_1))^2 - 4k_v k_c T_2}}{2(T_2 - k_v k_c T_1 L)}. \qquad (5.42)$$

By the controller gain k_c we have some liberty to choose the position of the closed loop poles. By choosing a double pole, the contribution from the square root is zero, and the equation

$$(k_v k_c (L+T_1))^2 - 4k_v k_c T_2 = 0 \qquad (5.43)$$
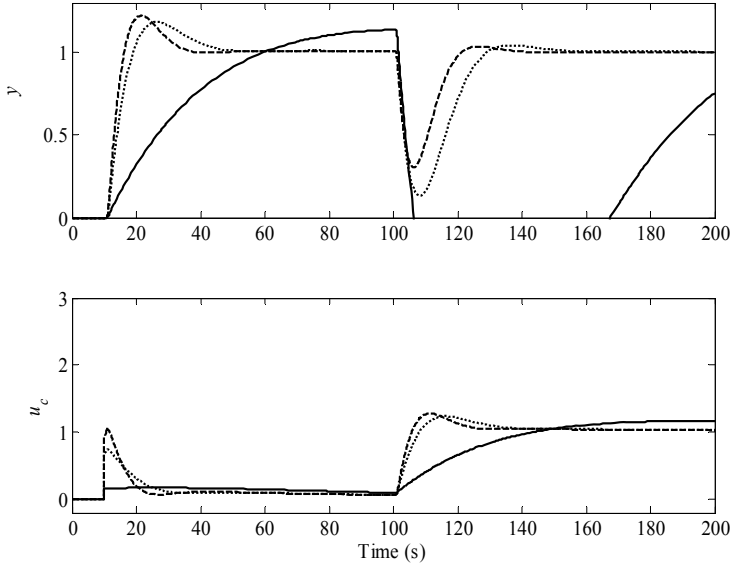
Figure 5.29 Evaluation of Nelson-Gardner's pole placement rule (5.44) for PI control (solid line) given the process in (5.17). Also shown is the IPZ-tuning for $M_s = 1.2$ (dotted) and $M_s = 1.3$ (dashed).

is fulfilled. This gives us the tuning rule

$$k_c = \frac{4T_2}{k_v (L + T_1)^2}, \quad T_i = T_2.$$ (5.44)

and the double pole is then positioned in

$$-\frac{2}{T_1 - L}$$ (5.45)

Assuming the process given in (5.17), the controller settings are

$$\text{PI: } k_c = 0.16, \, T_i = 20, \quad M_s = 1.04,$$ (5.46)

The simulation result is shown in Figure 5.29 and we can immediately see that this is not a satisfying controller. We can also see that it is a rather robust controller, since the M_s-value is fairly small. Further investigations show that this method gives a quite robust controller with M_s-values

below 1.05 for short time delays ($L \approx 1$). Larger time delays or shorter T_2 give $M_s \approx 1.1-1.2$, and relatively fine simulation results. The disadvantage with this method is the lack of any design parameter but it gives a reasonable tuning.

PID control

The poles of a second order process with one zero, can be placed independently of one another by a PID controller. By assuming that the time delay can be neglected, the IPZ-process fits into this model structure. Then the process is given by

$$P(s) = k_v \frac{(1 + sT_1)}{s(1 + sT_2)}, \tag{5.47}$$

and the controller is

$$C(s) = k_c \frac{1 + T_i s + T_i T_d s^2}{sT_i}. \tag{5.48}$$

The closed loop system then becomes

$$G_{ry}(s) =$$

$$= \frac{k_v k_c (1 + T_i s + T_i T_d s^2)(1 + T_1 s)}{T_i (k_v k_c T_1 T_d + T_2)s^3 + T_i (1 + k_v k_c T_1 + k_v k_c T_d)s^2 + k_v k_c (T_1 + T_i)s + k_v k_c}. \tag{5.49}$$

A suitable characteristic polynomial for a third-order system is

$$(s + \omega_1)(s^2 + 2\zeta\omega_0 s + \omega_0^2) \tag{5.50}$$

By equating coefficients of equal power in s, we get the following system of equations

$$\begin{cases} \dfrac{k_v k_c}{k_v k_c T_1 T_i T_d + T_2 T_i} = \omega_1 \omega_0^2 \\[3mm] \dfrac{k_v k_c (T_1 + T_i)}{k_v k_c T_1 T_i T_d + T_2 T_i} = 2\omega_0 \omega_1 \zeta + \omega_0^2 \\[3mm] \dfrac{T_i (1 + k_v k_c T_1 + k_v k_c T_d)}{k_v k_c T_1 T_i T_d + T_2 T_i} = 2\omega_0 \zeta + \omega_1 \end{cases} \qquad (5.51)$$

The solution is given by

$$k_c = \frac{\omega_0 (2T_1 \omega_1 \zeta + T_1 T_2 \omega_0 \omega_1 + T_1 \omega_0 - 2T_2 \omega_1 \zeta - T_2 \omega_0 - T_1^2 \omega_0 \omega_1)}{k_v (T_1^3 \omega_1 \omega_0^2 + T_1 \omega_1 + 2T_1 \omega_0 \zeta - 2\omega_0 \omega_1 \zeta T_1^2 - T_1^2 \omega_0^2 - 1)},$$

$$T_i = \frac{2\omega_1 \zeta + \omega_0 - T_1 \omega_0 \omega_1}{\omega_0 \omega_1}, \qquad (5.52)$$

$$T_d = \frac{T_1^2 T_2 \omega_0^2 \omega_1 - 2T_1 T_2 \omega_0 \omega_1 \zeta - T_1 T_2 \omega_0^2 + T_2 \omega_1 + 2T_2 \omega_0 \zeta - 1}{\omega_0 (2T_2 \omega_1 \zeta + T_2 \omega_0 - T_1 T_2 \omega_0 \omega_1 - 2T_1 \omega_1 \zeta - T_1 \omega_0 + T_1^2 \omega_0 \omega_1)}.$$

Even though any ω_0, ω_1, and ζ can be realized there should be some relation between the process and the desired closed loop poles, to give a controller with satisfactory performance. E.g. requesting a bandwidth that is too high for the closed loop system gives very high controller gain. This injects much noise into the loop, can be damaging to actuators, and might make the system unstable due to neglected process dynamics.

From (5.52) the controller settings can easily be calculated for a given closed loop response. As an example, we select to place the poles in

$$\omega_0 = \frac{3}{2T_1}, \quad \omega_1 = \frac{3}{4T_2}, \quad \zeta = \frac{3}{4}. \qquad (5.53)$$

The solution is then

$$k_c = \frac{9T_2 (T_1 - T_2)}{k_v T_1^2 (3T_1 - 4T_2)}, \quad T_i = \frac{4}{3} T_2, \quad T_d = \frac{T_1^2}{9(T_1 - T_2)}. \qquad (5.54)$$
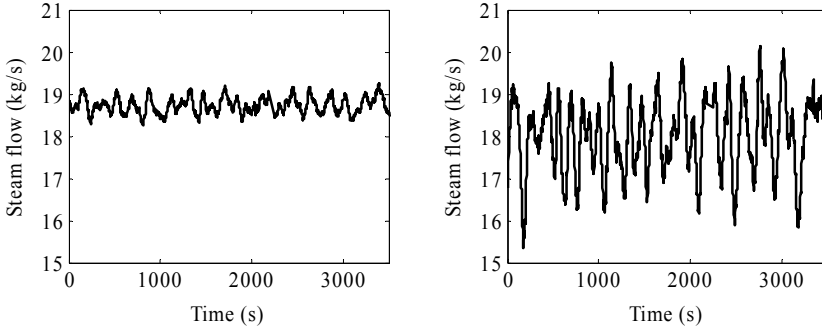
Figure 5.30 A case study − before (left) and after (right) an aggressive retuning of the steam pressure controllers in a drying section. Both figures show the total steam usage by the drying section. To the left is before retuning of the steam pressure controllers and to the right is after. The retuning gave both better set point following and disturbance rejection, but it had severe implications for the steam producers who could not handle the large variations in demand.

If this is a good tuning depends on how well we can neglect the time delay, but also on the other process parameters. Large T_1, for example, tends gives very small k_c.

Remark
Trying to place any of the closed loop poles in $-1/T_1$ gives infinite controller gain. This matches what was observed with PI control. Controller parameters T_i and T_d will have finite values though.

5.7.5 Some concluding remarks

In this section, a few different tuning methods have been evaluated to see how well they match the IPZ-tuning rule. A few of them give a reasonable tuning in some region of process parameters but only modest performance outside this region. The reason is that they do not fit well to the IPZ-process, since they often are derived from another process structure. It is always important to not only look at the process output but also the control signal. Ziegler-Nichols tuning rule gives a very fast response but also large variations in the control signal, which is particularly undesirable for the steam distribution system, see Figure 5.30. How large variations that are acceptable is a case-by-case matter, and it is therefore vital to have a design parameter to adjust the tradeoff between robustness and performance. Many other methods lack this design parameter. All this is the motivation for a specific tuning rule for the IPZ process.
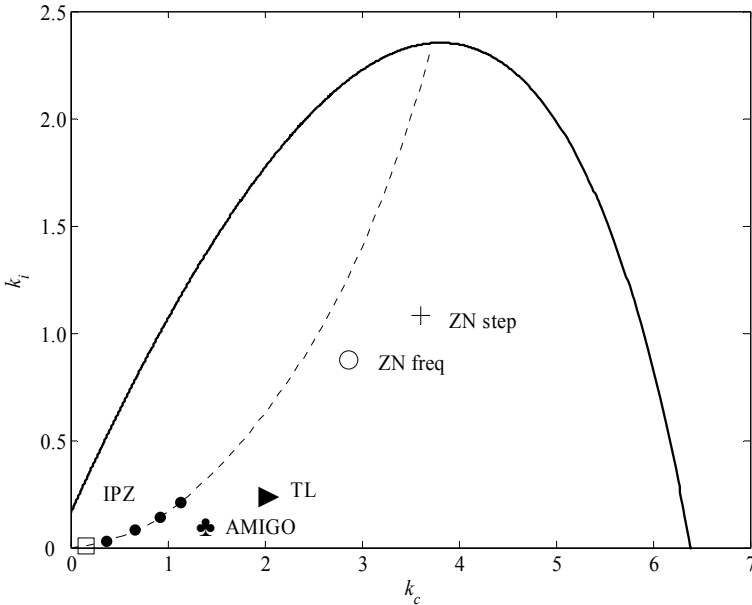
Figure 5.31 Stability region for the process in (5.17) controlled by a PI controller. The different tuning rules examined in this section are also indicated, ○ Ziegler-Nichols frequency method, + Ziegler-Nichols step test method, ► Tyreus-Luyben's modified rule, ♣ the AMIGO tuning rule, □ Nelson-Gardner, and ● IPZ-tuning ($M_s = 1.1-1.4$). The dashed line shows the contour that the IPZ-tuning follows. For large M_s values, the tuning method is moving towards the peak of the stability region, namely the maximum k_i.

To see the difference between the evaluated tuning methods from another perspective, the proposed controller settings by the different methods for PI control of (5.17) are indicated in the stability region for the process, see Figure 5.31. The two Ziegler-Nichols methods distinguish themselves by grouping together away from the other methods. All four settings from the IPZ-tuning are shown in the figure. It was previously concluded that the AMIGO tuning rule and Tyreus-Luyben's rule give satisfactory controller settings for this set of process parameters. Therefore, it seems reasonable that their controller settings are in the vicinity of the IPZ-tuning. The example of Nelson-Gardner's pole placement is also in that neighborhood but closer to the origin, which gives a much more robust control. Remember that it is only the IPZ tuning among the evaluated methods that have a design parameter and that give good performance for a wide range of different parameters of the IPZ model.

Finally, a robustness test is given in Figure 5.32, showing a simulation of the different methods tuned for (5.17) but where the time delay is
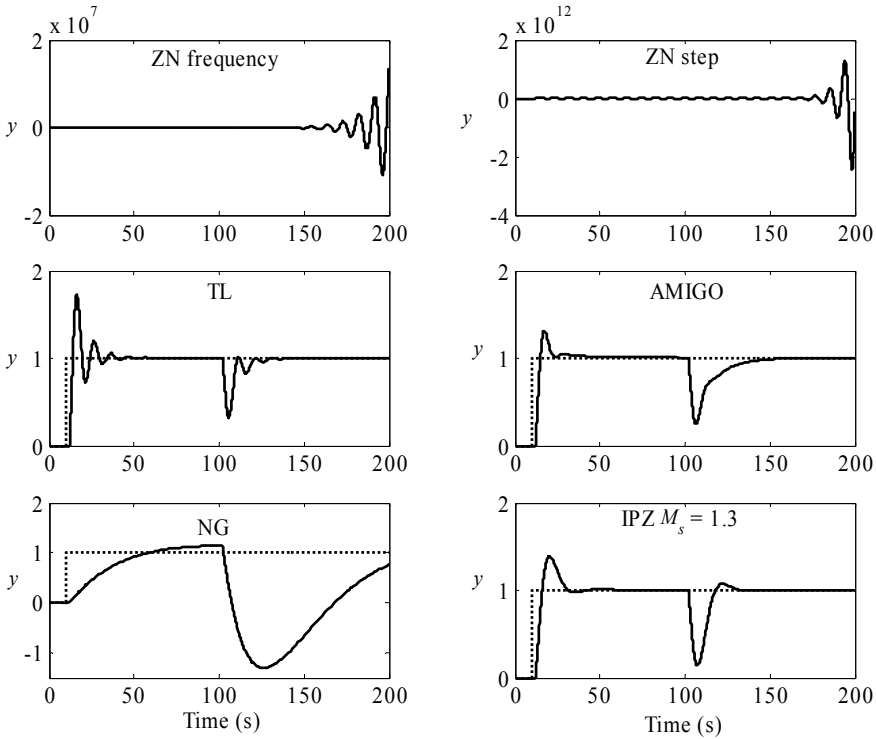
Figure 5.32 Robustness analysis of the tuning methods used in comparison with the IPZ tuning. The time delay in (5.17) is changed from 1 to 2 seconds.

multiplied by a factor of two. Both Ziegler-Nichols methods become unstable and Tyreus-Luyben is close to the point of instability. This clearly shows the necessity to not only consider performance but also robustness. Overall, the IPZ tuning appears to give the best result when weighing together all the comparisons given in this section.

5.8 Summary

In this chapter, a tuning method for PI and PID control of the IPZ model has been presented. It is based on optimized load disturbance rejection subject to a robustness constraint. To calculate the controller parameters, the method requires the four process parameters of the IPZ-model and a design parameter that is defined by the user. The process parameters can easily be obtained from an open loop step response. Since the dead time has a significant effect on the method, good quality dead time estimation

is essential. The advantage with the IPZ-tuning is that the equations are simple and it is easy to use. From experiments on several paper machines at different mills, the method has been validated and proved to perform well.

A few other tuning methods found in the literature have been compared to the proposed tuning method. The conclusion is that there is a need for a new method, since neither of the other give good result when they are evaluated for different process parameters.

Since the method is based on optimized load disturbance rejection it can with advantage be combined with a set point filter. Examples of this are the β and γ factors in (3.19), or the more general 2DOF-controller described in Section 3.3.

The IPZ structure can be used in many other process areas, apart from modeling the steam pressure in cylinders [Forsman, 2005]. Therefore the tuning method has a much wider field of applications than solely drying section control.

Part 2

Modeling and control of paper moisture in the drying section

Papermaking in the early 1900s, painted by Thomas M. Dietrich. It shows the dry end of the paper machine at the Fox River Paper mill in Appleton, Wisconsin. The man is checking the feel and transparency of the sheet for its thickness and formation. The paper has moved from right to left in this painting, passing through the dryers, calender stack, and reel. By courtesy of Fox Valley Corporation.

6

Enhanced Moisture Control Using the Air System

The drying section is enclosed inside a drying hood. The main purposes of the hood are to create a controlled environment for the drying process, improve energy utilization, and also to establish good working conditions in the machine room. The exhaust air removes the evaporated water from the paper web while preheated dry air is added to the hood by the supply air. Traditionally, these two variables are used to control the humidity and pressure inside the hood. This chapter proposes using the supply air, in combination with the steam cylinders, to control the moisture in the sheet. Trials have shown that the supply air has a fairly large and fast impact on moisture. This suggests that using the supply air would give a closed loop system with higher performance compared to conventional steam pressure control. However, the drying capacity of the steam cylinder process is much larger than the drying capacity of the air process and both processes are therefore essential to obtain a well functioning control system. The two manipulated variables are combined in a mid-ranging structure to control the moisture.

The proposed control structure is evaluated by simulations of a physical model of the drying section.

## 6.1 A literature review of drying section models

Mathematical modeling of cylinder drying started with the pioneer work by [Nissan and Kaye, 1955]. An extensive review of drying models up to 1980 with some 130 references is given in [McConnell, 1980]. Many drying models with different approximations and objectives have been proposed in the last decade. In [Ramesh, 1991], [Wilhelmsson, 1995], and [Reardon, *et al*, 2000] models based on non-linear steady-state relations are given. [Berrada, *et al*, 1997] develop a linear state-space model from physical relations. In [Rao, *et al*, 1994] a simplified dynamic model is developed, where the whole drying section is modeled as one or only a few large cylinders. Some physical properties are then adjusted to fit the assumption. A combination of statistical multivariate models and physical models can be found in [Viitamäki, 2004]. In [Chen, 1995], [Menani, *et al*, 1998], [Skoglund, *et al*, 2000], and [Sun, *et al*, 2000] different kinds of black-box models are used. In [Sadeghi, 2003] and [Sadeghi and Douglas, 2004] a model that includes different transport phenomena within the paper sheet is presented but only in steady-state. Both [Mori, *et al*, 2000] and [Gaillemard and Johansson, 2004] give a physical model but omit the steam system. [Perré, *et al*, 2004] shows a simulation model for drying of coated paper that is implemented in Excel, but neglects the steam system and [Videau and Lemaitre, 1982] develops a static simulator used for analysis of paper production and energy consumption.

This chapter describes a physical simulation model of a drying section, implemented in Simulink. The model contains approximately 10^5 states and is capable of dynamically describing moisture gradients and other properties inside the paper sheet. This model is used for simulations in this chapter and also in Chapter 7.

6.2 The model

The model used for simulation and analysis in this chapter and Chapter 7 is developed at the Department of Chemical Engineering, Lund University, see [Karlsson and Stenström, 2005a] and [Karlsson and Stenström, 2005b]. In this thesis, the model is not described in detail but a general overview is given. It is adapted to a board machine at a paper mill in Sweden. It consists of 93 steam cylinders divided in 12 groups. It is assumed that the machine speed is 430 m/min and the dry basis weight is 267 g/m^2.
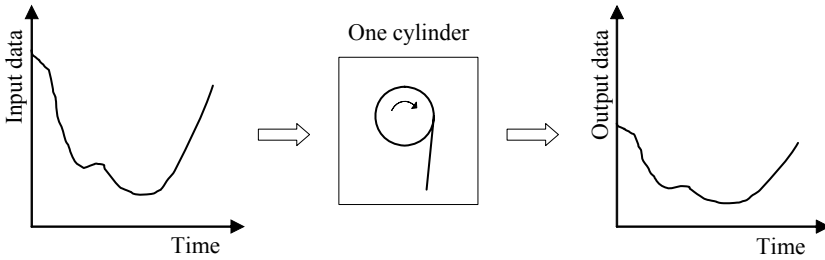
Figure 6.1 Illustration of the simulation method, where one cylinder with a following free draw is simulated at a time.

The model is built on basic physical relations, in terms of mass and energy balances, and algebraic equations. The continuity equation forms a basis for all the balances. Written as a partial differential equation (PDE) it is given by

$$\frac{\partial \Phi}{\partial t} = -\nabla \cdot J + k, \tag{6.1}$$

where Φ is some extensive system property (properties that are strictly additive, normally mass or energy), J is flow and k is net consumption or generation. It states that the amount of property entering a infinitesimal volume element either leaves that volume, accumulates within it, or is consumed, see [Hangos and Cameron, 2001] or [Sparr and Sparr, 2000].

Algebraic relations describing transport for mass and energy in combination with (6.1), gives balances for water, vapor, air, and fibre in the web. This means that properties like gas pressure inside the paper web, different transport mechanisms, and moisture gradients and shrinkage in the thickness direction can be simulated. The cylinder shell and the surrounding air are also included in the model, but not the dynamics for the steam inside the cylinder. The model is calibrated to steady-state measurements by adjusting two parameters, heat transfer coefficients for the contact between the cylinder and the paper, and for the condensate inside the cylinder.

The set of PDEs are converted into a set of ordinary differential equations (ODEs) by discretization. There are 10 nodes in the thickness direction and 2005 nodes in the machine direction. The model is implemented in Simulink with the ODEs written in C-code to reduce the simulation time. To reduce the requirements for internal memory storage in the computer, one cylinder at a time is simulated, see Figure 6.1. The result from a simulation of one cylinder is then used as input data for the
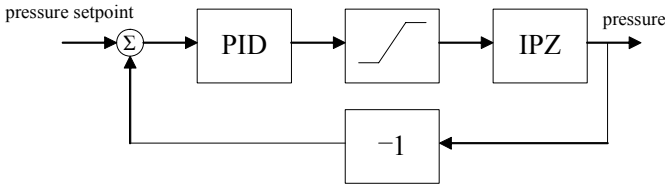
145

Figure 6.2 The model used to simulate the closed loop steam pressure dynamics.

simulation of the next cylinder, by following the flow of the paper. In this way, the number of nodes in each simulation is greatly reduced, and the memory requirement is reduced from gigabytes to megabytes. Simulations shown in this chapter still take 1−2 days on a standard computer. The simulation technique will have some implications for simulation of the closed loop system, as it will be shown later.

Modeling of the steam pressure dynamics

Since the physical model does not include the steam pressure dynamics inside the cylinders, the IPZ model given in Chapter 3 is used. It is combined with a PID controller and a valve saturation to give a model of the closed loop steam pressure system, see Figure 6.2. From a step response in each group in the drying section of the real machine, parameters of an IPZ model are estimated, see Figure 6.3 and Figure 6.4. By including the PID parameters, used by the mill for each pressure controller, a simulation model for each group is obtained that is linked to the physical model described previously. This gives a complete simulation model of the drying section, including both steam system, cylinder shell and paper sheet.

Modeling of the air system

The air system is of special interest in this chapter and is therefore further discussed. Figure 6.5 shows an example of how the blow boxes can be configured in a drying section. A blow box is the unit through which the main part of the supply air is distributed. The other part comes from leakage air through the hood, which is roughly 20−30 % of the total air flow in modern machines [Karlsson, 2000]. Apart from bringing dry supply air close to the sheet, the blow box also improves runnability by reducing sheet flutter. The areas where the most of the evaporation from the sheet occurs are indicated in the figure. To model this it is assumed that there is a specific volume of air around each cylinder that is involved

146

Figure 6.3 Graphical output from the modeling tool [Wallén, 2000] used to identify the steam pressure dynamics included in the simulation model. The solid lines are process signals and dotted lines the obtained models (also given as transfer functions). The unit of y is kPa (gauge) and the unit of u_c is %. The figure shows group 1−8.
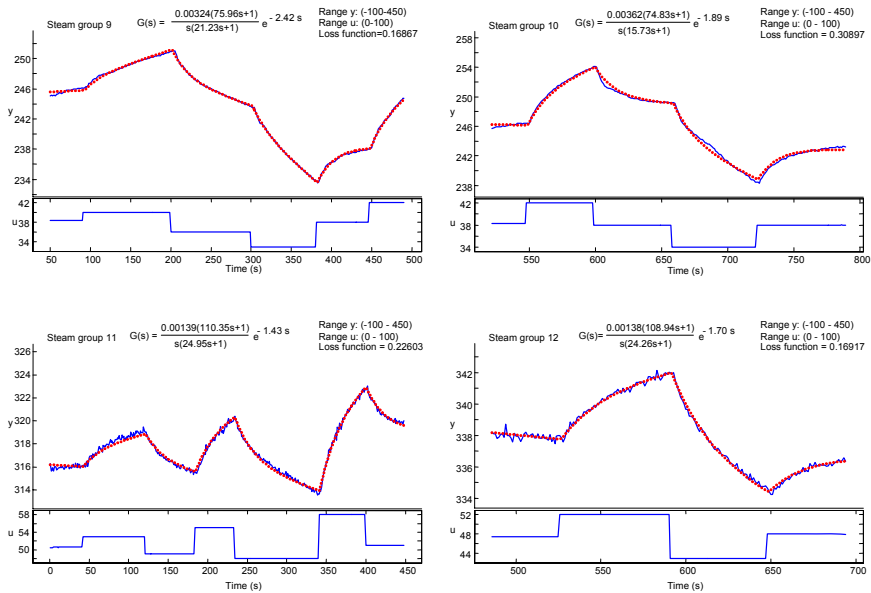
Figure 6.4 Graphical output from the modeling tool [Wallén, 2000] used to identify the steam pressure dynamics included in the simulation model. The solid lines are process signals and dotted lines the obtained models (also given as transfer functions). The unit of y is kPa (gauge) and the unit of u_c is %. The figure shows group 9−12.

Figure 6.5 An example of blow box configuration in both a single-tier (above) and two-tier (below) machine. The oval areas indicate the region where most evaporation occurs. The active air volume is essentially bounded by machine equipment and fabrics. The large arrow indicates the direction of the paper and a few blow boxes are indicated by smaller arrows. By courtesy of Metso Paper.
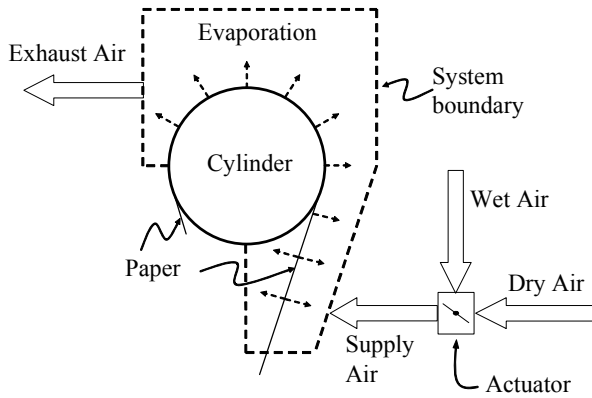
Figure 6.6 A picture of the air system used in the model.

in the dynamics, see Figure 6.6, and the volume was set to 10 m^3. With a nominal total supply air flow of 50 m^3/s divided to 93 cylinders, this corresponds to a residence time of 18.6 s. Dry air is mixed with recirculated moist air and in this way, the dew point of the supply air is manipulated while the flow rate is constant. The idea is to prevent runnability problems due to web flutter in case of aggressive use of the supply air.

6.3 A prestudy

To investigate the potential to use the supply air as an actuator, a step test has been performed on a board machine, see Figure 6.7. The machine speed is 724 m/min and the basis weight is 134 g/m^2. The step test is performed on the last third of the drying section (the after dryer), while both the moisture and basis weight controller are put in manual mode (the steam pressure controllers are still in automatic). The air flows are manipulated by variable speed fan motors (some machines have air flow dampers instead). Measurements prior to the experiment showed that 67 % control signal corresponds to 41.4 m^3/s supply air and 70.3 m^3/s exhaust air. Both the supply air and exhaust air are changed equally during the step test to maintain the air balance in the hood. Because of the instrumentation at the particular mill, it is not possible to automatically log the signal to the fans, therefore the control signal shown in the figure has been recreated afterwards from notes taken during the experiment. In addition, the change in supply air is done 5−10 s after the change in exhaust air, since it is done manually by one person. The moisture and

149
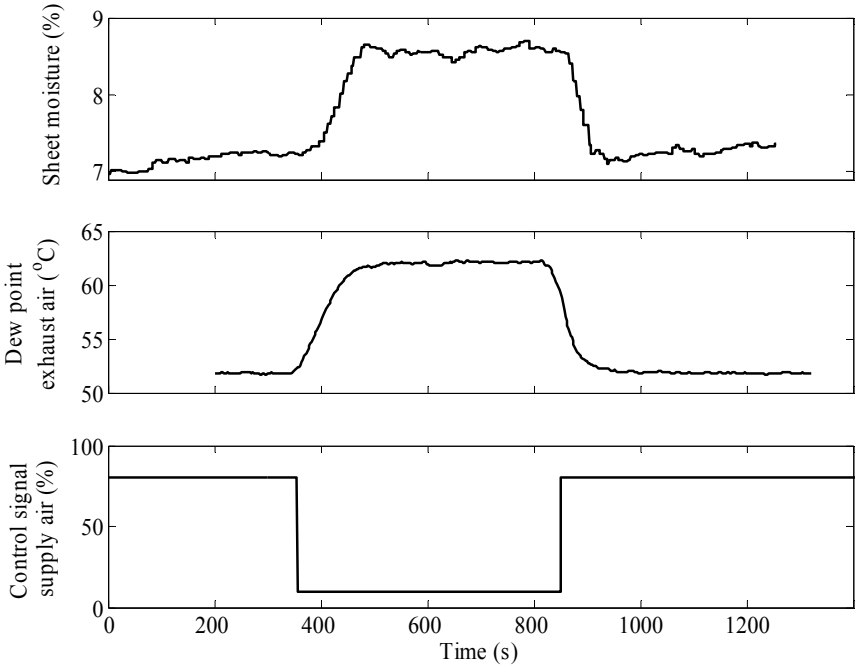
Figure 6.7 Results of the prestudy where it is shown that the supply air has a large impact on the sheet moisture, measured at the reel-up. The dew point of the exhaust air is also shown.

dew point are logged in two different systems and are synchronized at a later stage by the time tags from the internal system clocks. Therefore, it is considered somewhat uncertain to make a dynamic model from the experiment result, but it still clearly gives an idea of the potential to use the air system as an actuator for the moisture controller.

The experiment gives a promising result. The response is distinct, the change in sheet moisture is rather significant and the time constant is somewhere between 15−25 s if it is modeled as a first order process, see Figure 6.7. This also agrees well with the residence time of the air system in the model described in Section 6.2.

6.4 Mid-ranging

As described previously, the steam and air system is combined by mid-ranging control. Generally, mid-ranging refers to control problems where there is one process output and two or more manipulated inputs, see
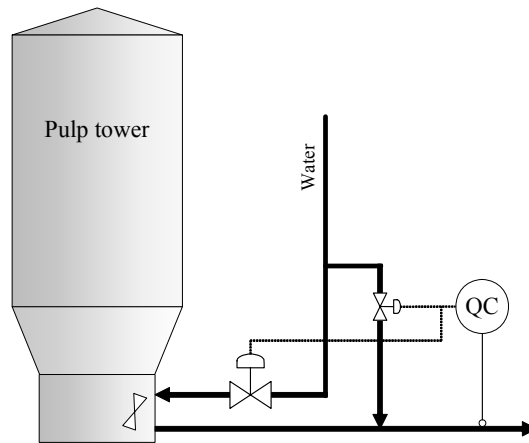
Figure 6.8 The consistency in the pulp tower is typically 8−12 %. Dilution to pumpable suspension takes place at the bottom of the tower by injection of dilution water. An agitator helps the mixing.

[Shinskey, 1978], [Allison and Isaksson, 1998] and [Allison and Ogawa, 2003]. A common example in the pulp and paper industry is consistency control of the pulp that is pumped from the storage tower, see Figure 6.8. The controller has two actuators, a large dilution valve and a smaller valve for fine adjustments. The main purpose of the water through the large valve is to make the pulp pumpable. Nevertheless, it is also important to avoid letting too much water being injected at the bottom of the tower to prevent the small valve from being closed, and vice versa, since the small valve often has a smaller operating range and finer resolution. One solution is to let the small valve return to its midpoint or target value in steady state. This is known as *mid-ranging*. In general, the effect of the inputs differs significantly in both range and speed, and sometimes in cost. When there is a cost tied to the inputs, the optimal target value for the expensive input is often not the midpoint.

Four types of mid-ranging structures

There exist several different alternatives to implement a mid-ranging controller, and four different structures are described below. It is assumed that P_1 is a fast process with a small range, and P_2 is a slow process with a large range. The signals u_1 and u_2 are control signals for P_1 and P_2, respectively, and r_1 is set point for y and r_2 set point for u_1. The last three mid-ranging structures are evaluated in [Allison and Isaksson, 1998]. The

151
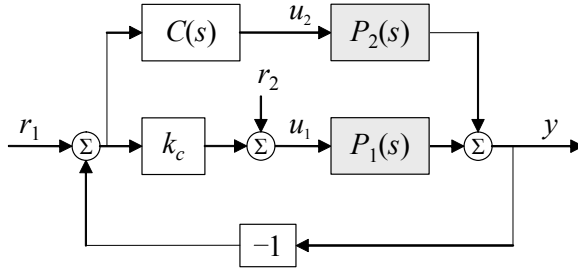
Figure 6.9 The structure of the simple mid-ranging controller. The set point r_2 is the bias of the P-controller. In practice, $C(s)$ is often chosen as a PI controller

conclusion is that the MPC solution is superior compared to the other two, and the valve position controller comes in second hand.

Simple Mid-ranging
This is probably the simplest way to implement mid-ranging and it consists of only one feedback loop but two controllers in parallel with the same set point, see Figure 6.9. The controller manipulating u_1 is a P controller, whereas the controller manipulating u_2 is a controller with integral action. When the integral action in C removes the control error, the output u_1 is the offset of the P controller. By adjusting the offset, the target value for u_1 is set. The disadvantage with this solution is that P_1 is limited to be controlled by a P controller. This gives a slow response to both set point changes and disturbance rejections, since the P controller gives a steady-state error which is removed by C through a much slower process P_2.

Valve Position Controller
The valve position controller in Figure 6.10 is probably the most common implementation of mid-ranging found in industry today, see [Shinskey, 1978] and [Allison and Ogawa, 2003]. Controller C_1 controls the output y with input u_1, while C_2 controls u_1 with u_2. In the literature describing the valve position controller, the decoupling filter C_D is seldom included. An exception is [Allison and Isaksson, 1998], where it is briefly discussed without any details. The filter is not necessary for the function of the control system but it improves the performance. If the decoupling filter is removed, the only way for C_2 to control u_1 is through the error r_1-y, consequently introducing disturbances into y. The decoupling should ideally be chosen as
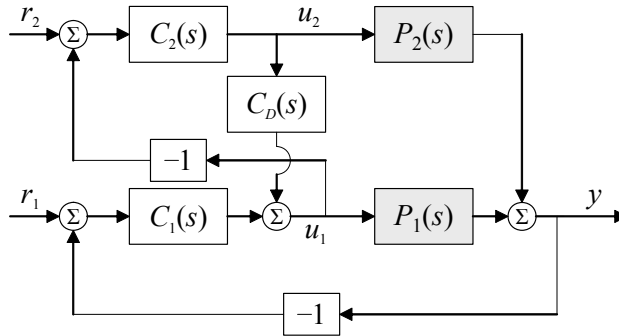
Figure 6.10 The structure of the valve position controller.

$$C_D(s) = -\frac{P_2(s)}{P_1(s)}, \tag{6.2}$$

which is realizable as long as the time delay of P_1 is shorter or equal to the time delay of P_2, and P_1 and P_2 have the same unstable zeros. In addition, the pole excess of P_2 should be at least as large as the pole excess of P_1. It is assumed that both P_1 and P_2 have stable poles or integrators. With (6.2), changes in u_2 do not affect y, and the transfer function from u_2 to $r_2 - u_1$ is equal to $-C_D$. If the ideal decoupling is not realizable, approximations have to be used.

This implementation does not require anti-windup protection in C_1 since u_1 is a controlled variable. Regardless if u_1 saturates or not during an upset, controller C_2 brings u_1 back to r_2 in steady-state. However, depending on the speed of controller C_2, anti-windup protection in C_1 might be beneficial, see [Haugwitz, *et al*, 2005].

Hybrid Mid-ranging
An approach, originally used to control pressure of a steam header, is the hybrid mid-ranging [Love, 1994]. It consists of one PI controller, two saturations, a low pass filter, and three gains, see Figure 6.11. The parameter R_m, should be chosen as

$$R_m = \frac{100k_1}{k_1 + k_2}, \tag{6.3}$$

where k_1 and k_2 are the steady-state gains of P_1 and P_2, respectively. The filter in combination with the direct term creates the mid-ranging function. The transfer function from the output of the PI controller to the

153
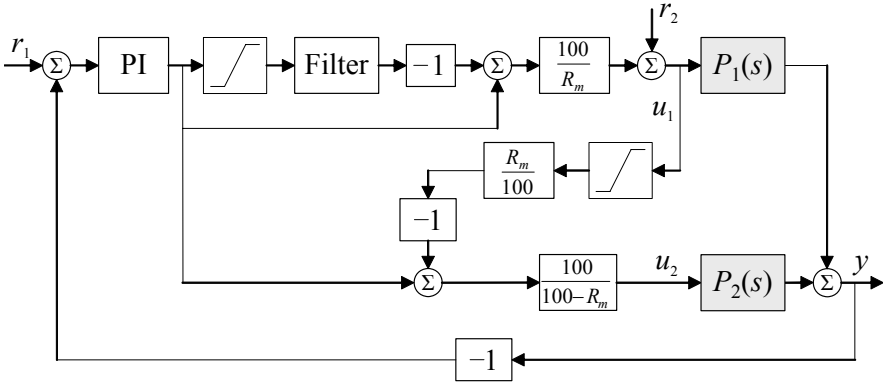
Figure 6.11 The structure of the hybrid mid-ranging controller.

summation after the filter is in effect a low pass filtered derivative. The purpose of the saturation block preceding the filter is to allow an offset in u_1 when u_2 is reaching its limit. By this, the controller combines mid-ranging (normal operation) with split-range (saturated u_2) in a nice way. The purpose of the other saturation block is to immediately engage control signal u_2 when u_1 reaches its limit.

The PI controller can, without losing the mid-ranging function, be replaced by any SISO controller.

Mid-range MPC
In [Allison and Isaksson, 1998] a mid-ranging controller is implemented in the MPC (model predictive control) approach, see Figure 6.12. By letting the minimized cost function be given by

$$J(k) = \sum_{i=1}^{H_p} \left\| \begin{bmatrix} r_1(k+i) - \hat{y}(k+i\,|\,k) \\ r_2(k+i) - u_1(k+i) \end{bmatrix} \right\|_Q^2 + \sum_{i=1}^{H_u} \left\| \begin{bmatrix} \Delta u_1(k+i) \\ \Delta u_2(k+i) \end{bmatrix} \right\|_R^2, \quad (6.4)$$

and the weighting matrices chosen as

$$Q = \begin{bmatrix} \text{large} & 0 \\ 0 & \text{small} \end{bmatrix}, \quad R = \begin{bmatrix} \text{large} & 0 \\ 0 & \text{small} \end{bmatrix}, \quad (6.5)$$
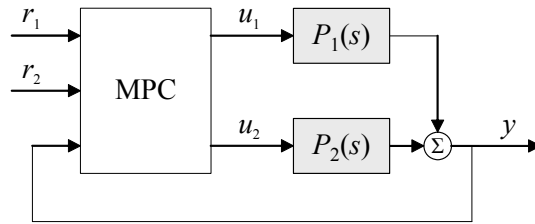
Figure 6.12 The structure of the mid-range MPC.

the desired behavior is achieved. Since the MPC formulation is inherently discrete-time, the cost function is given as a summation. Notation $\hat{y}(k + i \mid k)$ denotes the i step-ahead prediction, and analogously for u_1 and u_2. H_p is the prediction horizon, H_u is the control horizon, and Δ is the difference operator ($\Delta = 1 - z^{-1}$, where z^{-1} is the backward shift operator). The main advantage with the MPC formulation is that it takes constraints into account explicitly and integrator windup is no issue. The main tuning parameters are the prediction horizon H_p, the control horizon H_u, and the weights Q and R. It is possible to omit the weight on the control increments, R, in (6.4), without losing the mid-ranging function. However, the formulation is less flexible since there in practice is only one weighting parameter (one of the parameters in Q can be set to e.g. one).

6.5 Moisture control by mid-ranging the air system

A mid-ranging strategy to control the sheet moisture by a combination of both the blow boxes and steam cylinders, is evaluated by simulations of disturbance rejection, using the model introduced in Section 6.2. The results are compared to conventional moisture control, where only the steam pressure in the cylinders is used.

6.5.1 Modeling and control design

The valve position controller is chosen as the mid-ranging structure to be used, both for its flexibility and for being the most common approach in industry, see Figure 6.13. The process consists of one controlled variable, the sheet moisture, and two manipulated variables, the steam pressure set point and the air flow actuator. The control signal u_1 manipulates the air flow actuator while u_2 is a set point for the steam pressure. The motivation for not manipulating the steam valves directly is both to preserve the
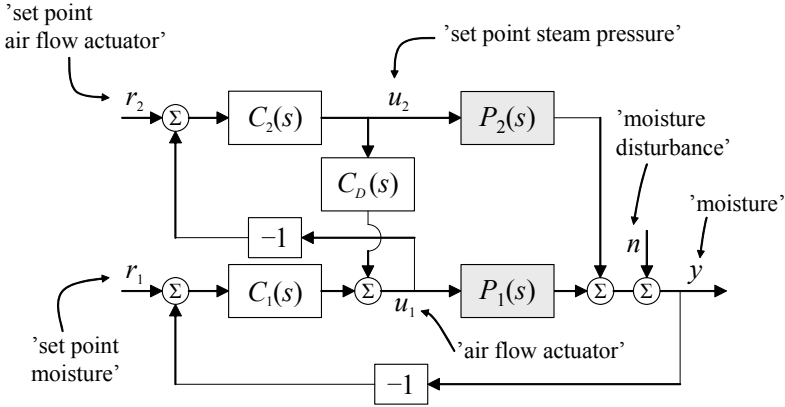
Figure 6.13 The mid-ranging structure used in the simulations where the different variables are also given. Note that u_1 manipulates the air flow actuator while u_2 is the set point to the steam pressure controllers.

function of the cascade system in the condensate system and for paper quality reasons, as described in Section 2.3.

Since the paper drying process includes a significant transport dead-time, the two controllers C_1 and C_2 are based on the IMC concept, which is well known as an effective dead-time compensator for a stable process with long time-delays [Morari and Zafiriou, 1989]. The transfer function of an IMC can be written as

$$C(s) = \frac{H_f(s)P^+(s)}{1 - H_f(s)P^+(s)P(s)},\qquad(6.6)$$

where P is the process model, P^+ is the realizable inverse of the process model, and H_f is a low pass filter with steady-state gain one that determines the closed loop performance.

The process transfer functions are obtained from open-loop step responses, see Figure 6.14 and Figure 6.15, and are modeled as

$$P_1(s) = -\frac{0.2548s + 0.04887}{617.3s^2 + 35.66s + 1}e^{-10s},\qquad(6.7)$$

and

$$P_2(s) = -\frac{0.1365}{61.5s + 1}e^{-40s}.\qquad(6.8)$$
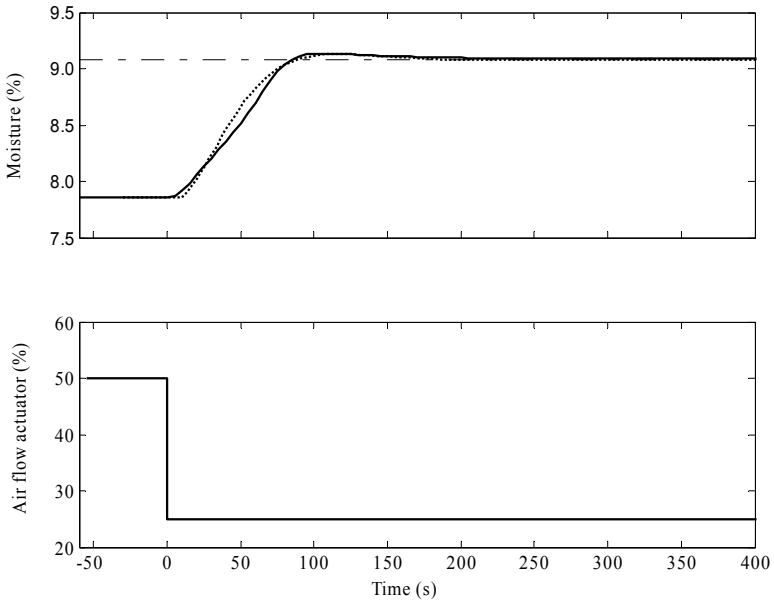
Figure 6.14 Step response of the air flow − moisture process (solid) and the obtained model (dotted), also given in (6.7). The dash-dotted line indicates the final value.
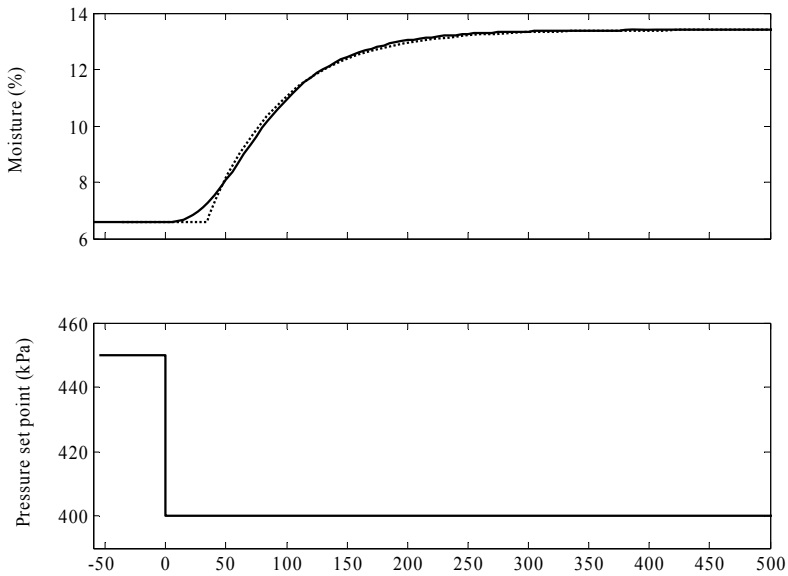
Figure 6.15 Step response of the steam pressure − moisture process (solid) and the obtained model (dotted), also given in (6.8).

157

The model from air flow actuator to moisture, P_1, has two complex conjugated poles to capture the dynamics. The physical explanation for the overshoot is a combination of both dynamics in the paper and cylinder. When the air flow is decreased, the amount of moisture in the air around the sheet is increased. This reduces the evaporation of water from the paper and the paper moisture increases. This also decreases the paper temperature which makes the energy flow to the paper to increase, and this in turn will increase the evaporation. However, the dynamics in the cylinder is much slower than the air-paper process and the increased evaporation due to increased energy flow to the paper lags behind the increase in sheet moisture due to reduced air flow, which gives an over-shoot in the paper moisture.

Notice the resemblance between the prestudy experiment in Figure 6.7 and the open-loop simulation in Figure 6.14. The moisture in Figure 6.7 reaches a new steady-state promptly in a manner that does not appear as a process with only one or two real poles. However, it is difficult to distinguish the over-shoot in the response because of disturbances.

P_1 has both faster dynamics and shorter time delay compared to P_2. The design parameter for the IMC is the filter H_f. For C_1 it is chosen as

$$H_{f1}(s) = \frac{1}{\left(1 + \dfrac{\tau_1}{\omega}s\right)^2},\qquad(6.9)$$

where $\tau_1 = 1$ (nominal value) implies that the closed-loop poles are real and placed at the same distance from the origin as the open-loop poles, see Figure 6.16. A value of τ_1 greater than one makes the closed-loop system slower, and vice versa. Apart from the two poles, P_1 also has a zero. However, it has been observed that a simpler model, with only two complex conjugated poles and no zero, is sometimes sufficient for the airflow − moisture process. Therefore, a second order filter is chosen in (6.9), to make the controller C_1 realizable in both cases.

Ideally, the only term affecting C_2 is C_D and the controller is tuned for that process. This can be seen by inserting C_2 into the structure in Figure 6.13, assuming perfect process models. The purpose of C_2 is to slowly restore the signal u_1 to its desired value. In practice, it can not be assumed to have an ideal decoupling filter, and therefore it is important that C_1 and C_2 do not interfere with each other. The closed-loop time constant of C_2 is therefore related to the fast loop and the IMC filter is chosen as

$$H_{f2}(s) = \frac{1}{1 + \dfrac{\tau_2}{\omega} s} . \qquad (6.10)$$

The value of τ_2 is set to be significantly larger (at least five to ten times) than τ_1, to separate the controllers C_1 and C_2 in frequency.

The mid-ranging controller is compared to the case when only the steam pressure in the cylinders are used to control the sheet moisture, here denoted as *steam pressure control*. It is assume that the steam pressure control is based on an IMC tuned for the process in (6.8) and the corresponding filter is chosen as

$$H_{f3}(s) = \frac{1}{1 + 61.5\tau_3 s} , \qquad (6.11)$$

where $\tau_3 = 1.5$. To obtain an adequate comparison between the two moisture control systems, the mid-ranging controller is tuned to have the same maximum value of the sensitivity function, M_s, as the steam pressure control, see Figure 6.17. In this way they have the same robustness to modeling errors and are in that sense comparable. The value of M_s is chosen to 1.3 and this gives $\tau_1 = 1.2$. Also given in the figure is the frequency response from moisture set point to sheet moisture, which in this case is also equal to the complementary sensitivity function. Observe
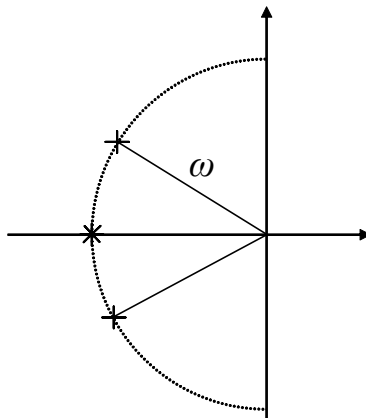
Figure 6.16 The open-loop poles (+) and the closed-loop double pole (∗) of the air flow − sheet moisture process. The parameter ω is the distance between the open loop poles and the origin.
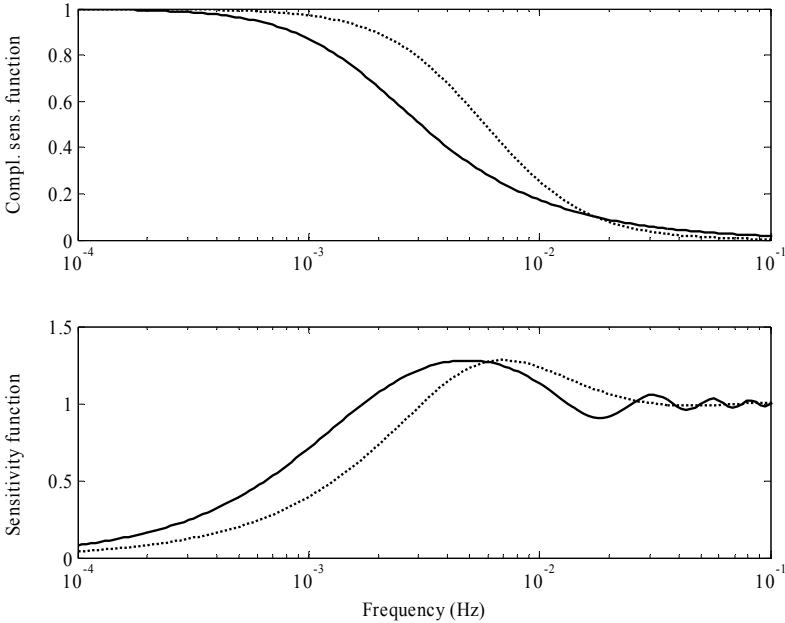
Figure 6.17 Frequency plot for the mid-ranging system (dotted line) and steam pressure control (solid line). The sensitivity function represents the transfer function from disturbance *n* to sheet moisture *y*, see Figure 6.13. The complementary sensitivity function is, for this control structure, equal to the transfer function from set point *r* to output *y*.

that ideally, both the sensitivity and complementary sensitivity functions are independent of controller C_2 and consequently also τ_2, because of the decoupling filter C_D. The bandwidth of the closed loop system with the mid-ranging controller is more than twice as large, compared to steam pressure control. This is a good indication that taking advantage of the air system together with the steam cylinders gives a higher performance than solely using the steam system. There is a region in the sensitivity plot where the mid-ranging controller has a higher amplification of disturbances compared to steam pressure control. Compared to the estimated level of noise in moisture given in Figure 2.18, there are no severe variations in that region and the amplification of noise in that frequency region by the mid-ranging is therefore not a problem for that specific example. However, the noise distribution should be regarded before implementing the mid-ranging controller on a drying section.

Remark

The air flow − moisture process can also be modeled with two real poles and slow zero. The overshoot is then due to the lead action of the zero. In this work, the process was identified by using System Identification Toolbox in Matlab which gave a model with two complex conjugated poles.

6.5.2 Simulation results

Because of the simulation technique, described in Section 6.2, where one cylinder at a time is simulated in the physical model of the drying section, it is not possible to attach a continuous control system to it. During a simulation, the resulting change in sheet moisture is not known until the last cylinder is simulated, which is when the whole simulation is performed. Therefore, continuous feedback control is not achievable and the control system is discretized. A sample time of 5 s is chosen and when the controller puts out a new control signal, the paper machine is simulated for 5 s and the moisture after the last cylinder is fed back to the controller. Obviously, this solution is not a disadvantage since it imitates the procedure of a control system in reality.

All simulations show the response to a disturbance in inlet moisture to the drying section. This can be interpreted as changed conditions in either the wire section or press section of the paper machine. The inlet moisture is changed from 62.12 to 62.82 % (this corresponds to adding 50 grams of extra water to each kg of dry solids). The size of the step disturbance and nominal supply air flow are chosen so that the air flow actuator is not saturated. This means that only the linear part of the control system is analyzed. However, windup protection and saturations in mid-ranging control is further discussed in Chapter 8.

In Figure 6.18, the response in sheet moisture due to the change in inlet moisture is shown. The mid-ranging has a significantly better disturbance rejection than the steam pressure control. There is a slight fluctuation in sheet moisture, for the mid-ranging case, after $t = 300$ s. This is because of imperfect models in the decoupling filter, C_D, and it becomes more prominent when pushing the performance level for the controller ($\tau_1 = 0.7$). When u_2 mid-ranges u_1 by increasing the steam pressure, C_D reduces the air flow accordingly but the compensation is not perfect which affects the process output. This issue would probably benefit from changing model (6.8) to a two-pole model, see also Figure 6.15.
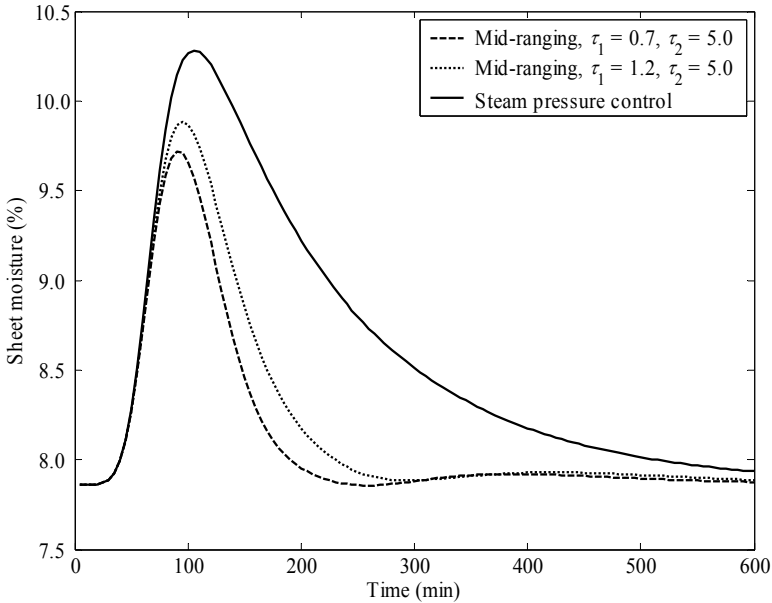
Figure 6.18 Comparison between the mid-ranging control system ($\tau_2 = 5.0$) and steam pressure control. The steam pressure control should be compared to mid-ranging with $\tau_1 = 1.2$.
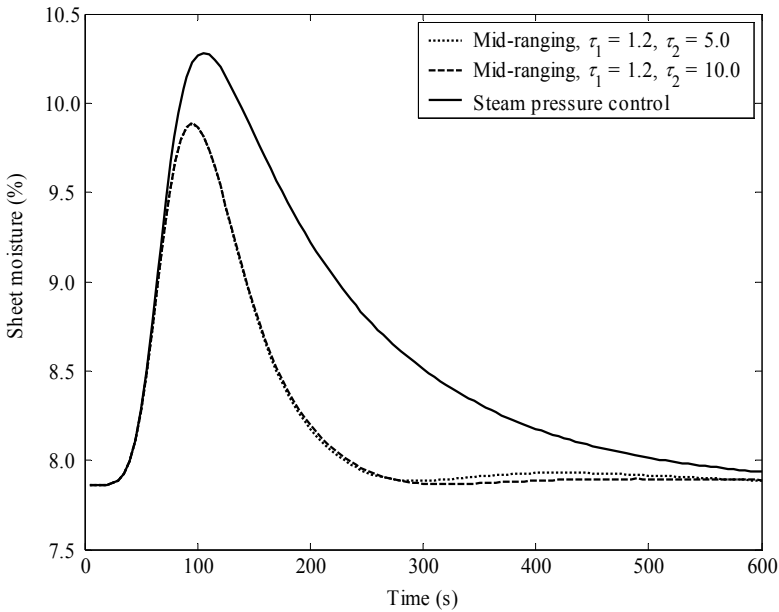
Figure 6.19 Moisture in paper for two different τ_2.

Figure 6.19 shows that the response in sheet moisture is practically independent of τ_2. However, there is a slight difference at the second half of the simulation. Larger values of τ_2 reduce the fluctuation since the steam system is less aggressive in its attempt to 'mid-range' the air system. Figure 6.20 and Figure 6.21 show the corresponding dew point of the air and steam pressure in the lead group. It is evident that both the steam and air process becomes less aggressive with larger τ_2. However, the larger τ_2 is, the more the control system becomes 'single-loop' and the advantages of mid-ranging are reduced.

Figure 6.21 also shows the steam pressure in the lead group for steam pressure control. The steam pressure is not increased as rapidly by the mid-ranging control as by steam pressure control. In the mid-ranging case, the fast moisture transients are handled by the air system and the steam system is only used to restore the air system in steady-state. Less variations in steam pressure is advantageous since it reduces the injection of disturbances in the steam and condensate system, which has negative effect on both steam production and other steam users, see also Section 2.4.

Remark 1
One drawback of using the air flow (and thus the dew point) to control the sheet moisture, is the risk of reduced efficiency in the heat recovery. A well optimized drying section ventilation has a dew point close to the allowed maximum. For the proposed control technique to function well, the dew point then needs to be decreased which leads to higher energy costs. This should be taken into account by weighing the gain of reduced variability in sheet moisture against increased energy usage [Lindell and Stenström, 2004], when evaluating the control principle for a specific drying section.

Remark 2
Physically, the dew point is a driving force for the evaporation of water in the sheet. A low dew point implies a low vapor partial pressure in the air, and high difference in vapor pressure between sheet and air. It can be interpreted as a low dew point pulls out the moisture in the sheet. This is the opposite of an increase in steam pressure which increases the evaporation by increasing the vapor pressure in the sheet, and pushes out the moisture in the sheet. In [Karlsson and Stenström, 2005b] it is shown that a high vapor pressure inside the sheet can cause delamination
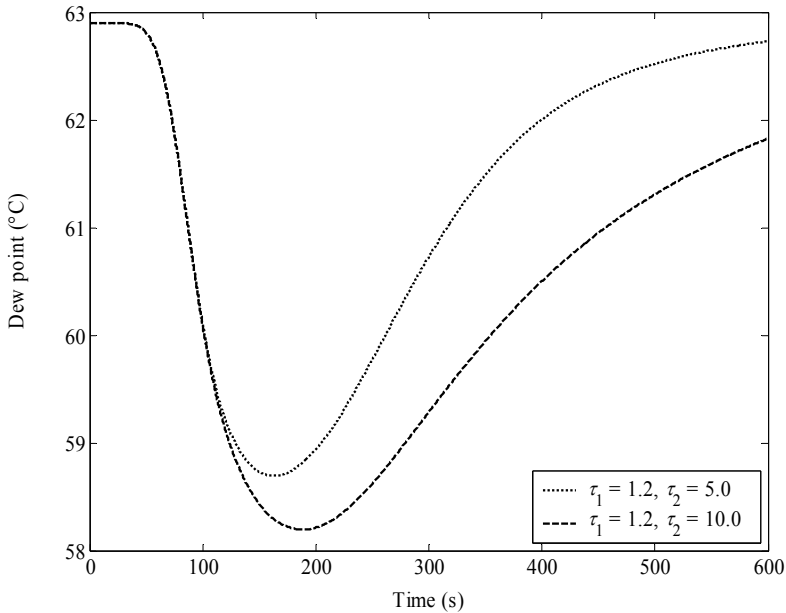
Figure 6.20 Change in dew point (mid-ranging).
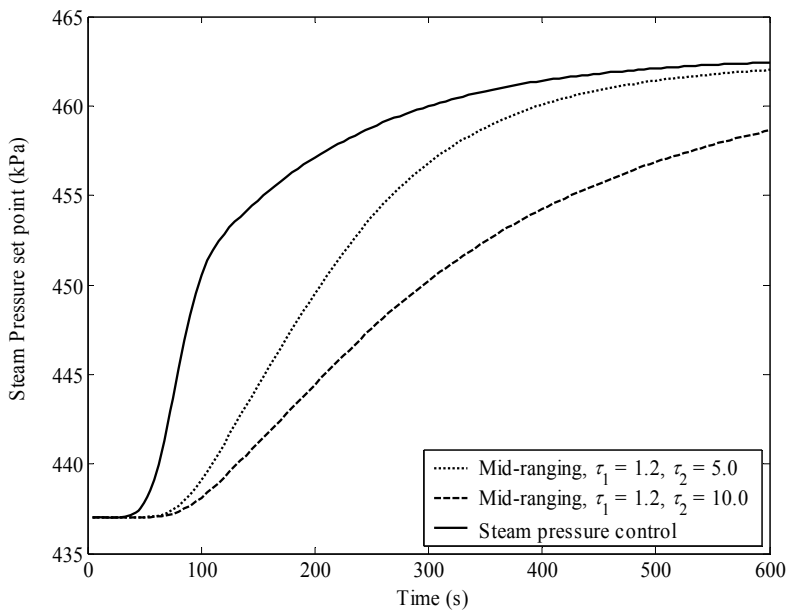
Figure 6.21 Steam pressure in the last steam group (lead group) when comparison steam pressure control and mid-ranging.

(different pulp layers are separated) problems in board machines. Since the mid-ranging control presented here, gives smaller variations in steam pressure it should reduce this problem.

Remark 3

An alternative control configuration is to let the dew point be the inner part of a cascade loop with the moisture control. Controller C_1 then gives a set point to the dew point controller, which is included in P_1, compare with Figure 6.13. However, the dew point is normally measured in the exhaust air, far from the sheet. Experiments in [Forsman and Birgerson, 1999] show that the time constant in the process from air flow actuator to dew point is around 1.5 minutes due to the large volume of air in the hood. This would give a slow moisture control loop, unless the dew point is measured close to the paper (in the pocket). The experiment in Figure 6.7 gives a time constant for the actuator − dew point process around 30 seconds. Also in this case the dew point needs to be measured closer to the sheet to be useful in a cascade control configuration.

6.5.3   Zero-level and dew point control

There are two important variables to control in the air inside the dryer hood, the dew point and zero-level, see Figure 6.22. Normally the supply
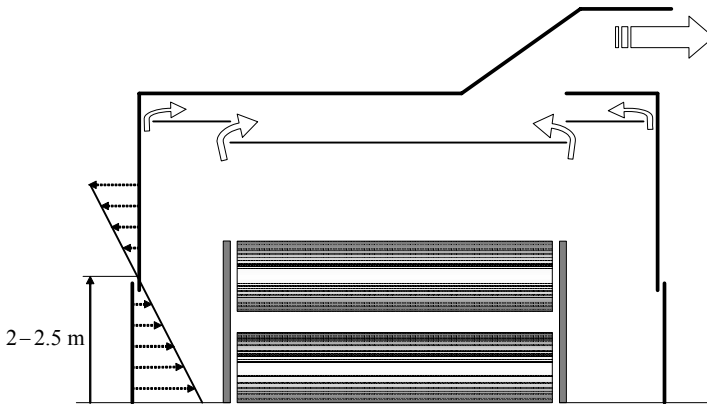
Figure 6.22 The air balance in the hood. The large unfilled arrows indicate the exhaust air. To provide uniform air flows around the cylinders, there is a *false ceiling*. The smaller arrows indicate the pressure inside the hood. Below the doors of the hood, there is an under pressure to prevent moist air to leak into the machine room. The height where the air pressure inside the hood equals the outside pressure, is called *zero-level*, [Karlsson, 2000].
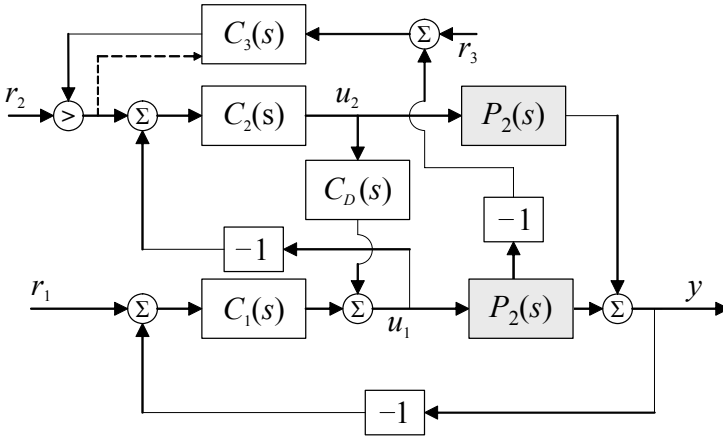
Figure 6.23 By allowing the dew point to adjust the air flow actuator set point, it is possible to set an upper constraint on the dew point. The output from the selector is fed back to the integral mode of C_3 to avoid windup.

air is used to control the zero-level, and the exhaust air to control the dew point [Forsman and Birgerson, 1999]. The dew point is often measured in the exhaust air channel.

The proposed control strategy in this chapter uses the supply air to control the sheet moisture. That means that the exhaust air must be used to control the zero-level. It is vital to have an upper constraint on the dew point to prevent condensation that might cause dripping on the sheet and corrosion on machine units. A possible solution, in the mid-ranging structure, is shown in Figure 6.23. By adding an extra controller, C_3, that controls the dew point in the exhaust air through a selector that is shared with set point r_2, the air flow actuator set point is increased if the dew point exceeds set point r_3.

6.6 Summary

A new control strategy has been developed for the multi-cylinder drying section, to reduce sheet moisture variability. The air system in the blow boxes are used to control sheet moisture, in combination with the steam system. A previously developed physical model for the drying section is used in simulations, where the performance of the control system is compared with a conventional moisture control.

The result is that by combining the conventional steam control loop with the supply air system, it is possible to significantly improve the disturbance rejection of the sheet moisture feedback loop, without changing the level of robustness. This is shown in both in simulations and by observing that the bandwidth for the disturbance rejection is more than twice as large for the mid-ranging control. The physical reason for this is the fast response of the dewatering rate to changes in air dew point.

There are two design parameters in the selected mid-ranging structure, τ_1 and τ_2. The performance of the closed loop system is determined by τ_1 and τ_2 determines how fast the steam system should restore the air system to its original level. Ideally, these two parameters can be chosen independently but in practice it is recommended to let $\tau_2 \geq 10\tau_1$. Letting $\tau_1 = 1$, means that the closed loop poles have the same distance to the origin as the open loop poles.

7

Feedforward from a Paper Surface Temperature Measurement

The paper machine is often run with constant set points for all quality variables for a long period of time, typically several hours or even days. The primary function of the control system is then to maintain the desired properties in the presence of disturbances. In Chapter 6, it is shown that the air in the surrounding hood can beneficially be integrated with the steam pressure control system by mid-ranging. The mid-ranging control system proved to be far more efficient than using only the steam pressure as manipulated variable. By using a combination of both the fast but low-capacity air system and the slow but high-capacity steam system, the mid-ranging control system was able to significantly reduce the effect of moisture disturbances.

Due to the long time constants and time delays in the process, there is a large potential gain in disturbance rejection by introducing feedforward to the control system. It is essential that the disturbance signal is measured early in the process to make the feedforward effective. Installation of a moisture scanner between the press and drying section is possible and the moisture measurement can be used for feedforward control. However, the space between the press and drying section is often very small and a scanner is also a fairly large investment for the mill.

Therefore, a new signal to be used for feedforward control of the paper moisture content is presented. The signal is based on the paper surface temperature in a few positions in the machine direction. The drying process generates large moisture gradients in the thickness direction of the paper and the surface becomes dry before the center of the sheet. When the paper surface becomes dry the surface temperature quickly increases to a value above 100°C. The general idea is therefore to estimate the position where the paper surface becomes dry by measuring the surface temperature. The possibility to measure the signal is verified by measurements on a real paper machine. The control system is evaluated by simulations of the drying section model presented in Chapter 6. Similar work for the wire section, where new feedforward signals have been proposed, can be found in [Larsson and Gustafsson, 1998] and [Li, *et al*, 2001].

7.1 The peak position − the position of a dry surface

An important physical aspect in paper drying are the concepts of free water and bound water. The amount of energy required to evaporate the
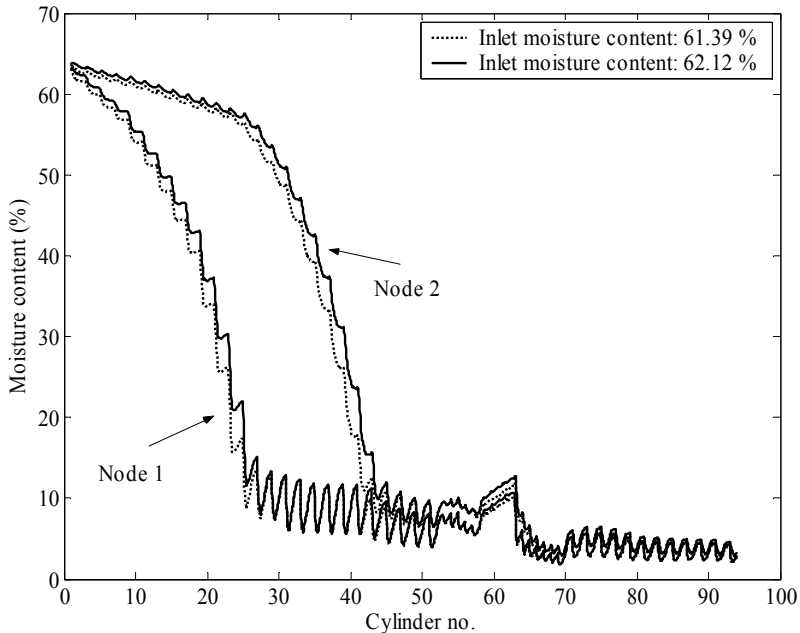
Figure 7.1 Moisture content at the first two nodes in the thickness direction. Note that when the first node reaches a moisture content of 10 %, the second node is still at 60 %.

free water is equal to the latent heat of vaporization. The bound water, however, is tightly bound to the fibres by hydrogen bonds, and requires more energy to evaporate compared to the free water. This means that the paper is more difficult to dry in presence of only bound water. The proposed feedforward structure uses this indirectly by measuring the surface temperature.

As described in Section 6.2, the discretization of the paper sheet model in the thickness direction is set to 10 nodes. A steady-state simulation of the moisture content at the two first nodes seen from the lower surface, is shown in Figure 7.1. The first layer reaches the bound water region at cylinder number 25. This can be seen since the evaporation rate changes significantly. The same event happens to the second fibre layer at cylinder number 43. The paper surface then contains a low moisture content at the same time as a lot of free water is still present in the middle of the paper structure.

To validate the model in terms of simulated paper surface temperature, the temperature has been measured on the paper machine the model is adapted for. By using an IR-camera which gives the surface temperature in a two-dimensional window, temperature values along a line in the
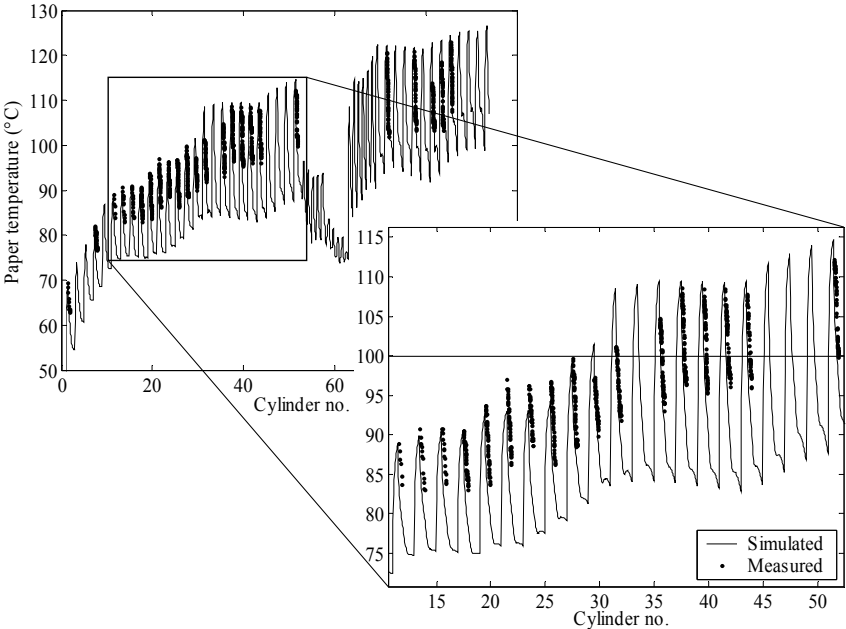
Figure 7.2 Comparison between measured and simulated paper surface temperature. The most important section for the feedforward structure in enlarged and the 100°C-level is indicated.
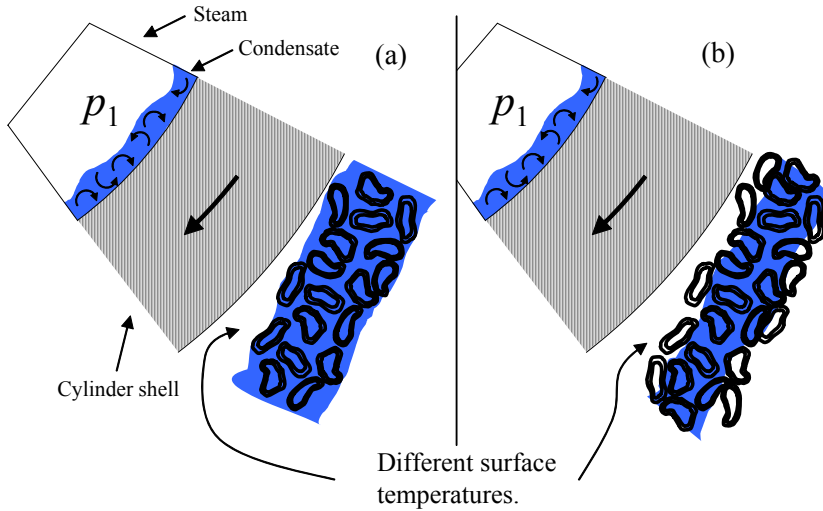
Figure 7.3 Schematic picture that shows the changed properties as the paper surface dries out. A wet surface (a) will act differently compared to a dry surface (b), given the same external conditions.

machine direction are singled out and the results are shown in Figure 7.2. The simulations show both the temperature for the free draw and the part where the paper is in contact with the cylinder. Since the paper in the contact zone is not visible due to the dryer fabrics, the temperature is only measured in the free draw. The simulated values show very good agreement with the measured values. Observe that this is a pure validation without any adjustment of the model, at an operating point different from the one where the model was fitted. Paper temperatures exceeding 100°C are first observed in the free draw section after cylinder number 27 and this phenomenon appears more frequently after cylinder number 35.

The layer of surface fibres without any surrounding free water show totally different properties when it comes to both evaporation and heat transfer mechanisms, compared to fibres surrounded by free water. Since the evaporation requires a large amount of energy, the absence of free water will cause the paper temperature to increase. This can also be considered from another viewpoint. If the surface temperature is above 100°C, there can not exist any free water on the surface since it would instantly evaporate to the surrounding air. The important event is thus the formation of a dry fibre layer since the paper surface temperature will change as the free water is removed. An illustration of the phenomenon is shown in Figure 7.3.

Suggested measuring
position
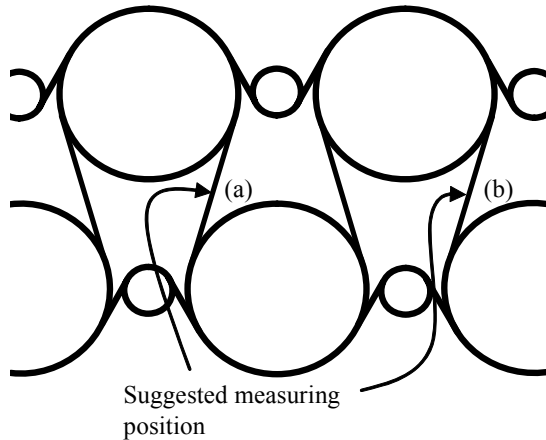
Figure 7.4 Description of the suggested measuring position. It is important to measure on the same side of the paper surface since the drying often is uneven in the thickness direction.

The paper surface temperature measurements shown in Figure 7.2 indicate that the paper surface moisture content is at a low level at cylinder number 27, otherwise the observed high temperatures are not possible. The measurements thus confirm the large moisture gradients in the thickness direction, suggested by the model. The paper surface temperature signal is reliable and showed little variation during the time of the measurements.

The appealing aspect here is that variations in the the inlet moisture content to the drying section affects the position where the paper surface reaches the bound water region. It can therefore serve as an indirect moisture measurement. The paper surface temperature itself is not interesting but the point where there is a sudden increase in temperature indicates that the surface is dry. By measuring the temperature in the middle of a free draw in a number of positions a temperature curve is obtained, see Figure 7.4 and Figure 7.5.

The paper surface temperature obviously also changes when the paper sheet reaches a new steam group (with a different steam pressure inside its cylinders) and it is then not possible to distinguish the occurrence of a dry surface. Measurement of the feedforward signal therefore requires that the paper surface dries out in the middle of a steam group. The steam pressures are also shown in Figure 7.5 to mark the different steam groups. Within each group, the paper surface temperature reaches a constant level but in group 3 and 4 the paper temperature suddenly increases in the middle of the steam group, which corresponds to the first and second node reaching the bound water region. The differences in temperature between
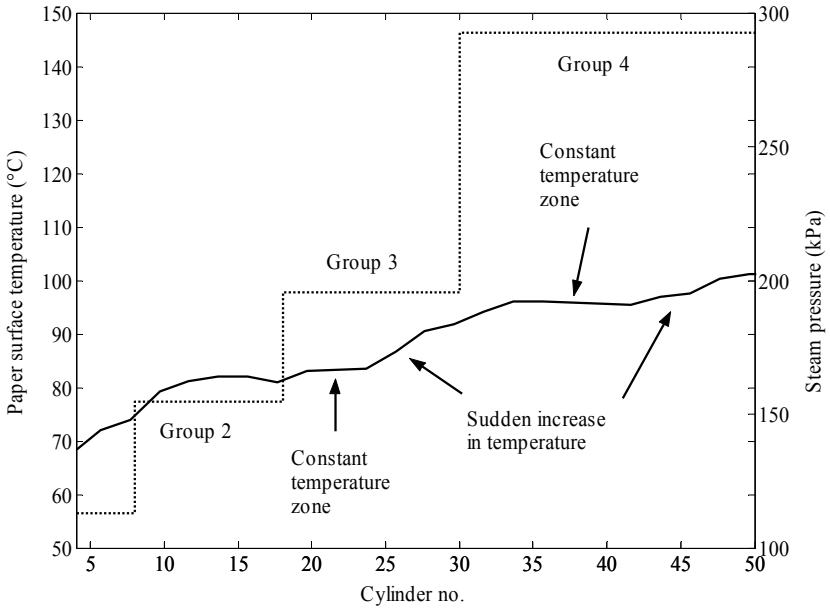
Figure 7.5 The temperature curve obtained by measuring the surface temperature as indicated in Figure 7.4. The steam pressures in the different groups are also shown.
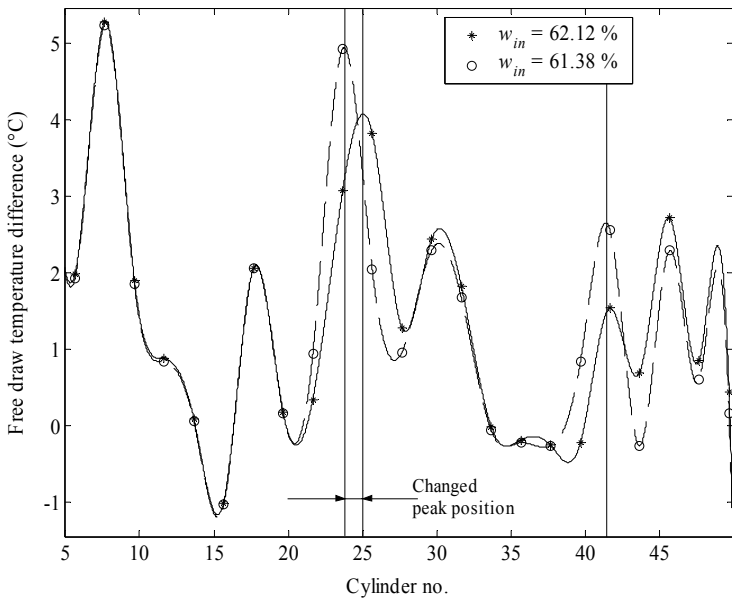
Figure 7.6 A temperature curve calculated by taking the difference between two adjacent temperature measurements, as indicated in Figure 7.4.

173

two adjacent measurements are shown in Figure 7.6. All the differences in free draw paper temperature that deviate from zero are either due to a new steam group or because the paper surface has dried out. The paper surface temperature differences were fitted to cubic splines and the position the maximum of these splines (originated from a dried-out surface) will hereafter be called "peak position".

Two different cases with different inlet paper moisture ratios are shown in Figure 7.6. The paper temperature is affected differently at the two positions where the two first fiber layers dry out but shows the same behavior for the positions of all other peaks (representing the heat-up periods). The peak at cylinder number 43 is a reaction of the free water removal in the second node and does not show large variation in position (cylinder number).

Note that there might well be a difference in peak position and the position where the paper surface actually dries out. The maximum of the temperature difference shows where the dry surface causes maximum effect and not the exact location of a dry surface. For instance, if position (a) in Figure 7.4 show 1 °C higher temperature than the previous measuring position and position (b) show 6 °C higher temperature than (a), the surface may still have dried out just before (a). The effect of the dry surface is however radically increased as the paper reaches (b). The physical meaning of the signals, however, is of minor importance as long as it indicates changes in paper moisture. Both the peak position and the sheet moisture at the reel up will be affected by a disturbance in inlet moisture content and the peak position can therefore be used in feedforward control.

To measure the peak position, an IR camera should be positioned in the free draws around the position where the surface becomes dry. It is crucial to measure at the same position in each free draw to obtain relevant comparisons of the temperatures. Here, the chosen position is the middle of the free draw. The peak position may however be difficult to measure online with the current available measuring technique. The measuring devices must e.g. withstand the humid environment inside the hood and problems with fibre coating on the device must be dealt with. Also, the measuring depth could cause problems if several fibre layers are visible by the measuring equipment. During the experiments it was also observed that both the viewing angle and distance to the paper is important for the result.
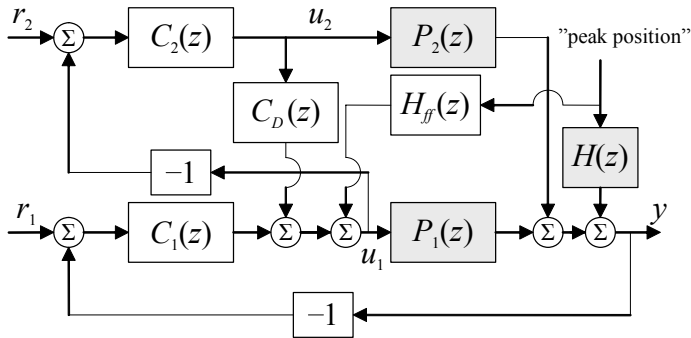
Figure 7.7 A simplified block diagram of the control structure used in the simulations.

7.2 Design of a feedforward controller

Figure 7.7 shows a somewhat simplified block diagram of the mid-ranging control system together with the feedforward. H is the process from peak position to moisture content, H_{ff} is a feedforward block and the definition of the other parts are given in Chapter 6, see Figure 6.13. Since
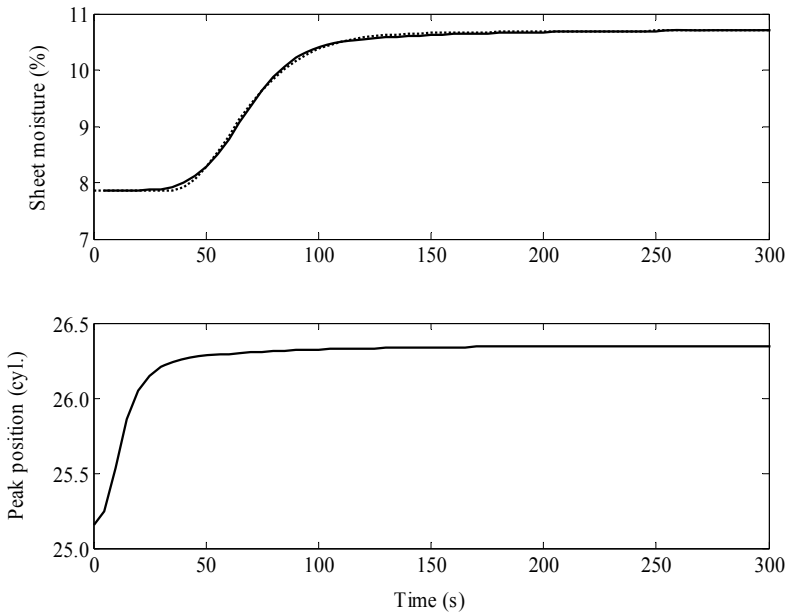
Figure 7.8 The experiment used for identification of H. The solid lines are the result of the simulation and the dotted line is the obtained simplified model given in (7.1).
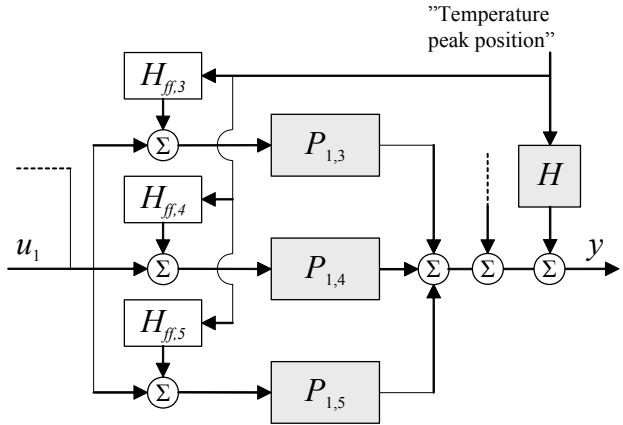
Figure 7.9 A block diagram of the feedforward structure used in the simulations.

the simulation model is very large ($\sim 10^5$ states) it needs to be simplified before it can be used for control design. This is done by system identification of a low order model. To excite the peak position a step change in inlet moisture content to the drying section is performed. The identification of the process and the design of the control system is done in discrete time, where the sample time is 5 seconds. This differs from the procedure in Chapter 6 where the modeling and design are done in continuous time and the discretized right before the implementation. To identify the process H, the moisture controller is put in manual mode (while the steam pressure control is in automatic mode), and a step disturbance is introduced in the moisture content at the inlet of the drying section. The result is shown in Figure 7.8 and the obtained discrete model of the process is

$$H(z) = \frac{0.185z^{-6}}{1 - 1.528z^{-1} + 0.599z^{-2}}. \tag{7.1}$$

The feedforward can be implemented as described above but it is slightly modified. The air system is divided into five groups so that the disturbance compensation from the feedforward "follows" the paper through the machine. More specifically, when there is an indication of a moisture disturbance in the peak position (which is at the first part of the drying section) it is unfavorable to compensate it directly at the end of the drying section. From step responses it is found that the time delay from the first and second air flow actuator to moisture is longer than the time

176
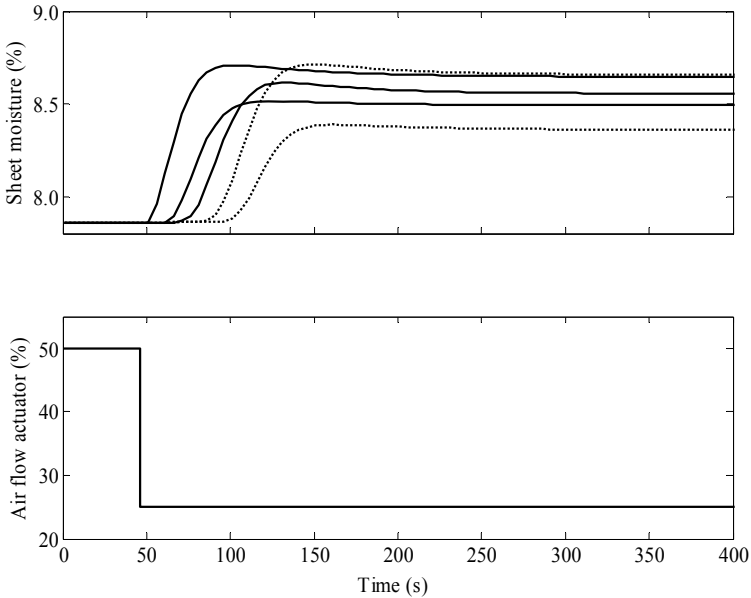
Figure 7.10 Step responses from the five air flow actuators to moisture content at the reel up. The two dashed lines are the first two air groups which are not used for the feedforward control.

delay of H. Consequently, feedforward is not realizable for those groups and only the three last air groups were used. This means that when a disturbance is measured, it is more effective to use the last three air groups. Figure 7.9 shows the configuration, with the three utilized parts of P_1. Since the impact of the disturbance at y is to be eliminated, the condition

$$H + P_{1,3}H_{ff,3} + P_{1,4}H_{ff,4} + P_{1,5}H_{ff,5} = 0, \tag{7.2}$$

holds. For simplicity the feedforward filters were selected as

$$H_{ff,3} = -\frac{H}{3P_{1,3}}, H_{ff,4} = -\frac{H}{3P_{1,4}}, H_{ff,5} = -\frac{H}{3P_{1,5}}. \tag{7.3}$$

The control signals of the last three air groups now might be different and therefore C_2 was set to control the actuator signal of the first two groups (u_1). Another possible solution is to let C_2 control the mean value of all

five air flow actuators or to introduce multivariable control in the steam system so that each air group is mid-ranged by a steam group.

Just as in the case of *H*, the air groups are identified from step responses, shown in Figure 7.10, and are given by

$$P_{1,3}(z) = \frac{-0.00411 + 0.00198z^{-1}}{1 - 1.609z^{-1} + 0.685z^{-2}} z^{-6},$$

$$P_{1,4}(z) = \frac{-0.00476 + 0.00224z^{-1}}{1 - 1.490z^{-1} + 0.590z^{-2}} z^{-4}, \qquad (7.4)$$

$$P_{1,5}(z) = \frac{-0.00537 + 0.00214z^{-1}}{1 - 1.537z^{-1} + 0.639z^{-2}} z^{-1}.$$

7.3 Simulations

The feedforward system in (7.3) is simulated with a step disturbance in inlet moisture ratio. It is then compared to simulations with conventional steam pressure control and with the previously developed mid-ranging control system in Chapter 6. The sheet moisture is shown in Figure 7.11.
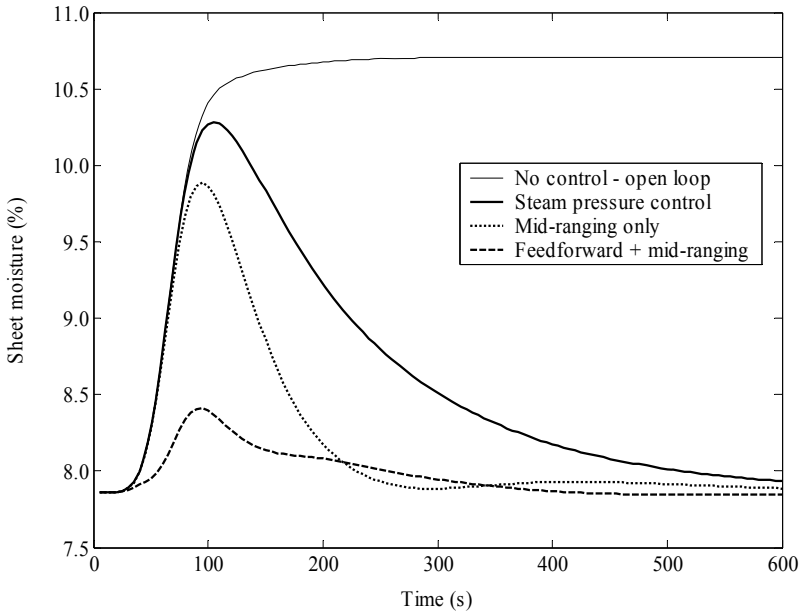
Figure 7.11 Comparison of different control systems.
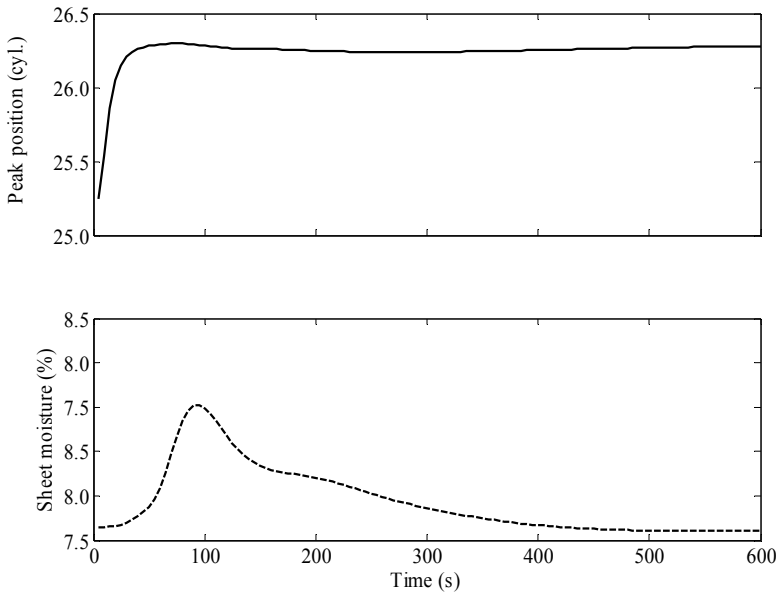
Figure 7.12 Peak position and sheet moisture during the closed loop simulation.
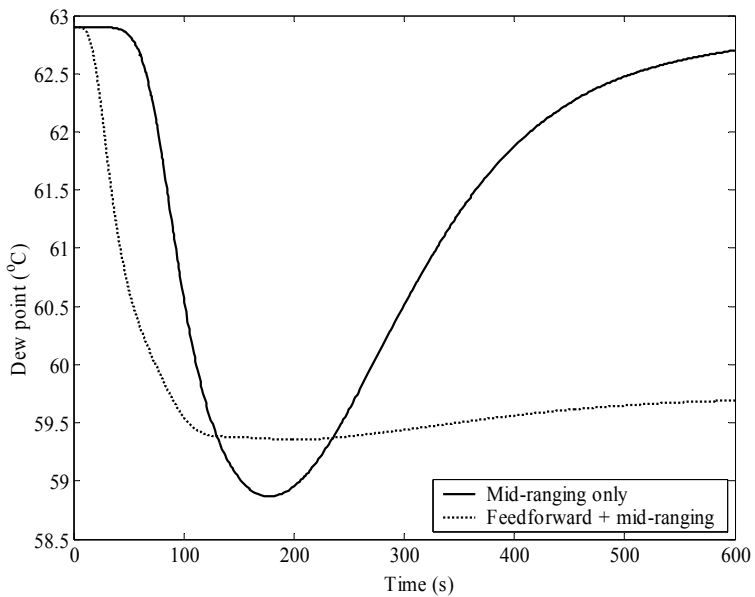
Figure 7.13 Change in dew point.
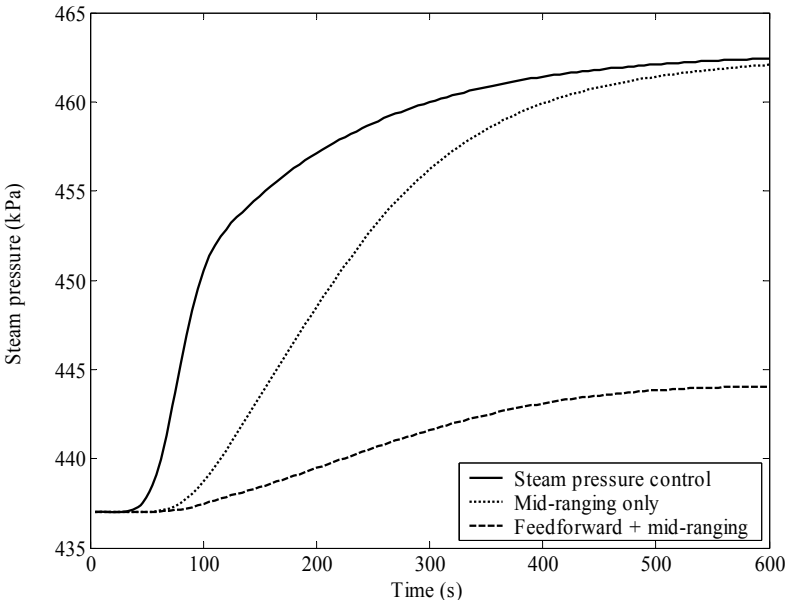
Figure 7.14 Comparison of the steam pressure in the lead group by the different control system.
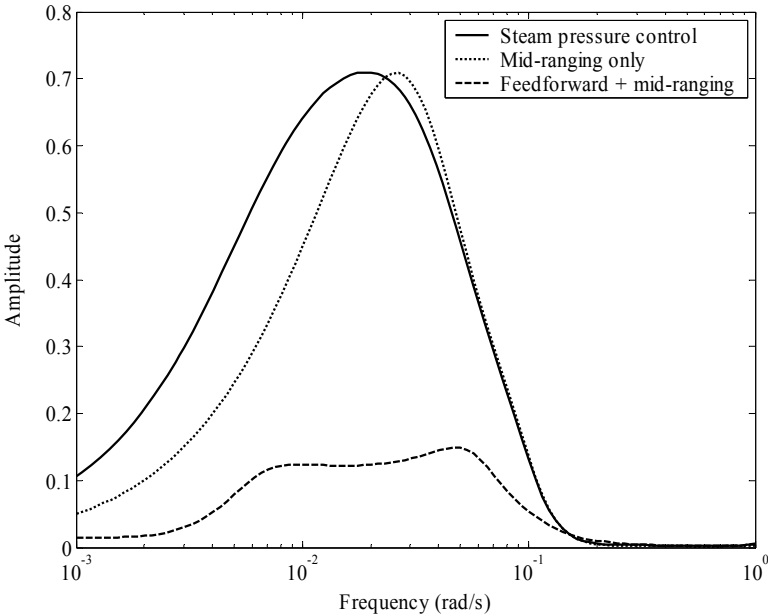
Figure 7.15 Frequency plot, showing how the disturbances in inlet moisture propagate, for the different control systems.

The most apparent result is that the disturbance is greatly attenuated. After 150 seconds the decreasing rate of the moisture content restoration is reduced for the feedforward system. The reason for this can be seen in Figure 7.12, where the peak position is shown for the same simulation. When the control system compensates for the disturbance by increasing the control signal, it also slightly affects the peak position. The feedforward signal is thus affected but this dynamic relation from u_1 to the peak position in Figure 7.7 is neglected. By considering this in (7.2) the feedforward could probably be slightly improved. For comparative reasons Figure 7.11 also shows the moisture deviation when all control systems are switched off (open loop).

The dew points in $P_{1,3}$ are shown in Figure 7.13 and the steam pressures are shown in Figure 7.14. Notable for the two feedforward control systems is that the air flow actuators are not restored to their original positions by the mid-ranging part. This was also noted in Section 7.2. Multivariable control of the air and steam groups could be introduced to give maximum manoeuvring range to the individual air flow actuators, if desired.

The different control systems are also compared by evaluating their disturbance rejection in the frequency domain, see Figure 7.15. The figure is generated by identifying the process from inlet moisture content to moisture content at the reel-up and the figure simply shows the Bode plot of the identified model. The feedforward control shows to be superior. Due to the low pass characteristics of the process, all systems attenuate high frequencies similarly. For low frequencies the difference between the systems is considerable. Since there are both slow dynamics and long time delays in the process, the feedback systems can only attenuate extremely slow disturbances (note that 10^{-3} rad/s is a variation with a period time of almost two hours). The feedforward can beneficially use its prior information about the disturbances acting on the system.

The feedforward assumes linear systems while the system is nonlinear. With the presented technique to obtain the control parameters it is therefore not possible to completely eliminate the effect of disturbances.

Remark

The implementation of the feedforward does not require a mid-ranging control system. It might as well be combined with any other moisture control structure. The mid-ranging controller is chosen here to give natural connection to Chapter 6.

7.4 Summary

A new measured signal, called the peak position, has been presented that can be used for feedforward in moisture control. The signal is based on measurements of paper surface temperature in several free draw zones. By observing the position at which the paper dries out on the surface it is possible to compensate for moisture disturbances before they are measured by the moisture scanner at the reel-up.

With the addition of the peak position in combination with a process model, it is possible to significantly reduce the transients from inlet moisture disturbances. From the studied step disturbance it is clear that the feedforward signal greatly improves the performance of the paper moisture control system.

The peak position may be difficult to measure with the current available technique. The potential increase in performance is, however, large and the signal may be replaced by any other suitable signal that indicates disturbances in moisture content. Equipment that measure the surface moisture content are being developed [Boström, 2002]. This signal would be very suitable for feedforward control. What type of signal that is finally chosen is of minor importance, as long as it can be used as a disturbance indication.

8

Object-Oriented Modeling and Predictive Control of the Moisture Content

The model used in Chapter 6 and Chapter 7 is capable of dynamically describing moisture gradients and other properties inside the paper sheet. This is necessary for the simulation of feedforward from surface temperature measurements (the peak position). However, the model contains approximately 10^5 states which make simulations fairly tedious. It also lacks a physical model for the steam system, where it instead uses a black-box model. Therefore a less complex model is developed that is based purely on physical relations. The objective is control of the moisture at the reel-up and not to accurately describe micro-scale moisture variations inside the sheet. The model is built on heat and mass balances for steam, cylinder, and paper. The core of the model is based on work by [Wilhelmsson, 1994], [Persson, 1998], and [Slätteke and Åström, 2005].

The model is implemented in the object-oriented modeling language Modelica, see [Mattsson and Elmqvist, 1997], [Mattsson, *et al*, 1998], and [Fritzson, 2004]. Like any object-oriented programming language, Modelica provides the notions of classes and objects, also called instances, as the fundamental tool. Properties like inheritance and abstract classes provide a structured approach to implement equations. The advantages of such a modeling tool are (i) it is built on a non-causal equation structure (ii) it is possible to create model components that

correspond to physical objects in the real world, in contrast to modeling techniques that require conversion to signal blocks (iii) it permits mixing of physics with empirical models (iv) it is easy to go from simple models to high fidelity models by drag and drop features (v) it is easy to build and exchange model libraries and (vi) it is suited for modeling in several engineering domains.

The obtained model is used to investigate how the heat transfer coefficient affects some dynamic properties and this is compared to some of the results presented in Chapter 4. It is also validated against measurements on a real paper machine. Finally, the model is used to evaluate a new MPC strategy to control the moisture that has similar ideas as the mid-ranging structure in Chapter 6.

8.1 The model

This chapter describes a physical simulation model of a drying section, implemented in an object oriented modeling language. A similar attempt is [Bergström and Dumont, 1998] and [Bortolin, *et al*, 2004], where the object oriented modeling technique is demonstrated by modeling the stock preparation (the process section that precedes the paper machine) and the wet end, and the commercial process simulator APROS [Silvennoinen, *et al*, 1989], [Niemenmaa, *et al*, 1996]. The objective is to develop a non-linear model that captures the key dynamical properties for a wide operating range. The equations for the steam and cylinder process are taken from Chapter 4, apart from a few exceptions. For completeness, they are all shown here.

The steam and cylinder process

Let q_s be the mass flow rate of steam into the cylinder, q_c be the condensation rate, q_{bt} the blow through steam, and q_w be the siphon flow rate. Also, let V_s and V_w be the volume of steam and water in the cylinder, and let ρ_s and ρ_w be the densities. The mass balances for water and steam are then

$$\frac{d}{dt}\left(\rho_s V_s\right) = q_s - q_c - q_{bt},$$
$$\frac{d}{dt}\left(\rho_w V_w\right) = q_c - q_w. \tag{8.1}$$

The energy balances for steam, water, and metal are

$$\frac{d}{dt}(\rho_s u_s V_s) = (q_s - q_{bt})h_s - q_c h_s,$$

$$\frac{d}{dt}(\rho_w u_w V_w) = q_c h_s - q_w h_w - Q_m, \qquad (8.2)$$

$$\frac{d}{dt}(mC_{p,m}T_m) = Q_m - Q_p,$$

where Q_m is the power supplied from the water to the metal, Q_p is the power supplied from the metal to the paper, h_s is the steam enthalpy, h_w is the water enthalpy, m the mass of the cylinder shell, $C_{p,m}$ the specific heat capacity of the shell, T_m the mean temperature of the metal, u_s and u_w are the specific internal energies of steam and water. The steam and water volumes add up to the total cylinder volume,

$$V = V_s + V_w. \qquad (8.3)$$

The power flow to the metal is given by

$$Q_m = \alpha_{sc} A_{cyl}(T_s - T_m), \qquad (8.4)$$

where α_{sc} is the heat transfer coefficient from the steam-condensate interface to the centre of the cylinder shell, A_{cyl} is the inner cylinder area, and T_s the steam temperature. The power flow to the paper is

$$Q_p = \alpha_{cp} A_{cyl} \eta (T_m - T_p), \qquad (8.5)$$

where T_p is the paper temperature, α_{cp} the heat transfer coefficient from the cylinder shell to the paper, and η is the fraction of dryer surface covered by the paper web. In Chapter 4, α_{sc} is used to calibrate the model against plant data. Here, both α_{cp} and α_{sc} are possible candidates for that purpose. Experiments have shown that α_{sc} depends on both condensate thickness, machine speed, and the number of spoiler bars, see [Pulkowski and Wedel, 1988] and [Wilhelmsson, 1995]. However, the condensate has a turbulent behavior and the heat transfer coefficient has proven to be difficult to model, see Figure 8.1. Therefore α_{sc} is used as a free variable to calibrate the model with. Empirical models for α_{cp} have been
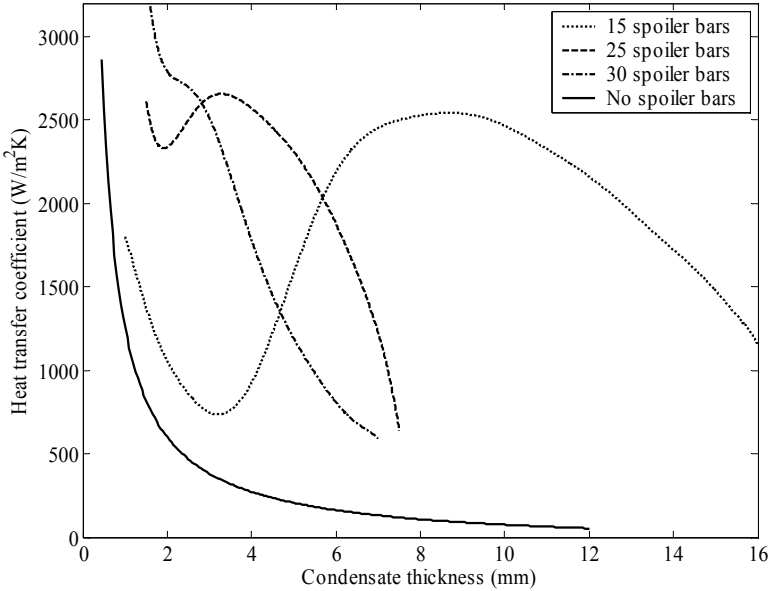
Figure 8.1 Steady-state measurements of how the number of spoiler bars affect the heat transfer coefficient for the condensate [Pulkowski and Wedel, 1988]. It also depends on machine speed and bar size, and is difficult to model due to the turbulent behavior.

developed. From [Wilhelmsson, 1995] a linear relation with moisture ratio u is given

$$\alpha_{cp}(u) = \alpha_{cp}(0) + 955u, \tag{8.6}$$

is obtained, where $\alpha_{cp}(0)$ varies between 200 and 500 W/(m^{2}K). It is well known that α_{cp} depends on other things, e.g. the web tension, and surface smoothness of both paper and cylinder, but this is omitted here.

Since the steam flow to the cylinder cannot be manipulated directly, a valve model is also needed. From [Thomas, 1999] we have

$$q_s = C_v f_v(x_v)\sqrt{(p_{sh} - p)\rho_s}, \tag{8.7}$$

where C_v (m^2) is the valve conductance, x_v is the position of the valve stem and the function f_v is the valve characteristics called valve trim. The valve stem varies from 0 (minimum valve opening) to 1 (maximum valve opening). The supply pressure at the steam header is p_{sh}. We use equal
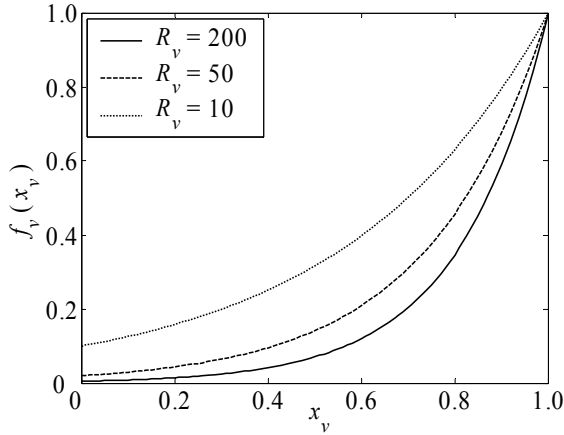
Figure 8.2 Equal percentage valve characteristic.

percentage trim, since it is the most common characteristic in the process industry [Hägglund, 1991], see Figure 8.2. It is given by

$$f_v(x_v) = R_v^{x_v-1}. \tag{8.8}$$

R_v is a constant known as the "rangeability" since it is the ratio between the maximum and minimum valve opening.

For simplicity, all steam within the cylinder cavity is assumed to be homogeneous with the same pressure and temperature. We also assume that the steam in the cylinder is saturated. This means that the enthalpy, density, and temperature are functions of the pressure only. Fitting polynomials to the tabulated values for saturated steam in [Schmidt 1969], gives

$$\begin{aligned}
T_s &= 0.1723(\ln p)^3 - 3.388(\ln p)^2 + 37.71\ln p - 148.7, \\
h_s &= [-0.07402(\ln p)^4 + 2.887(\ln p)^3 - 39.58(\ln p)^2 \\
&\quad + 260\ln p + 1824]\cdot 10^3, \\
h_w &= [0.8842(\ln p)^3 - 18.77(\ln p)^2 + 200\ln p - 748.5]\cdot 10^3, \\
\rho_s &= [0.005048p + 64.26]\cdot 10^{-3}, \\
\rho_w &= -0.3136(\ln p)^3 + 6.792(\ln p)^2 - 52.43\ln p + 1141.
\end{aligned} \tag{8.9}$$

Equations (8.1) − (8.9) are a crude nonlinear model for the steam-cylinder process. By choosing p, V_w, and T_m as state variables and using partial

derivatives, the system can be rewritten into a third order state equation (most steps are omitted here), where f_1, f_2, and f_3 are defined as the right hand side of the equations.

$$e_{11}\frac{dp}{dt} + e_{12}\frac{dV_w}{dt} = C_v f_v(x_v)\sqrt{(p_{sh} - p)\rho_s} - q_w - q_{bt} = f_1,$$

$$e_{21}\frac{dp}{dt} + e_{22}\frac{dV_w}{dt} = C_v f_v(x_v)\sqrt{(p_{sh} - p)\rho_s}h_s$$

$$- q_{bt}h_s - q_w h_w - \alpha_{sc} A_{cyl}(T_s - T_m) = f_2, \qquad (8.10)$$

$$e_{33}\frac{dT_m}{dt} = \alpha_{sc} A_{cyl}(T_s - T_m) - (\alpha_{cp}(0) + 955u)A_{cyl}\eta(T_m - T_p) = f_3,$$

where

$$e_{11} = (V - V_w)\frac{d\rho_s}{dp} + V_w\frac{d\rho_w}{dp},$$

$$e_{12} = \rho_w - \rho_s,$$

$$e_{21} = h_s(V - V_w)\frac{d\rho_s}{dp} + \rho_s(V - V_w)\frac{dh_s}{dp} + h_w V_w \frac{d\rho_w}{dp} + \rho_w V_w \frac{dh_w}{dp} - V,$$

$$e_{22} = \rho_w h_w - \rho_s h_s,$$

$$e_{33} = mC_p.$$

$$(8.11)$$

In the rewritings of the energy balances above the specific internal energy has been eliminated by the definitions $u_s = h_s - p/\rho_s$ and $u_w = h_w - p/\rho_w$. Using f_1, f_2, and f_3 the system can be further rewritten into an explicit state form.

$$\frac{dV_w}{dt} = \frac{e_{33}e_{21}f_1 - e_{11}e_{33}f_2}{e_{33}(e_{21}e_{12} - e_{11}e_{22})},$$

$$\frac{dp}{dt} = \frac{e_{12}e_{33}f_2 - e_{33}e_{22}f_1}{e_{33}(e_{21}e_{12} - e_{11}e_{22})}, \qquad (8.12)$$

$$\frac{dT}{dt} = \frac{f_3}{e_{33}}.$$
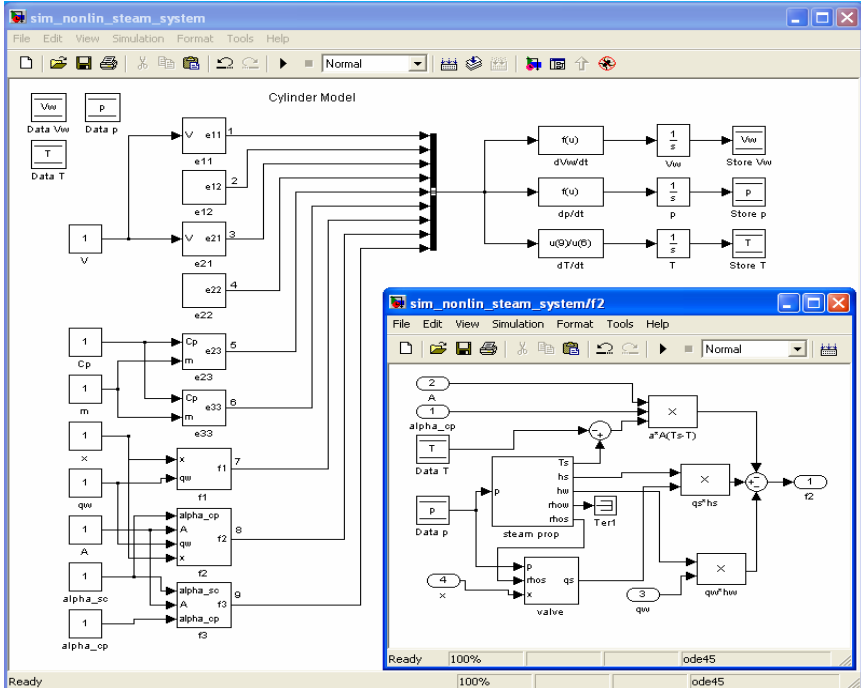
Figure 8.3 A Simulink model of (8.12). The submodel f_2 is also opened, which in turn contains submodels.

```
model Cylinder

  equation
  Ms = rhos*Vs;
  der(Ms) = qs - qc - qbt;                  % (8.1)
  Mw = rhow*Vw;
  der(Mw) = qc - qw;

  Es = rhos*us*Vs;
  us = hs - p/rhos;
  der(Es) = (qs - qbt)*hs - qc*hs;
  Ew = rhow*uw*Vw;                          % (8.2)
  uw = hw - p/rhow;
  der(Ew) = qc*hs - qw*hw - Qm;
  Em = m*Cp*Tm;
  der(Em) = Qm - Qp;

  V = Vs + Vw;                              % (8.3)
  Qm = alpha_sc*Acyl*(Ts - Tm);            % (8.4)
  Qp = alpha_cp*Acyl*eta*(Tm - Tp);        % (8.5)

end Cylinder;
```

Figure 8.4 Code segment of the Modelica model of the steam cylinder. In addition, equations for steam properties are required to give a complete simulation model.

In this form the model can be directly implemented and simulated in e.g. Simulink, see Figure 8.3. By using Modelica instead the tedious and error prone procedure of transforming the system to explicit form is avoided and we let the simulation environment decide the state realization. Since the transformation of equations is automated, it is also easier to change the model at a later stage. Equations (8.1) − (8.5) are put into the simulation environment as they are, see Figure 8.4.

The paper web process

We will now expand the model to also include dynamics for the paper sheet. To describe the moisture in the paper we need a mass balance and to describe the paper temperature we need an energy balance. Starting with the mass balance, we describe how much water is evaporating from the paper surface to the air. From [Persson, 1998] we get the Stefan equation

$$q_{evap} = \frac{p_{tot} K M_w}{R_g T_p} \ln\left(\frac{p_{tot} - p_{v,a}}{p_{tot} - p_{v,p}} \right), \tag{8.13}$$

where q_{evap} is the evaporation rate (kg/m^{2}s), K is the mass transfer coefficient (m/s), M_w is the molecular weight of water (kg/mole), p_{tot} the total pressure (Pa), $p_{v,a}$ the partial pressure for water vapor in the air (Pa), $p_{v,p}$ the partial pressure for the water vapor at the paper surface, R_g the gas constant (J/mole·K), and T_p the paper temperature (K). The partial pressure $p_{v,a}$ is given by the moisture content of air, x (kg water vapor/kg dry air), and the total pressure,

$$p_{v,a} = \frac{x}{x + 0.62} p_{tot}. \tag{8.14}$$

The vapor partial pressure at the paper surface is

$$p_{v,p} = \varphi \, p_{v0}, \tag{8.15}$$

where p_{v0} is the partial vapor pressure for free water. This is given by Antoine's equation
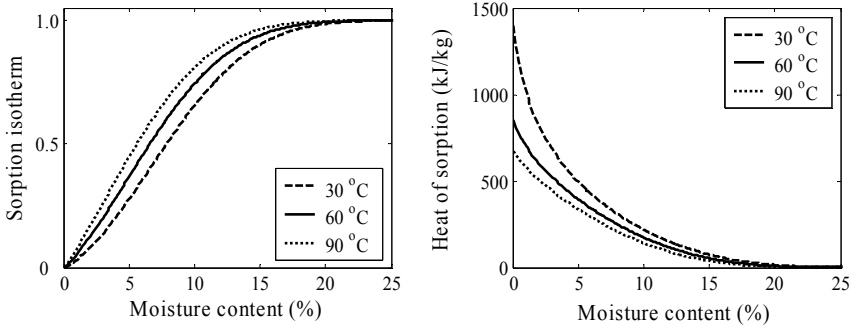
Figure 8.5 Sorption isotherm, φ, and heat of sorption, ΔH_s given by (8.17) and (8.21).

$$p_{v0} = 10^{\left(10.127 - \frac{1690}{T_p - 43.15}\right)}. \tag{8.16}$$

As long as capillary transport can bring new water to the paper surface, the vapor partial pressure at the paper surface is equal to the partial pressure for free water. When the paper becomes dryer a correction factor called sorption isotherm, φ, is invoked which has a value between zero and one, see Figure 8.5. The sorption isotherm of a paper web depends on its composition and temperature. It is not very well investigated when compared to other materials [Pettersson and Stenström, 2000], but [Heikkilä, 1993] gives an empirical expression for paper pulp, namely

$$\varphi = 1 - \exp(-47.58u^{1.877} - 0.10085(T_p - 273)u^{1.0585}), \tag{8.17}$$

where u is the moisture ratio (kg moisture/kg fiber). Also, let v_x be the speed of the paper web (m/s), d_y the width of the paper web (m), A_{xy} the area of the dryer surface covered by paper (m^2), and g the dry basis weight (kg/m^2). Then the mass balance of moisture in the paper web can be written as

$$\frac{d(ugA_{xy})}{dt} = d_y v_x g u_{in} - A_{xy} q_{evap} - d_y v_x g u. \tag{8.18}$$

Figure 8.6 shows a schematic picture of the mass flows in the model. To model the energy balance, introduce
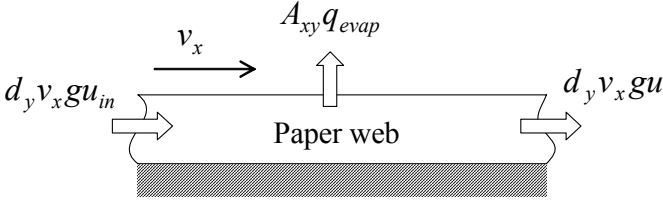
Figure 8.6 The mass balance for moisture in the paper web. The shaded area is the cylinder wall

$$C_{p,p} = \frac{C_{p,fiber} + uC_{p,w}}{1+u},$$
(8.19)

where $C_{p,p}$, $C_{p,fiber}$, and $C_{p,w}$ is the specific heat capacity for the paper, fiber and water, respectively (J/kg·K). As we can see, $C_{p,p}$ is a weighted sum of the heat capacities of the parts. From [Wilhelmsson, 1995] we have $C_{p,fiber}$ = 1256 J/(kg·K).

Also, let T_p be the paper temperature and ΔH be the amount of energy needed to evaporate the water. Analogously to the discussion about the mass balance, if the web is wet enough this energy is equal to the latent heat of vaporization for free water. When the paper becomes dryer an extra amount of energy ΔH_s (the heat of sorption) is necessary besides the latent heat of vaporization for free water. The heat of sorption can be derived from the sorption isotherm by thermodynamic theory and this relation is known as the law of Clausius-Clapeyron

$$\Delta H_s = -\frac{R_g}{M_w} \left[\frac{d(\ln \varphi)}{d(1/T_p)} \right],$$
(8.20)

and by applying this on (8.17), we get

$$\Delta H_s = 0.10085 u^{1.0585} T_p^2 R_g \frac{\varphi - 1}{M_w \varphi}.$$
(8.21)

The amount of energy required to evaporate the water from the surface of the web is the given by

$$\Delta H = \Delta H_{vap} + \Delta H_s,$$
(8.22)

$$A_{xy}q_{evap}(\Delta H_{vap} + \Delta H_s)$$

$$d_y v_x g(1+u_{in})C_{p,p}T_{p,in} \qquad\qquad d_y v_x g(1+u)C_{p,p}T_p$$

Paper web

$$Q_p$$
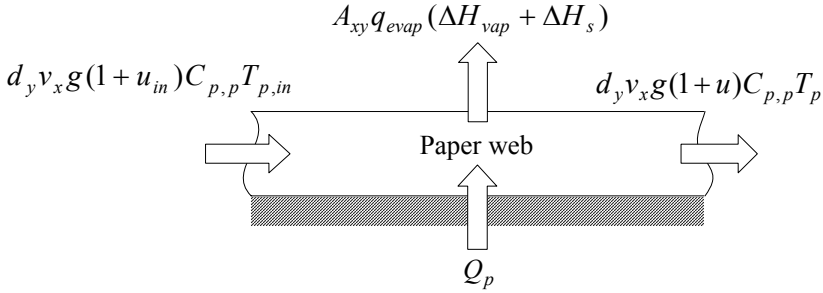
Figure 8.7 The energy balance of the paper web. The shaded area is the cylinder wall.

where ΔH_{vap} is the latent heat of vaporization, equal to 2260 kJ/kg (at atmospheric pressure).

Reference [Pettersson and Stenström, 2000] investigates some sorption isotherms found in the literature. Many of those give a heat of sorption that goes to infinity as u goes to zero. This is physically unrealistic since the bond energy between the last fraction of water and a cellulose fiber must be finite. From [Heikkilä, 1993], a finite heat of sorption at the origin which matches the hydrogen bond energy between water−fiber is given and is therefore found to be most appropriate. The heat loss in the paper due to mass evaporation is dominating the heat conduction and radiation, which therefore can be neglected. In addition, since water is an incompressible medium there is no pressure volume work on the surroundings and we write the energy balance as a change in enthalpy. The energy balance of the paper web is thus modeled as

$$\frac{d\left(g(u+1)A_{xy}C_{p,p}T_p\right)}{dt} = d_y v_x g(1+u_{in})C_{p,p}T_{p,in} \tag{8.23}$$
$$- A_{xy}q_{evap}(\Delta H + \Delta H_s) - d_y v_x g(1+u)C_{p,p}T_p,$$

see Figure 8.7. In addition, we let the heat transfer coefficient from the cylinder to the paper web depend on the moisture content in the web.

To summarize the complete drying section model, it is given by the balances in (8.1), (8.2), (8.18), and (8.23), together with the algebraic relations given in (8.3)−(8.9), (8.13)−(8.17), (8.19), (8.21), and (8.22). Equation (8.1) and (8.2) define the dynamics of a cylinder, and one set of these equations are needed for each cylinder in the drying section. The dynamics of a lumped paper web model is given by (8.18) and (8.23). By connecting a series of these equations a discretized model is obtained,
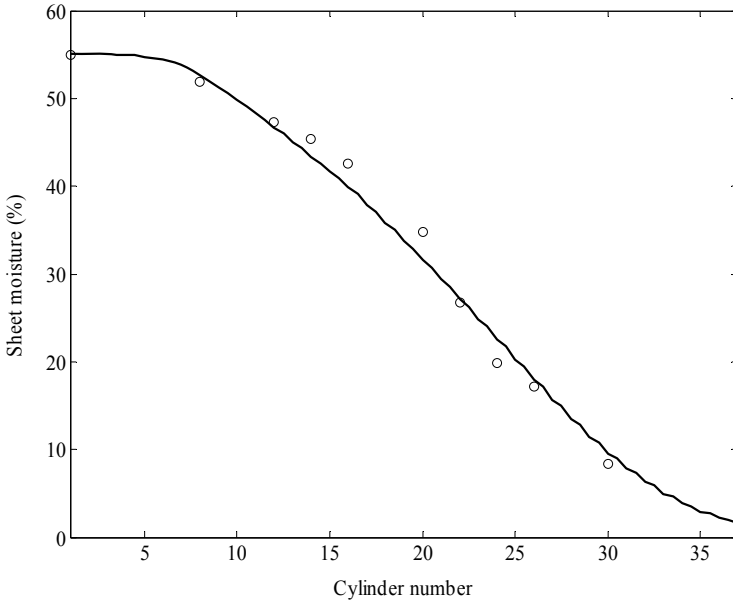
Figure 8.8 Validation by comparing steady-state simulations with moisture measurements on a fine paper machine.

where the outflow of paper of one component becomes the inflow of the next component.

8.2 Steady-state model validation

The two partial models in Section 8.1, are validated separately in [Slätteke and Åström, 2005] and [Persson, 1998]. To assure that the combined model is satisfying it has been validated against steady-state data taken from a paper machine producing fine paper [Stenström, et al, 1994]. The machine is running at 708 m/min with a basis weight of 80 g/m^2. The paper is over dried to a final moisture content of only 0.012 kg/kg, since this is a predryer which is immediately followed by a size press (a unit where starch is applied to the surface to obtain strength and water resistance) where a certain amount of rewetting occurs.

The moisture content is measured in 11 different positions, which can be seen in Figure 8.8 together with the simulation result. The heat transfer coefficient α_c is used as fitting parameter with the same value in all cylinders and 1100 W/(m^2·K) is found to give the best fit by visual inspection. The agreement between model and measurements is good even
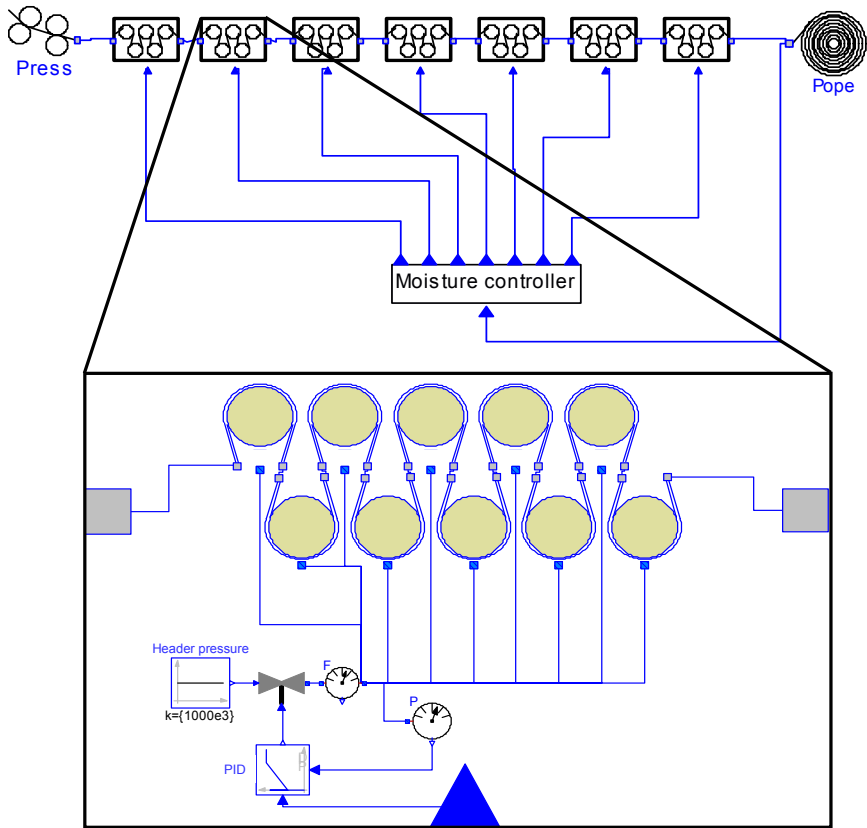
Figure 8.9 The Modelica model of the drying section used in the simulations. The component of the second dryer group is expanded, showing the cylinders, steam valve, and PID controller. It is assumed that the temperature and moisture are constant at a single cylinder due to the high machine speed, hence modeled as one control volume.

though this is rough validation without using all possible degrees of freedom, e.g. by assuming different α_c in different cylinders. The model also captures the three zones in the drying process, the heating phase, the constant drying rate phase, and the falling drying rate phase [Karlsson, 2000]. In the heating phase (cyl. 1−5) most steam energy is used to heat the web and the evaporation rate is low. In the constant rate phase (cyl. 6−30), energy to the web is equal to the energy consumed for water vaporization. In the falling rate phase (cyl. 31−37), drying rate begins to decrease due to the hygroscopic nature of the fibres.

8.3 Open loop simulations

A simulation model of a fictitious drying section is used in simulations to investigate different properties. It consists of 60 drying cylinders divided in 7 drying groups, see Figure 8.9. The machine speed is chosen to 1100 m/min, the machine width is 7.15 m, and the dry weight of the paper sheet is 77 g/m^2. This is also the drying section model used in Section 8.5 to evaluate MPC control of the moisture.

In Chapter 4 the IPZ model is deduced from physical relations. It is concluded that a slow pole in the process dynamics can be regarded as an integrator if the heat transfer coefficient of the steam-condensate interface is much larger than the heat transfer coefficient of the cylinder-paper interface, $\alpha_{sc} \gg \alpha_{cp}$, see (4.3) and (4.4). In Figure 8.10 response in steam pressure during a step in valve position is shown for two different cases of heat transfer coefficient α_{cp}. This implies that in this analysis α_{cp} is set to a constant value instead of the linear relationship (8.6) to define it independently of u. It is clear from Figure 8.10 that for the case with
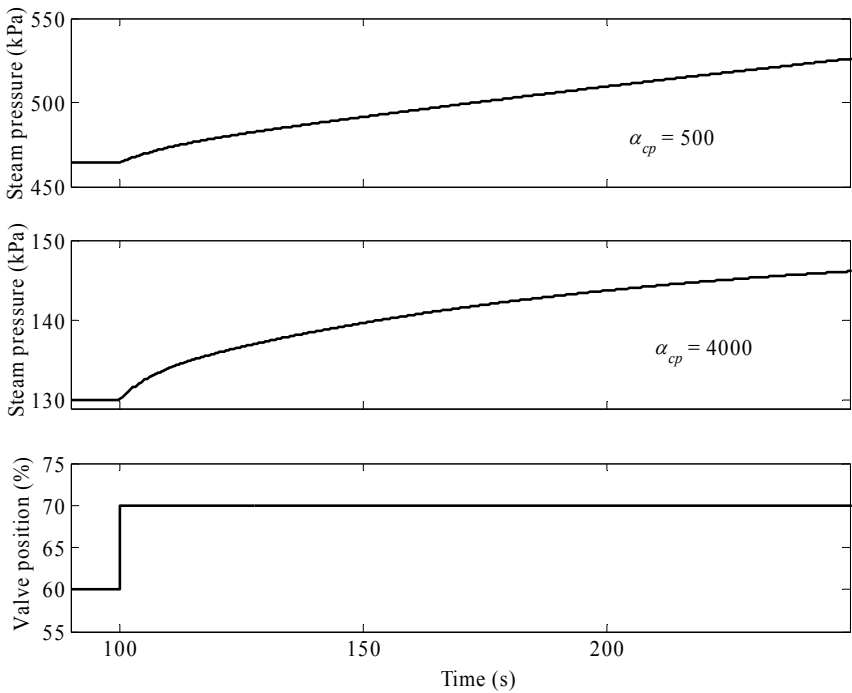
Figure 8.10 Pressure response for a step in valve position for two different values of α_{cp}. Heat transfer coefficient $\alpha_{sc} = 4000$.
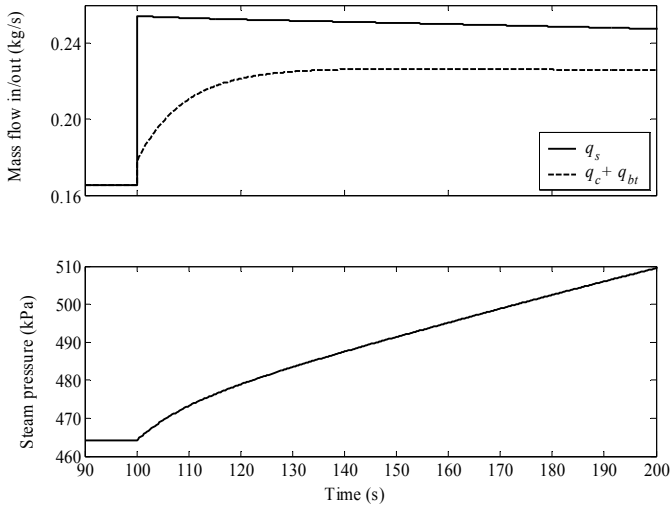
Figure 8.11 Open loop step response in pressure with $\alpha_{sc} = 4000$ W/(m²·K). Heat transfer coefficient α_{cp} is set to a constant value 500 W/(m²·K).
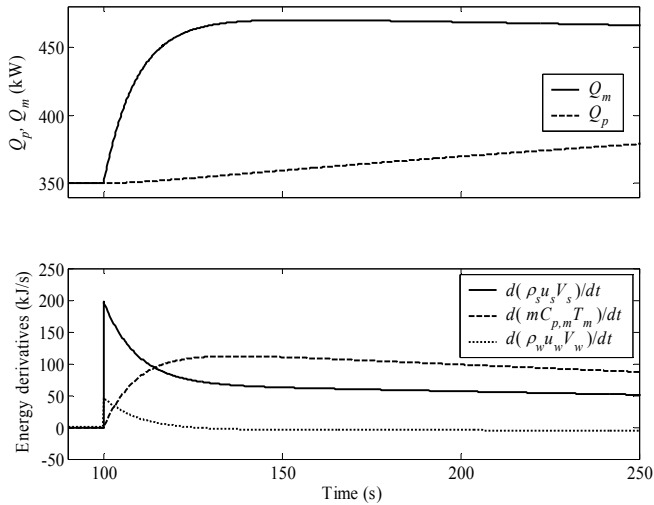
Figure 8.12 Open loop step response in pressure with $\alpha_{sc} = 4000$ W/(m²·K). Heat transfer coefficient α_{cp} is set to a constant value 500 W/(m²·K).

$\alpha_{cp} = 500$ W/(m²·K), the process can be modeled with an integrator plus some dynamics for the given time frame (in reality we know that the integrator is a slow pole). However, for the response with $\alpha_{cp} = 500$ W/(m²·K) an IPZ model is not sufficient. Note that since the heat transfer coefficients are different in the two figures, the steady-state solutions are

also different and the two simulations start from different steady-state steam pressures. The conclusion is unaffected if the two responses start at the same pressure.

Figure 8.11 gives an explanation for the characteristic appearance of the open loop step response of the steam pressure. When the steam valve position is increased, it will increase the steam pressure inside the cylinder and consequently the saturation temperature of the steam and the condensation rate. However, the increasing condensation rate lags behind the increasing steam inlet flow as the condensate layer heats up to the new steady state temperature. Therefore, there will be a fast initial build-up in steam pressure, before the steam consumption has reached its new value. This is also noted in Chapter 3.

Figure 8.12 shows the energy flows to the cylinder and paper, and also the energy derivatives. In the derivation of the linear model in Chapter 4, it is simplified by assuming that the thermal dynamics of the water is fast compared to the dynamics of steam and metal. The energy balance is therefore replaced by a static model by defining its derivative as zero.
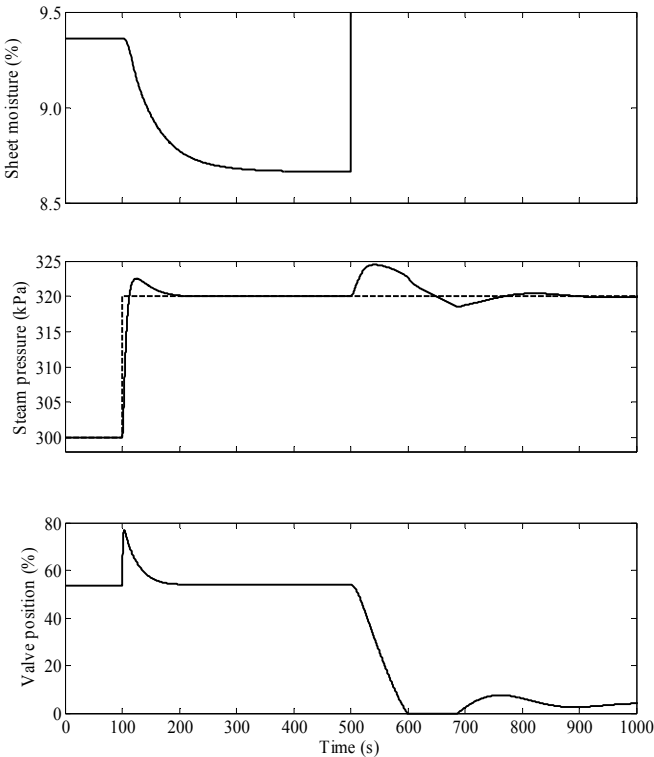
Figure 8.13 Simulation of set point change in steam pressure and a web break.

Figure 8.12 shows that this assumption is valid. Since the cylinder shell acts as a thermal filter Q_p is increasing more slowly that Q_m.

Figure 8.13 shows a simulation where the steam pressure controllers are in closed loop while the moisture is uncontrolled. The pressure is controlled by a PI controller tuned according to the method in Chapter 5 with $M_s = 1.2$. At $t = 100$ s there is a steam pressure set point change. The valve position returns to its initial position when the set point is reached due to the integral action in the process. Note that the characteristic over-shoot in steam pressure does not result in an over-shoot in the moisture. At $t = 500$ s there is a web break and the moisture quickly reaches a level around 60 % since the sheet has lost the energy source for its evaporation, and the curve is out of the scale in the figure. Since the main energy sink is lost for the cylinders, the control valve is almost closed to keep the desired steam pressure.

Figure 8.14 shows two simulations of moisture response for a set point change in steam pressure: One with a medium heat transfer coefficient and one with a high heat transfer coefficient. Modeling the two responses as a first order process, they are given by

$$P(s) = -\frac{0.109}{46.2s + 1} e^{-16.1s} \qquad \alpha_{sc} = 2000 \text{ W/m}^2\text{K} \qquad (8.24)$$

and

$$P(s) = -\frac{0.0917}{21.2s + 1} e^{-16.6s} \qquad \alpha_{sc} = 4000 \text{ W/m}^2\text{K} \qquad (8.25)$$

The difference in dynamics between the two processes is significant and will greatly affect the performance of the closed loop system. This clearly shows that effective condensate removal and the cylinder design in terms of spoiler bars are important.

The simulation time for the figures in this section is a few minutes. This should be compared to the more complex model used in Chapter 6 and Chapter 7, where the simulation time is counted in days.

8.4 Control of moisture by mid-range MPC

In the last decade, MPC (model predictive control) has received large attention in the process industry. It has been described as one of the most
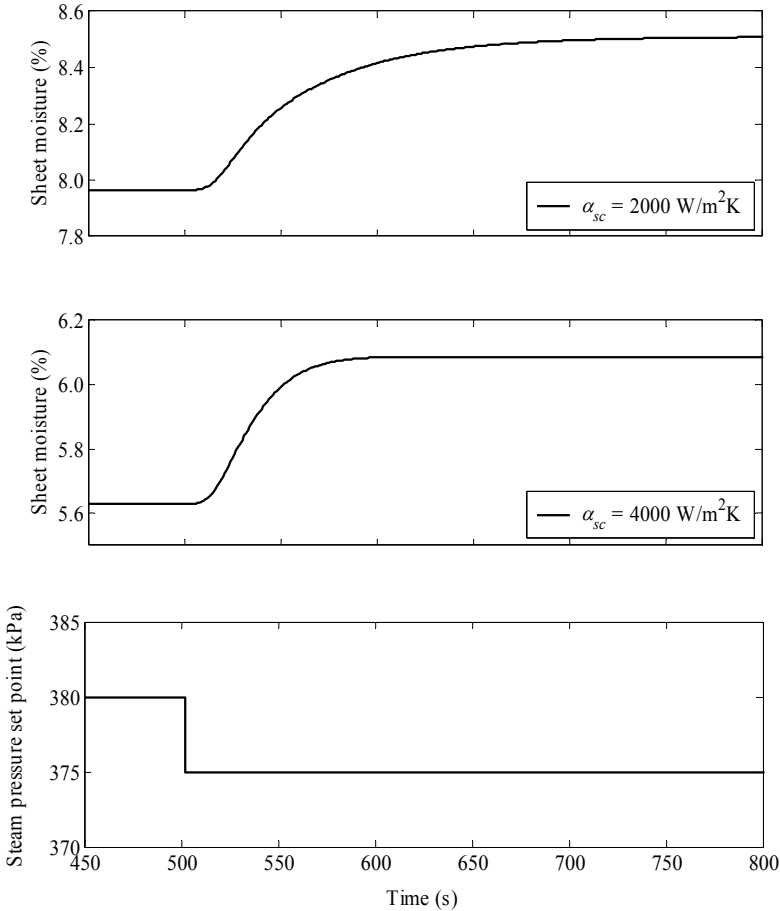
Figure 8.14 Response in moisture to step change in steam pressure set point for two different values of heat transfer coefficient α_{cp}.
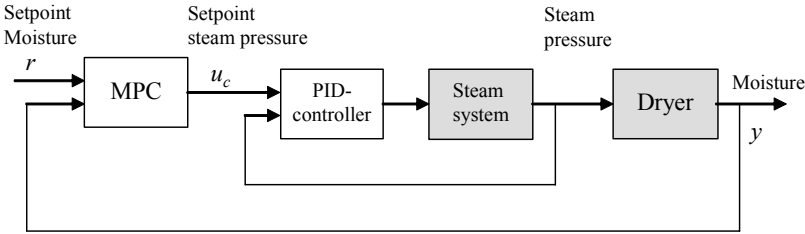
Figure 8.15 Moisture control by single loop MPC.
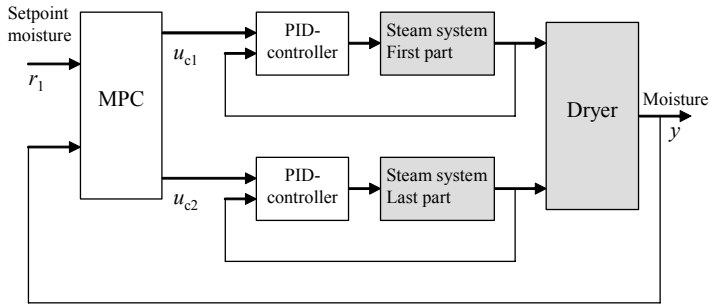
Figure 8.16 The proposed moisture control loop.

significant developments in process control [Doyle, 1999] and the only methodology to handle constraints in a systematic way [García, *et al*, 1989]. In this section, a new strategy to control the moisture in paper production is evaluated. It is implemented in a MPC structure and the analysis is done by simulations of the paper machine model shown in Figure 8.9. A Matlab toolbox for MPC [Åkesson, 2003] is linked to the Modelica environment. In this way, the advantages of the simple modeling technique in Modelica and the rich family of toolboxes in Matlab are used.

Figure 8.15 shows a block diagram where the moisture is controlled by MPC. The steam pressure set point is distributed to the dryer groups as described in Chapter 2, see Figure 2.12. The performance of this closed loop system is limited by the long transport dead-time in the drying section. By manipulating the steam pressure in the cylinders of the last part of the machine independently of the first part, a more effective moisture control system can be derived, see Figure 8.16. The objective is still to control the moisture in the sheet with the steam pressure in the cylinders but now the process has two inputs (and the same output as before) and this extra degree of freedom can be taken advantage of.

By identification of step responses on the high-order nonlinear physical model, a simple black-box model is achieved. In the Laplace domain, it is given by

$$Y = -\frac{0.098}{48s+1}e^{-14s}U_{c1} - \frac{0.010}{48s+1}e^{-5s}U_{c2}, \qquad (8.26)$$

where y is the moisture content, u_{c1} is the steam pressure set point to the first 50 cylinders, and u_{c2} the set point to the last 10 cylinders. The PID-controllers in the inner loops are tuned according to the IPZ-tuning

derived in Chapter 5. The response from u_{c2} has a significantly shorter time delay but also smaller process gain. The advantage of the high gain from u_{c1} and fast dynamics from u_{c2} is utilized in a mid-ranging MPC structure.

The simplified model for the singe-loop case in Figure 8.15, obtained correspondingly to (8.26), is given by

$$Y = -\frac{0.11}{48s + 1} e^{-13s} U_c, \qquad (8.27)$$

The cost function being minimized in the mid-ranging MPC is

$$J(k) = \sum_{i=1}^{50} \left\| \begin{bmatrix} r_1(k+i) - \hat{y}(k+i\,|\,k) \\ r_2(k+i) - u_{c2}(k+i) \end{bmatrix} \right\|_Q^2 + \sum_{i=1}^{4} \left\| \begin{bmatrix} \Delta u_{c1}(k+i) \\ \Delta u_{c2}(k+i) \end{bmatrix} \right\|_R^2, \qquad (8.28)$$

where r_1 is the set point for the moisture, and r_2 the set point for u_{c2}. Notation $\hat{y}(k+i\,|\,k)$ denotes the i step-ahead prediction and Δ is the difference operator. Since the MPC formulation is inherently discrete, the cost function is given as a summation. The idea of (8.28) is to let u_{c2} take care of the variations in paper moisture and let u_{c1} be positioned at a level where u_{c2} has an adequate control range in both directions in steady-state. In this way, the first part of the drying section serves as the base level of the drying while the last part controls the moisture. This is done by choosing appropriate weighting matrices, Q and R. For the simulations in this chapter they are chosen as

$$Q = \begin{bmatrix} 500 & 0 \\ 0 & 10^{-3} \end{bmatrix}, \quad R = \begin{bmatrix} 100 & 0 \\ 0 & 10^{-4} \end{bmatrix}. \qquad (8.29)$$

There is obviously a larger weight on deviations from r_1 than from r_2, since moisture control is the main objective. The weight on Δu_{c1} is larger than on Δu_{c2} making the controller to primarily use signal u_{c2} when acting on disturbances in moisture or on set point changes. The MPC settings in (8.29) are found from a combination of these 'rules of thumb' and evaluation of performance by simulations. The sample time is 5 s, the prediction horizon is chosen to 50 and the control horizon is chosen to 4, see (8.28). The prediction horizon is set to approximately match five time constants of the open-loop system (to assure that the prediction 'sees' the
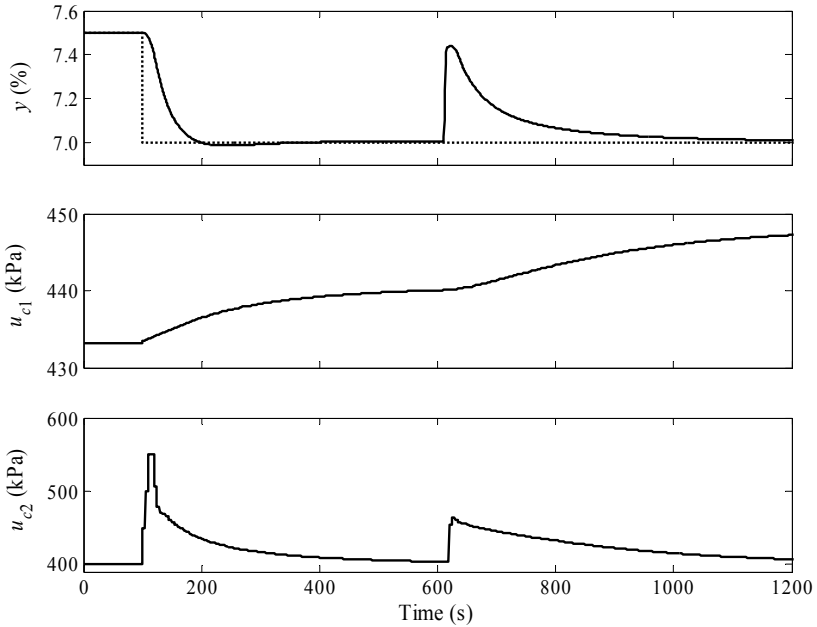
Figure 8.17 Simulation of mid-range MPC. There is a set point change at $t = 100$ s and a disturbance in inlet moisture content to the drying section from 60.0 % to 60.5 % at
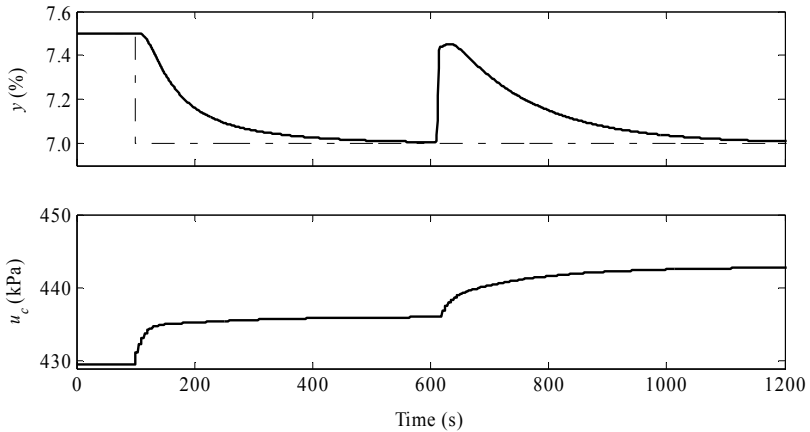
Figure 8.18 Simulation of single loop MPC. A set point change occurs at $t = 100$ s and a disturbance in inlet moisture content from 60.0 % to 60.5 % at $t = 600$ s.
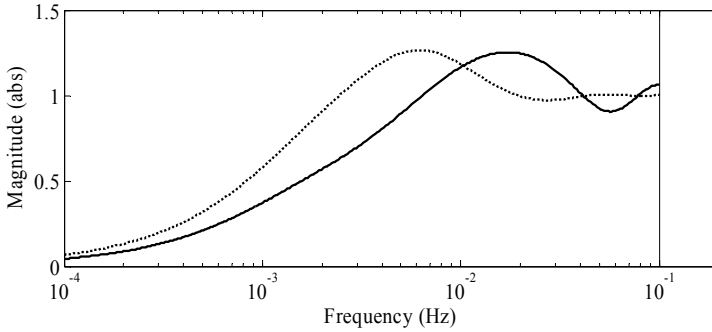
Figure 8.19 The sensitivity function for single loop MPC (dotted) and mid-range MPC (solid), using the linearized model (8.26). The maximum sensitivity is chosen to 1.25. The difference in limit frequency for the two systems is around a factor two.

full response of a change in Δu_{c1} and Δu_{c2}) and a small control horizon to limit the computational effort for the MPC. There is also a rate constraint for the control signals

$$\left|\Delta u_{c1}\right| \leq 10 \text{ kPa}, \quad \left|\Delta u_{c2}\right| \leq 50 \text{ kPa}. \tag{8.30}$$

The purpose of this is to avoid severe injections of disturbances into the steam system by allowing large variations in steam usage, which has negative effect on both steam production and other steam users.

Figure 8.17 shows a simulation of the mid-range MPC and it clearly visualizes the thought of mid-ranging. The signal u_{c2} is used to quickly react to set point changes and disturbances while u_{c1} is used to push u_{c2} back to its set point in steady-state. Both during the set point change and disturbance, the rate constraint for u_{c2} is initially active. This reduces the performance of the controller slightly but is important for the steam consumption, as described above. Simulations show that leaving out the constraints gives a more aggressive use of u_{c2}, but it is of course not 'free' to use since there still is a cost from (8.28).

To make an evaluation of the proposed control structure, the mid-ranging MPC is compared to single-loop MPC, see Figure 8.18. The tuning is chosen so that the two control systems have the same maximum value of the sensitivity function, see Figure 8.19. This implies that they, in some sense, have the same degree of robustness. However, due to the constraint handling, MPC is nonlinear and the comparison only serves as guidance. The cost function for the single-loop MPC is given by
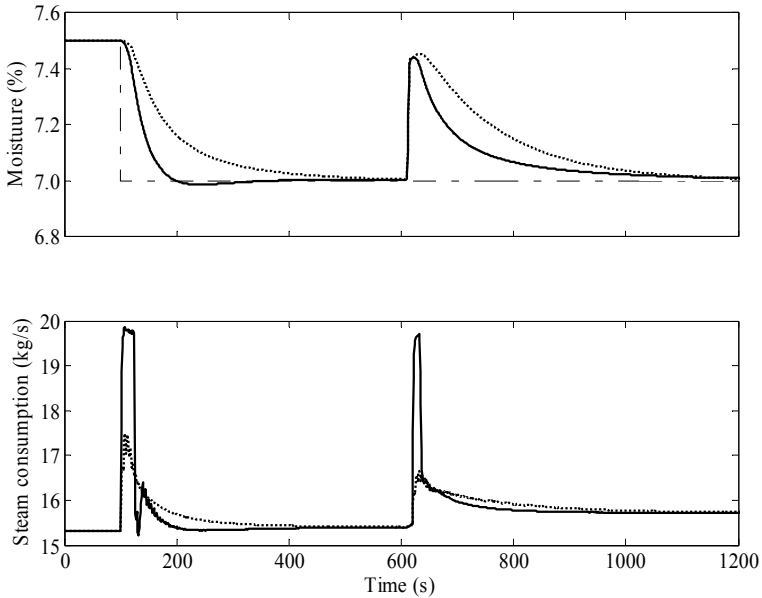
Figure 8.20 Comparison between mid-range MPC (solid) and single loop MPC (dotted), showing the moisture content and steam consumption.

$$J(k) = \sum_{i=1}^{50} \left\| \left[r(k+i) - \hat{y}(k+i \mid k) \right] \right\|_Q^2 + \sum_{i=1}^{4} \left\| \Delta u_c(k+i) \right\|_R^2, \qquad (8.31)$$

and the chosen weights that give the sensitivity in Figure 8.19, and constraint are

$$Q = 10, \quad R = 1, \quad \left| \Delta u_c \right| \le 10 \text{ kPa} \qquad (8.32)$$

Figure 8.19 also indicates the difference in performance between the two controllers, at least in the non-constrained case. The mid-range MPC has a limit frequency almost twice as large as the limit frequency of the single loop MPC. Since paper machines often are run from several hours to days with the same set point, disturbance rejection is important and it therefore makes sense to look at this property.

Figure 8.20 shows the moisture response for the two different controllers together with the steam flow in the header. The difference in performance is apparent. The mid-range MPC has both better set point following and disturbance rejection. However, the transient steam
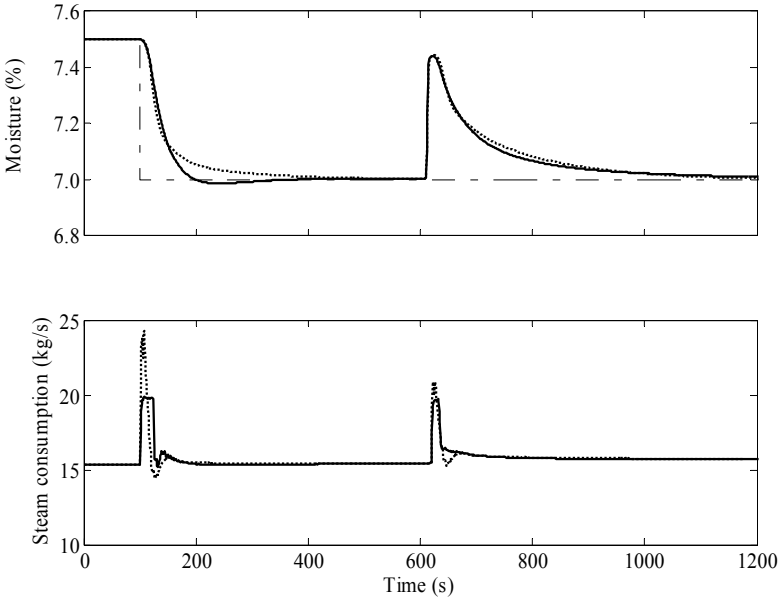
Figure 8.21 Comparison between mid-range MPC (solid) and single loop MPC (dotted), showing moisture content and steam consumption when tuned to give similar performance in disturbance rejection.

consumption is twice as large for the mid-range MPC. This is the price being paid for the extra performance.

In Figure 8.21, the single loop MPC has been tuned to give similar performance in disturbance rejection as the mid-range MPC, shown in Figure 8.17 and Figure 8.20. The output of the single loop MPC is in this case much more aggressive than it was in Figure 8.18 and therefore the transient steam consumption is much larger. This to be able to match the performance of the mid-range MPC. The maximum value of the sensitivity is also larger, hence the control system is less robust, see Figure 8.22.

The advantage with the proposed control structure is that, in general, it does not require any rebuild of the drying section. The cylinders are normally divided into different groups even though all groups follow the same set point. Therefore, it is simply a matter of changing the controller software and a majority of the main system vendors have the possibility to include a MPC package into their DCS system. However, it is an advantage if the flash steam from the last group is recirculated through a thermo compressor, see Figure 2.5. If the flash steam is reused by another group it is important to let the steam pressure of the last group be constrained so that its pressure never falls below the steam pressure of the
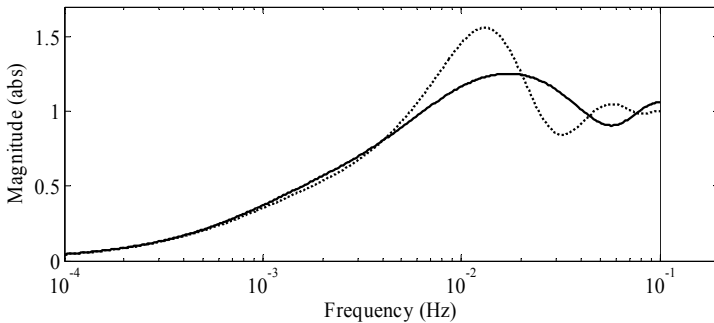
Figure 8.22 The sensitivity function for single loop MPC (dotted) and mid-range MPC (solid), when tuned to give similar performance

receiving group. This guarantees that the steam flows in the intended direction.

This mid-ranging MPC has two essential advantages compared to the mid-ranging structure used in Chapter 6, see Figure 6.10. Firstly, the MPC does not require any decoupling filter, C_D, since the complete multi-variable process model is given in the cost function. The MPC therefore automatically balances the two process inputs to get a desired output and there is no need for the extra 'fix' with a decoupling filter between the two process inputs as in Figure 6.10. Secondly, the MPC has a systematic implicit way to treat constraints. For the structure in Chapter 6, this has to be taken care of explicitly and not as a part of the tuning phase. A disadvantage can be that it is a bit more difficult to tune a mid-range MPC compared to e.g. the IMC or Dahlin controller used by many mills today.

8.5 Summary

A physical model, implemented in the object-oriented modeling language Modelica, for a drying section has been given. Components for steam cylinder, control valve, paper web, and different moisture controllers have been developed and collected in a model library. All equations are based on mass and energy balances, and algebraic constraints. By drag-and-drop features it is easy to build a simulation model of virtually any existing drying section. It is also easy to expand the model library with components for press and wire section.

The model has been validated against measurements on a real paper machine. By simply adjusting one parameter, the heat transfer coefficient for the condensate, a good fit is obtained.

The model is linked to a MPC toolbox in Matlab to evaluate a new strategy to control the moisture in the drying section. The strategy utilizes the possibility to divide the drying section into two parts. By controlling this multi-variable process with a mid-range structure, the performance of the closed loop system is greatly improved. The mid-ranging MPC is compared with single-loop MPC and the evaluation is done by comparing performance in terms of sensitivity function, disturbance rejection and steam consumption. An important advantage of the mid-ranging MPC is that it does not require any rebuild of the physical process.

The advantage of this model compared to the one used in Chapter 6 and Chapter 7 is the simulation time, which is a few minutes instead of a few days. The model used in the previous two chapters is capable of simulating microscopic phenomena like water and vapor transport, and moisture gradients, inside the paper sheet. The model described in this chapter neglects this and assumes a homogeneous paper in the thickness direction. For the purpose of the feedback control investigated in this thesis, this assumption sufficient. However, the feedforward control in Chapter 7 requires a model that takes differences in the thickness direction into account to observe the peak position.

9

Conclusions

9.1 Summary

In this thesis, modeling and control of the paper machine drying section is presented. The treatment is divided into two main parts, control of the steam and condensate system, and moisture control.

The steam and condensate system

The main task for the steam and condensate system is to deliver sufficient amount of energy to the evaporation process in the paper sheet. It is shown that the process response from the steam valve to steam pressure inside the drying cylinder can be described by a linear second order black-box model. Written as a transfer function, it consists of a pole, a zero, an integrator, and a time delay. The model structure is referred to as the IPZ model. A simple graphical identification procedure is given that estimates the four model parameters from two asymptotes of an open loop step response.

From the black-box model, a tuning rule for PI and PID control is derived. It is based on optimized load disturbance rejection subject to a robustness constraint and is referred to as IPZ tuning. To give the user the

option to balance between robustness and performance the tuning rule has a design parameter. A nice property of the tuning rule is that the controller settings are easily calculated from the process parameters of the IPZ model. It is successfully verified from experiments on real paper machine at different mills. The IPZ structure can be used in many other process areas, apart from modeling the steam pressure in cylinders. Therefore the tuning method has a much wider field of applications than solely drying section control.

The IPZ model is used to examine some properties of the closed loop system and to investigate two different control structures. The main objective is to avoid resonance peaks in the closed-loop frequency response from set point to process output, and this is accomplished by a set-point feedforward controller (two-degree-of-freedom controller) and a state feedback controller. The two types of structures solve the objective differently but they roughly give the same performance. However, the two-degree-of-freedom controller is recommended since it is best suited for implementation in today's industrial control systems. As this controller structure separates the servo and regulation problem it also fits well to the IPZ tuning. The set-point feedforward design gives the desired response from set-point to output, while a PID controller based on IPZ tuning takes care of the disturbance rejection in the feedback loop.

By making some assumptions and a linearization, it is shown that the black-box model can be derived from a few simple mass and energy balances. This means that the process parameters of the black-box model are directly related to physical quantities as cylinder dimension, valve characteristics, and steam properties. The model is validated against measurements from a real paper machine and the heat transfer coefficient from steam to cylinder is used as calibration parameter.

Moisture control

Traditionally the moisture in the paper sheet is controlled by manipulating the pressure in the steam cylinders. To improve the performance of the closed loop moisture control system both feedforward and feedback is investigated. A new measurement signal, called the peak position is introduced. It is based on measurements of the paper surface temperature and indicates the position where the surface becomes dry. It is shown that peak position can significantly improve the control performance by feedforward.

The feedback is carried out by two types of mid-ranging controllers. The first uses the air supply system in combination with the steam system.

The advantage of the fast impact from the supply air and the high capacity of the steam system are combined to enhance the performance of the closed loop system. The second mid-ranging structure utilizes similar advantages by combining the last drying group with the remaining part of the dryers to improve performance. Two different of mid-ranging controllers are used. The first mid-ranging structure combines two single-loop controllers, in this case IMC, together with a decoupling filter and a method to tune the system is given. The second structure is implemented in a MPC. The advantages of the mid-ranging MPC are that the decoupling filter is not needed and that constraints are explicitly taken into account.

From mass and energy balances, a dynamic simulation package of a drying section is implemented in the object-oriented modeling language Modelica. By drag-and-drop features, a simulation model of practically any drying section can easily be built. It can be used to investigate effects of a rebuild, different controller structures, and different ways to operate the machine. All this can be done for web breaks, grade changes, start-ups, and normal run.

9.2 Future work

The proposed solutions for moisture control, two mid-ranging controllers and a feedforward structure, have to this point only been verified by simulations. The next step is to evaluate them experimentally on a pilot or full-scale paper machine.

The simulation package in Modelica contains components for cylinder and paper sheet. However, it lacks models for the pipings, condensate tanks, and hood. By adding components for these objects, cross-couplings between cylinders, caused by the cascade configurations in the condensate system, can be investigated. The modeling package would also benefit from more validation with real plant data. It is desirable to validate the model for a number of different operating points to assure that it is valid in a wide operating range.

The modeling package can also be used for optimization. Some examples of this are minimization of the total energy usage by finding the optimal steam distribution between the dryer groups; and minimization of the time for a grade change by finding the optimal trajectories for machine speed, basis weight, and steam pressure, with respect to given rate constraints.

The differential pressure loop has only been treated briefly. A deeper analysis and a tuning rule, like the one for the pressure loop, are desired. This loop will probably benefit from a feedforward structure since it is greatly affected by the operation of the pressure loop.

From the linear model of the cylinder dynamics there is a potential of making a recursive identification of the heat transfer coefficient for fault detection with respect to condensate evacuation. This would be very beneficial since the heat transfer coefficient have a large impact on the dynamics of the moisture process and consequently its control performance.

A systematic analysis of moisture control where different control paradigms as MPC, Smith-predictor, IMC, PID, deadbeat control, minimum-variance, or LQG, are compared would be valuable. Every control system vendor use their control structure but no thorough comparison have been published in the literature.

Appendix A

Glossary

This glossary contains explanations from the following websites:
`www.afandpa.org`, `www.internationalpaper.com`, `www.instituteofpaper.com`, and `www.paperonline.org`.

Ash content: The amount of residue when a sample of paper is burned under controlled conditions so that all ignitable matter is removed. The ash derives from the mineral loading in the paper.

Basis weight: Weight in grams of one square metre of paper or board; also called grammage.

Black liquor: Mixture of cooking chemicals and dissolved wood material remaining after sulphate cooking; recovered during pulp washing, concentrated by evaporation and burned in the recovery boiler to regenerate the cooking chemicals and generate energy.

Board: Generic term for stiff paper usually made in several layers with a substance normally varying from 160 to 500 g/m^2, for certain grades even higher; widely used for packaging (e.g. folding cartons) and graphic applications.

Broke: Papermakers own waste paper created during papermaking process. It is usually repulped.

Bulk: Specific volume, inverse of density of the paper.

Caliper: The thickness of a sheet of paper or board. Also known as thickness or bulk. Usually measured in nanometers.

Chemical pulp: Pulp in which wood fibres have been separated by chemical, rather than mechanical, means.

Chemi-thermomechanical pulp (CTMP): Chemi-mechanical pulp produced by treating wood chips with chemicals (usually sodium sulphite) and steam before mechanical defibration.

Coated paper: The uniform application of a coating yields a more even and more closed surface of printing papers, which is suitable for the reproduction of fine screen artwork. The coating is applied in separate coaters or in the paper machine.

Conditioned basis weight: dsd

Corrugated board: Formed fluting that is faced with a liner on both sides.

Curl: The degree of curvature, measured when paper is positioned flat.

Dry end: Final part of the paper machine from the drying section onwards.

Dry weight: Mass of paper sheet excluding the moisture.

Fabric tension: The tension of the fabric creates contact pressure between the wet web and cylinder. Higher contact pressure gives higher heat transfer.

Filler: A material or substance that is added to the furnish to smooth out the spaces between fibers, enhancing the printing properties of the paper.

Fine paper: A broad term including printing, writing, and cover papers, as distinguished from wrapping papers and paper not generally used for printing purposes, which are generally referred to as coarse papers.

Fines: Small fragments of fibres produced, for example, in the course of beating or refining.

Fluting: Paper that has been formed into the flutes that make up the ridged part of the corrugated board between the liners.

Formation: The arrangement of fibers in a sheet of paper; can be seen by holding it up to a light source.

Freeness: A measure of the drainability of an aqueous suspension of stock, determined and expressed as specified in a standard method of test.

Furnish: The ingredients or constituents of which the paper is made. Fibrous furnish concerns only the types and proportions of the fibres present.

Grade: (1) A class or level of quality of a paper or pulp which is ranked, or distinguished from other papers or pulps, on the basis of its use, appearance, quality, manufacturing history, raw materials, or a combination of these factors. Some grades have been officially identified and described; others are commonly recognized but lack official definition. (2) With reference to one particular quality, one item (q.v.) differing from another only in size, weight, or grain; e.g., an offset book paper cut grain long is not the same grade as the same paper cut grain short.

Fiber orientation: The direction of the fibers in paper.

Kraft paper: A paper made essentially from wood pulp produced by a modified sulfate pulping process. It is a comparatively coarse paper particularly noted for its strength, and in unbleached grades is primarily used as a wrapper or packaging material. It can be watermarked, striped, or calendered, and it has an acceptable surface for printing. Its natural unbleached color is brown but by the use of semibleached or fully bleached sulfate pulps it can be produced in lighter shades of brown, cream tints, and white. In addition to its use as a wrapping paper, it is converted into such products as: grocery bags, envelopes, gummed sealing tape, asphalted papers, multiwall sacks, tire wraps, butcher wraps, waxed paper, coated paper, as well as specialty bags and sacks.

Liner: A paper that is used as the facing material in the production of corrugated and solid fibre shipping containers.

Mechanical pulp: Pulp consisting of fibres separated entirely by mechanical rather than chemical means.

Newsprint: A lightweight paper, made mainly from mechanical wood pulp, engineered to be bright and opaque for the good print contrast needed by newspapers. Newsprint also contains special tensile strength for repeated folding. It does not includes printing papers of types generally used for purposes other than newspapers such as groundwood printing papers for catalogs, directories, etc.

Opacity: The ability of a sheet of paper to prevent light transmission through it. Opacity prevents print that is on one side of a sheet of paper from showing through to the other side.

Packaging papers: These papers are used to wrap or package consumer and industrial products such as grocer's bags and sacks, shopping and merchandise bags, and multiwall shipping sacks used for shipping such products as cement, flour, sugar, chemicals and animal food. "Specialty" packaging papers are used for cookies, potato chips, ice cream, and similar products.

Paper Stock: A mix of pulp fibers, water, additives, chemicals and dyes that will be pumped onto the paper machine to form paper.

Picking: Fibers in the paper which tend to pull away from the surface during the drying process.

Recovery boiler: In wood pulping, a unit for concentrating black liquor to a stage where the residual carbon is then burned out and the inorganic sodium salts melted and recovered.

Refiner: A machine, usually equipped with discs or with a cone and plug, intended for the treatment of fibrous materials in an aqueous medium to give them some of the properties needed for the manufacture of pulp or paper with the necessary characteristics.

Retention: Proportion of fibre and filler retained on the paper machine wire.

Sheet (or Web): A continuous length of paper, such as paper when it is on the paper machine or on roll-feed equipment.

Sizing: This process can either be applied on the surface of the sheet or in the sheet: in the first case starch is applied to the surface to increase its strength and to resist the penetration of oil-based inks (this process is carried out at the size press, which is about two-thirds of the way down the dry end); in the second case chemicals are added to the stock at the pulping stage before the sheet is formed: this is called internal or engine sizing and its purpose is to stop penetration of water-based inks into the sheet.

Smoothness: It is a measured property of paper that describes or rates the flatness and evenness of a sheet's surface.

Stock: The wet pulp before it is fed onto a paper making machine, or during the paper making processes before it becomes a sheet of paper; contains around 99% water and 1% fibre.

Stock preparation: Collective term for all treatment necessary for the preparation of the stock before it reaches the making machine.

Tissue: Collective term for papers of a grammage of less than 30 g/m^2 that differ in application and composition but have the common feature of being thin. Examples of different types of tissue papers include sanitary grades such as toilet, facial, napkin, towels, wipes, and special sanitary papers. The extremely thin Japanese tissue papers are sometimes produced in grammages as small as 6 to 8 g/m^2. Other examples of tissue papers are decorative and laminated tissue papers and crepe papers, often used in gift wrapping and to decorate. Desirable characteristics here are appearance, strength, and durability.

Wet end: First part of the paper machine up to the drying section.

White water: The filtrate from the wet end of the paper machine

Winding: An operation in which the paper or board from the paper machine is slit and wound into the roll widths ordered by the customer.

Woodfree paper: Paper consisting of chemical pulp fibres. It does not contain any mechanical pulp beyond a permissible content of 5 % by mass.

Appendix B

Conservation Balance for Energy in Compartmental Models

The models developed in Chapter 4 and Chapter 8 are based on mass and energy balances, together with a few constitutive relations. The balance equations come from the fundamental conservation principle in physics, that mass and energy are neither destroyed nor created but simply change their form. Putting up a mass balance is rather straightforward but the energy balance is not always so evident, particularly not for gas systems.

In this appendix the energy balance for the steam and condensate in the cylinder model is discussed. It will be shown why change in internal energy depends on in- and outflow of enthalpy, see Figure A.1.
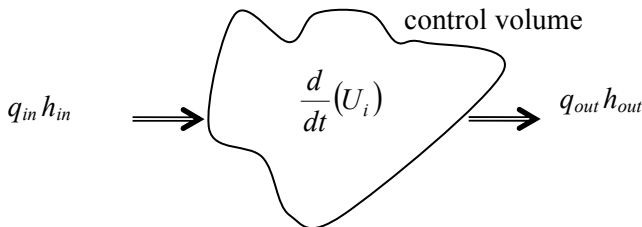
Figure A.1 The general energy balance for steam and condensate, used in this thesis. q is mass flow, h specific enthalpy, and U_i internal energy. The change in internal energy depends on inflow and outflow of enthalpy.

B.1 The energy balance

Starting from a general energy balance, the total energy of a system comprises of three principal components

- internal energy U_i
- kinetic energy E_k
- potential energy E_p

Observe that we here use internal energy U_i [J] and not specific internal energy u_i [J/kg]. Energy flows into the system in terms of

+ heat input (conductive energy flow)
+ work input (mechanical work)
+ energy brought into the control volume by the incoming fluid (convective energy flow)
+ work done on the control volume by the incoming fluid (flow work)

and energy flows out of the system in terms of

− heat output
− work output
− energy leaving the control volume with the outgoing fluid
− work done by the outgoing fluid

Conductive energy flow
This is energy that flows in and out of the system through conductive heat transfer mechanisms. We call this Q_c [J/s].

Convective energy flow
This is the energy carried by means of the mass flow into and out of the control volume. It consists of internal, kinetic, and potential energy.

$$\text{Convective inflow:} \quad q_{in}(u_{i,in} + e_{k,in} + e_{p,in})$$

$$\text{Convective outflow:} \quad q_{out}(u_{i,out} + e_{k,out} + e_{p,out})$$

where q_{in} and q_{out} are mass flows [kg/s], and e_k and e_p are specific energies [J/kg].

Mechanical work

This is denoted as W_m [J/s] and can be both shaft work and expansion work. Shaft work is the work done by the fluid or surrounding through a moving part (e.g. a pump rotor). Expansion work accounts for work done in expansion or contraction of the control volume. This term is often not present especially not when the control volume is fixed. Work done on the system is positive work.

Flow work

This term relates to the work done on the fluid as it moves into and out of the control volume. This is expressed as

$$\text{Work by inflow: } q_{in} p_{in} v_{in}$$

$$\text{Work by outflow: } q_{out} p_{out} v_{out}$$

where p_{in} and p_{out} are pressures [Pa] at inlet and outlet, and v_{in} and v_{out} are specific volumes [m^3/kg] at inlet and outlet. To see this, consider a unit volume of fluid across the boundary at the input, see Figure A.2. Let the element have a length l [m/kg] and the cross-sectional area of the inlet be A [m^2] Then the energy required to push the element across the boundary is given by the *force* times *length*,

$$(p_{in} A_{in}) \times l = p_{in} v_{in}$$

Similarly it can be shown that the flow work at the outlet is given by

$$p_{out} v_{out}$$

Putting it all together

The principle of conservation of energy gives us

$$\frac{d}{dt}(U_i + E_k + E_p) = q_{in}(u_{i,in} + e_{k,in} + e_{p,in}) - q_{out}(u_{i,out} + e_{k,out} + e_{p,out})$$

$$+ q_{in} p_{in} v_{in} - q_{out} p_{out} v_{out} + Q_{c,in} - Q_{c,out} + W_{m,in} - W_{m,out}$$

The sum of specific internal energy and the *pv* term is called specific enthalpy, and is given by the symbol *h* (*h* = *u* + *pv*). We can therefore write the energy balance as

$$\frac{d}{dt}(U_i + E_k + E_p) = q_{in}(h_{in} + e_{k,in} + e_{p,in}) - q_{out}(h_{out} + e_{k,out} + e_{p,out})$$
$$+ Q_{c,in} - Q_{c,out} + W_{m,in} - W_{m,out}$$

When the steam cylinder model is developed in Chapter 4, the kinetic and potential energies are neglected, which is applicable to most systems in the process industry. Also, there are evidently no mechanical work terms acting on the system and the internal energy of the control volume is written as *specific internal energy* times *mass*. It is then simplified to

$$\frac{d}{dt}(\rho u_i V) = q_{in}h_{in} - q_{out}h_{out} + Q_{c,in} - Q_{c,out}$$

where ρ is density [kg/m^3] and V volume [m^3].
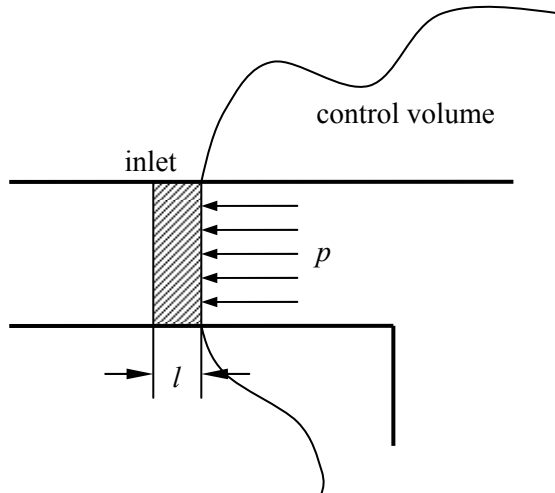
Figure A.2 A small section at inlet to the system. There is an expenditure in energy to push the fluid across the boundary.

Appendix B. Conservation Balance for Compartmental Models

If we are dealing with an incompressible liquid, there is no pressure-volume work done on the system, and the energy balance can be further simplified to

$$\frac{d}{dt}(\rho h V) = q_{in} h_{in} - q_{out} h_{out} + Q_{c,in} - Q_{c,out}$$

This is the case when considering the water phase (moisture) in the paper web.

Appendix C

Solution to the One Dimensional Heat Equation

The general heat equation is a partial differential equation, describing heat conduction in solids in a given region over time, of the following form

$$\rho c \frac{\partial T}{\partial t} - \nabla \cdot (\lambda \nabla T) = k, \qquad (C.1)$$

where ρ (kg/m^3) is the density, λ (W/m°C) is the thermal conductivity, c (J/kg°C) the specific heat capacity, and k (W/m^3) the added heat per unit volume and time. Assuming homogeneous material, no added or subtracted heat inside the given region, and a one-dimensional problem, it can be written as

$$\frac{\partial T}{\partial t} - a \frac{\partial^2 T}{\partial x^2} = 0, \qquad (C.2)$$

where a (m^2/s) is the thermal diffusivity, defined as

$$a = \frac{\lambda}{\rho c}. \qquad (C.3)$$
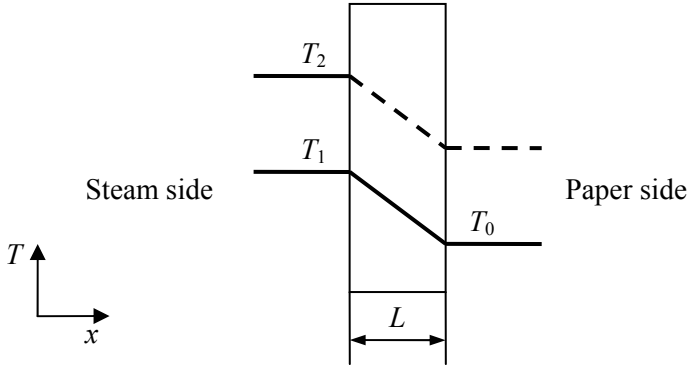
Figure C.1 At $t = 0$, the temperature on the steam side is changed from T_1 to T_2. The two steady-state solutions are shown in the figure.

Heat transfer through a cylinder wall with a step change in temperature

A steam filled cylinder with wall thickness L, has the temperature T_1 on the steam side and temperature T_0 on the paper side, in steady-state. At $t = 0$ the steam temperature is suddenly changed to T_2, see Figure C.1. Also, the heat flow to the paper is assumed to be Q (W/m^2) . Thus, the system is given by

$$
\begin{cases}
\dfrac{\partial T}{\partial t} - a\dfrac{\partial^2 T}{\partial x^2} = 0, & 0 < x < L, t > 0 \\[2mm]
T(x,0) = T_1 + \dfrac{x}{L}(T_0 - T_1) \\[2mm]
T(0,t) = T_2, & t > 0 \\[2mm]
-\lambda \dfrac{\partial T(L,t)}{\partial x} = Q
\end{cases}
\tag{C.4}
$$

From theory of Hilbert Spaces and eigenfunctions the solution to (C.4) can be written as [Sparr and Sparr, 2000]

$$T(x,t) = T_{stat}(x) + v(x,t) = T_2 - \frac{Q}{\lambda}x + \sum_{k=1}^{\infty} c_k e^{-a\mu_k t} \sin \beta_k x$$

$$= T_2 - \frac{Q}{\lambda}x + \sum_{k=1}^{\infty} \frac{4(T_1 - T_2)}{(2k-1)\pi} e^{-a\left(k-\frac{1}{2}\right)^2 \frac{\pi^2}{L^2}t} \sin\left(k - \frac{1}{2}\right)\frac{\pi}{L}x. \tag{C.5}$$

The solution can be thought of as the sum of the steady-state temperature distribution (given by $T_2 - Qx/\lambda$) which is independent of time, and a transient solution (given by the series) that tends to zero as $t \to \infty$.

Figure C.2 and Figure C.3 shows the temperature distribution, given by (C.5). Since we have assumed constant energy flow Q, the slope of the initial temperature curve and the steady-state temperature curve are equal. Also, the initial discontinuity in temperature is quickly smoothened out. The heat equation is a parabolic PDE and this is a typical character of this type of equation [Sparr and Sparr, 2000]. Figure C.4 shows how the temperature at the paper side varies as a consequence of the step in steam temperature. The response is similar to a step response of a system with order higher than one. However, the mean temperature of the cylider shell, shown in figure C.5, has more resemblance to the step response of a first-order system. The mean temperature of the cylinder is what is used in Chapter 4 when putting up a lumped model this system and it is then described by a first-order linear model.

In Chapter 4, the heat equation (C.1) is compared to a simplified static relation

$$Q = \alpha A(T_1 - T_2), \tag{C.6}$$

where the heat equation is assumed to be the correct description of heat transfer. However, it is important to remember that the heat equation is also an approximation. To show this it will be solved it for an infinitely long rod.

Appendix C. Solution to the One Dimensional Heat Equation
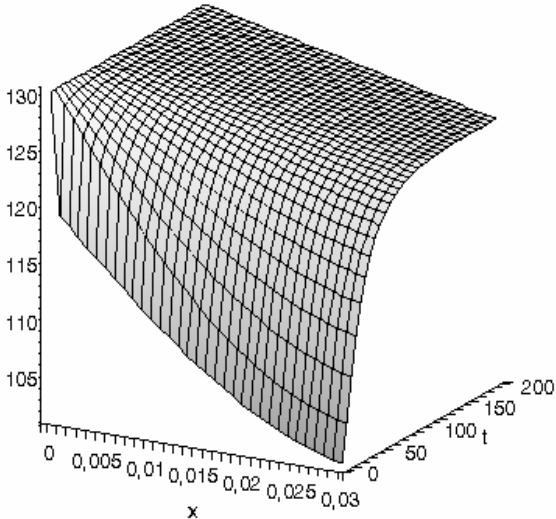
Figure C.2 The temperature as a function of both position x and time t (given in seconds). $T_1 = 120°C$, $T_2 = 130°C$, $L = 0.03$ m, $c = 500$ J/(kg°C), $\lambda = 50$ W/(m²°C), $\rho = 7000$ kg/m³, $Q = 10$ kW.
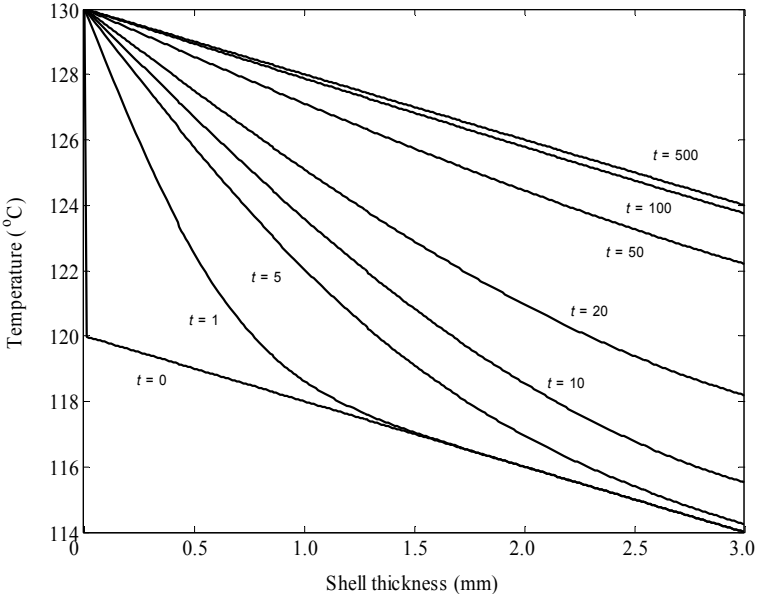
Figure C.3 The temperature as a function of position x for different points of time.
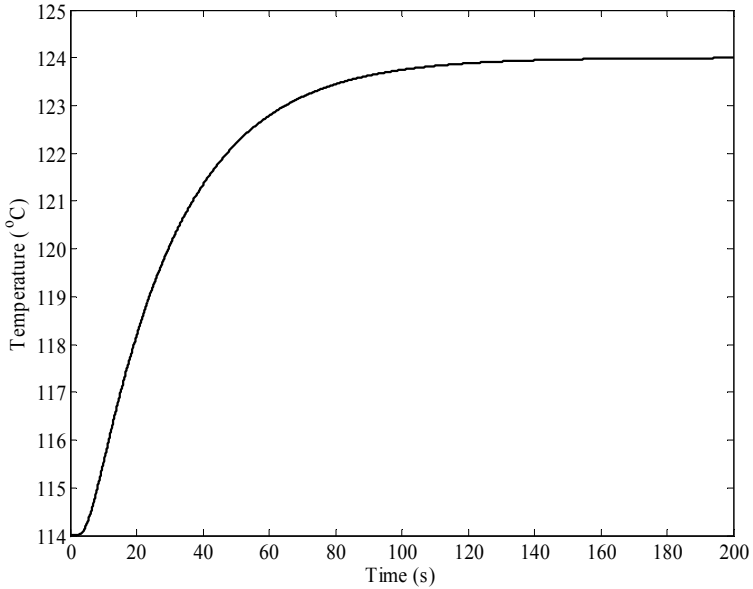
Figure C.4 The temperature at the cylinder surface (paper side) as a function of time. The response is similar to a step response of a higher order system.
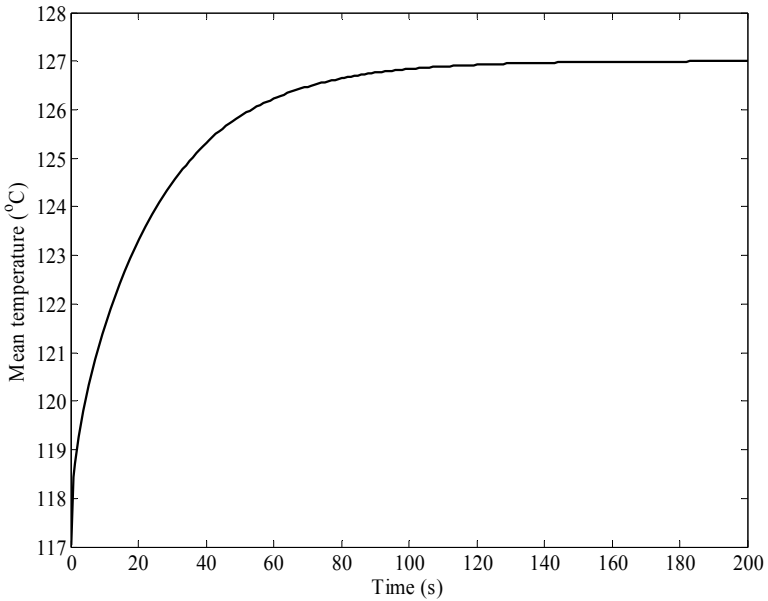
Figure C.5 The mean temperature of the cylinder shell as a function of time. The response is similar to a step response of a first-order system.

Heat conduction in an infinitely long rod

Regard the heat equation for an infinitely long rod

$$\begin{cases} \dfrac{\partial T}{\partial t} - a\dfrac{\partial^2 T}{\partial x^2} = 0, & x \in \mathfrak{R}, t > 0 \\ T(x,0) = g(x) \end{cases} \tag{C.7}$$

This equation can be solved by the Fourier or Laplace transform and the solution is given by the convolution formula

$$T(x,t) = G * g(x,t) = \int_{-\infty}^{\infty} G(x-\alpha)g(\alpha)d\alpha, \tag{C.8}$$

where

$$G(x,t) = \frac{1}{\sqrt{4\pi a t}} e^{-x^2/4at}. \tag{C.9}$$

G is called the Green function for the heat equation. If we assume that the initial condition is given by the Dirac pulse, the solution to (C.7) is

$$T(x,t) = G * \delta = \int_{-\infty}^{\infty} G(x-\alpha)\delta(\alpha)d\alpha = \frac{1}{\sqrt{4\pi a t}} e^{-x^2/4at}. \tag{C.10}$$

Figure C.6 shows this solution as a function of both time and space. The integral of (C.10) over the whole space is proportional to the thermal energy in the rod, and evaluates to

$$\int_{-\infty}^{\infty} \frac{1}{\sqrt{4\pi a t}} e^{-x^2/4at} dx = 1, \tag{C.11}$$

independently of t and a. This because no energy leaves the rod and the Dirac pulse has unit area.

The implication of (C.10) is that the energy impulse in the origin affects the temperature in each point x for all $t > 0$. In other words, all points in space will sense the impulse instantaneously, and the model

228

(C.1) leads to an infinite propagation velocity for the heat at the starting point. This is due to the averaging effect of the integral in (C.8). Loosely speaking, the heat equation does not admit any discontinuous solutions.

This non-physical property of the heat equation has been extensively discussed in the literature, first explicitly solved by [Cattaneo, 1948]. The theory has become known as extended thermodynamics, and is a field of research still today [Herwig and Beckert, 2000], [Pulko, *et al*, 2002], and [Belevich, 2004]. [Joseph and Preziosi, 1989] gives a good overview of the field. Often the drawback of infinite velocity is overcome by adding an extra term to (C.1) involving a derivative of second order in time. It then becomes a hyperbolic function which can be regarded as a "wave equation for heat" (with a certain speed of the heat wave).
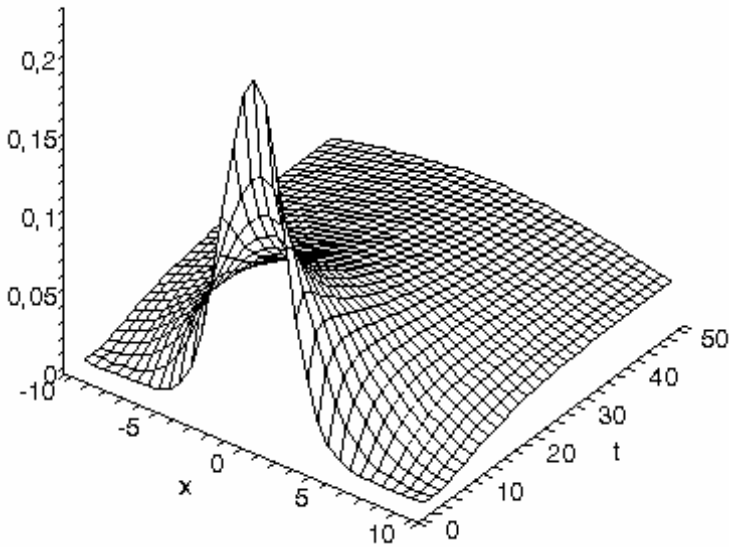
Figure C.6 Temperature as a function of both position *x* and time *t* (given in seconds), for the normalized case *a* = 1.

References

Åkesson, J., *Operator interaction and optimization in control systems*, Licentiate thesis, ISRN LUTFD2/TFRT--3234--SE, Department of Automatic Control, Lund Institute of Technology, 2003. Download can be found at `www.control.lth.se/user/johan.akesson/mpctools`.

Allison, B. J., A. J. Isaksson, and A. Karlström (1997): "Grey-box identification of a TMP refiner." *Pulp and Paper Canada*, 98(4), pp. 123−126.

Allison, B. J., and A. J. Isaksson (1998): "Design and performance of mid-ranging controllers." *Journal of Process Control*, 8(5−6), pp. 469−474.

Allison, B. J., and S. Ogawa (2003): "Design and tuning of valve position controllers with industrial applications." *Transactions of the Institute of Measurements and Control*, 25(1), pp. 3−16.

Asensio, M. C., and J. Seyed-Yagoobi (1992): "Theoretical drying study of single-tier versus conventional two-tiered dryer configurations." *Tappi Journal*, 75(10), pp. 203−211.

Åström, K. J. (1967): "Computer control of a paper machine − an application of linear stochastic control theory." *IBM Journal of Research and Development*, 11(4), pp. 389−405.

Åström, K. J. (1998): "Design of PI controllers based on non-convex optimization." *Automatica*, 34(5), pp. 585-681.

Åström, K. J. (2000a): "Control problems in paper making – revisited." In *Preprints Control Systems 2000*, pp. 129−136, Canada.

Åström, K. J. (2000b): "Limitation on control system performance." *European Journal of Control*, 6(1), pp. 2−20.

Åström, K. J. (2003): Personal communication.

Åström, K. J., and R. D. Bell (2000): "Drum boiler dynamics." *Automatica*, 36(3), pp. 363−378.

Åström, K. J., and T. Hägglund (2001): "The future of PID control." *Control Engineering Practice*, 9, pp. 1163−1175.

Åström, K. J., and T. Hägglund (2004): "Revisiting the Ziegler-Nichols step response method for PID control." *Journal of Process Control*, 14(6), pp. 635−650.

Åström, K. J., and T. Hägglund (2005): *Advanced PID control*, Instrument Society of America, Research Triangle Park, NC.

Åström, K. J. and B. Wittenmark (1997): *Computer-controlled systems − theory and design*, 3rd ed., Prentice-Hall, Upper Saddle River, NJ.

Balchen, J. G. (1999): "How have we arrived at the present state of knowledge in process control? Is there a lesson to be learned?" *Journal of Process Control*, 9(2), pp. 101−108.

Belevich, M. (2004): "Causal description of heat and mass transfer." *Journal of Physics A: Mathematical and General*, 37, pp. 3053−3069.

Bequette, B. W. (1998): *Process dynamics − modeling, analysis, and simulation*, Prentice Hall, Upper Saddle River, NJ.

References

Bergström, J., and G. Dumont (1998): "An object oriented framework for developing dynamic models of a paper machine." *Dynamic Modeling Control Applications for Industry Workshop, IEEE Industry Applications*, pp. 63−69.

Berrada, M., S. Tarasiewicz, M. Elkadiri, and P. Radziszewski (1997): "A state model for the drying paper in the paper product industry." *IEEE Trans. on Industrial Electronics*, vol. 44, no. 4, pp. 579−586.

Bialkowski, W. L. (1996): "Effectiveness of deadtime compensators for basis weight and moisture control." In *Proceedings Control Systems 1996*, pp. 61−67, Halifax, Canada.

Bohlin, T. (1994): "A case study of grey box identification." *Automatica*, 30(2), pp. 307−318.

Bohlin, T. and S. Graebe (1995): "Issues in nonlinear stochastic Grey-Box identification." *International Journal of Adaptive Control and Signal Processing*, 9(6), pp. 465−490.

Borisson, U. and B. Wittenmark (1974): "An industrial application of a self-tuning regulator." In 4th *IFAC/IFIP Symposium on Digital Computer Applications to Process Control*, pp. 76−87, Zürich, Switzerland.

Bortolin, G., S. Borg, and P. O. Gutman (2004): "Modeling of the wet end part of a paper mill with Dymola." *Mathematics and Computers in Simulation*, 65, pp. 31−38.

Boström, B (2002): "Measurement of dynamic moisture gradients in the z-direction." *Preprints 7th New Available Technologies,* pp. 60−64, Stockholm, Sweden.

Brown, T., and D. Millard (1993): "New model-based machine direction control algorithm." In *Proceedings TAPPI Process Control Conference*, pp. 15−20, Nashville, TN.

Carlberg, M. (ed) (1989): *Teknisk uppkäftighet*, Skogsindustrierna and Bokförlaget Bra Böcker.

Cattaneo, C. A. (1958): "A form of heat conduction equation which eliminates the paradox of instantaneous propagation." *Comptes Rendus Academie Science*, 247, pp. 431−433.

CEPI (2004): "European pulp and paper industry − Annual statistics." *Confederation of European Paper Industries*, 2004, Download can be found at `www.cepi.org`.

Chang, D.-M., C.-C. Yu, and I.-L. Chien (2000): "Design sensor trajectory for control: application to sheet-forming processes." *AIChE Journal*, 46(8), pp. 1581−1592.

Chen, S.-C. (1992): "Full-width sheet property estimation from scanning measurements." in *Proceedings Control Systems '92*, Whistler, Canada.

Chen, S.-C. (1995): "Modelling of paper machines for control: theory and practice." *Pulp and Paper Canada*, 96(1), pp. 17−21.

Chen, S.-C., and R. Subbarayan (1999): "Cross-machine direction response modeling with two-dimensional sheet variations measurements." in *Proceedings of American Control Conference*, pp. 3082−3086, San Diego, CA.

Chidambaram, M., R. P. Sree (2003): "A simple method of tuning PID controllers for integrator/dead-time processes." *Computers and Chemical Engineering*, 27(2), pp. 211−215.

Chien, K. L., J. A. Hrones, and J. B. Reswick (1952): "On the automatic control of generalized passive systems." *Transactions of American Society of Mechanical Engineers*, 74, pp. 175−185.

Choi, S., W. Yu, D. M. France, and M. W. Wambsganss (2001): "A novel multiport cylinder dryer." *Tappi Journal*, 84(2), pp. 47.

Clapperton, R. H. (1967): *The paper-making machine, its invention, evolution and development*, Pergamon Press.

Cohen, G. H., and G. A. Coon (1953): "Theoretical consideration of retarded control." *Transactions of American Society of Mechanical Engineers*, 75, pp. 827−834.

References

Crotogino, R. H. (2001): "The mysteries of technology transfer. Luck versus good planning." *Drying Technology*, 19(10), pp. 2559−2575.

Dagens Industri (2004): "Skogsindustrierna tappar mark i tuff konkurrens." *Dagens Industri (a swedish daily paper)*, published 2004-02-14.

Dahlin, E. B. (1968): "Designing and tuning digital controllers." *Instruments and Control Systems*, 41(6), pp. 77−83.

Doyle, F. J., (1999): "Computational issues in the application of model-based control to the pulp and paper industry." *AIChE Symposium Series No. 322*, vol. 95, pp. 165−172.

Dumont, G. A (1986): "Applications of advanced control methods in the pulp and paper industry − a survey." *Automatica*, 22(2), pp. 143−153.

Dumont, G. A. (1988): "Challenges and opportunities in pulp and paper process control." *Proceedings of the 1988 American Control Conference*, pp. 1959−1964, Atlanta, GA.

Dumont, G. A., M. S. Davies, and K. Natarajan (1993): "Estimation of moisture variations on paper machines." *IEEE Transactions on Control Systems Technology*, 1(2), pp. 101−113.

Dumont, G. A., M. S. Davies, K. Natarajan, C. Lindeborg, F. Ordubadi, Y. Fu, K. Kristinsson, and L. Jonsson (1991): "An improved algorithm for estimating paper machine moisture profiles using scanned data." *Proceedings IEEE Control and Decision Conference*, pp. 1857−1862, Brighton, England.

Duncan, S. (2003): "Editorial." *Transactions of the Institute of Measurements and Control*, 25(1), pp. 1−2.

Fellers, C., and B. Norman (1998): *Pappersteknik*, Institutionen för pappersteknik, KTH.

FFIF (2004): "Paper and wood, yearbook 2004, statistics 2003." *Finnish Forest Industries Federation*, Download can be found at `www.forestindustries.fi`.

Forsman, K (2005): *Reglerteknik för processindustrin*, Studentlitteratur, Lund, Sweden.

Forsman, K, and J. Birgersson (1999): "Modelling and control of the process air in a paper machine hood." *Proceedings of the 53rd Appita annual conference*, Rotura, New Zealand.

Foss, B., B. Lohmann, and W. Marquardt (1998): "A field study of the industrial modeling process." *Journal of Process Control*, vol. 8, no. 5, pp. 325−338.

Fritzson, P. (2004): *Object-oriented modeling and simulation with Modelica 2.1*, John Wiley & sons, New York, USA.

Gaillemard, C., and A. Johansson (2004): "Modeling of the moisture content of the paper in the drying section of a paper mill." In *Proc. of Control Systems 2004*, Quebec, Canada, pp. 183−187.

García, C. E., D. M. Prett, and M. Morari (1989): "Model predictive control: theory and practice − a survey." *Automatica*, vol. 25, no. 3, pp. 335−348.

Gavelin, G. (ed.) (1972): *Drying of paper and paperboard*, Lockwood Publishing, New York.

Gavelin, G. (1998): *Paper machine design and operation*, Angus Wilde Publications, Vancouver, Canada.

Hangos, K., and I. Cameron (2001): *Process modelling and model analysis*, Academic Press.

Haugwitz, S., M. Karlsson, S. Velut, and P. Hagander (2005): "Anti-windup in mid-ranging control." *Proceedings of 44th IEEE Conference on Decision and Control and European Control conference*, Seville, Spain.

Heaven, E. M., I. M. Jonsson, T. M. Kean, M. A. Manness, and R. N. Vyse (1994): "Recent advances in cross machine profile control." *IEEE Control System Magazine*, 14(5), pp. 35−46.

References

Heikkilä, P. (1993): *A study on the drying process of pigment coated paper webs*, PhD thesis, Department of Chemical Engineering, Åbo Akademi, Åbo, Finland.

Henson, M. A., B. A. Ogunnaike, and J. S. Schwaber (1995): "Habituating control strategies for process control." *AIChE Journal*, 41(3), pp. 604−618.

Herwig, H., and K. Beckert (2000): "Fourier versus non-fourier heat conduction in materials with a nonhomogeneous inner structure." *Journal of Heat Transfer*, 122(2), pp. 363−365.

Hill, K. C. (1993): "Analyzing the dryer section's steam and condensate system." *Tappi Journal*, 76(6), pp. 105−114.

Ho, W. K., O. P. Gan, E. B. Tay, and E. L. Ang (1996): "Performance and gain and phase margins of well-known PID tuning formulas." *IEEE Transactions on Control Systems Technology*, 4(4), pp. 473−477.

Ho, W. K., C. C. Hang, and L. S. Cao (1995): "Tuning of controllers based on gain and phase margin specifications." *Automatica*, 31(3), pp. 497−502.

Hägglund, T. (1991): *Process control in practice*, Studentlitteratur, Lund, Sweden.

Isaksson, A. J., and S. F. Graebe (2002): "Derivative filter is an integral part of PID design." *IEE Proceesings of Control Theory and Applications*, 149(1), pp. 41-45.

Jansson, J. and B. Nordgren (1958): "Om torkning av papper på filttäckta torkcylindrar." *Svensk Papperstidning*, 61(19), pp. 834−843.

Joseph, D. D., and L. Preziosi (1989): "Heat waves." *Reviews of Modern Physics*, 61(1), pp. 41−73.

Karlsson, I. (2002): "Förfarande vid torkning av ett banformigt material." Swedish patent, 0004851-2 (SE518049).

Karlsson, M. (ed) (2000): *Paper making part 2, drying*, Tappi Press.

Karlsson, M., O. Slätteke, B. Wittenmark, and S. Stenström (2003): "Evaluation of models for the steam supply system." *Tappi Spring Technical Conference & Trade Fare*, Chicago, IL.

Karlsson, M., and S. Stenström (2005a): "Static and dynamic modelling of cardboard drying, part I: theoretical model." *Drying Technology*, 23(1−2), pp. 143−163.

Karlsson, M., and S. Stenström (2005b): "Static and dynamic modelling of cardboard drying, part II: simulation and experimental results." *Drying Technology*, 23(1−2), pp. 165−186.

Karlsson, M., S. Stenström, and E. Baggerud (2002): "Dynamic simulation of the steam supply system for a multi-cylinder dryer" *Nordic Pulp and Paper Research Journal*, 17(1), pp. 66−70.

Kastanakis, G., and A. Lizr (1991): "Interaction between the MD and CD control processes in paper making and plastics machines." *Tappi Journal*, 74(2), pp. 77−83.

Kjaer, A. P., W. P. Heath, and P. E. Wellstead (1995): "Identification of cross-directional behaviour in web production: techniques and experience." *Control Engineering Practice*, 3(1), pp. 21−29.

Krumenacker, R. (ed) (1997): *Paper machine steam and condensate systems*, 5th edition, Tappi Press.

Kuang, H.-D., J. Thibault, R. Chen, and B. Grandjean (1995): "Pilot scale investigation of infrared drying of paper." *Tappi Journal*, 78(7), pp. 129−137.

Kuusisto, R., M. Kosonen, J. Shakespeare, and T. Huhtelin (2002): "Multivariable control of paper machine grade changes." *Pulp and Paper Canada*, 103(10), pp. 260−263.

Larsson, J. E., and T. Gustafsson (1998): "Paper machine dry line position control during grade changes." *Proceedings of the American Control Conference*, pp. 2997−3001, Philadelphia, PA.

References

Lehtinen, J. (1995): "Condebelt drying of paper and paperboard for optimizing quality and production for many grades." *Drying technology*, 13(8), pp. 2049−2068.

Li, P. Y., P. J. Bjegovic, and S. Ramaswamy (2001): "Preemptive control of multiply actuated processes: application to moisture content control in paper manufacturing using surrogate measurements." *Proceedings of 2001 ASME International Mechanical Engineering Congress and Exposition*, New York, NY.

Lindell, K., and S. Stenström (2004): "Assessment of different paper drying processes to reduce the total energy costs from a mill perspective." *Proceedings of the 14th International Drying Symposium*, Sao Paulo, Brazil.

Ljung, L. (1999): *System identification - Theory for the user*, 2nd edition, Prentice Hall.

Ljung, L. (2004): *System identification toolbox − user's guide version 6*, Mathworks, Natick, MA.

Love, W. C. (1994): "Innovative control technique improves control rangeability and resolution in paper mill applications." *Tappi Journal*, 77(2), pp. 195−199.

Makkonen, A., R. Rantanen, A. Kaukovirta, H. Koivisto, J. Lieslehto, T. Jussila, H. N. Koivo, and T. Huhtelin (1995): "Three control schemes for paper machine MD-control." *Control Engineering Practice*, 3(10), pp. 1471−1474.

Martinez, D. M., M. Drotz, R. Lai, and A. R. Matin (2001): "Dryness and physical properties of paper webs in laboratory-scale impulse processing." *Drying Technology*, 19(10), pp. 2435−2450.

Mattsson, S. E., and H. Elmqvist (1997): "Modelica − An international effort to design the next generation modeling language." *7th IFAC symp. on computer aided control systems design*, Gent, Belgium.

Mattsson, S. E., H. Elmqvist, and M. Otter (1998): "Physical system modeling with Modelica." *Control Eng. Practice*, vol. 6, pp. 501−510.

McConnell, R. (1980): *A literature review of drying research in the pulp and paper industry*, Drying '80, Ed. A. Mujumdar, Hemisphere Publishing, NY, pp. 330−337.

McLain, R. B, M. J. Kurtz, and M. A Henson (1996): "Habituating control for non-square nonlinear processes." *Proceedings of IEEE International Conference on Control Applications*, pp. 273−278, Dearborn, MI.

Menani, S., H. Koivo, T. Huhtelin, and R. Kuusisto (1998): "Dynamic modelling of paper machine from grade change data." In *Proceedings of Control Systems*, Porvoo, Finland pp. 79−86.

Morari, M., and E. Zafiriou (1989): *Robust process control*, Prentice-Hall, Englewood Cliffs, N. J.

Mori, Y., H. Shimizu, and K. Takao (2000): "Development of a new automatic grade change control system for paper machine." *Proc. Control Systems 2000*, pp. 231−234, Victoria, Canada.

Murphy, T. F., and S.-C. Chen (1999): "Transition control of paper-making processes: paper grade change." *Proceedings of the 1996 IEEE International Conference on Control Applications*, pp. 1278−1283, Kohala Coast-Islands of Hawaii, Hawaii.

Murphy, T. F., S. Yurkovich, and S.-C. Chen (1996): "Intelligent control for paper machine moisture control." *Proceedings of the 1996 IEEE International Conference on Control Applications*, pp. 826−833, Dearborn, Michigan.

Morud, J., and S. Skogestad (1996): "Dynamic behaviour of integrated plants." *Journal of Process Control*, 6, pp. 145−156.

Natarajan, K., G. A. Dumont, and M. S. Davies (1988): "An algorithm for estimating cross and machine direction moisture profiles for paper machines." *IFAC/IFORS Symposium*, pp. 1091−1096, Beijing, PRC.

Nelson, D., and T. Gardner (1996): "Optimizing paper machine control - a case study." *Pulp and Paper Canada*, 97(11), pp. 43−49.

References

Niemenmaa, A., J. Lappalainen, K. Juslin, and I. Laukkanen (1996): "Dynamic modelling and simulation of paper machine drying section." *Proceedings of the 10th International Drying Symposium (IDS'96)*, vol. B, pp.1157−1164, Kraków, Poland.

Nissan, A., and W. Kaye (1955): "An analytical approach to the problem of drying thin fibrous sheets on multicylinder machines." *Tappi Journal*, vol. 38, no. 7, pp. 385−398.

Orloff, D. I., and J. W. Crouse (1999): "Impulse drying: status of the pilot-scale research program." *Tappi Journal*, 82(9), pp. 143−149.

Pauksta, P. M. (1998): "Paper machines of tomorrow, drying to speed." *Tappi Journal*, 81(7), pp. 46−52.

Peng, S. W., K. Mizukami, W. Liu, N. Sebe, T. Takeba (1997): "An experimental study of condensation heat transfer in a horizontally rotating cylinder with a scraper." *Experimental Thermal and Fluid Science*, 14, pp 205−212.

Perrault, R. D. (1991): "Troubleshooting design and operation of the dryer section." in *TAPPI Practical Aspects of Pressing & Drying Short Course*, pp. 249−277, Atlanta, GA.

Perré, P., Y. Lescanne, and Y. Brocard (2004): "Modelling of paper drying: a comprehensive computational model used by the industry." *Proceedings of the 14th International Drying Symposium (IDS'2004)*, vol. B, pp. 1263−1270, São Paulo, Brazil.

Persson, H. (1998): *Dynamic modelling and simulation of multi-cylinder paper dryers*, Licentiate thesis, Department of Chemical Engineering, Lund Institute of Technology.

Petterson, M., and S. Stenström (2000): "Experimental evaluation of electric infrared dryers." *Tappi Journal*, vol. 83, no. 8.

Poulin É., and A. Pomerleau (1999): "PI settings for integrating processes based on ultimate cycle information." *IEEE Transactions on Control Systems Technology*, 7(4), pp. 509−511.

Pulko, S. H., A. J. Wilkinson, and A. Saidane (2002): "TLM representation of the hyperbolic heat conduction equation." *International Journal of Numerical Modelling*, 15, pp. 303−315.

Pulkowski, J. H., and G. L. Wedel (1988): "The effect of spoiler bars on dryer heat transfer." *Pulp and Paper Magazine of Canada*, 89(8), pp. 61−66.

Ramesh, R. (1991): *Modeling of multicyliner drying of light-weight paper*, PhD thesis, State University of New York, Col. of Environmental Science and Forestry.

Rao, M., Q. Xia, and Y. Ying (1994): *Modeling and advanced control for process industries: application to paper making processes*, Springer-Verlag, New York.

Reardon, S., M. Davis, and P. Doe (2000): "Computational modelling of paper drying machines." *Tappi Journal*, vol. 83, no. 9.

Retulainen, E. (2001): "Key development phases of Condebelt: long journey from idea to commercial product." *Drying Technology*, 19(10), pp. 2451−2467.

Sadeghi, M. (2003): *Modeling and simulation of transport phenomena in paper drying*, PhD thesis, McGill University, Montreal, Canada.

Sadeghi, M., and W. J. M. Douglas (2004): "From tissue to linerboard: validation of a microscale simulator for single technique and hybrid dryers." *Proceedings of the 14th International Drying Symposium (IDS'2004)*, vol. A, pp. 444−451, São Paulo, Brazil.

Schmidt, E. (1969): *Properties of water and steam in SI-units*, Springer Verlag, Berlin, Germany.

Schweiger, C. A., and J. B. Rudd (1994): "Prediction and control of paper machine parameters using adaptive technologies in process modelling." *Tappi Journal*, 77(11), pp. 201−208.

Sell, N. J. (ed) (1995): *Process control fundamentals - for the pulp and paper industry*, Tappi Press.

References

Seyed-Yagoobi, J., S. J. Sikirica, and K. M. Counts (2001): "Heating/drying of paper sheet with gas-fired infrared emitters − pilot machine trials." *Drying Technology*, 19(3&4), pp. 639−651.

Shinskey, F. G. (1978): "Control systems can save energy." *Chemical Engineering Progress*, 43, pp. 43−46.

Silvennoinen, E., K. Juslin, M. Hänninen, O. Tiihonen, J. Kurki, and K. Porkholm (1989): *The APROS software for process simulation and model development*, Technical Research Centre of Finland, Research report 618, Espoo, Finland.

Skogestad, S. (2003): "Simple analytic rules for model reduction and PID controller tuning." *Journal of Process control*, 13, pp.291−309.

Skoglund, A., A. Brundin, and C.-F. Mandenius (2000): "A multivariate process model for grade change in a paperboard machine." *Nordic Pulp and Paper Research Journal*, vol. 15, no. 3, pp. 183−188.

Slätteke, O., and K. J. Åström (2005): "Modeling of a steam heated rotating cylinder – a grey-box approach." *American Control Conference 2005*, Portland, Oregon.

Slätteke, O., K. Forsman, T. Hägglund, and B. Wittenmark (2002). "On identification and control tuning of cylinder dryers" In *Proceedings Control Systems 2002*, pp. 298−302, Stockholm, Sweden

Sparr, G. and A. Sparr (2000): *Kontinuerliga System*, Studentlitteratur, Lund, Sweden.

Stenström, S., M. Karlsson, O. Slätteke, K. Forsman, and B. Wittenmark (2002): "Productivity increase from a better understanding of dynamic processes and control of the paper dryer." *Preprints 7th New Available Technologies,* pp. 70−73, Stockholm, Sweden.

Stenström, S., and T. Svanquist (1991): "A general model for calculating pressure drop in siphons and siphon riser tubes − Part 2: experimental results", *Tappi Journal*, 74(12), pp. 157−162.

Stenström, S., B. Wilhelmsson, L. Nilsson, R. Krook, and R. Wimmerstedt (1994): "Measurement of reference experimental

drying data for the multi-cylinder paper dryer." *Proceedings of the 9th International Drying Symposium (IDS'94)*, Gold Coast, Australia, pp. 1179−1186.

Stewart, G. E., D. M. Gorinevsky, and G. A. Dumont (2003): "Feedback controller design for a spatially distributed system: the paper machine problem." *IEEE Transaction on Control Systems Technology*, 11(5), pp. 612−628.

Sun, X., K. Yi, and Y. Sun (2000): "The modeling and control of basis weight and moisture content." *Proceedings 3rd World Congress on Intelligent Control and Automation*, Heifei, P. R. China, pp. 3724−3728.

Thomas, P. (1999): *Simulation of industrial processes − for control engineers*, Butterworth-Heinemann, Oxford, Great Britain.

Tyreus, B. D., and W. L.. Luyben (1992): "Tuning PI controllers for integrator/dead time processes." *Industrial and Engineering Chemistry Research*, 31, pp. 2625−2628.

VanAntwerp, J. G, and R. D. Braatz (2000): "Fast model predictive control of sheet and film processes." *IEEE Transactions on Control Systems Technology*, 8(3), pp. 408−417.

Videau, J. L., and A. Lemaitre (1982) *An improved model of a paper machine multicylinder drying section*, Drying '82, Ed. A. Mujumdar, Hemisphere Publishing, NY, pp. 129−138.

Viitamäki, P. (2004): *Hybrid modeling of paper machine grade changes*, PhD-thesis, Department of Automation and Systems Technology, Helsinki University of Thechnology, Finland.

Visioli, A. (2001): "Optimal tuning of PID controllers for integral and unstable processes." *IEE Proceedings of Control Theory Applications*, 148(2), pp. 180−184.

Wallén, A. (2000): *Tools for autonomous process control*, PhD-thesis, Department of Automatic Control, Lund Institute of Technology, Sweden.

References

Wang, H. (1996): "Applying neuro-fuzzy modelling and control to MD moisture content systems in paper machines." *Proceedings of IEEE International Conference on Control Applications*, pp. 229−234, Dearborn, MI.

Wang, Y.-G., W.-J. Cai (2001): "PID tuning for integrating processes with sensitivity specification." *Proceedings Conference on Decision and Control*, pp. 4087−4091, Orlando, FL.

Wells, C. H. (1999): "Robust multivariable IMC control for paper machines." *Tappi Journal*, 82(7), pp. 140−144.

Wilhelmsson, B. (1995): *An experimental and theoretical study of multi-cylinder paper drying*, PhD thesis, Department of Chemical Engineering, Lund Institute of Technology.

Wilhelmsson, B., L. Fagerholm, L. Nilsson, and S. Stenström (1994): "An experimental study of contact coefficients in paper drying." *Tappi Journal*, 77(5), pp. 159−168.

Xia, Q, M. Rao, and J. Qian (1993): "Model algorithmic control for paper machines." *Proceedings of the IEEE Conference on Control Applications*, pp. 203−208, Vancouver, Bristish Columbia.

Zhuang, M., and D. P. Atherton (1993): "Automatic tuning of optimum PID controllers." *IEE Proceedings D. Control Theory and Applications*, 140(3), pp. 216−224.

Ziegler, J. G., and N. B. Nichols (1942): "Optimum settings for automatic controllers." *Transactions of American Society of Mechanical Engineers*, 64, pp. 759−768.

List of Symbols

A_{cyl}	m^2	Inner cylinder area
A_{xy}	m^2	Area of paper covering the cylinder
$C_{p,m}$	$J/(kg \cdot K)$	Specific heat capacity of cylinder shell
$C_{p,p}$	$J/(kg \cdot K)$	Specific heat capacity of paper
C_v	m^2	Valve conductance
$C(s)$	−	Controller transfer function
d	−	Load disturbance
d_v	$kg/(s \cdot \%)$	Valve constant
d_y	m	Width of paper sheet
g	kg/m^2	Dry basis weight of paper
$G(s)$	−	General transfer function
h_s	J/kg	Enthalpy of steam
h_w	J/kg	Enthalpy of condensate
ΔH_s	J/kg	Heat of sorption
ΔH_{vap}	J/kg	Latent heat of vaporization
ΔH	J/kg	Energy required to evaporate water from the paper surface
J	−	Cost function in MPC
k_c	−	Gain of the PID controller
K	m/s	Mass transfer coefficient for paper sheet
m	kg	Mass of cylinder shell
M_s	−	Maximum value of sensitivity function
M_w	$kg/mole$	Molecular weight of water

List of Symbols

n	–	Noise
p	Pa	Steam pressure inside cylinder
p_{sh}	Pa	Steam pressure in header
p_{tot}	Pa	Standard pressure (101.325 kPa)
p_{v0}	Pa	Partial vapor pressure for free water
$p_{v,a}$	Pa	Partial pressure for water vapor in the air
$p_{v,p}$	Pa	Partial pressure for water vapor at paper surface
$P(s)$	–	Process transfer function
q_{bt}	kg/s	Blow through steam
q_c	kg/s	Condensation rate
q_{evap}	kg/(m²·s)	Evaporation rate
q_s	kg/s	Inflow of steam to cylinder
q_w	kg/s	Outflow of condensate
Q	–	Weighting matrix for MPC
Q_m	W	Energy flow to cylinder shell
Q_p	W	Energy flow to paper
r	–	Set point
R	–	Weighting matrix for MPC
R_g	J/(mole·K)	Gas constant (≈ 8.31)
R_v	–	Valve rangeability
T_d	s	Derivative time of the PID controller
T_i	s	Integral time of the PID controller
T_m	K	Temperature of cylinder shell
T_p	K	Temperature of paper
u	kg/kg	Moisture ratio
u_c	–	Controller output
u_s	J/kg	Internal energy of steam
u_w	J/kg	Internal energy of condensate

V	m^3	Volume inside cylinder
V_s	m^3	Volume of steam
V_w	m^3	Volume of condensate
v_x	m/s	Speed of paper sheet
w	%	Moisture content
x	kg/kg	Water content in air
x_v	−	Valve opening
y	−	Process output
α_{sc}	W/(m^2·K)	Heat transfer coefficient steam − cylinder
α_{cp}	W/(m^2·K)	Heat transfer coefficient cylinder − paper
δ_{cyl}	m	Cylinder thickness / 2
φ	−	Sorption isotherm
λ_{cyl}	W/(m·K)	Thermal conductivity of cylinder shell
η	−	Fraction of dryer surface covered by paper
ρ_s	kg/m^3	Density of steam
ρ_w	kg/m^3	Density of condensate
τ_1 and τ_2	−	Tuning parameters of mid-ranging controller